dc_836_14

MTA doktori értekezés

A sejtosztódás és sejtnövekedés matematikai modelljei

Dr. Csikász-Nagy Attila

Pázmány Péter Katolikus Egyetem

Információs Technológiai és Bionikai Kar

2016

dc_836_14

Tartalomjegyzék

dc_836_14

Összefoglalás

Az egyedi sejtek osztódásának precíz szabályozása kulcsfontosságú az élőlények fejlődéséhez és növekedési egyensúlyának fenntartásához. A sejtek túlszaporodása rákhoz, míg az osztódások hiánya fejlődési rendellenességekhez vezet. Az eukarióta sejtek osztódását egy komplex molekuláris regulációs hálózat szabályozza. A fő szabályozó molekulák és azok kölcsönhatásai nagymértékben konzerváltak. A sejtciklus periodicitásáért az ugyancsak evolúciósan konzervált Ciklin-Függő Kinázok aktivitásának oszcillációja felel. Ezeket a központi sejtciklus regulátorokat szabályzó jelátviteli utak és az őáltaluk szabályozott molekulák azonban már nagyobb diverzitást mutatnak. Munkám folyamán a központi konzervált rendszer, valamint az alsóbb és felsőbb jelátviteli útvonalak dinamikus viselkedését vizsgáltam matematikai modellekkel.

Tér- és időbeli szimulációkkal, valamint a nemlineáris dinamika módszereivel vizsgáltam a sejtosztódási ciklust szabályozó hálózatot és annak kapcsolatát a sejtnövekedést, valamint a napi ritmust szabályozó hálózatokkal. A munka legnagyobb része élesztőkön megfigyelt kísérleti eredményekre támaszkodik és modelljeink jóslásait is élesztőkön teszteltük, azonban modelljeink szerint a legtöbb megállapítás magasabb szervezettségű eukariótákra is érvényes.

Saccharomyces cerevisiae, sarjadzó élesztő modellünkből kiindulva megállapítottuk, hogy a sejtciklus központi regulációs moduljának molekuláris kapcsoltságában megfigyelhető pozitív visszacsatolások felelősek a sejtciklusátmenetek pontos sorrendjéért. Hasadó élesztő, *Schizosaccharomyces pombe* sejtekre kidolgoztuk a sejtnövekedés és a sejtosztódási ciklus kapcsolatának matematikai és hálózati modelljeit, és azok predikcióit kísérletesen igazoltuk. A napi ritmus és a sejtciklus kapcsolatának matematikai modelljei segítettek minket megérteni és később kísérletesen vizsgálni ezt a kapcsolatot *Neurospora crassa* modell organizmusban. Ezeken kívül számos megfigyelést tettünk a molekuláris szabályozó hálózatok általános dinamikai viselkedésére, és módszereket fejlesztettünk ki a modellek rendszerszintű vizsgálatára is. Eredményeink hozzájárulnak a sejtosztódás szabályozásának alaposabb megismeréséhez, és ezáltal megteremtik a rák kialakulásának és megfékezésének rendszerszintű vizsgálatának lehetőségét.

dc_836_14

Köszönetnyilvánítás

Köszönetemet szeretném kifejezni mindazoknak, akik támogattak tudományos karrierem alatt. Novák Béla és John J. Tyson professzorok voltak a mentoraim, ők alapozták meg tudásom, tőlük kaptam a tudományos szemléletet, ami segített ide eljutni. Rengeteg kiváló kutatót neveltek ki, akik közül sokaknak köszönöm az együttműködést és a barátságot, ami végig elkísért karrieremen. Különös köszönet Győrffy Bélának, Sveiczer Ákosnak, Kathy Chennek, Laurence Calzone-nak, Andrea Cilibertonak, Kapuy Orsolyának, Tóth Attilának.

Szintén köszönet illeti a rengeteg együttműködő kollégát, akik hittek modellezési eredményeimben, és kísérletesen tesztelték azokat. Kiemelt köszönet Christian I. Hongnak, Rafael Carazo-Salasnak, Marti Aldea-nak, Sean Thomasnak és Azeddine SiAmmournak, akikkel továbbra is öröm együtt dolgozni. Köszönöm az együttműködést azoknak, akiktől új elméleti módszereket és tudást kaptam: Luca Cardelli, Matteo Cavaliere, Ivan Mura, Lars Juhl Jensen, Orkun Soyer. Köszönöm korábbi intézetvezetőimnek, Corrado Priaminak, Duccio Cavalierinek, Malcolm Irvingnek és Anne Ridley-nek, hogy megadták a lehetőséget új kutatási irányok felfedezésére.

Köszönet illeti a velem dolgozó briliáns posztdoktorokat, Federico Vaggit és Sean Sedwardst, valamint a korábbi és mostani doktoránsaimat (Zámborszky Judit, Archana Bajpai, Sreeharish Muppirisetty, Valentina Cappelletti, Dúl Zoltán, Rosa Hernansaiz Ballesteros, Kirsten Jenkins és Evguenia Usoskina), hogy mindig bíztak bennem, felfedeztek velem együtt és megtanítottak olyasmikre, amiket néha nekem kellett volna nekik tanítani.

Köszönet számos kollégának a Pázmány Péter Katolikus Egyetem Információs Technológiai és Bionikai Karán, különösen Szolgay Péter dékán úrnak a belém vetett bizalomért és Pongor Sándornak, azért mert visszavezetett a magyar tudományos életbe.

Családom nélkül ez biztos nem sikerült volna, sok lemondással és alkalmazkodással lehetővé tették, hogy a tudományra és ezzel a karrieremre és egyben a hobbimra fókuszáljak.

dc_836_14

Rövidítések jegyzéke

CDK: **C**iklin-Függő (**D**ependens) **K**ináz

TF: **T**ranszkripciós **F**aktor

FFL: Előrecsatolási hurok (**F**eed **F**orward **L**oop)

SIN: **S**zeptációt **I**ndukáló Hálózat (Network)

ÖV: **Ö**reg **V**ég

ÚV: **Ú**j **V**ég

Glu: Glükóz

Gal: Galaktóz

Raf: Raffinóz

Eth: Etanol

dc_836_14

1. Bevezetés

A sejtek egészséges fejlődéséhez és szaporodásához elengedhetetlen, hogy az osztódási ciklusuk pontos ellenőrzés alatt álljon, és a sejtciklus egyes fázisai kötött sorrendben kövessék egymást. Egy komplex regulációs hálózat felelős a sejtciklus pontos szabályozásáért. A sejtciklust szabályozó molekulák kölcsönhatásai bonyolult előre- és visszacsatolási hurkokat hoznak létre a szabályozó hálózatban, és ezek által szabályozzák a sejtciklus fázisainak átmeneteit. A sejtciklust szabályozó molekulák nagy részét ismerjük, és a kapcsoltságukról is rendelkezünk információkkal, de sokkal kevésbé értjük, hogy a komplex kölcsönhatásaik hogyan vezetnek a megfigyelt fenotípusos válaszokhoz. A számításos rendszerbiológia módszereinek alkalmazásával vizsgálni tudjuk, hogy a kísérletes alapon feltételezett regulációs hálózatok milyen dinamikai viselkedéshez vezethetnek, és ezek mennyire egyeznek más, független kísérletes eredményekkel. Matematikai modellekkel összefoglalhatjuk eddigi tudásunk, és vizsgálhatjuk, hogy azok mennyire képesek a valóságot leírni (1. ábra). A modell egyezése a kísérlettel a rendszer megértését segítheti, míg ha a modell csak részben egyezik a kísérletekkel, akkor predikciók megalkotásában és a további kísérletes munka tervezésében segíthet.

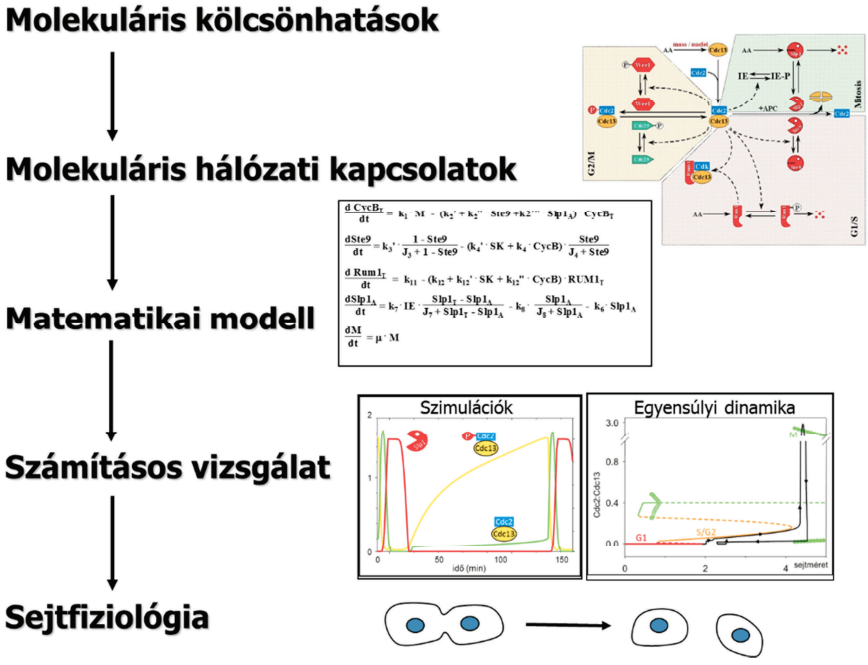

1. ábra: **Biológiai rendszerek matematikai modellezéses vizsgálatának lépései.**

dc_836_14

A biológiai rendszerek vizsgálatához az ismert molekuláris kölcsönhatások hálózata alapján egy egyenletrendszert állítunk fel. Az egyenleteket szimulációkkal és a dinamikai rendszerek vizsgálati módszereivel elemezzük, és ezáltal megpróbáljuk megérteni a sejtek fiziológiai viselkedését. Az 1. ábrán bemutatott példában a hasadó élesztő sejtciklus szabályozó hálózata alapján egy differenciálegyenlet-rendszert állítottunk fel, és az egyenletek megoldásának időbeni lefutását, valamint az egyensúlyi állapotok közötti átmeneteket vizsgáltuk. A szimulációs görbék alakja és az egyensúlyi állapotok megfeleltethetők a sejtek fiziológiai viselkedésének, így a módszer alkalmas arra, hogy megvizsgáljuk, hogy az ismert tudásanyag alapján képesek vagyunk-e megfelelően leírni a sejtek viselkedését.

Kutatásaim során a sejtciklust szabályozó központi regulációs hálózat és az ahhoz kapcsolt fiziológiai viselkedésért felelős jelátviteli útvonalakat vizsgáltam a fent bemutatott módszerekkel. Munkám során a következő kérdésekre kerestem a választ:

- Milyen molekuláris interakciók felelősek a sejtciklus fázisok közötti átmenetek pontos sorrendjéért?
- A sejtciklusszabályzás központi rendszerének dinamikai viselkedése mennyire konzervált eukariótákban?
- A sejtosztódási és sejtnövekedési ciklus hogyan kapcsolódik egymáshoz?
- A napi ritmus hogyan hat a sejtciklus periodicitására?

Doktori tézisem három részből áll: a második fejezetben összefoglalom a sejtciklus központi szabályozó hálózatának vizsgálatára irányuló munkánkat, a harmadik fejezetben e központi hálózat és a lokalizált sejtnövekedés, valamint sejtméret-szabályozás kapcsolatát ismertetem, míg a negyedik fejezetben a sejtciklus és a napi ritmus kapcsoltságát vizsgáló munkáinkat mutatom be. A fejezetek logikai felépítése azonos: irodalmi adatok alapján felállítunk egy, az 1. ábrának megfelelő modellt, azt különböző matematikai módszerekkel vizsgáljuk, majd az eredmények alapján javaslatokat teszünk a rendszer viselkedésének korábban ismeretlen pontjára, és sok esetben újabb kísérleteket javasolunk a rendszer pontosabb megértéséhez.

dc_836_14

2. A sejtciklus-szabályozás matematikai modelljei

A sejtciklus központi szabályozó molekulái a Ciklin-Függő Kinázok (CDK). A szubsztrát felismerő ciklin molekulák a sejtciklus alatt periodikusan szintetizálódnak, és a CDK-val komplexet képezve több száz fehérjét foszforilálnak a sejtciklus különböző fázisaiban. A ciklin molekulák specificitása és a CDK saját foszforilációs állapota, valamint sztöchiometrikus inhibitorok felelősek a CDK aktivitásának periodikus szabályozásáért. Ugyanakkor a CDK-szabályozó molekulák nagy része a CDK-nak direkt szubsztrátja is, így a CDK szabályozza saját regulátorait is. Mind a ciklinek, a CDK és a visszacsatolási hurkok jelenléte is konzervált eukarióta sejtekben, ezáltal feltételezhetjük, hogy a visszacsatolásoknak is jelentős szerepük van a pontos sejtciklus-szabályozásban. Kutatásainkban azt vizsgáltuk, hogy milyen dinamikai viselkedéshez vezetnek a kísérletesen megfigyelt kölcsönhatások, és hogy a modellek számítógépes szimulációi mennyire egyeztethetőek össze az egyes mutáns sejtek fenotípusos viselkedésével. Az alább ismertetett eredményeket két összefoglaló cikkben is tárgyaltam korábban (Tyson és mtsai. 2002, Csikász-Nagy 2009).

2.1. Célkitűzések

- **Az élesztő sejtciklusok dinamikájának a vizsgálata**

A legtöbb sejtciklus-szabályozó hálózattal foglalkozó kísérletes eredmény sarjadzó és hasadó élesztőn végzett kísérletekből származik. Először ezeket az eredményeket használtuk fel matematikai modelljeink megalkotására, és a modell paramétereinek beállítására.

- **A sejtciklus konzervált dinamikai funkcióinak vizsgálata**

A szabályozó molekulák és azok kapcsoltságának konzervációját felhasználva megnéztük, hogy az élesztőn megfigyeltek mennyire terjeszthetők ki fejlettebb eukariótákra is.

- **Egyedi sejtek viselkedésének szimulációja**

A legújabb kísérletes technológiák már az egyedi sejtek sejtciklusáról is képesek adatot szolgáltatni. Fenti, átlag sejtet leíró modelljeinket kiterjesztjük egyedi sejtek vizsgálatára is.

dc_836_14

2.2. Eredmények

Az élesztő sejtciklusok dinamikájának a vizsgálata

Az eukarióta szervezetek közül a *Saccharomyces cerevisiae* sarjadzó élesztő sejtciklusát ismerjük a legrészletesebben. Ez volt az első eukarióta, amelynek genomját leszekvenálták, és az első, amelyben teljes genomot átfogó vizsgálatokat végeztek. A központi sejtciklus-szabályozó rendszer kapcsoltsági hálóját megalkottuk, és egy átfogó matematikai modellt készítettünk, amely szimulálja a sejtciklus kezdő (G1-S) és befejező (M-G1) átmeneteinek dinamikáját (Chen és mtsai. 2004). A modell paraméterei úgy lettek beállítva, hogy az képes szimulálni 131 mutáns viselkedését (életképesség, sejtméret, sejtciklus fázisok hosszai). A modell részletes dinamikai elemzése megmutatta, hogy a sejtciklus két különböző időskálán mozog, egy lassú, a sejtek növekedésétől függő periódust egy megfutó periódus követ. A lassú fázisok megfeleltethetőek G1 és G2 fázisoknak, míg a gyors, autokatalítikus fázisok a sejtciklus átmeneteknél figyelhetőek meg (Lovrics és mtsai. 2006). A modell paramétereinek érzékenységanalízise megmutatta, hogy az egyes paraméterek elhangolása által okozott dinamikai változások mely más paraméterek változtatásával kompenzálhatóak (Lovrics és mtsai. 2008).

A sejtcikluskutatás második legismertebb élesztő tesztorganizmusa a *Schizosaccharomyces pombe* hasadó élesztő. Kísérletes partnerekkel együttműködve vizsgáltuk, hogy a sejtek hogyan reagálnak arra, ha az egyes sejtciklus-szabályozó génekből több kópiát tartalmaznak. Matematikai modellünk képes volt szimulálni a korábban leírt sejtciklus génhiányos mutánsok, valamint az újonnan megalkotott gén túlkifejezéses mutánsok viselkedését is (Moriya és mtsai. 2011).

A sejtciklus konzervált dinamikai funkcióinak vizsgálata

A két élesztő sejtciklusának vizsgálata rávilágított arra, hogy számos hasonló szabályozásbeli, molekuláris és dinamikai funkció konzervált a két organizmus között. Ebből kiindulva egy összehasonlító elemzést végeztünk a két élesztő, az afrikai karmos béka *Xenopus laevis* és egy általános emlős sejtciklus modell között. Megállapítottuk, hogy a különböző élőlények sejtciklus-szabályozó rendszere hasonlóan kapcsolt, és egy általános

dc_836_14

modellt is megalkottunk, amely egyedi paraméter készletekkel képes szimulálni az összes vizsgált organizmus sejtciklusát (Csikász-Nagy és mtsai. 2006). Az általános eukarióta sejtciklus vizsgálatával megállapítottuk, hogy a sejtciklus központi regulációs moduljának molekuláris kapcsoltságában megfigyelhető pozitív visszacsatolások felelősek a sejtciklusátmenetek egyirányúságáért (Novák és mtsai. 2007) (2. ábra). Szinén megmutattuk, hogy a CDK által szabályozott transzkripciós – poszttranszlációs előrecsatolási hurkok felelősek a sejtciklus fázisok pontos sorrendjéért (Csikász-Nagy és mtsai. 2009). Ezekben az előrecsatolási hurkokban a CDK foszforilezéssel szabályozza a sejtciklusátmenetek legfőbb transzkripciós faktorait (TF) és az azok által indukált sejtciklusátmenet-indító fehérjéket is (2. ábra). A CDK indukált foszforiláció és a transzkripicós faktorok is lehetnek pozitív és negatív hatással is a fehérjék képződésére és aktiválódására. Ez a két hatás különböző időskálán hat a fehérjékre, a foszforiláció sokkal gyorsabban változtatja meg a fehérjék aktivitását, mint ahogy a transzkripció változásai hatnak a fehérjeszintre. A CDK így egy lassú és egy gyors hatást is kifejthet ugyanarra a fehérjére. Modelljeink azt jósolták, hogy a különböző sejtciklusátmeneteknél ezeknek a hatásoknak az előjele változik. A különböző sejtciklus fázisoknál és azok átmeneteinél a gyors és lassú hatások előjelet válthatnak (CDK foszforilációval egyes fehérjéket aktivál, másokat gátol), és ezáltal a CDK képes egyedül kontrollálni a sejtciklus összes fázisának kulcsfehérjéit. Protein-protein interakciós és transzkripciós regulációt tartalmazó adatbázisok (http://string.embl.de/ és http://www.yeastract.com/) segítségével elemeztük az élesztőben előforduló CDK regulált előrecsatolási hurkokat. Az eredmények egyértelműen afelé mutatnak, hogy a sejtciklus különböző fázisaiban valóban másfajta topológiájú előrecsatolási hurkok működnek, a G1 fázisban a CDK mindkét ágon gátolja a fehérjéket, a G1-S átmenetnél a CDK transzkripciósan gátol, míg foszforilációsan aktivál, G2 és korai M fázisban mindkét módon aktivál, a mitózis meta-anafázis átmeneténél pedig transzkripciósan aktivál, közvetlenül pedig gátol (Csikász-Nagy és mtsai. 2009). Bioinformatikai és modellezéses módszerekkel szintén megmutattuk, hogy a CDK-aktivitást, és ezáltal a sejtciklusátmeneteket szabályozó fehérjék periodikus transzkripciója egyedi mintát mutat. Különböző élőlényekben az átmenetek más és más szabályozója íródik át periodikusan, annak függvényében, hogy az adott élőlény melyik sejtciklusátmenetet szabályozza a legkörültekintőbben (Romanel és mtsai. 2012). (2. ábra)

dc_836_14

Az általános modellekből kiindulva kidolgoztunk egy modellt az emlős sejtek restrikciós pontjának szabályozására is, és a modell metabolikus kontroll analízise által megállapítottuk, hogy a p27 gátló hatása a Cdk2-CycE komplexekre a restrikciós pont egyik fő kulcsreakciója (Conradie és mtsai. 2010).

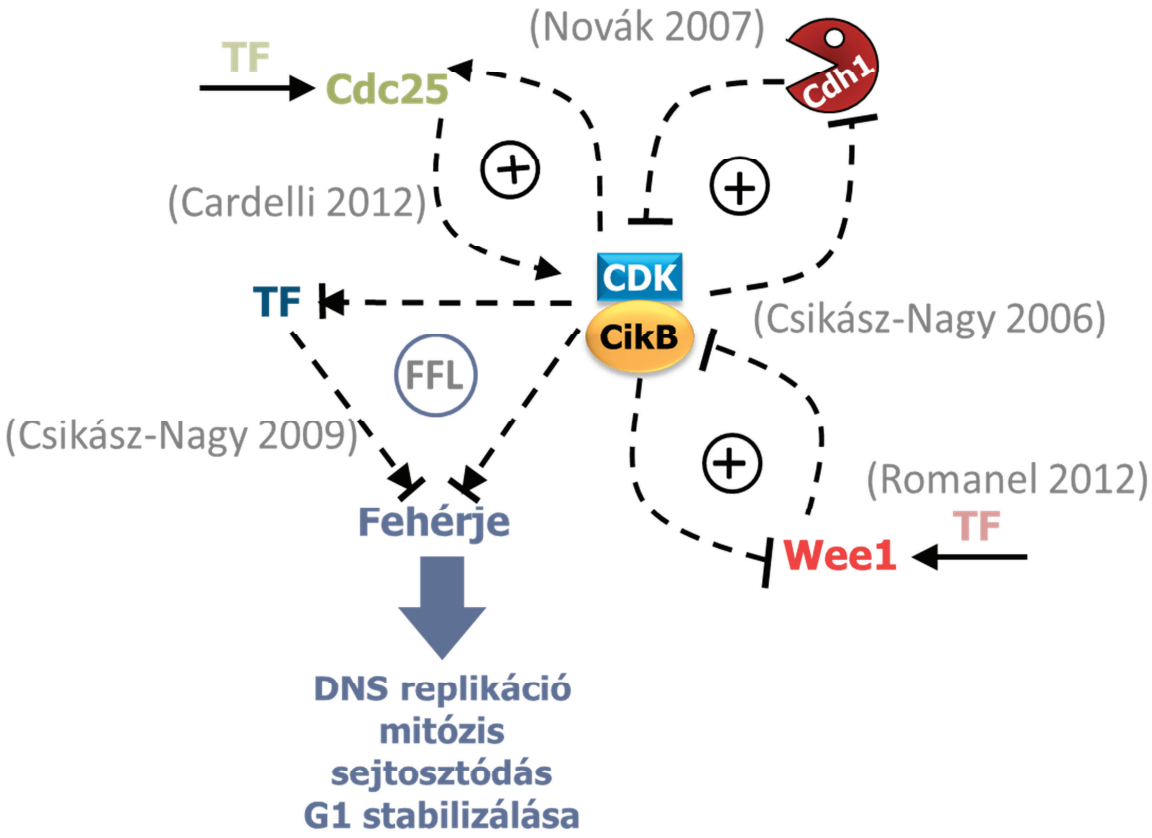

2. ábra: **A sejtciklus kulcslépéseinek szabályozása a CDK - ciklin B komplexek által pozitív és negatív visszacsatolási és előrecsatolási (FFL) hurkok által. Az egyes lépéseket leíró főbb modelljeink referenciái szürkével jelölve. (TF: Transzkripciós Faktor)**

Egyedi sejtek viselkedésének szimulációja

A fent ismertetett differenciálegyenlet-rendszer alapú modellek egy átlagos sejt viselkedését tudják leírni. Azonban, hála a legújabb mikroszkópiás technikáknak, tudjuk, hogy egy sejtpopulációban egymástól sokban eltérő viselkedésű sejtek is megfigyelhetőek. A fent említett sarjadzó élesztő modellt (Chen és mtsai. 2004) a Petri Net modellezési módszer felhasználásával átalakítottuk olyan rendszerré, amelyben az egyedi molekulák fluktuációit is le tudjuk írni, és a Gillespie-féle sztochasztikus szimulációs algoritmus segítségével vizsgáltuk

dc_836_14

az egyedi sejtciklusok dinamikáját. Megállapítottuk, hogy a sejtciklushossz eloszlása a sarjadzó élesztő számos mutánsánál sokkal szélesebb, mint a vad típusú sejteknél. Ezzel magyarázatot tudtunk adni arra a megfigyelésre, hogy ezek a törzsek populáció szinten életképesek, de sok egyedi sejt képtelen a sejtosztódásra (Mura és Csikász-Nagy 2008). Sztochasztikus szimulációkkal megmutattuk, hogy az mRNS-ek többlépéses képződése és lebomlása adhat magyarázatot a kísérletesen megfigyelt alacsony molekuláris zajszintre (Csikász-Nagy és Mura 2010). Hasonló módszerekkel megállapítottuk, hogy a sejtciklusátmenetek szabályozóinak egyed szinten regulált transzkripciója szabhatja meg a sejtciklus egyes szakaszainak hosszát (Romanel és mtsai. 2012). Szintén a sztochasztikus sejtciklus modellek segítettek abban, hogy megmutassuk, hogy a sejtciklus G2 és M fázisa közötti átmenetet szabályozó Cdk-Cdc25-Wee1 hálózat mind dinamikájában, mind struktúrájában hasonlít a számítástechnikában, a disztributív rendszerek szabályozására egyik leggyakrabban használt algoritmus viselkedéséhez (Cardelli és Csikász-Nagy 2012). Később azt is megmutattuk, hogy ez a hasonlóság fennáll akkor is, ha a sejtciklus különböző komplexitású modelljeit hasonlítjuk össze egymással (Cardelli és mtsai. 2016)

dc_836_14

3. A sejtnövekedés és a sejtciklus összehangolása

A sejtek osztódási ciklusa szorosan kapcsolt a növekedési ciklussal. A DNS-állomány megduplázása az S-fázis és két új sejtmagba osztása a mitózis alatt össze van hangolva a sejtek növekedésével, és a sejtosztódás csak akkor következhet be, ha a mitózis rendben befejeződött. A sarjadzó élesztőben az S-fázis, míg a hasadó élesztőben a mitózis áll úgynevezett sejtméretkontroll alatt, azaz ezek a sejtciklus szakaszok csak akkor kezdődhetnek el, ha a sejtek elértek egy kritikus méretet. Mindkét élesztő sejt képes polarizált sejtnövekedésre. A sarjadzó élesztők a sarj megjelenésekor, a hasadó élesztők egész interfázisuk alatt csak a sejtmembrán egy kis lokalizált területén növekednek. Ez a polarizált növekedés a G2-fázisban a sarjadzó élesztőnél átvált a sarj izotrópikus növekedésére, a hasadó élesztő sejtek pedig ekkor aktiválnak egy második polarizált növekedési zónát. A növekedés és a sejtciklus regulációjának kapcsoltságára számos matematikai modellt készítettünk.

3.1. Célkitűzések

- **A lokalizált sejtnövekedés sejtciklusos kontrolljának vizsgálata**

A hasadó élesztő sejtek a sejtciklus folyamán többször is változtatják a lokális növekedési zónáik helyzetét. Célunk az volt, hogy a kísérleteket helyesen szimuláló tér- és időbeni matematikai modelleket dolgozzunk ki a rendszer vizsgálatára, elemezzük a szabályozó molekuláris hálózatot, és ezek alapján kísérleteket javasoljunk a rendszer pontosabb megismerésére.

- **A sejtosztódást szabályozó regulációs hálózat matematikai modellezése**

A hasadó élesztő sejtosztódása egy komplex molekuláris regulációs hálózat által szabályozott. A sejtosztódás indításáért felelős molekuláris szabályozó hálózat viselkedését akartuk megérteni a rendszer tér- és időbeni matematikai modelljeinek vizsgálatával.

dc_836_14

- **A sejtméret szabályozásának vizsgálata**

Homeosztatikus állapotban a legtöbb eukarióta sejt egy viszonylag szűk tartományban tartja méretét, és ez a sejtpopulációban egy kontrollált sejtméreteloszlást eredményez. Matematikai modellekkel vizsgáltuk a méretkontroll-szabályozó rendszert élesztőkben és azt, hogy ez hogyan módosul a környezeti paraméterek megváltoztatásával.

3.2. Eredmények

A lokalizált sejtnövekedés sejtciklusos kontrolljának vizsgálata

Számtalan eukarióta sejttípusnál megfigyelhető az egyes intracelluláris és membrán struktúrák polarizált lokalizációja. Neuronok, hámszöveti sejtek, makrofágok és egysejtű organizmusok is képesek a sejtmembrán egy adott zónájára lokalizálni bizonyos molekulákat. Ezek a molekulák fontosak lehetnek irányított kommunikáció, mozgás, vagy polarizált növekedés szabályozásában. A rúd alakú hasadó élesztő sejtek a növekedési zónájukat lokalizálják a rúd végeire, és csak itt nőnek. Méghozzá a sejtciklus G1 fázisában csak azon a végen, amelyik már létezett az előző hasadásos sejtosztódás előtt (un. Öreg Vég – ÖV), és a G2 fázis kezdetekor aktiválják az Új Véget (ÚV), és egészen a mitózisig mindkét végen nőnek (3. ábra). A növekedésért a lokalizáltan polimerizált aktin felelős, míg a pontos lokalizációért a mikrotubulusokon szállított fehérjekomplexek felelnek. Érdemes megjegyezni, hogy a legfontosabb szabályozó fehérjék, amelyek felelősek a lokalizációért, konzerváltak az eukarióták között.

dc_836_14

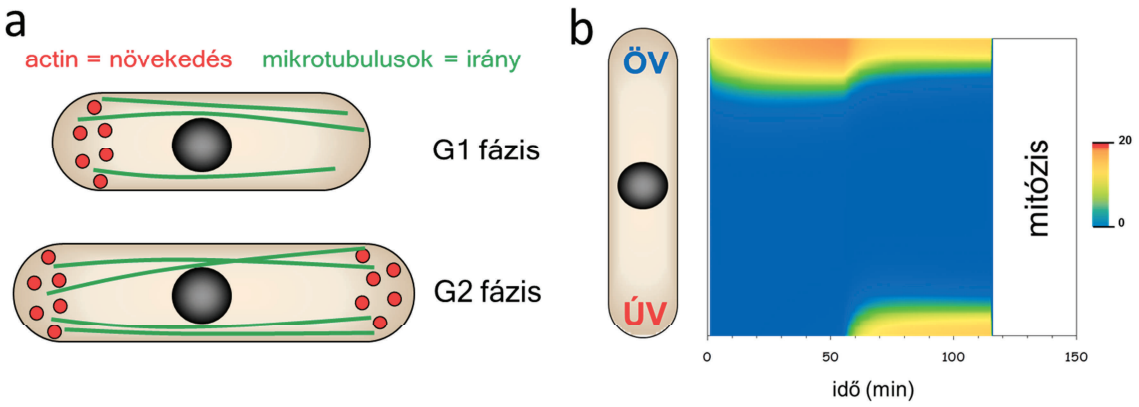

3. ábra: **Hasadó élesztő növekedési mintázata (a) és a rendszer matematikai modelljének szimulációja (b).**

A rendszer vizsgálatára kidolgoztunk egy reakció-diffúziós matematikai modellt, amelyben lassan diffundáló autokatalítikusan polimerizálódó, szubsztrát limitált komplexek indukálják a sejtnövekedést (Csikász-Nagy és mtsai. 2008). Ez a modell képes szimulálni az egyirányú növekedésből a kétirányú növekedésre váltást (3. b ábra), és különböző mutánsok fenotípusát is helyesen írja le. A későbbiekben kísérletes együttműködő partnereinkkel közösen megállapítottuk, hogy a sejtek végén a molekulák klasztereket képeznek, és ezek kialakulásáért a modellünkben feltételezett autokatalítikus asszociáció a felelős (Dodgson és mtsai. 2013) (4. ábra).

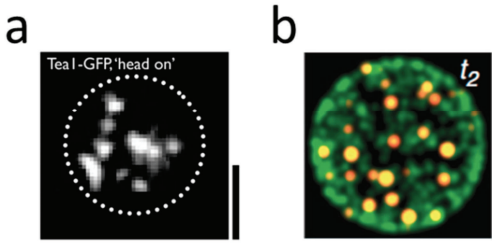

4. ábra: **Hasadó élesztő sejt végén lokalizált fehérjék klaszterezett elrendeződése kísérletesen (a) és szimulációnkban (b).**

Az eredeti modellünket több lépésben továbbfejlesztettük, és a legújabb kísérletes eredmények alapján kiegészítettük a szimpla autokatalítikus aktivátort egyinhibitorral. Ezzel a publikálás alatt álló modellel már a legújabb kísérleti eredményeket is sikeresen tudjuk szimulálni.

dc_836_14

Mindezek az eredmények magyarázatot adnak arra, miért kell a sejteknek egy kritikus méretet elérniük az új vég növekedésének aktiválásához, de nem ad magyarázatot arra, miért szükséges, hogy a sejtek G2 fázisban legyenek ekkor. Hogy molekuláris szinten ezt megértsük, a hasadó élesztő sejtpolarizációjával összefüggésbe hozott több mint 80 különböző fehérjét és azoknak a leírt kölcsönhatásait vizsgáltuk a gráfelmélet hálózati analízis módszereivel (Vaggi és mtsai. 2012). Kidolgoztunk egy új hálózati mérőszámot, ami segít felderíteni, hogy mely molekulák szolgálhatnak információátvivőként a sejtciklus és a sejtpolaritás szabályozó hálózata között. Ezzel a módszerrel jutottunk el az Sts5 RNS kötő fehérjéhez, mint potenciális kapcsolóelemhez a sejtciklus és a sejtpolarizáció között. Korábban felderítették, hogy ez a fehérje fontos a második növekedési vég aktiválódásához, és együttműködő partnereink kísérletei igazolták, hogy az Sts5 lokalizációja a sejtciklus által szabályozott (Vaggi és mtsai. 2012). A hálózati megközelítést alkalmazva számos egyéb predikciót tudtunk tenni a sejtpolarizációt szabályozó hálózat kölcsönhatásaira. Ezek a jóslások jelenleg kísérletes tesztelés alatt állnak.

Sejtpolarizációs kutatási eredményeink alapján meghívást kaptam, hogy a Philosophical Transactions of the Royal Society Biological Sciences folyóirat egy különszámának társszerkesztője legyek. Egy szerkesztői közleményben mutattuk be a téma különböző kutatási eredményeit, és foglaltuk össze a sejtmorfológiai kutatások legnagyobb sikereit (Csikász-Nagy és mtsai. 2013).

A sejtosztódást szabályozó regulációs hálózat matematikai modellezése

Az eukarióta sejtek osztódása csak azután indulhat meg, hogy a mitózis befejeződött. Molekuláris szinten ez úgy szabályozódik, hogy a mitózisos CDK-ciklin B komplexek inaktiválódása szükséges a sejtosztódás megindulásához. A hasadó élesztő sejtek, mint azt a nevük sugallja, a sejt közepén kialakuló szeptum segítségével, hasadással osztódnak. A szeptum kialakulásának (szeptáció) több lépése van. Mitózis közben egy aktin gyűrű alakul ki a sejt közepén, ami a CDK-aktivitás csökkenésének hatására összehúzódik, és ahogy az aktin gyűrű záródik, a sejtmembrán betüremkedik, és új sejtfal szintetizálódik, ami elválasztja a két leánysejtet egymástól. A következő lépésben a leánysejteket összetartó szeptum rész feloldódik, és a sejtek elválnak egymástól. A szeptációt indukáló jelátviteli útvonal (SIN – **S**eptation **I**nitiation **N**etwork) aktiválódása indítja a szeptációt. Egy matematikai modellt

dc_836_14

dolgoztunk ki annak megértésére, hogy a CDK-aktivitás mitózisos magas, majd azutáni alacsony szintje hogyan szabályozza azt, hogy a sejtosztódás a sejtciklus folyamán csak egyszer történik meg (Csikász-Nagy és mtsai. 2007)(5. ábra). A modell leírja a vadtípusú sejtek és számos mutáns viselkedését, és segített annak megértésében, hogy a CDK egy előrecsatolásos hurkon keresztül éri el, hogy a sejtosztódás csak egyszer történhet meg. Ez a megfigyelés vezetett a 2. fejezetben tárgyalt későbbi munkához, amelyben beláttuk, hogy a CDK ilyen előrecsatolásos hurkokon keresztül képes az összes sejtciklusátmenetet szabályozni (Csikász-Nagy és mtsai. 2009).

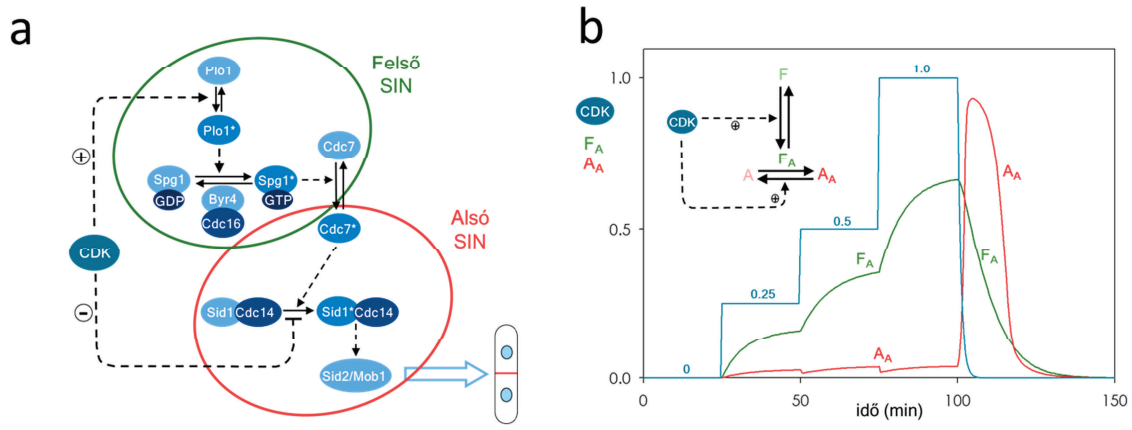

5. ábra: **Hasadó élesztő sejtosztódását szabályozó hálózat (a), és a hálózat matematikai modelljének szimulációja mutatja, hogy a SIN alsó útvonalai csak a CDK-aktivitás csökkenése után aktiválódnak (b).**

Azt is megfigyelték, hogy a SIN minden komponense az élesztők sejtmagjába ágyazódott centroszómájához kötődik, és a mitózis elején a mindkét leány centroszómán aktiválódnak a SIN felső elemei. Ugyanakkor az alsó elemek aktiválódásukkor a kezdeti szimmetrikus eloszlásból aszimmetrikusra váltanak. Így a SIN alsó jelátviteli útja csak az egyik centroszómán aktiválódik, miközben a másikon az egész SIN inaktiválódik. Korábbi kísérleti eredmények kimutatták, hogy a SIN aktiválódása az egész SIN lokalizációjáért felelős Cdc11 molekulák foszforilezéséhez vezet. Az is ismert volt, hogy a CDK is képes a Cdc11-et foszforilezni, más helyeken. Arra voltunk kíváncsiak, hogy ezek a foszforilációs lépések hogyan hatnak a SIN aszimmetriájának kialakulására. Különböző matematikai modelleket dolgoztunk ki a foszforiláció esetleges hatásainak a vizsgálatára. A modellek közül sikerült kiválasztanunk egyet, amely a SIN komponenseinek időbeni lokalizációs változásait helyesen

dc_836_14

írja le (6. ábra). A kiválasztott modell kísérletes tesztelésére javaslatot adtunk, és együttműködés keretein belül igazoltuk is, hogy a SIN aszimmetriájának kialakításáért a Cdc11 többlépéses foszforilációja a felelős (Bajpai és mtsai. 2013).

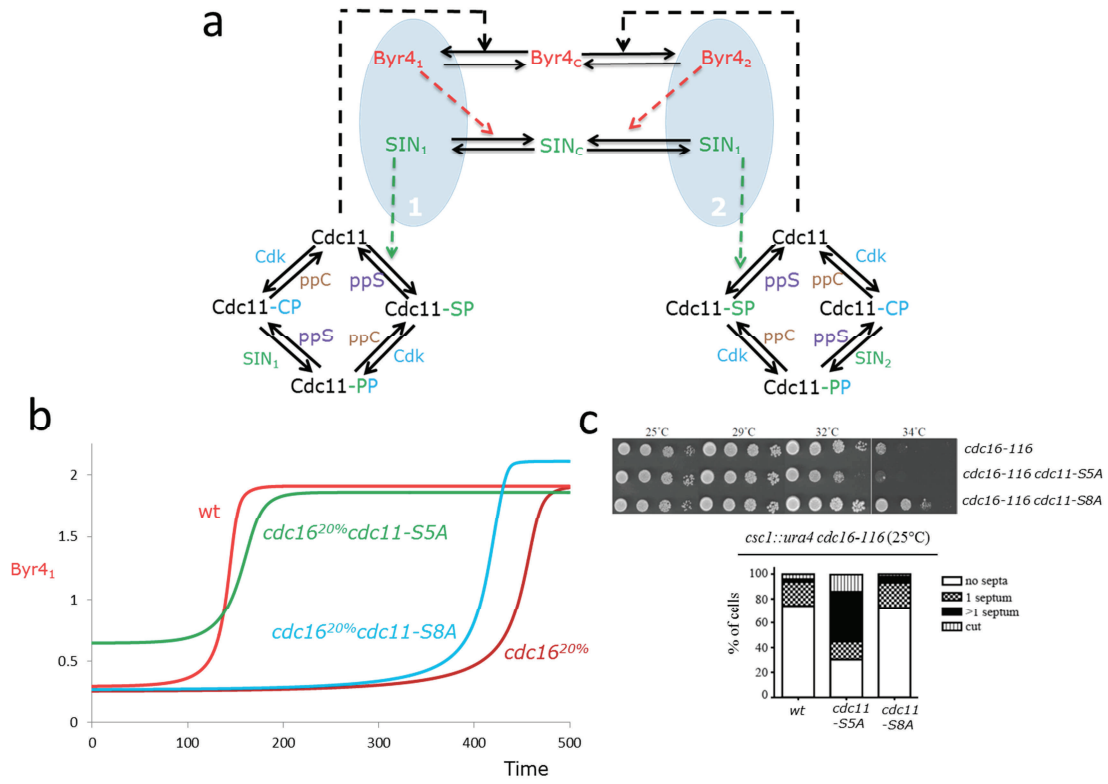

6. ábra: **Hasadó élesztő sejtosztódását szabályozó hálózat aszimmetrikus aktivációja. (a) A kísérleteket helyesen leíró hálózat a két centroszóma (kék alapon számmal jelölve) és az azokhoz kapcsolódó Cdc11, SIN és Byr4 molekulák interakciójára. b) A modell szimulációja azt mutatja, hogy *cdc16*^{ts} mutáns sejtekben a SIN által indukált foszforilációk gátlása (zöld, *cdc11-S5A* mutáns) nem, míg a CDK által indukált foszforilációk gátlása (kék, *cdc11-S8A* mutáns) késlelteti az aszimmetria kialakulását. (c) A *cdc11-S5A* mutánsok valóban nem képesek késleltetni a szeptációt *cdc16*^{ts} háttérben, azonban a *cdc11-S8A* mutánsok képesek erre, és ezáltal elősegítik a *cdc16*^{ts} mutáns sejtek túlélését és normális szeptációját.**

dc_836_14

A sejtméret szabályozásának a vizsgálata

A legtöbb eukarióta sejttípus egy viszonylag állandó mérettartományban tartja térfogatát azáltal, hogy két sejtosztódás között annyit nőnek a sejtek, hogy az újonnan megszülető leánysejtek az anyasejt kezdeti méretéhez hasonlóak lesznek. Ez a sejtméret homeosztázis úgy érhető el, hogy a sejtek csak akkor kezdik meg a sejtciklus egy kritikus lépését, ha már elértek egy bizonyos méretet. Ezt a kapcsoltságot a sejt osztódási és növekedési ciklusa között nevezzük méretkontrollnak. Több sejttípusnál azt is megfigyelték, hogy a tápanyagban gazdagabb táptalajon növesztett sejtek nagyobb, míg a minimális táptalajon növesztett sejtek kisebb méretnél osztódnak. Egyedi sarjadzó élesztő sejtek mikroszkópos vizsgálatával megfigyeltük, hogy egy adott populációban is igaz, hogy a gyorsabban növő sejteknek egy nagyobb kritikus méretet kell elérniük, hogy átmenjenek a sejtciklus START eseményén (az emlős sejtek restrikciós pontjának megfeleltethető átmenet, amikor az S-fázist indító transzkripciós faktorok aktiválódnak). Azt is megállapítottuk, hogy különböző táptalajokon növesztett egyedi sejtekre is igaz, hogy nem a táptalaj maga, hanem a sejtek egyedi növekedési sebessége határozza meg kritikus méretüket (7. a ábra). A mérési adatok alapján felállított modellel egyrészt reprodukálni tudtuk ugyanezt az eloszlást (7. b ábra), másrészt a leánysejtek és a populáció kritikus méreteit (7. c ábra), és ezek jó egyezést mutattak a kísérleti eredményekkel (7. d ábra). A modell segített annak megértésében, hogy a kritikus méret kapcsoltsága a növekedési sebességgel milyen evolúciós előnyt ad a populációnak egy olyanhoz képest, amelyben minden sejt azonos kritikus méretet kell, hogy elérjen (Ferrezuelo és mtsai. 2013). A kísérleti eredmények megmutatták, hogy ez a kapcsoltság eltűnik több START szabályozó molekula együttes kiütésekor, de akkor is, ha az egyik sejtciklus szabályozásban is fontos dajkafehérjét (Ydj1, élesztő HSP40) kiütjük a sejtekből. Legújabb munkánkban azt vizsgáljuk, hogy milyen molekuláris mechanizmus áll ennek a kapcsoltságnak a hátterében.

Komoly tudományos vita folyik a méretkontroll szerepéről az emlős sejtek sejtciklus szabályzásában. Különböző kísérletek egymástól eltérő eredményt találtak arról, hogy mennyire fontos a méretkontroll különböző emlős sejttenyészetekben. Ennek a diszkrepanciának a feloldására a 4. fejezetben részletesen ismertetett napi ritmus és a sejtciklus kapcsoltságát vizsgáló egyik modellünk adott egy javaslatot. A szimulációink azt

dc_836_14

sugallták, hogy a sejtek növekedési sebessége itt is hatással lehet a kritikus méretre, de ez a hatás elveszik, ha a sejtek a 24 órás, a napi ritmusnak megfelelő növekedési sebességgel nőnek, mert ekkor a sejtciklus fő szabályozója a napi ritmus (Zámborszky és mtsai. 2007).

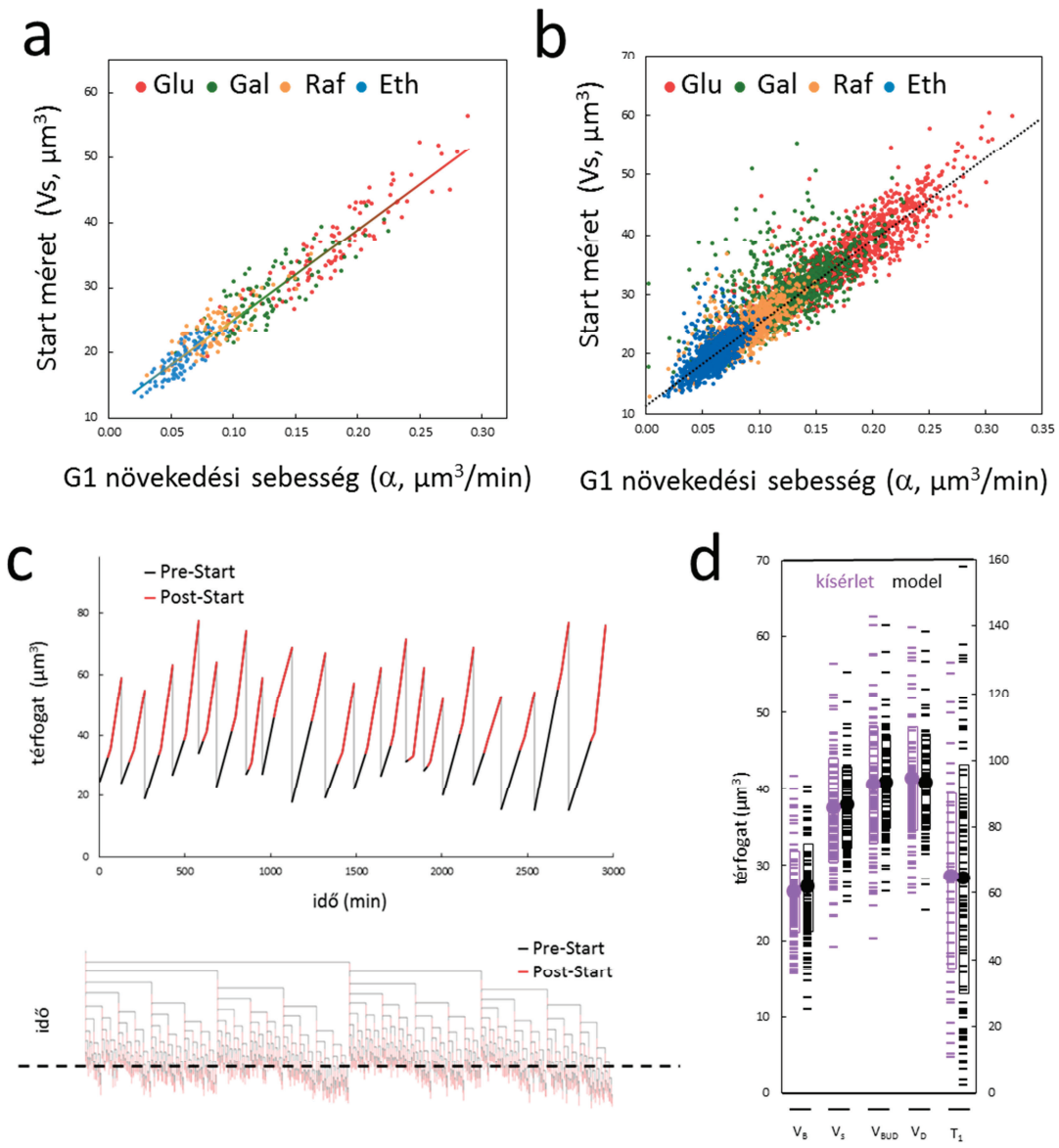

7. ábra: **A sarjadzó élesztő sejtek kritikus mérete (V_S) függ az egyedi sejtek növekedési sebességétől. (a) Kísérleti eredmények egyedi sejteken, (b) egyedi sejtciklusok szimulációs eredményei. (c) Felső ábra: egyedi leánysejt-vonal szimulációja, alsó ábra: egy anyasejt összes leszármazottjának szimulációja (fentről lefelé, a leánysejtek mindig jobbra jelennek meg az anyasejtek mellett, az osztódás időpillanatában). (d) Aszinkron populációk kísérleti és szimulációs (szaggatott vonal a c panel alsó ábráján) eredményeinek összevetése.**

dc_836_14

4. A sejtciklus és a napi ritmus kapcsoltságának vizsgálata

Számos fiziológiai és sejtfunkció 24 órás periodicitást mutat, és ez az oszcilláló viselkedés sok esetben állandó körülmények (fény, hőmérséklet, stb.) között is fennmarad. Egy, a napi ritmust szabályozó molekuláris hálózat képes fenntartani ezeket az oszcillációkat, és ezáltal az élőlények és egyedi sejtek is képesek előre megjósolni a környezet változásait, és ahhoz alkalmazkodni. A napi ritmust szabályozó molekuláris hálózat több helyen is megjelent az evolúció folyamán, így a szabályozó molekulák nem konzerváltak, de az élőlények legnagyobb része egy transzkripciós – poszttranszlációs késleltetett negatív visszacsatolásos hurkon alapuló oszcillátorral kontrollálja napi ritmusát. Sok élőlényben a sejtosztódási ciklus is hasonló 24 órás periódust mutat. Emiatt feltételezték, hogy a két periodikus rendszer kapcsolt, így a sejtciklus kritikus pillanatai (DNS-replikáció, mitózis) megfelelő napszakhoz köthető. Ezt a kapcsoltságot kimutatták emlős sejtekre is, és azt is megfigyelték, hogy a DNS-károsodás jelátviteli útvonala képes a napi ritmust is megzavarni, ezáltal a sejtciklus is vissza tud hatni a napi ritmusra. Ez a kapcsoltság napi ritmus, sejtciklus és DNS-károsodás jelátvitele között egészségügyileg is nagyon fontos. Rákos betegek kronoterápiás kezelésekor a DNS-károsító gyógyszereket vagy sugárzást a nap egy adott szakaszában adják, hogy ezzel elkerüljék a 24 órás periódusú normális sejtek megzavarását, és minimalizálják a mellékhatásokat, miközben a gyorsan szaporodó, napi ritmusukat vesztett rákos sejteket effektíven roncsolja. A rendszer jobb megértéséhez matematikai modelleket dolgoztunk ki, amelyekben vizsgáltuk a napi ritmus hatását a sejtciklus idejére, a DNS-károsodás hatását a napi ritmusra, és modelljeink alapján kifejlesztettünk egy módszert e kapcsolatok kísérletes vizsgálatára az egyik közkedvelt napi ritmus tesztorganizmusban. Eredményeink jó alapot nyújthatnak a terápiás célú DNS-károsító beavatkozások ideális napi időzítésének megjóslásának kifejlesztésére.

4.1. Célkitűzések

- **A napi ritmus sejtciklusra gyakorolt hatásának matematikai modellezése**

Kísérleti eredmények rámutattak, hogy a sejtciklus G2-M átmenetének egyik szabályozófehérjéje a napi ritmus kontrollja alatt áll. Meg akartuk érteni, hogy ez a kapcsoltság hogyan hat a sejtciklusok periodicitására.

dc_836_14

- **Napi ritmus és sejtciklus kapcsolatának vizsgálata *Neurospora crassa* rendszerben**

A más élőlényekben megfigyelt kapcsoltságot megpróbáltuk átültetni a napiritmus-kutatás egyik kedvenc tesztorganizmusára, amelynek azonban még nem volt ismert a sejtciklus szabályozása. Matematikai modellek és kísérletek kombinációjával vizsgáltuk, hogy a napi ritmus képes lehet-e szinkronizálni a fonalas gomba sejtmagjainak osztódási ciklusát.

4.2. Eredmények

A napi ritmus sejtciklusra gyakorolt hatásának matematikai modellezése

Az emlős sejtek sejtciklusa gyakran 24 órás periódussal fut, de számos már organizmus is összekapcsolja a sejtciklusát a napi ritmussal. Fiziológiai megfigyelések már több mint ötven éve leírták ezt a kapcsoltságot, de a kapcsolat molekuláris háttere csak a 2000-es évek eleje óta kezd ismertté válni. A napi ritmus szabályozásáért felelős molekulák egy késleltetett negatív visszacsatolásos hurkon (8. a ábra) keresztül indukálják a BMAL1/CLOCK transzkripciós faktor komplex 24 órás periodikus aktiválódását. Ugyanez a transzkripciós faktor a sejtciklus G2-M átmenet egyik inhibitorának, a Wee1 kináznak az átírását is indukálja. Ezáltal a napi ritmus képes lehet szinkronizálni egy sejtpopulációban a sejtciklusokat, és azokat a 24 órás napi ritmushoz kapcsolni. Matematikai modelleket fejlesztettünk ki a két oszcillátor kapcsoltságának vizsgálatára(8. a ábra). Vizsgáltuk, hogy milyen feltételekkel tudja a napi ritmus elérni, hogy a sejtciklusok is 24 órás periódussal fussanak. Megállapítottuk, hogyha a sejtek tömegduplázódási ideje közel áll a 24 órához, akkor a napi ritmus 24 órás periódusát követik a szinkron sejtciklusok, de ha a sejtek növekedési sebessége ettől nagyban eltér, akkor a sejttömeg kompenzálása miatt egy sejtpopulációban a sejtciklusidő többcsúcsú elosztást mutat (8. b ábra) (Zámborszky és mtsai. 2007). Azaz, a populációban sejtek rövidebb és hosszabb ciklusidővel is előfordulnak, így hosszabb távon elérve, hogy az egyedi sejtek mérete ne térjen el túlzottan egymástól. Ez az eredményünk adhat magyarázatot arra, hogy a harmadik fejezetben már tárgyalt méretkontroll mechanizmus kölcsönhatása a napi ritmussal lehet felelős az irodalomban már megfigyelt kvantált sejtciklusidő eloszlásért (8. c ábra).

dc_836_14

Szintén vizsgáltuk, hogy a DNS meghibásodásától aktiválódó jelátviteli útvonalak hogyan hatnak a napi ritmusra. Több napiritmus-modell összehasonlító vizsgálatával megállapítottuk, hogy a napi ritmus szabályozási hálózatában egy pozitív visszacsatolási hurok kell, hogy szerepeljen, máskülönben a modellek nem képesek leírni a kísérletesen megfigyelt viselkedést (Hong és mtsai. 2009). Az irodalomban megtalálható, pusztán negatív visszacsatoláson alapuló napiritmus-modellekhez nem tudtunk olyan paraméterkészletet találni, hogy azok pontosan leírják az indukált DNS-meghibásodás utáni válaszreakciókat. A modellekhez egy pozitív visszacsatolást hozzáadva viszont a kísérletekkel jó egyezést mutattak.

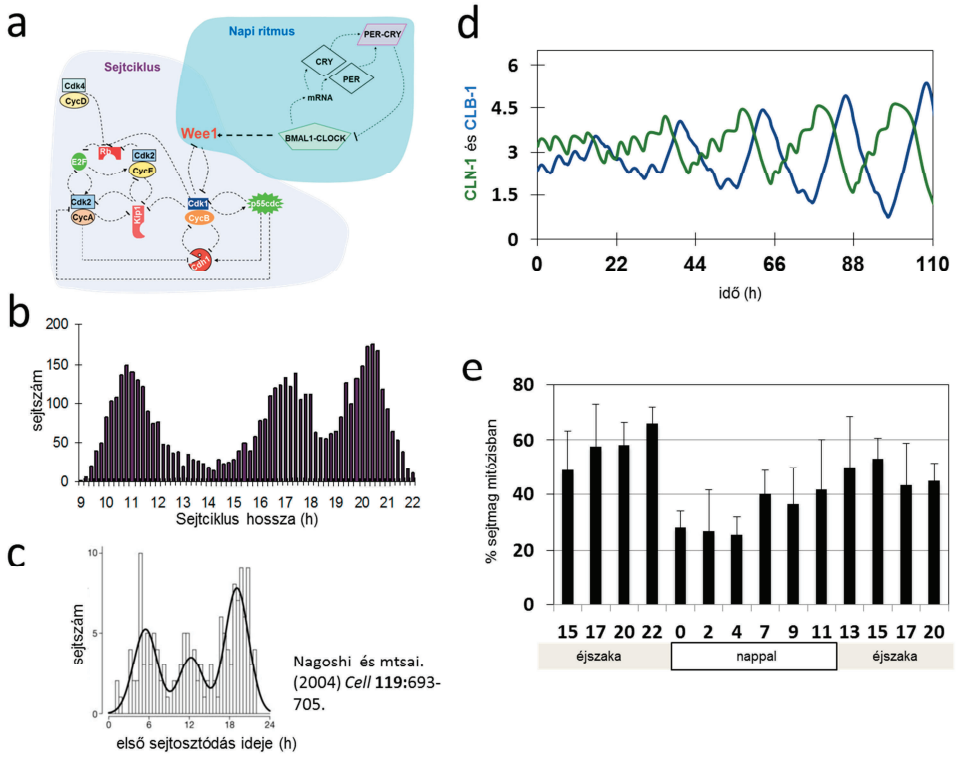

8. ábra: **A napi ritmus és a sejtciklus kapcsolatának következményei. (a) A napi ritmus és a sejtciklus kapcsolatának modellje. (b) Egyedi sejtek osztódási periódus idejének eloszlása, amikor a napi ritmus 24h, a növekedési sebesség pedig 16h periódus időt diktál. (c) Kísérleti eredmény, napi ritmus szinkronizált sejtek első sejtciklusának hosszeloszlása (Nagoshi és mtsai. 2004 alapján). (d) Különböző kezdeti sejtciklus fázisokból elindított *Neurospora crassa* sejtmagok (30 db) G1-es (CLN-1) és G2-es (CLB-1) ciklinjeinek populáció szintű szinkronizációjának a szimulációja. (e) A mitózisban lévő sejtmagok százalékos eloszlása szinkronizált napi ritmusú *Neurospora crassa* fonalas gombában.**

dc_836_14

Napi ritmus és sejtciklus kapcsolatának vizsgálata *Neurospora crassa* rendszerben

Matematikai modellezéses eredményeinket és azok jóslásait *Neurospora crassa* fonalas gombák tenyészetében kísérletesen teszteltük. A *Neurospora crassa* szélesen alkalmazott tesztorganizmusa a napiritmus-kutatásnak, de mivel ennek a fonalas gombának a sejtmagjai egy közös citoplazmában helyezkednek el, és azok aszinkron osztódnak, így sejtciklusáról korábban szinte semmit sem tudtunk. Genetikailag a *Neurospora crassa* nagyfokú hasonlóságot mutat egyéb élesztőkkel, és mivel teljes genomja leszekvenált, fehérjéi jelölhetőek és géndeléciók nagy hatásfokkal indukálhatók, így megvizsgáltuk, hogy a sejtciklust szabályozó fehérjék hogyan viselkednek a napi ritmus kontrollja alatt. Matematikai modellünk azt jósolta, hogy a sejtciklusszabályzó fő ciklinek 24 órás periódust mutatnak majd populáció szinten (8. d ábra), és ettől a sejtmagok szinkron tudnak osztódni. Ha ilyen teljes fokú kapcsoltság nem is, de világos 24 órás periódusú mitózisos hullámokat figyeltünk meg (8. e ábra), és a CLN-1 és CLN-2 fehérjék periodicitása is megfelelt a modell által jósoltaknak (Hong és mtsai. 2014). Eredményeink rámutatnak, hogy a fonalas gomba sejtciklusa kontrollálható, és ezáltal ez az organizmus használható a napi ritmus és a sejtciklus kapcsolatának vizsgálatára. Az ezáltal kínálkozó kísérletes lehetőségeket és az eddigi eredményeket egy összefoglaló cikkben mutattuk be (Zámborszky és mtsai. 2014).

dc_836_14

5. Az új tudományos eredmények összefoglalása

Tudományos eredményeim a sejtciklust szabályozó molekuláris rendszer és az azzal kölcsönható jelátviteli utak dinamikai viselkedésének megértésében tettek jelentős lépéseket.

Megmutattuk, hogy a sejtciklus fázisai közötti átmenetek pontos sorrendjéért a molekuláris szabályozó hálózatban található pozitív visszacsatolási és előrecsatolási hurkok felelősek. Matematikai modelljeink szintén igazolták, hogy a sejtciklus központi szabályozórendszerének dinamikai viselkedése konzervált eukariótákban.

Modelljeink alapján megjósoltuk, és kísérletesen bizonyítottuk, hogy a központi sejtciklust szabályzó rendszer milyen molekulákon keresztül indukál változásokat a hasadó élesztő sejtek polarizált növekedésében, és hogyan szabályozza a sejtek osztódását.

Matematikai modelljeinkkel és később kísérletesen is megmutattuk, hogy a napi ritmust szabályozó molekuláris hálózat milyen esetekben képes a sejtciklus periodicitását befolyásolni.

Ezeket és az ezekhez kapcsolódó egyéb eredményeket az alábbi pontokban foglalnám össze (a pontokhoz kapcsolódó két legfontosabb publikáció kiemelésével):

1. A sejtciklus szabályozásának rendszerszintű matematikai modelljeivel megmutattuk, hogy a sejtciklus fázisainak pontos dinamikájáért pozitív visszacsatolási és különböző előrecsatolási hurkok felelősek.

   Csikász-Nagy A., Kapuy O., Toth A., Pal C., Jensen LJ., Uhlmann F., Tyson JJ. & Novák B. (2009) Cell cycle regulation by feed-forward loops coupling transcription and phosphorylation. *Mol Sys Biol***5**:236

   Csikász-Nagy A., Battogtokh D., Chen KC., Novák B. & Tyson JJ. (2006) Analysis of a generic model of eukaryotic cell cycle regulation. *Biophys J* **90**, 4361-4379

dc_836_14

2. Kidolgoztuk a sejtnövekedés és a sejtosztódási ciklus kapcsolatának matematikai és hálózati modelljeit, és azok predikcióit kísérletesen igazoltuk.

Bajpai A., Feoktistova A., Chen JS., McCollum D., Sato M., Carazo-Salas RE., Gould KL., **Csikász-Nagy A.** (2013) Dynamics of SIN Asymmetry Establishment. *PLOS Comp Biol***9(7):**e1003147

Vaggi F., Dodgson J., Bajpai A., Chessel A., Jordan F., Sato M., Carazo-Salas RE., **Csikász-Nagy A.** (2012) Linkers of cell polarity and cell cycle regulation in the fission yeast protein interaction network. *PLoS Comp Biol***8(10):** e1002732

3. A napi ritmus és a sejtciklus kapcsolatának matematikai modelljei segítettek minket megérteni, és később kísérletesen vizsgálni ezt a kapcsolatot *Neurospora crassa* modell organizmusban.

Hong CI., Zámborszky J., Baek M., Labiscsak L., Ju K., Lee H., Larrondo LF., Goity A., Chong HS., Belden WJ., **Csikász-Nagy A.** (2014) Circadian Rhythms Synchronize Mitosis in *Neurospora crassa*. *Proc Natl Acad Sci USA***111(4):**1397-402

Zámborszky J., Hong CI. & **Csikász-Nagy A.** (2007) Computational Analysis of Mammalian Cell Division Gated by a Circadian Clock: Quantized Cell Cycles and Cell Size Control. *J Biol Rhythms*, **22:** 542-53.

Ezek az alapkutatási eredmények hosszabb távon a rákkutatás és a sejtciklus-szabályozás egyéb betegségeinek megértését segíthetik elő. Modelljeink továbbfejlesztésével állatkísérleteket lehet majd kiváltani, különböző gyógyszeres beavatkozások kimenetele számítógépesen szimulálható, és a sejtek viselkedése ez alapján jósolható lehet. A kifejlesztett módszereknek és eredményeknek így messzire ható tudományos és egészségügyben felhasználható alkalmazásai lehetnek.

dc_836_14

6. Közlemények

6.1. Az értekezés témakörében a PhD óta megjelent közlemények

26. Cardelli L., **Csikász-Nagy A.**, Dalchau N., Tribastone M., Tschaikowski M. (2016) Noise Reduction in Complex Biological Switches. *Scientific Reports*. 6:20214.

Impakt faktor: 5.578

25. Zámborszky J., **Csikász-Nagy A.,** Hong CI**.** (2014) Neurospora crassa as a model organism to explore the interconnected network of the cell cycle and the circadian clock. *Fungal Genet Biol***71:**52-7 **Impakt faktor: 3.262**

24. Hong CI., Zámborszky J., Baek M., Labiscsak L., Ju K., Lee H., Larrondo LF., Goity A., Chong HS., Belden WJ., **Csikász-Nagy A.** (2014) Circadian Rhythms Synchronize Mitosis in *Neurospora crassa*. *Proc Natl Acad Sci USA***111(4):**1397-402 **Impakt faktor: 9.737**

23. Bajpai A., Feoktistova A., Chen JS., McCollum D., Sato M., Carazo-Salas RE., Gould KL., **Csikász-Nagy A.** (2013) Dynamics of SIN Asymmetry Establishment. *PLOS Computational Biology*9(7):e1003147 **Impakt faktor: 4.829**

22. Dodgson J., Chessel A., Yamamoto M., Vaggi F., Cox S., Rosten E., Albrecht D., Geymonat M., **Csikász-Nagy A.**, Sato M., Carazo-Salas RE. (2013) Spatial segregation of polarity factors into distinct cortical clusters is required for cell polarity control. *Nature Communications***4:**1834 **Impakt faktor: 10.742**

21. **Csikász-Nagy A.,** Sato M., Carazo-Salas RE. (2013) Projecting cell polarity into the next decade. *Philos Trans R Soc Lond B Biol Sci.* 368(1629):20130001.

Impakt faktor: 6.230

20. Vaggi F., Dodgson J., Bajpai A., Chessel A., Jordan F., Sato M., Carazo-Salas RE., **Csikász-Nagy A.** (2012) Linkers of cell polarity and cell cycle regulation in the fission yeast protein interaction network. *PLoS Computational Biology***8(10):** e1002732

Impakt faktor: 4.867

dc_836_14

19. Cardelli L., **Csikász-Nagy A.** (2012) The Cell Cycle Switch Computes Approximate Majority. *Scientific Reports***2:**656 **Impakt faktor: 2.927**

18. Ferrezuelo F., Colomina N., Palmisano A., Garí E., Gallego C., **Csikász-Nagy A.** & Aldea M. (2012) The critical size is set at a single-cell level by growth rate to attain homeostasis and adaptation. *Nature Communications***3:**1012 **Impakt faktor: 10.015**

17. Romanel A., Cardelli L., Jensen LJ., **Csikász-Nagy A.** (2012) Transcriptional regulation is a major controller of cell cycle transition dynamics. *PLoS One***7:** e29716 **Impakt faktor: 3.730**

16. Moriya H., Chino A., Kapuy O., **Csikász-Nagy A.**, Novak B. (2011) Overexpression limits of fission yeast cell-cycle regulators in vivo and in silico. *Mol Sys Biol***7**:556 **Impakt faktor: 8.626**

15. Conradie R., Bruggeman FJ., Ciliberto A., **Csikász-Nagy A.,** Novák B., Westerhoff HV., Snoep JL.(2010) Restriction point control of the mammalian cell cycle via the cyclin E/Cdk2:p27 complex. *FEBS J.***277(2):**357-67 **Impakt faktor: 3.129**

14. **Csikász-Nagy A.,** Mura I.(2010) Role of mRNA gestation and senescence in noise reduction during the cell cycle. *In Silico Biol.***10:**0006. **Impakt faktor: ?**

13. **Csikász-Nagy A.** (2009) Computational Systems Biology of the Cell Cycle. *Brief Bioinform.***10(4):**424-34 **Impakt faktor: 7.329**

12. Hong CI., Zámborszky J. & **Csikász-Nagy A.** (2009) Minimum Criteria for DNA Damage-Induced Phase Advances in Circadian Rhythms. *PLoS Comput Biol.***5(5):**e1000384 **Impakt faktor: 5.759**

11. **Csikász-Nagy A.,** Kapuy O., Toth A., Pal C., Jensen, L.J. Uhlmann, F. Tyson, J.J. & Novák B. (2009) Cell cycle regulation by feed-forward loops coupling transcription and phosphorylation. *Mol Sys Biol***5**:236 **Impakt faktor: 12.125**

10. Mura I, **Csikász-Nagy A.** (2008) Stochastic Petri Net extension of a yeast cell cycle model. *J Theor Biol.***254(4)**, 850-60. **Impakt faktor: 2.454**

dc_836_14

9. Lovrics A, Zsély IG, **Csikász-Nagy A,** Zádor J, Turányi T, et al. (2008) Analysis of a budding yeast cell cycle model using the shapes of local sensitivity functions. *Int J Chem Kinet***40:** 710-720. **Impakt faktor: 1.370**

8. **Csikász-Nagy, A.,** Győrffy, B., Alt, W., Tyson, J.J. & Novák, B., (2008) Spatial controls for growth zone formation during the fission yeast cell cycle. *Yeast*, **25:** 59–69. **Impakt faktor: 2.622**

7. Zámborszky J., Hong CI. &**Csikász-Nagy A.** (2007) Computational Analysis of Mammalian Cell Division Gated by a Circadian Clock: Quantized Cell Cycles and Cell Size Control. *J Biol Rhythms*, **22:** 542-53. **Impakt faktor: 4.211**

6. Novák B., Tyson JJ., Győrffy B. &**Csikász-Nagy A.** (2007) Irreversible cell cycle transitions due to systems-level feedback. *Nat Cell Biol,***9**, 724 – 728 **Impakt faktor: 17.774**

5. **Csikász-Nagy A.,** Kapuy O., Győrffy B., Tyson, J.J. & Novák, B.,(2007) Modeling the Septation Initiation Network (SIN) in Fission Yeast Cells. *Curr Genet*, **51,** 245-255 **Impakt faktor: 2.507**

4. Lovrics A.,**Csikász-Nagy A.,** Zsély I.G., Zádor J., Turányi T. & Novák B. (2006) Time scale and dimension analysis of a budding yeast cell cycle model. *BMC Bioinformatics*, **7**, 494 **Impakt faktor: 3.617**

3.**Csikász-Nagy A.,** Battogtokh D., Chen KC., Novák B. & Tyson JJ. (2006) Analysis of a generic model of eukaryotic cell cycle regulation. *Biophys J* **90**, 4361-4379 **Impakt faktor: 4.757**

2. Chen KC., Calzone L., **Csikász-Nagy A.,** Cross FR., Novak B., Tyson JJ. (2004) Integrative Analysis of Cell Cycle Control in Budding Yeast. *Mol Biol Cell***15**, 3841-3862. **Impakt faktor: 7.517**

1. Tyson, J.J., **Csikász-Nagy A.** & Novák, B. (2002): The Dynamics of Cell Cycle Regulation. *Bioessays***24**, 1095-1109 **Impakt faktor: 7.888**

dc_836_14

6.2. Az értekezéshez közvetlenül nem kapcsolódó PhD óta publikált közlemények

13. Rizzetto S., Priami C., **Csikász-Nagy A.** (2015) Qualitative and Quantitative Protein Complex Prediction Through Proteome-Wide Simulations. *PLoS Comput Biol*. 11(10):e1004424. doi: 10.1371/journal.pcbi.1004424 **Impakt faktor: 4.62**

12. Rivero D., Berná L., Stefanini I., Baruffini E., Bergerat A., **Csikász-Nagy A.**, De Filippo C., Cavalieri D. (2015) Hsp12p and PAU genes are involved in ecological interactions between natural yeast strains. *Environ Microbiol*. doi: 10.1111/1462-2920.12950. **Impakt faktor: 6.201**

11. Kakui Y., Sunaga T., Arai K., Dodgson J., Ji L., **Csikász-Nagy A.**, Carazo-Salas R., Sato M. (2015) Module-based construction of plasmids for chromosomal integration of the fission yeast Schizosaccharomyces pombe. *Open Biol*5(6). pii: 150054 **Impakt faktor: 5.784**

10. Honeth G., Schiavinotto T., Vaggi F., Marlow R., Kanno T., Shinomiya I., Lombardi S., Buchupalli B., Graham R., Gazinska P., Ramalingam V., Burchell J., Purushotham AD., Pinder SE., **Csikász-Nagy A.**, Dontu G. (2015) Models of Breast Morphogenesis Based on Localization of Stem Cells in the Developing Mammary Lobule. *Stem Cell Reports* 4,: 699-711. **Impakt faktor: 5.365**

9. Fernandes de Abreu D.A., Caballero A., Fardel P., Stroustrup N., Chen Z., Lee K., Keyes W.D., Nash Z.M., López-Moyado I.F., Vaggi F., Cornils A., Regenass M., Neagu A., Ostojic I., Liu C., Cho Y., Sifoglu D., Shen Y., Fontana W., Lu H., **Csikász-Nagy A.,** Murphy C.T., Antebi A., Blanc E., Apfeld J., Zhang Y., Alcedo J. and Ch'ng Q. (2014). An Insulin-to-Insulin Regulatory Network Orchestrates Phenotypic Specificity in Development and Physiology. *PLoS Genet***10**: e1004225. **Impakt faktor: 8.167**

8. Vaggi F., Schiavinotto T., Lawson JLD., Chessel A., Dodgson J., Geymonat M., Sato M., Carazo-Salas RE., **Csikász-Nagy A.** (2014) A network approach to mixing delegates at meetings. *eLife***3:**e02273 **Impakt faktor: 8.519**

dc_836_14

7. **Csikász-Nagy A.**, Escudero LM., Guillaud M., Sedwards S., Baum B., Cavaliere M. (2013) Cooperation and competition in the dynamics of tissue architecture during homeostasis and tumorigenesis. *Seminars in Cancer Biology***23:**293-298 **Impakt faktor: 7.436**

6. Amara F., Colombo R., Cazzaniga P., Pescini D., **Csikász-Nagy A.**, Muzi Falconi M., Besozzi D., Plevani P., (2013) In vivo and in silico analysis of PCNA ubiquitylation in the activation of the Post Replication Repair pathway in S. cerevisiae. *BMC Systems Biology***7:**24 **Impakt faktor: 2.982**

5. Cavaliere M., Sedwards S., Tarnita CE., Nowak MA., **Csikász-Nagy A.** (2012) Prosperity is associated with instability in dynamical networks. *J Theor Biol***299:**126-138 **Impakt faktor: 2.351**

4. **Csikász-Nagy A.**, Cardelli L., Soyer OS. (2011) Response dynamics of phosphorelays suggest their potential utility in cell signaling *J R Soc Interface***8(57):**480-8 **Impakt faktor: 4.241**

3. Soyer OS., Kuwahara H., **Csikász-Nagy A.** (2009) Regulating the total level of a signaling protein can vary its dynamics in a range from switch like ultrasensitivity to adaptive responses. *FEBS J.***276(12),** 3290-3298 **Impakt faktor: 3.042**

2. **Csikász-Nagy A.,** Soyer OS. (2008) Adaptive dynamics with a single two-state protein. *J R Soc Interface.***Suppl 1**:S41-7. **Impakt faktor: 3.621**

1. Sveiczer Á., **Csikász-Nagy A.** & Novák, B. (2002): Morphogenetic checkpoint in fission yeast? Yes! *Microbiology* **148,** 2270-2271 **Impakt faktor: 2.897**

dc_836_14

6.3. Tudománymetriai Adatok

Tudományos folyóiratcikkek száma: **47**

Ezekre kapott hivatkozások száma (önhivatkozások nélkül): **1779 (1437)**

Hirsch index: **20**

Összesített impakt faktor: **225**

Első szerzős folyóiratcikkek száma: **13**

Utolsó szerzős folyóiratcikkek száma: **13**

PhD elnyerése utáni folyóiratcikkek száma: **42**

Utolsó 10 év tudományos folyóiratcikkek száma: **39**

Utolsó 10 év tudományos folyóiratcikkekre kapott hivatkozások száma: **509**

Utolsó 10 év tudományos folyóiratcikkek közül a folyóiratok felső negyedébe rangsorolt: **33**

Utolsó 10 év tudományos folyóiratcikkek közül a folyóiratok felső 10%-ba rangsorolt: **25**

Összes meghívott előadás: **35**

Egyéb konferencia előadás: **23**

dc_836_14

7. A dolgozathoz csatolt publikációk

7.1 A sejtciklus egy általános modelljének analízise

Csikász-Nagy A., Battogtokh D., Chen KC., Novák B. & Tyson JJ. (2006) Analysis of a generic model of eukaryotic cell cycle regulation. *Biophys J* **90**, 4361-4379

Impakt faktor: 4.757

Biophysical Journal Volume 90 June 2006 4361–4379

Analysis of a Generic Model of Eukaryotic Cell-Cycle Regulation

Attila Csikász-Nagy,*† Dorjsuren Battogtokh,* Katherine C. Chen,* Béla Novák,† and John J. Tyson*
*Department of Biological Sciences, Virginia Polytechnic Institute and State University, Blacksburg, Virginia 24061-0406; and †Molecular Network Dynamics Research Group of the Hungarian Academy of Sciences and Department of Agricultural and Chemical Technology, Budapest University of Technology and Economics, H-1521 Budapest, Hungary

ABSTRACT We propose a protein interaction network for the regulation of DNA synthesis and mitosis that emphasizes the universality of the regulatory system among eukaryotic cells. The idiosyncrasies of cell cycle regulation in particular organisms can be attributed, we claim, to specific settings of rate constants in the dynamic network of chemical reactions. The values of these rate constants are determined ultimately by the genetic makeup of an organism. To support these claims, we convert the reaction mechanism into a set of governing kinetic equations and provide parameter values (specific to budding yeast, fission yeast, frog eggs, and mammalian cells) that account for many curious features of cell cycle regulation in these organisms. Using one-parameter bifurcation diagrams, we show how overall cell growth drives progression through the cell cycle, how cell-size homeostasis can be achieved by two different strategies, and how mutations remodel bifurcation diagrams and create unusual cell-division phenotypes. The relation between gene dosage and phenotype can be summarized compactly in two-parameter bifurcation diagrams. Our approach provides a theoretical framework in which to understand both the universality and particularity of cell cycle regulation, and to construct, in modular fashion, increasingly complex models of the networks controlling cell growth and division.

INTRODUCTION

The cell cycle is the sequence of events by which a cell replicates its genome and distributes the copies evenly to two daughter cells. In most cells, the DNA replication-division cycle is coupled to the duplication of all other components of the cell (ribosomes, membranes, metabolic machinery, etc.), so that the interdivision time of the cell is identical to its mass doubling time (1,2). Usually mass doubling is the slower process; hence, temporal gaps (G1 and G2) are inserted in the cell cycle between S phase (DNA synthesis) and M phase (mitosis). During G1 and G2 phases, the cell is growing and ''preparing'' for the next major event of the DNA cycle (3). ''Surveillance mechanisms'' monitor progress through the cell cycle and stop the cell at crucial ''checkpoints'' so that events of the DNA and growth cycles do not get out of order or out of balance (4,5). In particular, in protists (for sure) and metazoans (to a lesser extent), cells must grow to a critical size to start S phase and to a larger size to enter mitosis. These checkpoint requirements assure that the cycle of DNA synthesis and mitosis will keep pace with the overall growth of cells (6). Other checkpoint signals monitor DNA damage and repair, completion of DNA replication, and congression of replicated chromosomes to the metaphase plate (7).

Eukaryotic cell cycle engine

These interdependent processes are choreographed by a complex network of interacting genes and proteins. The main components of this network are cyclin-dependent protein kinases (Cdk's), which initiate crucial events of the cell cycle by phosphorylating specific protein targets. Cdk's are active only if bound to a cyclin partner. Yeasts have only one essential Cdk, which can induce both S and M phase depending on which type of cyclin it binds. Because Cdk molecules are always present in excess, it is the availability of cyclins that determines the number of Cdk/cyclin complexes in a cell (8). Cdk/cyclin complexes can be downregulated a), by inhibitory phosphoryation of the Cdk subunit and b), by binding to a stoichiometric inhibitor (cyclin-dependent kinase inhibitor (CKI)) (9).

Some years ago Paul Nurse (10) proposed, and since then many experimental studies have confirmed, that the DNA replication-division cycle in all eukaryotic cells is controlled by a common set of proteins interacting with each other by a common set of rules. Nonetheless, each particular organism seems to use its own peculiar mix of these proteins and interactions, generating its own idiosyncrasies of cell growth and division. The ''generic'' features of cell cycle control concern these common genes and proteins and the general dynamical principles by which they orchestrate the replication and partitioning of the genome from mother cell to daughter. The peculiarities of the cell cycle concern exactly which parts of the common machinery are functioning in any given cell type, given the genetic background and developmental stage of an organism. We formulate the genericity of cell cycle regulation in terms of an ''underlying'' set of nonlinear ordinary differential equations with unspecified kinetic parameters, and we attribute the peculiarities of specific organisms to the precise settings of these parameters. Using bifurcation diagrams, we show how specific physiological features of

Submitted January 12, 2006, and accepted for publication March 16, 2006.

Address reprint requests to John J. Tyson, Tel.: 540-231-4662; Fax: 540-231-9307; E-mail: tyson@vt.edu; or Attila Csikász-Nagy, E-mail: csikasz@mail.bme.hu.

0006-3495/06/06/4361/19 $2.00

doi: 10.1529/biophysj.106.081240

the cell cycle are determined ultimately by levels of gene expression.

Mathematical modeling of the cell cycle

The dynamic properties of complex regulatory networks cannot be reliably characterized by intuitive reasoning alone. Computers can help us to understand and predict the behavior of such networks, and differential equations (DEs) provide a convenient language for expressing the meaning of a molecular wiring diagram in computer-readable form (11). Numerical solutions of the DEs can be compared with experimental results, in an effort to determine the kinetic rate constants in the model and to confirm the adequacy of the wiring diagram. Eventually the model, with correct equations and rate constants, should give accurate simulations of known experimental results and should be pressed to make verifiable predictions. This method has been used for many years to create mathematical models of eukaryotic cell cycle regulation (12–29). The greatest drawback to DE-based modeling is that the modeler must estimate all the rate constants from the available data and still have some observations ''left over'' to test the model. In the case of cell cycle regulation, very few of these rate constants have been measured directly (30,31) although the available data provide severe constraints on rate constant values (15,32). To complement the important but tedious work of parameter estimation by data fitting, we need analytical tools for characterizing the parameter-dependence of solutions of DEs and for associating a model's robust dynamical properties to the physiological characteristics of living cells.

Bifurcation theory and regulatory networks

Bifurcation theory is a general tool for classifying the attractors of a dynamical system and describing how the qualitative properties of these attractors change as a parameter value changes. Bifurcation theory has been used successfully to understand transitions in the cell cycle by our group (33–37) and by others (12,26,38). In this article, we use bifurcation theory to examine a generic model of eukaryotic cell cycle controls, bringing out the similarities and differences in the dynamical regulation of cell cycle events in yeasts, frog eggs, and mammalian cells. To understand our approach, the reader must be familiar with a few elementary bifurcations of nonlinear DEs and how they are generated by positive and negative feedback in the underlying molecular network. For more details, the reader may consult the Appendix to this article and some recent review articles (36,37).

MATERIALS AND METHODS

In Fig. 1 we propose a general protein interaction network for regulating cyclin-dependent kinase activities in eukaryotic cells. (Fig. 1 uses ''generic'' names for each protein; in Table 1 we present the common names of each component in specific cell types: budding yeast, fission yeast, frog eggs, and

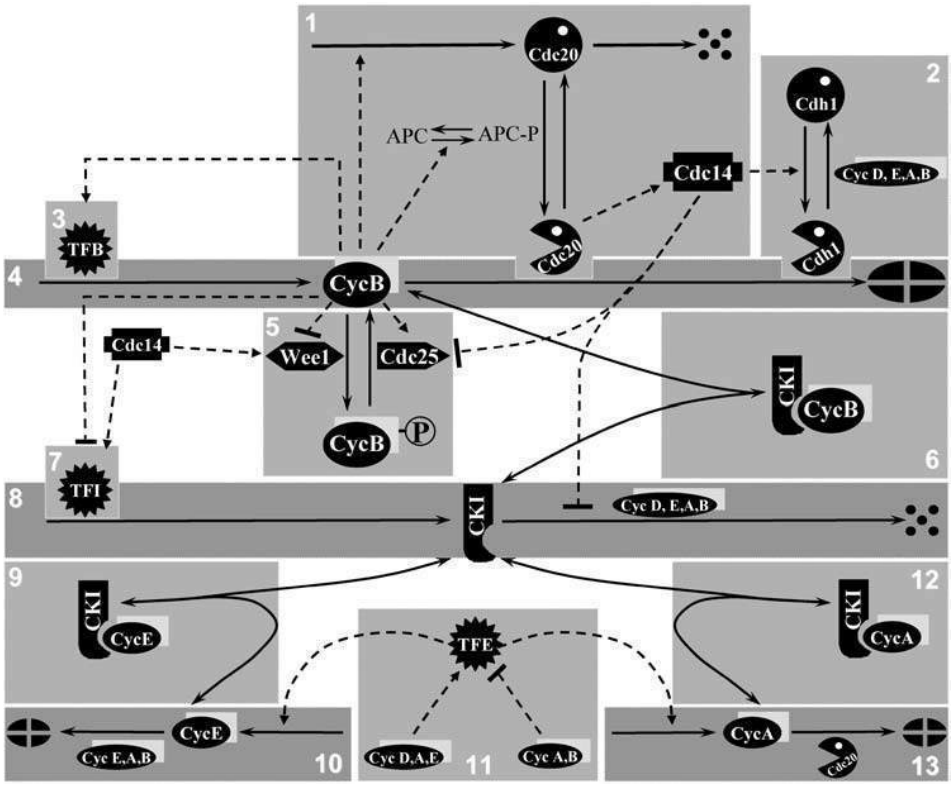

FIGURE 1 Wiring diagram of the generic cell-cycle regulatory network. Chemical reactions (*solid lines*), regulatory effects (*dashed lines*); a protein sitting on a reaction arrow represents an enzyme catalyst of the reaction. Regulatory modules of the system are distinguished by shaded backgrounds: (*1*) exit of M module, (*2*) Cdh1 module, (*3*) CycB transcription factor, (*4*) CycB synthesis/degradation, (*5*) G2 module, (*6*) CycB inhibition by CKI (also includes the binding of phosphorylated CycB, if that is present), (*7*) CKI transcription factor, (*8*) CKI synthesis/degradation, (*9*) CycE inhibition by CKI, (*10*) CycE synthesis/degradation, (*11*) CycE/A transcription factor, (*12*) CycA inhibition by CKI, (*13*) CycA synthesis/degradation. Open-mouthed PacMan represents active form of regulated protein; gray rectangles behind cyclins represent their Cdk partners. We assume that all Cdk subunits are present in constant, excess amounts.

TABLE 1 Protein name conversion table and modules used for each organism

In Fig. 1	Budding yeast	Fission yeast	*Xenopus* embryo	Mammalian cells	Function
CycB	Cdc28/Clb1,2	Cdc2/Cdc13	Cdc2/CycB	Cdc2/CycB	Mitotic Cdk/cyclin complex
CycA	Cdc28/Clb5,6	Cdc2/Cig2	Cdk1,2/CycA	Cdk1,2/CycA	S-phase Cdk/cyclin complex
CycE	Cdc28/Cln1,2	–	Cdk2/CycE	Cdk2/CycE	G1/S transition inducer Cdk/cyclin
CycD	Cdc28/Cln3	Cdc2/Puc1	Cdk4,6/CycD	Cdk4,6/CycD	Starter Cdk/cyclin complex
CKI	Sic1	Rum1	Xic1	$p27^{Kip1}$	Cdk/cyclin stoichometric inhibitor
Cdh1	Cdh1	Ste9	Fzr	hCdh1	CycB degradation regulator with APC
Wee1	Swe1	Wee1	Xwee1	hWee1	Cdk/CycB inhibitory kinase
Cdc25	Mih1	Cdc25	Xcdc25	Cdc25C	Cdk/CycB activatory phosphatase
Cdc20	Cdc20	Slp1	Fizzy	$p55^{Cdc}$	CycB, CycA degradation regulator with APC
Cdc14	Cdc14	Clp1/Flp1	Xcdc14	hCdc14	Phosphatase working against the Cdk's
TFB	Mcm1	–	–	Mcm	CycB transcription factor
TFE	Swi4/Swi6 Mbp1/Swi6	Cdc10/Res1	XE2F	E2F	CycE/A transcription factor (SBF+MBF in budding yeast)
TFI	Swi5	–	–	–	CKI transcription factor
APC	APC	APC	APC	APC	Anaphase promoting complex
Active modules	1, 2, 3, 4, 6, 7, 8, 10, 11, 12, 13, (5*)	1, 2, 4, 5, 6, 8, 11, 12, 13	1, 4, 5	1, 2, 3, 4, 6, 8, 9, 10, 11, 12, 13, (5*)	Modules of Fig. 1, used for simulation of organism

*Module 5 is not introduced into the first version of budding yeast and mammalian models.

mammalian cells.) Using basic principles of biochemical kinetics, we translate the generic mechanism into a set of coupled nonlinear ordinary differential equations (Supplementary Material, Table SI) for the temporal dynamics of each protein species. Although the structure of the DEs is fixed by the topology of the network, the forms of the reaction rate laws (mass action, Michaelis-Menten, etc.) are somewhat arbitrary and would vary from one modeller to another. We use rate laws consistent as much as possible with our earlier choices (15,18,25,39–41). In addition, most of the parameter values for each organism (Supplementary Material, Table SII) were inherited from earlier models.

For numerical simulations and bifurcation analysis of the DEs, we used the computer program XPP-AUT (42), with the ''stiff'' integrator. Instructions on how to reproduce our simulations and diagrams (including all necessary .ode and .set files, and an optional SBML version of the model) can be downloaded from our website (43).

All protein concentrations in the model are expressed in arbitrary units (au) because, for the most part, we do not know the actual concentrations of most regulatory proteins in the cell. Hence, all rate constants capture only the timescales of processes (rate constant units are min^{-1}). For each mutant, we use the same equations and parameter values except for those rate constants that are changed by the mutation (e.g., for gene deletion we set the synthesis rate of the associated protein to zero).

RESULTS

A generic model of cell cycle regulation

Since the advent of gene-cloning technologies in the 1980s, molecular cell biologists have been astoundingly successful in unraveling the complex networks of genes and proteins that underlie major aspects of cell physiology. These results have been collected recently in comprehensive molecular interaction maps (44–48). In the same spirit, but with an eye toward a computable, dynamic model, we collected the most important regulatory ''modules'' of the Cdk network. Our goal is to describe a generic network (Fig. 1) that applies equally well to yeasts, frogs, and humans. We do not claim that Fig. 1 is a complete model of eukaryotic cell-cycle controls, only that it is a starting point for understanding the basic cell-cycle engine across species.

Regulatory modules

The network, which tracks the three principal cyclin families (cyclins A, B, and E) and the proteins that regulate them at the G1-S, G2-M, and M-G1 transitions, can be subdivided into 13 modules. (Other, coarser subdivisions are possible, but these 13 modules are convenient for describing the similarities and differences of regulatory signals among various organisms.)

Modules 4, 10, and 13: synthesis and degradation of cyclins B, E, and A. Cyclin E is active primarily at the G1-S transition, cyclin A is active from S phase to early M phase, and cyclin B is essential for mitosis.

Modules 1 and 2: regulation of the anaphase promoting complex (APC). The APC works in conjunction with Cdc20 and Cdh1 to ubiquitinylate cyclin B, thereby labeling it for degradation by proteasomes. The APC must be phosphorylated by the mitotic CycB kinase before it will associate readily with Cdc20, but not so with Cdh1. On the other hand, Cdh1 can be inactivated by phosphorylation by cyclin-dependent kinases. Cdc14 is a phosphatase that opposes Cdk by dephosphorylating and activating Cdh1.

Module 8: synthesis and degradation of CKI (cyclin-dependent kinase inhibitor). Degradation of CKI is promoted by phosphorylation by cyclin-dependent kinases and inhibited by Cdc14 phosphatase.

Modules 6, 9, and 12: reversible binding of CKI to cyclin/Cdk dimers to produce catalytically inactive trimers (stoichiometric inhibition).

Modules 3, 7, and 11: regulation of the transcription factors that drive expression of cyclins and CKI. TFB is activated by cyclin B-dependent kinase. TFE is activated by some cyclin-dependent kinases and inhibited by others. TFI

is inhibited by cyclin B-dependent kinase and activated by Cdc14 phosphatase.

Module 5: regulation of cyclin B-dependent kinase by tyrosine phosphorylation and dephosphorylation (by Wee1 kinase and Cdc25 phosphatase, respectively). The tyrosine-phosphorylated form is less active than the unphosphorylated form. Cyclin B-dependent kinase phosphorylates both Wee1 (inactivating it) and Cdc25 (activating it), and these phosphorylations are reversed by Cdc14 phosphatase.

The model is replete with positive feedback loops (CycB activates TFB, which drives synthesis of CycB; CycB activates Cdc25, which activates CycB; CKI inhibits CycB, which promotes degradation of CKI; Cdh1 degrades CycB, which inhibits Cdh1), and negative feedback loops (CycB activates APC, which activates Cdc20, which degrades CycB; CycB activates Cdc20, which activates Cdc14, which opposes CycB; TFE drives synthesis of CycA, which inhibits TFE). These complex, interwoven feedback loops create the interesting dynamical properties of the control system, which account for the characteristic features of cell cycle regulation, as we intend to show.

The model (at present) neglects important pathways that regulate, e.g., cell proliferation in metazoans (retinoblastoma protein), mitotic exit in yeasts (the FEAR, MEN, and SIN pathways), and the ubiquitous DNA-damage and spindle assembly checkpoints. We intend to remedy these deficiencies in later publications, as we systematically grow the model to include more and more features of the control system.

Role of cell growth

In yeasts and other lower eukaryotes, a great deal of evidence shows the dominant role of cell growth in setting the tempo of cell division (2,49–52). In somatic cells of higher eukaryotes there are many reports of size control of cell-cycle events (e.g., (53–55)), although other authors have cast doubts on a regulatory role for cell size (e.g., (56,57)). For embryonic cells and cell extracts, the activation of Cdk1 is clearly dependent on the total amount of cyclin B available (58,59). To create a role for cell size in the regulation of Cdk activities, we assume, in our models, that the rates of synthesis of cyclins A, B, and E are proportional to cell ''mass''. The idea behind this assumption (see also Futcher (60)) is that cyclins are synthesized in the cytoplasm on ribosomes at an increasing rate as the cell grows. The cyclins then find a Cdk partner and move into the nucleus where they perform their functions. Presumably the effective, intranuclear concentrations of the cyclin-dependent kinases increase as the cell grows because they become more concentrated at their sites of action. Other regulatory proteins in the network, we assume, are not compartmentalized in the same way, so their effective concentrations do not increase as the cell grows. This basic idea for size control of the cell cycle was tested experimentally in budding yeast by manipulating the ''nuclear localization signals'' on cyclin proteins (8). As predicted by the model, cell size is larger in cells that exclude cyclins from the nucleus and smaller in cells that overaccumulate cyclins in the nucleus. A recent theoretical study by Yang et al. (61) may shed light on how cell size couples to cell division without assuming a direct dependence of cyclin synthesis rate on mass, but, for this article, we adopt the assumption as a simple and effective way to incorporate size control into nonlinear DE models for the control of cyclin-dependent kinase activities.

For simplicity, we assume that cell mass increases exponentially (with a mass doubling time (MDT) suitable for the organism under consideration) and that cell mass is exactly halved at division. Our qualitative results (bifurcation diagrams, etc.) are not dependent on these assumptions. Cell growth may be linear or logistic, and cell division may be asymmetric or inexact—it doesn't really matter to our models. The important features are that ''mass'' increases monotonically as the cell grows (driving the control system through bifurcations that govern events of the cell cycle) and that mass decreases abruptly at cell division (resetting the control system back to a G1-like state—unreplicated chromosomes and low Cdk activity).

Equations and parameter values

The dynamical properties of the regulatory network in Fig. 1 can be described by a set of ordinary differential equations (Supplementary Material, Table SI), given a table of parameter values suitable for specific organisms (Table SII). For each organism we analyze the effects of physiological and genetic changes on the transitions between cell cycle phases, in terms of bifurcations of the vector fields defined by the DEs (for background on dynamical systems, see the Appendix).

Frog embryos: *Xenopus* laevis

To validate our equations and tools, we first verified our earliest studies of bifurcations in the frog-egg model. The combination of modules 1, 4, and 5 of Fig. 1 was used to recreate the bifurcation diagram of Borisuk and Tyson (33); see Supplementary Material, Fig. S1. Our bifurcation parameter, ''cell mass'', can be interpreted as the rate constant for cyclin B synthesis. For small rates of cyclin synthesis, the control system is arrested in a stable ''interphase'' state with low activity of CycB-dependent kinase. For larger rates of cyclin synthesis, the model exhibits spontaneous limit cycle oscillations, which begin at a SNIPER bifurcation (long period, fixed amplitude). Eventually, as the rate of cyclin synthesis gets large enough, the oscillations are lost at a Hopf bifurcation (fixed period, vanishing amplitude). Beyond the Hopf bifurcation, the control system is arrested in a stable ''mitotic'' state with high activity of CycB-dependent kinase. These types of states of the control system are reminiscent of the three characteristic states of frog eggs: interphase arrest (immature oocyte), metaphase arrest (mature oocyte), and

spontaneous oscillations (fertilized egg). For more details, see Novak and Tyson (18) and Borisuk and Tyson (33).

Fission yeast: *Schizosaccharomyces pombe*

Wild-type cell cycle

The fission yeast cell cycle network, composed of modules 1, 2, 4, 5, 6, 8, 11, 12, and 13, is described in Fig. 2 in terms of a one-parameter bifurcation diagram (Fig. 2 *A*) and a simulation (Fig. 2 *B*). In the simulation, we plot protein levels as a function of cell mass rather than time, but because mass increases exponentially with time, one may think of the lower abscissa as $e^{\mu t}$. We present the simulation this way so that we can ''lift it up'' onto the bifurcation diagram: the gray curve in Fig. 2 *A* is identical to the solid black curve (actCycB) in Fig. 2 *B*. In Fig. 2 *A*, a stable, G1-like, steady state exists at very low level of actCycB (active Cdk/CycB dimers). This steady state is lost at a saddle-node bifurcation (SN1) at cell mass = 0.8 au. Between SN1 and SN2 (at cell mass = 2.6 au), the control system has a single, stable, steady-state attractor with an intermediate activity (~0.1) of cyclin B (an S/G2-like steady state). The other steady-state branches are unstable and physiologically unnoticeable. For mass >2.6 au, the only stable attractor is a stable limit cycle oscillation. This branch of stable limit cycles is lost by further bifurcations at very large mass (of little physiological significance for wild-type cells).

The gray trajectory in Fig. 2 *A* represents the path of a growing-dividing yeast cell projected onto the bifurcation diagram. Let us pick up the trajectory of a growing cell at mass = 2.2 au, where the cell cycle control system has been captured by the stable S/G2 steady state. As the cell continues to grow, it leaves the S/G2 state at SN2 and prepares to enter mitosis. At cell mass >2.6, the only stable attractor is a limit cycle. This limit cycle, which bifurcates from SN2, has infinite period at the onset of the bifurcation (hence, the onset point is commonly called a SNIPER—saddle-node-infinite-period—bifurcation). Because the limit cycle has a very long period at first, and the cell enters the limit cycle at the place where the saddle-node used to be, the cell is stuck in a semistable transient state (where the gray trajectory ''overshoots'' SN2). As the cell grows, it eventually escapes the semistable state (at cell mass ≈ 3), and then actCycB increases dramatically (note the log-scale on the ordinate), driving the cell into mitosis. Because the control system is now captured by the stable limit cycle, actCycB inevitably decreases and the cell is driven out of mitosis. We presume that the cell divides when actCycB falls below 0.1; hence, cell mass is halved (3.4 → 1.7), and the control system is now attracted to the S/G2 steady state (the only stable attractor at this cell mass). The newly divided cell makes its way to the S/G2 attractor by a circuitous route that looks like a brief G1 state (very low actCycB) but is not a stable and long-lasting G1 state. This transient G1 state is characteristic of wild-type fission yeast cells (62).

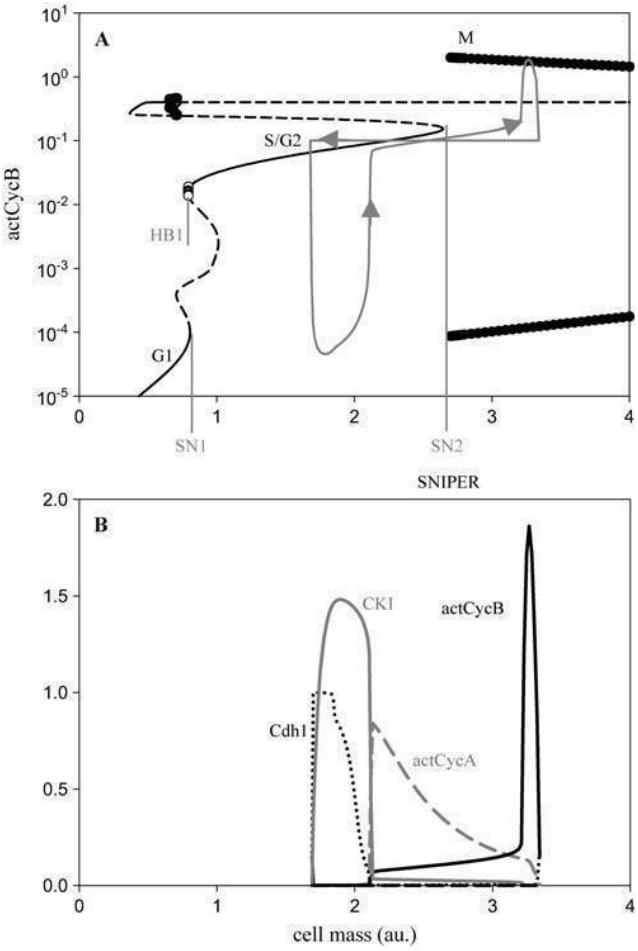

FIGURE 2 One-parameter bifurcation diagram (*A*) and cell-cycle trajectory (*B*) of wild-type fission yeast. Both figures share the same abscissa. Notice that cell mass is just the logarithm of age, because we assume that cells grow exponentially between birth (age = 0) and division (age = MDT). The gray curve in panel *A* (a ''cell-cycle trajectory'' for MDT = 120 min) is identical to the solid black curve in panel *B*. Key to panel *A*: solid line, stable steady state; dashed line, unstable steady state; solid circles, maxima and minima of stable oscillations; open circles, maxima and minima of unstable oscillations; SN1 (saddle-node bifurcation that annihilates the G1 steady state), SN2 (saddle-node bifurcation that annihilates the G2 steady state), and HB1 (Hopf bifurcation on the S/G2 branch of steady states that gives rise to endoreplication cycles). SN2 is a SNIPER bifurcation; i.e., it gives way to stable periodic solutions of infinite period (at the bifurcation point). The other (unmarked) bifurcation points in this diagram are not pertinent to cell-cycle regulation.

Overshoot of a SNIPER bifurcation point (as in Fig. 2 *A*) is a common feature of our cell cycle models, and recent experimental evidence (63) confirms this prediction in frog egg extracts. These authors located the position of the steady-state SN bifurcation in a nonoscillatory extract and then showed that during oscillations the Cdk-regulatory system overshoots the SN point by twofold or more.

The one-parameter bifurcation diagram in Fig. 2 *A* is a compact way to display the interplay between the DNA replication-segregation cycle (regulated by Cdk/CycB activity)

and the growth-division cycle (represented on the abscissa by the steady increase of cell mass and its abrupt resetting at division). The very strong ''cell size control'' in late G2 phase of the fission yeast cell cycle, which has been known to physiologists for 30 years (52), is here represented by growing past the SNIPER bifurcation, which eliminates the stable S/G2 steady state and allows the cell to pass into and out of mitosis (the stable limit cycle oscillation).

A satisfactory model of fission yeast must account not only for the phenotype of wild-type cells but also for the unusual properties of the classic *cdc* and *wee* mutants that played such important roles in deducing the cell-cycle control network. Mutations change the values of specific rate constants, which remodel the one-parameter bifurcation diagram and thereby change the way a cell progresses through the DNA replication-division cycle. For example (Fig. 3 *A*), for a *wee1*$^-$ mutant (reduce Wee1 activity to 10% of its wild-type value) SN2 moves to the left of SN1 and the infinite-period limit cycle now bifurcates from SN1. Hence, the cell cycle in *wee1*$^-$ cells is now organized by a SNIPER bifurcation at the G1/S transition: *wee1*$^-$ cells are about half the size of wild-type cells, they have a long G1 phase and short G2, and slowly growing cells pause in G1 (unreplicated DNA) rather than in G2 (replicated DNA).

In the Supplementary Material (Fig. S2) we present bifurcation diagrams for four other fission yeast mutants (*cig2*Δ, *cig2*Δ *rum1*Δ, *wee1*Δ *cdc25*Δ, *wee1*Δ *rum1*Δ), to confirm that our ''generic'' version is indeed consistent with the known physiology of these mutants. Because they have been described in detail elsewhere (37), we turn our attention instead to some novel results.

Endoreplicating mutants

On the wild-type bifurcation diagram (Fig. 2 *A*) we can notice a very small oscillatory regime at the beginning of the S/G2 branch of steady states (labeled as HB1, at cell mass = 0.79). This stable periodic solution is a consequence of a negative feedback loop whereby Cig2 inhibits its own transcription factor, Cdc10, by phosphorylation (64). (In the generic

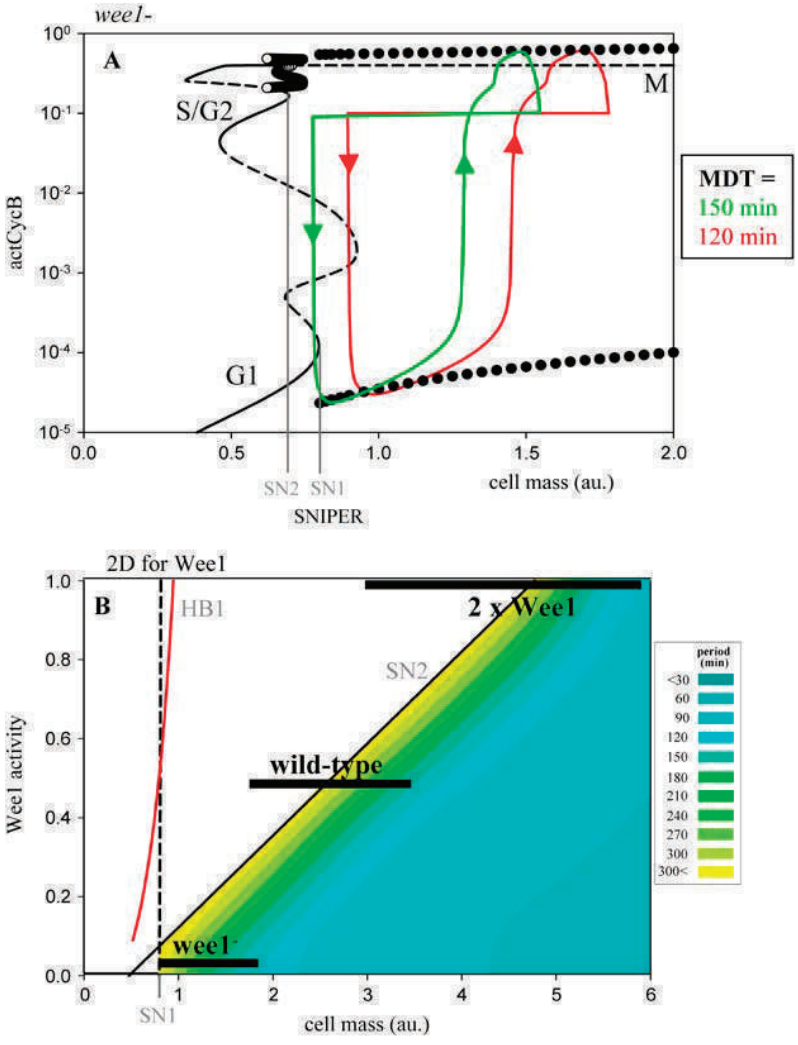

FIGURE 3 One-parameter (*A*) and two-parameter (*B*) bifurcation diagrams for mutations at the *wee1* locus in fission yeast. Panel *A* should be interpreted as in Fig. 2. Key to panel *B*: dashed black line, locus of SN1 bifurcation points; solid black line, locus of SN2 bifurcation points; red line, locus of HB1 bifurcation points; black bars, projections of the cell-cycle trajectories in Figs. 2 *A* and 3 *A* onto the two-parameter plane. Within regions of stable limit cycles, the color code denotes the period of oscillations. Notice that the period becomes very long as the limit cycles approach the locus of SNIPER bifurcations. The limit cycles switch their allegiance from SN2 to SN1 at Wee1 activity ~0.07 (by a complex sequence of codimension-two bifurcations that are not indicated here). Notice that *wee1*$^+$ overexpression leads to large cells, size-controlled at the G2-to-M transition, but *wee1* deletion leads to small cells (half the size of wild-type), size-controlled at the G1-to-S transition.

nomenclature, Cig2 is ''CycA'' and Cdc10 is ''TFE''.) The negative feedback loop can generate oscillations if there is positive feedback in the system as well, which is provided by the Cdk inhibitor (CKI). As CycA slowly accumulates, it is at first sequestered in inactive complexes with CKI, but eventually CycA saturates CKI and active (uninhibited) Cdk/CycA appears. ActCycA phosphorylates CKI, which labels CKI for proteolysis (65). As CKI is degraded, actCycA rises even faster because it is released from the inactive complexes. At this point the negative feedback turns on and CycA synthesis is blocked. With no synthesis but continued degradation, CycA level drops, which allows CKI to come back (provided there is no other Cdk activity that can phosphorylate CKI and keep its level low). CKI comeback returns the control system to G1. In wild-type cells, the CycA-TFE-CKI interactions cannot create stable oscillations because CycB takes over from CycA and keeps CKI low in G2 and M phases. But if CycB is absent (as in *cdc13*Δ mutants of fission yeast), then CKI and CycA generate multiple rounds of DNA replication without intervening mitoses (called ''endoreplication''), precisely the phenotype of *cdc13*Δ mutants (66).

In Fig. 4 *A* we show the bifurcation diagram of *cdc13*Δ cells. Over a broad range of cell mass, large amplitude stable oscillations of Cdk/CycA (from a SNIPER bifurcation at SN1) drive multiple rounds of DNA synthesis without intervening mitoses. Because this negative feedback loop also exists in metazoans, it may explain the core mechanism of developmental endoreplication (67).

Mutant analysis on the genetics-physiology plane

In our view, genetic mutations are connected to cell phenotypes through bifurcation diagrams. Mutations induce changes in parameter values, which may change the nature of the bifurcations experienced by the control system, which will have observable consequences in the cell's physiology. Mutation-induced changes in parameter values may be large or small: e.g., the rate constant for CycB synthesis = 0 in a *cdc13*Δ cell, but a *wee1*^{ts} (''temperature sensitive'') mutant

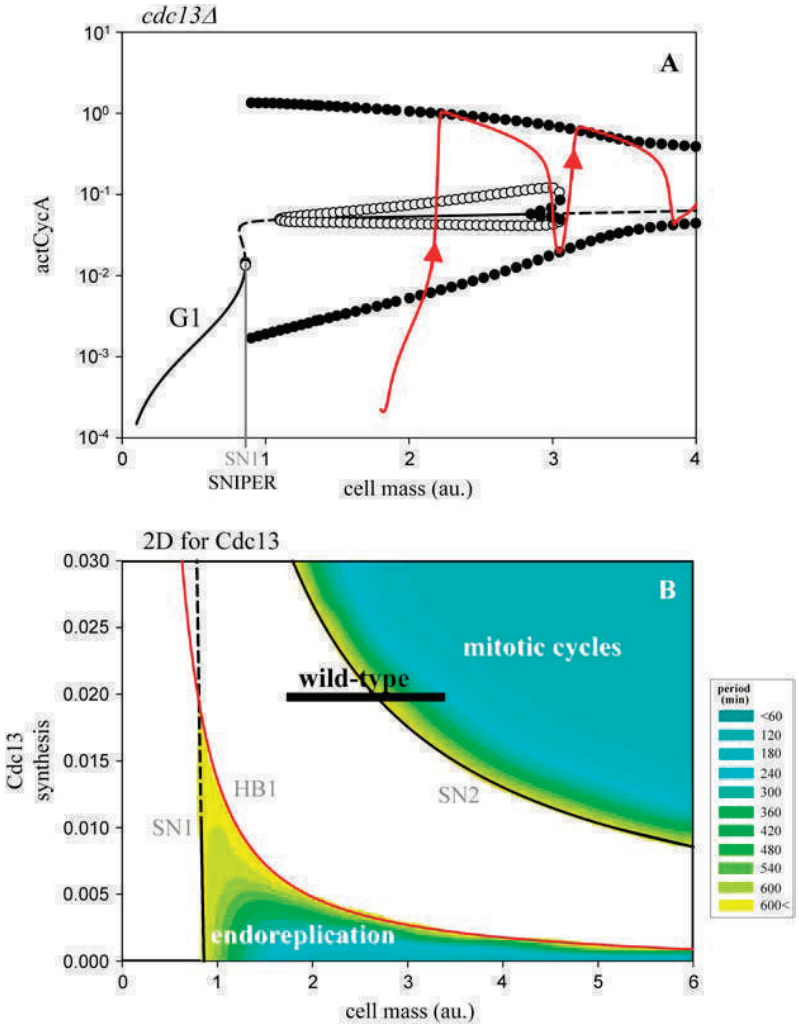

FIGURE 4 One-parameter (*A*) and two-parameter (*B*) bifurcation diagrams for mutations at the *cdc13* locus in fission yeast. Panels *A* and *B* should be interpreted as in Fig. 3. *cdc13*$^{+}$ overexpression has little effect on cell-cycle phenotype, but *cdc13* deletion prevents mitosis and permits endoreplication.

may cause only a minor change in the catalytic activity of Wee1 kinase. Whether these changed parameter values cause a qualitative change in bifurcation points on the one-parameter diagram (Figs. 2 *A* and 3 *A*), or merely a quantitative shift of their locations, depends on whether the parameter change crosses a bifurcation point or not. In principle, we can imagine a sequence of bifurcation diagrams (and associated phenotypes) connecting the wild-type cell to a mutant cell as the relevant kinetic parameter changes continuously (up or down) from its wild-type value. This theoretical sequence of morphing phenotypes can be captured on a two-parameter bifurcation diagram, where cell mass continues to stand in for the physiology of the cell cycle (growth and division) and the second parameter is a rate constant that varies continuously between 0 (the deletion mutant) and some large value (the overexpression mutant). Plotted this way, the two-parameter bifurcation diagram spans the entire range of molecular biology from genetics to cell physiology! (For more details on two-parameter bifurcation diagrams, see the Appendix.)

To illustrate this idea, we first consider *wee1* mutations. On the two-parameter bifurcation diagram in Fig. 3 *B* we follow the loci of bifurcation points (SN1, SN2, and HB1) from their position in wild-type cells (''Wee1 activity'' = 0.5) in the direction of overexpression (>0.5) or deleterious mutation (<0.5). The one-parameter bifurcation diagrams of wild-type (Fig. 2 *A*) and *wee1*$^-$ (Fig. 3 *A*) cells are cuts of this plane at the marked levels of Wee1 activity. For overexpression mutations, the SNIPER bifurcation moves toward larger cell mass, and the heavy bar shows where the simulation of 2 × *wee1*$^+$ cells projects onto the genetics-physiology plane. Clearly, the size of *wee1*^{op} cells increases in direct proportion to gene dosage (68). As Wee1 activity decreases below 0.5, e.g., in a heterozygote diploid cell (activity = 0.25) or in *wee1*^{ts} mutants, the SNIPER bifurcation moves toward smaller cell mass. Eventually, the SN1 and SN2 loci cross, and the infinite-period oscillations switch from SN2 to SN1 by a short but complicated sequence of codimension-two bifurcations (not shown on the diagram). Because SN1 is not dependent on Wee1 activity, the critical cell size at the SNIPER bifurcation drops no further as Wee1 activity decreases.

The two-parameter bifurcation diagram for cyclin B (Cdc13) expression (Fig. 4 *B*) shows how mitotic cycles are related to endoreplication cycles. As Cdc13 synthesis rate decreases from its wild-type value (0.02 min^{-1}), there is a dramatic increase of the critical cell mass for mitotic oscillations (the SNIPER bifurcation associated with SN2). In addition, endoreplication cycles appear at the intersection of HB1 and SN1 (by a sequence of codimension-two bifurcations, which we are not focusing on here). At first appearance, the endoreplication cycles have a very long period, but as Cdc13 synthesis rate decreases further, the period of endoreplication cycles decreases and the range of these oscillations increases.

The two-parameter bifurcation diagrams in Figs. 3 and 4 are incomplete: they do not show all loci of codimension-one bifurcations or any of the characteristic codimension-two bifurcations. Examples of more complete two-parameter bifurcation diagrams can be found in the Supplementary Material (Fig. S3) and on our web site (69).

Budding yeast: *Saccharomyces cerevisiae*

Our generic model of the budding yeast cell cycle is based on a detailed model published recently by Chen et al. (15). The generic model bypasses details of the mitotic exit network (MEN) in Chen's model, assuming instead that Cdc20 directly activates Cdc14. We had to change some parameters compared to Chen et al. (15) because of this and other minor changes in the network. We found these new parameter values by fitting simulations of wild-type and some mutant cells (15).

Wild-type cells

One-dimensional bifurcation diagrams of wild-type cells created by the full model (15) and by our generic model (Fig. 5, *A* and *B*) look very similar. Both figures show a stable G1 steady state that disappears at a SNIPER bifurcation (G1-S transition at cell mass = 1.13 au), giving rise to oscillations that correspond to progression through S/G2/M phases. There is no attractor representing a stable G2 phase in wild-type budding yeast cells. The green, red, and blue curves superimposed on the bifurcation diagram are ''cell cycle trajectories'' at mass doubling time of 150, 120, and 90 min, respectively (MDT = ln2/μ, where μ = specific growth rate). Notice that cells get larger as MDT gets smaller (as μ increases). For simplicity, we are neglecting the asymmetry of division of budding yeast in these simulations.

Two ways to achieve size homeostasis

Fig. 5 *A* shows that the relation of the cell cycle trajectory to the SNIPER bifurcation point depends strongly on MDT. At slow growth rates (MDT ≥ 150 min), newborn cells are smaller than the size at the SNIPER bifurcation; hence the Cdk-control system is attracted to the stable G1 steady state (seen more clearly in Fig. 5 *B* than in Fig. 5 *A*), and the cell is waiting until it grows large enough to surpass the SNIPER bifurcation. Only then can the cell commit to the S/G2/M sequence. This is a mathematical representation of the classic notion of ''size control'' to achieve balanced cell growth and division (49,50,52,70). At faster growth rates, however, newborn cells are already larger than the critical size at the SNIPER bifurcation, and they do not linger in a stable G1 state, waiting to grow large enough to start the next chromosome replication cycle. How then is cell-size homeostasis achieved, if the classic ''sizer'' mechanism is inoperative?

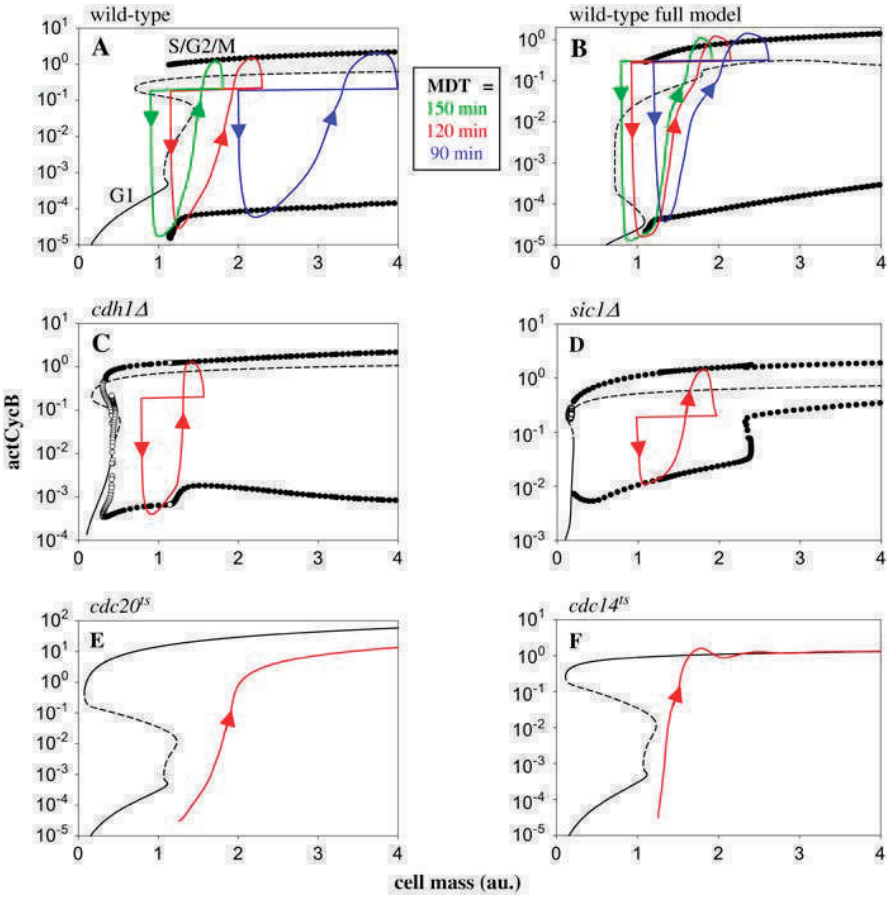

FIGURE 5 One-parameter bifurcation diagrams of budding yeast cells. (*A*) Wild-type (this article), (*B*) wild-type (Chen's 2004 model (15)), (*C*) *cdh1*Δ ($k_{ah1p} = k_{ah1pp} = 0$), (*D*) *cki*Δ ($k_{sip} = k_{sipp} = 0$), (*E*) *cdc20*Δ ($k_{s20p} = k_{s20pp} = 0$), (*F*) *cdc14*Δ ($[Cdc14]_{total} = 0$). See Fig. 2 for key to diagrams. (*A*, *B*, and *D*) The large-amplitude, stable limit cycles arise from SNIPER bifurcations; (*C*) they arise from a subcritical Hopf bifurcation followed by a cyclic fold bifurcation. Simulations are consistent with observed phenotypes: *cdh1*Δ and *cki*Δ are viable; *cdc20*Δ and *cdc14*Δ are inviable (blocked in late mitosis), with much higher activity of cyclin B-dependent kinase in *cdc20*Δ than in *cdc14*Δ.

Fig. 6 shows the relationship between limit cycle period and distance from the SNIPER bifurcation. For mass <1.13, there is no limit cycle; the stable attractor is the G1 steady state. For mass slightly >1.13, the limit cycle period is very long, approaching infinity as mass approaches 1.13 from above. Depending on MDT, the cell cycle trajectory finds a location on the cell-mass axis such that the average cell-cycle-progression time (time spent in G1/S/G2/M) is equal to the mass doubling time. For MDT = 90 min (*bottom curve* in Fig. 6), the cell is born at mass = 2 and divides at mass = 4, spending its entire lifespan in the oscillatory region, with an average cell-cycle-progression time of 90 min. As MDT lengthens to 120 min (*second curve from bottom*), the cell cycle trajectory shifts to smaller size, so that the average cell-cycle-progression time can lengthen to 120 min. Still slower growth rates (MDT $\geq$ 150 min) drive the newborn cell into the ''sizer'' domain, where the Cdk-control system can wait indefinitely at the stable G1 state until the cell grows large enough to surpass the SNIPER bifurcation. Notice that cell-size homeostasis is possible in the ''oscillator'' domain because of the inverse relationship between oscillator period and cell mass close to a SNIPER bifurcation.

Cell cycles that visit the ''sizer'' domain (*top two curves* in Fig. 6) show ''strong'' size control, i.e., interdivision time is strongly negatively correlated to birth size, and cell size at the size-controlled transition point (G1 to S in Fig. 6) shows little or no dependence on birth size (1,2). Cell cycles that live wholly in the ''oscillator'' domain (*bottom two curves* in Fig. 6) show ''weak'' size control, i.e., interdivision time is weakly negatively correlated to birth size and there is no clear ''critical size'' for any cell cycle transition. Nonetheless, such cycles still show balanced growth (interdivision time = mass doubling time) because the cell cycle trajectory settles on a size interval for which the average oscillatory period is identical to the cell's mass doubling time. Balanced growth and division is a consequence of the steep decline in limit cycle period with increasing cell size past the SNIPER bifurcation.

As Fig. 6 demonstrates, for cells in the ''oscillator'' domain, our model predicts a positive correlation between growth rate and average cell size (faster growing cells are bigger). This correlation is a characteristic and advantageous feature of yeast cells: rich media favor cell growth, poor media favor cell division (50,71). Although it is satisfying to see our model explain this correlation in an ''unforced'' way, we note that our interpretation of the dependence of cell size on growth rate is predicated on the assumption that one can vary mass doubling time without changing any rate constants in the Cdk-control system (i.e., without changing the location

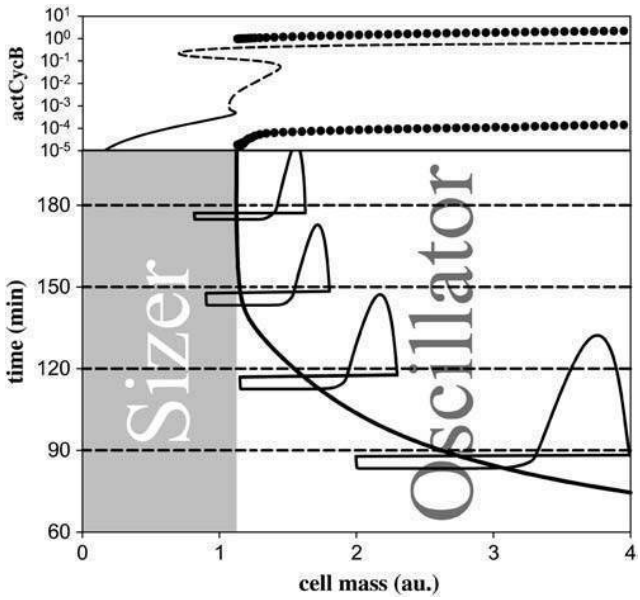

FIGURE 6 Achieving balanced growth at different growth rates. (*Upper panel*) Bifurcation diagram of the budding yeast network (same as Fig. 5 *A*). (*Lower panel*) Period of the oscillatory solutions. Cell cycle trajectories at different MDT (*solid curves*) are displayed at the corresponding period (*dashed lines*). Background shading shows the ''sizer'' and ''oscillator'' regimes of cell cycle regulation. Slowly growing cells spend part of their cell cycle in a stable G1-arrested state, until they grow large enough to surpass the SNIPER bifurcation and enter S/G2/M; these cells exhibit ''strong'' size control. Rapidly growing cells are large enough to stay always in the oscillatory regime, maintaining balanced growth and division by finding an average cell-cycle time = MDT. These cells display ''weak'' size control.

of the bifurcation points in Fig. 6). Unfortunately, this assumption is probably incorrect because changes in growth medium (sugar source, nitrogen source, etc.) likely induce changes in gene expression that move the SNIPER bifurcation points, with poorer growth medium favoring smaller size for completion of the cell cycle (see, e.g., (49,50)). We have yet to sort out all the complications of size regulation in yeast cells. In the meantime, Fig. 6 provides a useful paradigm for understanding ''strong'' and ''weak'' size control in eukaryotes.

Mutants of G1 phase regulation

In this section we present bifurcation diagrams for a few of the most important and interesting mutants described in great detail by numerical simulations in Chen et al. (15). We start with mutants missing the components that stabilize the G1 phase of the cell cycle: either Cdh1 (an activator of CycB degradation) (Fig. 5 *C*) or Sic1 (a cyclin B-dependent kinase inhibitor) (Fig. 5 *D*). In both cases the mutant cells are viable and apparently have a short G1 phase (72–74). On the bifurcation diagrams, however, a stable G1 steady state exists only at very small cell size. In both mutants, the cell cycle trajectory is operating in the ''oscillator'' domain of the size-homeostasis diagram, and consequently these mutant cells are expected to exhibit ''weak'' size control. In these cases, the G1 phase of the cell cycle is a transient state, as described above, and the START transition (G1-to-S) is governed by an oscillator not a sizer. Furthermore, if these mutant cells are grown from spores (i.e., very small size initially), they will execute START at a much smaller size than they do under normal proliferating conditions.

Two-parameter bifurcation diagrams (genetic-physiology planes) for both *SIC1* and *CDH1* are presented in the Supplementary Material (Fig. S3). The two types of mutations have quite a similar effect on cell physiology.

Mutants of mitotic exit regulation

Although both $cdc20^{ts}$ and $cdc14^{ts}$ mutants block mitotic exit, $cdc20^{ts}$ arrests at the metaphase-anaphase transition (75), whereas $cdc14^{ts}$ arrests in telophase (76,77). Hence, exit from mitosis must be a two-stage process (30), with two different stable-steady states in which the control system can halt. The one-parameter bifurcation diagrams (Fig. 5, *E* and *F*) reveal these two stable steady states. For $cdc20^{ts}$ the steady state has very large CycB activity (~60 au), whereas the $cdc14^{ts}$ mutant arrests in a state of much lower CycB activity (~2 au). Also, in the second case a damped oscillation is seen on the simulation curve. These effects all derive from the fact that if Cdc20 is inoperable, then cyclin degradation is totally inhibited, whereas if Cdc14 is not working, then Cdc20 can destroy some CycB—not enough for mitotic exit, but enough to create a stable steady state of lower CycB activity (30). The corresponding two-parameter bifurcation diagrams of $cdc20^{ts}$ and $cdc14^{ts}$ mutants (Supplementary Material, Fig. S3, *C* and *D*) are also qualitatively similar.

Lethality that depends on growth rate

To bind effectively to Cdc20, proteins of the core APC need to be phosphorylated (78). If these phosphorylation sites are mutated to nonphosphorylable alanine residues (the mutant is called *APC-A*), then Cdc20-mediated degradation of CycB is compromised, although the *APC-A* cells are still viable. We assume that APC-A has a constant activity that is 10% of the maximum activity of the normally phosphorylated form of APC in conjunction with Cdc20. Furthermore, we assume that APC-A has full activity in conjunction with Cdh1, in accord with the evidence (78). In simulations (Fig. 7 *A*), *APC-A* cells are viable and large. Because these mutant cells are delayed in exit from mitosis, the period of the limit cycle oscillations beyond the SNIPER bifurcation is considerably longer than in wild-type cells. Hence, they cycle in the ''oscillator'' regime even at MDT $>$ 150 min.

Double mutant cells, *APC-A* $cdh1\Delta$, are lethal at fast growth rates but partially viable at slow growth rates (30). Our bifurcation diagram (Fig. 7 *B*) shows a truncated oscillatory regime ending at a cyclic fold bifurcation at cell

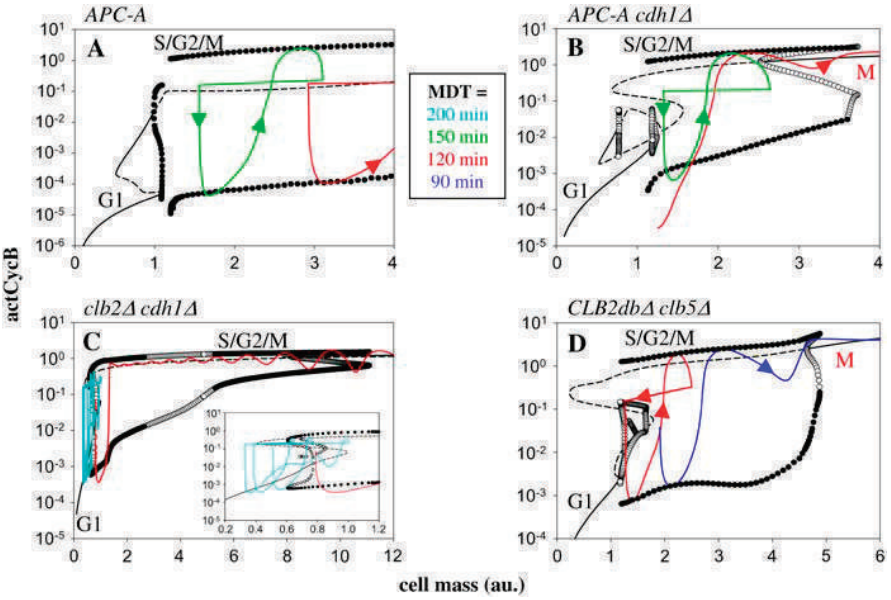

FIGURE 7 One-parameter bifurcation diagrams of budding yeast mutants defective in cyclin degradation. (*A*) *APC-A* ([APCP] = 0.1 au, constant value), (*B*) *APC-A cdh1*Δ ([APCP] = 0.1 au, $k_{ah1p} = k_{ah1pp} = 0$), (*C*) *clb2*Δ *cdh1*Δ ($k_{sbp} = 0.0015$ min^{-1}, $k_{sbpp} = 0.015$ min^{-1}, $k_{ah1p} = k_{ah1pp} = 0$), (*D*) *CLB2db*Δ *clb5*Δ ($k_{dbpp} = 0.03$ min^{-1}, $k_{dbppp} = k_{sap} = k_{sapp} = 0$). Notation as in Fig 2. (*A*, *B*, and *D*) The large-amplitude, stable limit cycles arise from SNIPER bifurcations; (*C*) they arise from a subcritical Hopf bifurcation followed by a cyclic fold bifurcation (*inset*). All these mutations compromise one or more of the negative feedback signals that promote exit from mitosis. The latter three show growth rate dependence of viability: slowly growing cells are viable, but rapidly growing cells become stuck in M phase.

mass = 3.6. Simulations show that at MDT = 150 min cells stay within the small oscillatory regime, but faster growing cells (MDT = 120 min) grow out of the oscillatory regime and get stuck in mitosis. Mutations of APC core proteins also show growth rate-dependent viability, e.g., *apc10-22* is viable in galactose (slow growth rate) but inviable in glucose (fast growth rate) (79).

The same dependence of viability on growth conditions was reported for *CLB2db*Δ *clb5*Δ mutant cells (CycB stablized, CycA absent) (30,80), and is illustrated in our bifurcation diagram (Fig. 7 *D*). In addition to these mutants, which are defective in cyclin degradation, Cross (30) found that the double mutant *clb2*Δ *cdh1*Δ also shows growth rate-dependent viability. In our model these cells are viable at MDT = 200 min, but lethal at MDT = 120 min (Fig. 7 *C*).

All of these mutations interfere with the negative feedback loop of CycB degradation. Weak negative feedback creates long-period oscillations that are stable attractors only at relatively small cell mass; at large mass the activity of CycB-dependent kinase is so strong that the mutant cells arrest in mitosis. Fast growing cells cannot find a period of oscillation that balances their MDT, so they overgrow the oscillatory region and get stuck in mitosis. These results suggest that other mutants affecting the negative feedback loop should be reinvestigated to see if viability depends on growth rate (for example, *APC-A sic1*Δ and *cdc20*^{ts} *pds1*Δ).

Cells that show this sensitivity to growth rate are also likely to be sensitive to random noise in the control system. Using a model similar to ours, Battogtokh and Tyson (34) showed that, for control systems operating close to a bifurcation to the stable M-like steady state, cells might get stuck in mitosis after a few cycles if a little noise is added to the system. This effect would show up as partial viability of a clone at intermediate growth rates.

Incorporation of the morphogenetic checkpoint

In modeling the budding yeast cell cycle so far, we have assumed that the G2 module of Cdk phosphorylation (module 5 in Fig. 1) plays no role during normal cell proliferation (81), but recently this view was challenged by Kellogg (82). In any event, all agree that the G2 module is necessary for the ''morphogenesis checkpoint'' in budding yeast, which arrests a cell in G2 if the cell is unable to produce a bud (81). It is a simple job to ''turn on'' module 5 in our generic version of the budding yeast cell cycle and to reproduce most of the results in Ciliberto et al. (83); see Supplementary Material, Fig. S4.

Mammalian cells

Many groups have modeled various aspects of the molecular machinery controlling mammalian cell cycles (22,26,84,85), including us (41). In this article, we insert parameter values from Novak and Tyson (41) into our generic model to simulate a ''generic mammalian cell'' (Fig. 8). As expected the bifurcation diagram of the mammalian cell (Fig. 8 *B*) is very similar to the budding yeast cell (there is no G2 module in either model). This yeast-like proliferation is observed in mammalian cells in early development and in malignant transformation, when the cell's main goal is rapid reproduction.

It has been recently discovered that mouse embryos deleted of all forms of CycD (86), deleted of both forms of CycE (87), or deleted of both Cdk4 and Cdk6 (88) can develop until late stages of embryogenesis and die from causes unrelated to the core cell cycle machinery. Mice lacking Cdk2 are viable (89), and mouse embryo fibroblast from any of these mutants proliferate normally. Our model is expected to reproduce these results. Indeed, simulation of CycE-deleted

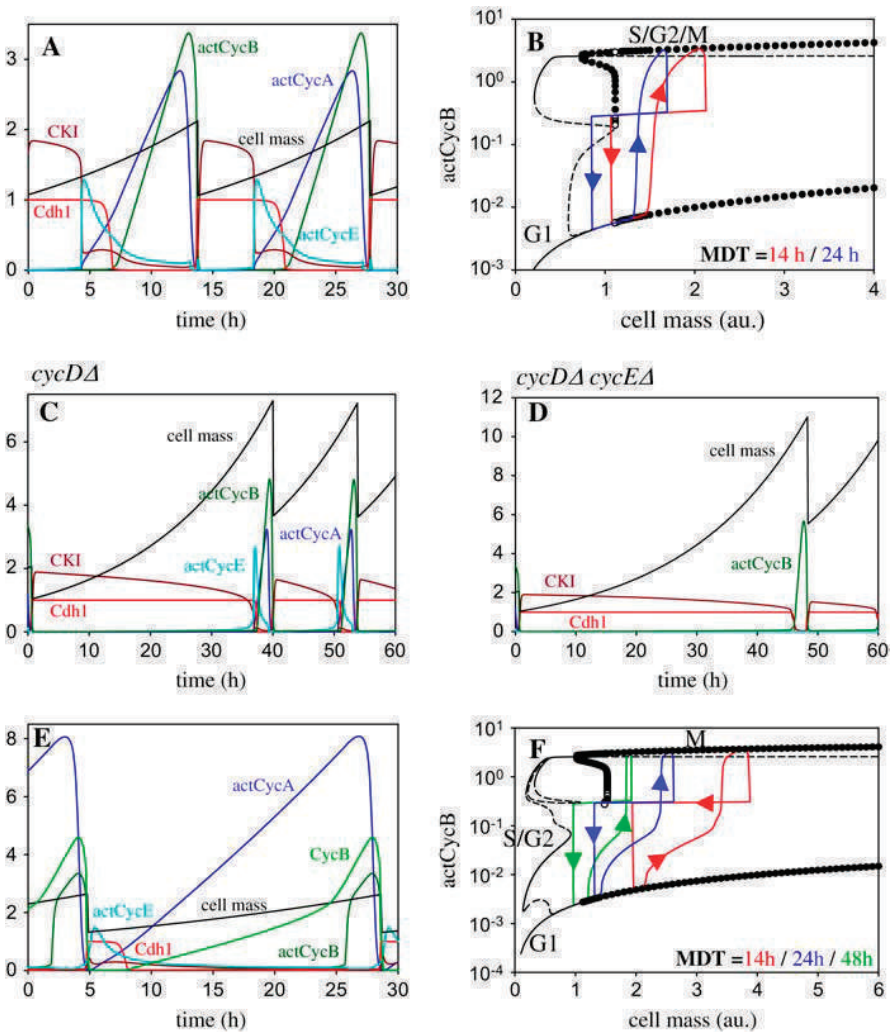

FIGURE 8 Analysis of a mammalian cell cycle model. Numerical simulations: (*A*) normal cell (without G2 module), (*C*) *cycD*Δ ($CycD^0 = 0$), (*D*) *cycD*Δ *cycE*Δ ($CycD^0 = 0$, $k_{sep} = k_{sepp} = 0$), (*E*) normal cell (with G2 module). One-parameter bifurcation diagrams for normal cell cycles without (*B*) and with (*F*) the G2 module.

cells show almost no defect in proliferation with a cell division mass 1.2 times wild-type cells (Supplementary Material, Fig. S5 *C*). The absence of CycD has a greater effect on the system, creating cycles with a division mass 3.6 times wild-type (Fig. 8 *C*). If we eliminate both CycD and CycE, we find that cells leave G1 phase at a mass equal to 5 times wild-type division mass (Fig. 8 *D*), which might be lethal for cells. These results are related to the corresponding experiments in budding yeast, where $cln3^-$ (CycD) and $cln1^-$ $cln2^-$ (CycE) mutants are viable but larger than wild-type (90), whereas the combined mutation is lethal (91).

From Chow et al. (92) we know that, although phosphorylation of Cdk2 (in complexes with CycE or CycA) plays no major role in unperturbed proliferation of HeLa cells, phosphorylation of Cdk1/CycB by Wee1 plays a role in normal cell cycling. These reactions (module 5 in Fig. 1) are easily added to the model, as we did in the previous section on budding yeast. For the parameter values chosen, the bifurcation diagram (Fig. 8 *F*) exhibits stable G1 and G2 steady states. The cell cycle trajectories in Fig. 8, *E* and *F*, are computed for cells proliferating at MDT = 24 h, that operate in the ''oscillator'' region of the size homeostasis curve (Fig. 6). More slowly proliferating cells (MDT = 48 h) pause in the stable G1 state until they grow large enough to surpass the SNIPER bifurcation at cell mass ~1. At all growth rates, there is a transient G2 state on the trajectory (the flattened regions of the red and blue curves at [actCycB] ~ 0.01–0.1).

With the G2-regulatory module in place, our model is now set up for serious consideration of the major checkpoint controls in mammalian cells: 1), restriction point control, by which cyclin D and retinoblastoma protein regulate the activity of transcription factor E; 2), the DNA-damage checkpoint in G1, which upregulates the production of CKI; 3), the unreplicated-DNA checkpoint in G2, which activates Wee1 and inhibits Cdc25; and 4), the chromosome misalignment checkpoint in M phase, which silences Cdc20. Building appropriate modules for these checkpoints and wiring them into the generic cell cycle engine will be topics for future publications and will provide a basis for modeling the hallmarks of cancer (93).

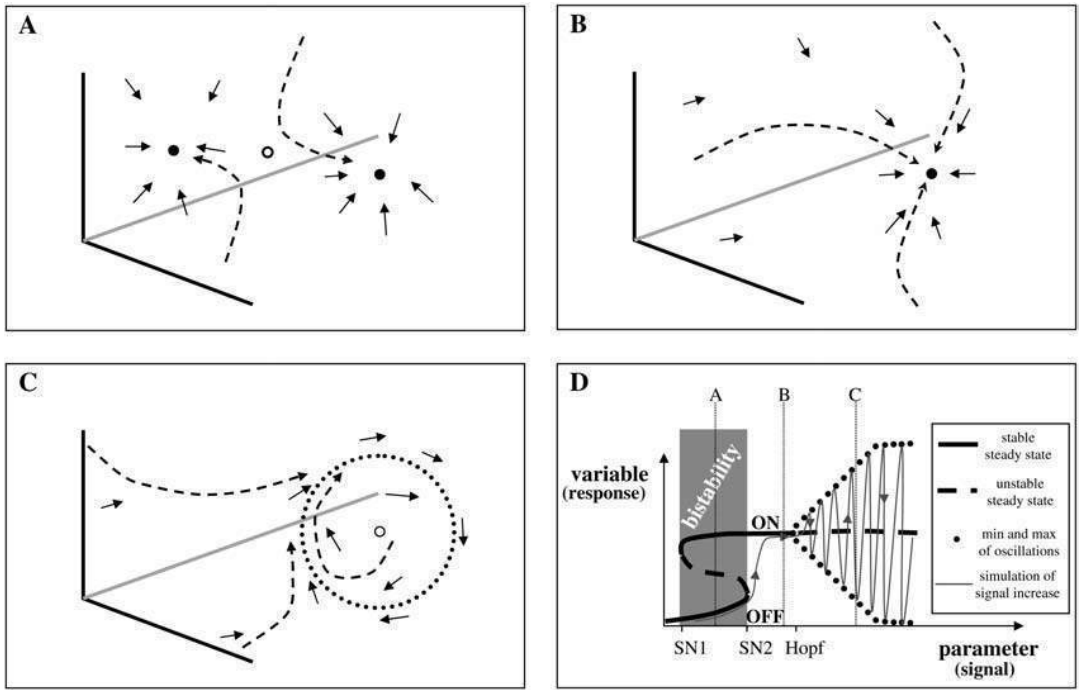

FIGURE 9 Attractors and their bifurcations. (*A–C*) Examples of vector fields in a three-dimensional state space. Solid arrows, vector field; dashed arrows, simulation results; solid circles, stable steady state; open circles, unstable steady state; dotted circle, stable limit cycle. (*D*) The transitions (bifurcations) between the vector fields of panels *A–C* are represented on a one-parameter bifurcation diagram. Solid line, locus of stable steady states; dashed line, locus of unstable steady states, black dots, maximum and minimum values of response variable on a periodic orbit; SN = saddle-node, HB = Hopf bifurcation. The light gray curve indicates a simulation of the response of the control system for a slow increase in signal strength. At SN2, the system jumps from the OFF state to the ON state, and at HB it leaves the steady state and begins to oscillate with increasing amplitude. Within the region of bistability, the control system can persist in either the OFF state or the ON state, depending on how it was prepared (a phenomenon called ''hysteresis'').

DISCUSSION

We propose a protein interaction network for eukaryotic cell cycle regulation that 1), includes most of the important regulatory proteins found in all eukaryotes, and 2), can be parameterized to yield accurate models of a variety of specific organisms (budding yeast, fission yeast, frog eggs, and mammalian cells). The model is built in modular fashion: there are four synthesis-and-degradation modules (''4, 8, 10, 13''), three stoichiometric binding-and-inhibition modules (''6, 9, 12''), three transcription factor modules (''3, 7, 11''), and three modules with multiple activation-and-inhibition steps (''1, 2, 5''). This modularity assists us to craft models for specific organisms (where some modules are more important than others) and to extend models with new modules embodying the signaling pathways that impinge on the underlying cell cycle engine.

To describe the differences in regulatory networks in yeasts, frog eggs, and mammalian cells, we subdivided the generic wiring diagram (Fig. 1) into 13 small modules. From a different point of view (36,37) we might lump some of these modules into larger blocks: bistable switches and negative feedback oscillators. One bistable switch creates a stable G1 state and controls the transition from G1 to S phase. It is a redundant switch, created by interactions between B-type cyclins and their G1 antagonists: CKIs (stoichiometric inhibitors) and APC/Cdh1 (proteolytic machinery). Either CKI or Cdh1 can be knocked out genetically, and the switch may still be functional to some extent. A second bistable switch creates a stable G2 state and controls the transitions from G2 to M phase. It is also a redundant switch, created by double-negative feedback between Cdk/CycB and Wee1 and positive feedback between Cdk/CycB and Cdc25. A negative feedback loop, set up by the interactions among Cdk/CycB, APC/Cdc20, and Cdc14 phosphatase, controls exit from mitosis. A second negative feedback loop, between CycA and its transcription factor, plays a crucial role in endoreplication. These regulatory loops are responsible for the characteristic bifurcations that (as our analysis shows) control cell cycle progression in normal cells and misprogression in mutant cells.

The many different control loops in the ''generic'' model can be mixed and matched to create explicit models of specific organisms and mutants. In this sense, there is no ''ideal'' or ''simplest'' model of the cell cycle. Each organism has its own idiosyncratic properties of cell growth and division, depending on which modules are in operation, which depends ultimately on the genetic makeup of the organism. Lethal mutations push the organism into a region of parameter space where the control system is no longer viable.

To deepen our understanding of the similarities and differences in cell cycle regulation in different types of cells, we analyzed our models of specific organisms and mutants with bifurcation diagrams. To show how cell growth drives transitions between cell cycle phases (G1/S/G2/M), we employ one-parameter bifurcations diagrams, where stable steady states correspond to available arrest states of the cell cycle (late G1, late G2, metaphase) and saddle-node and SNIPER bifurcation points identify critical cell sizes for leaving an arrest state and proceeding to the next phase of the cell cycle. In this view, cell cycle ''checkpoints'' (also called ''surveillance'' mechanisms) (4,5) respond to potential problems in cell cycle progression (DNA damage, delayed replication, spindle defects) by stabilizing an arrest state, i.e., by putting off the bifurcation to much larger size than normal (18,37,40,84,94).

The most important type of bifurcation, we believe, is a ''SNIPER'' bifurcation, by which a stable steady state (G1 or G2) gives rise to a limit cycle solution that drives the cell into mitosis and then back to G1 phase. At the SNIPER bifurcation, the period of the limit cycle oscillations is initially infinite but drops rapidly as the cell grows larger. SNIPER bifurcations are robust properties of nonlinear control systems with both positive and negative feedback. Not only are they commonly observed in one-parameter bifurcation diagrams of the Cdk network, but they persist over large ranges of parameter variations, as is evident from our two-parameter bifurcation diagrams. For example, in Figs. 3 *B* and 4 *B*, SNIPER bifurcations are observed over the entire range of gene expression for *wee1* and *cdc13* in fission yeast. The same is true for *SIC1* gene expression in budding yeast (Supplementary Material, Fig. S3 *B*), but not so for *CDC20* and *CDC14* genes (Fig. S3, *C* and *D*). In the latter cases, the SNIPER bifurcation is lost for low levels of expression of these essential (''cdc'') genes, and the mutant cells become arrested in late mitotic stages, as observed. Although SNIPER bifurcations are often associated with robust cell cycling in our models, they are not necessary for balanced growth and division, as is evident in our simulation of *cdh1*Δ mutants of budding yeast (Fig. 5 *C* and Supplementary Material, Fig. S3 *A*), where the stable oscillations can be traced back to a subcritical Hopf bifurcation.

The SNIPER bifurcation is very effective in achieving a balance between progression through the cell cycle (interdivision time (IDT)) and overall cell growth (mass doubling time (MDT)). Cell size homeostasis means that IDT = MDT. In Fig. 6 we show that cell size homeostasis is a natural consequence of the eukaryotic cell cycle regulatory system, and that it can be achieved in two dramatically different ways: by a ''sizer'' mechanism (characteristic of slowly growing cells) and an ''oscillator'' mechanism (employed by rapidly growing cells). In the sizer mechanism, slowly growing cells are ''captured'' by a stable steady state, either a G1-like steady state (as in budding yeast) or a G2-like steady state (as in fission yeast).

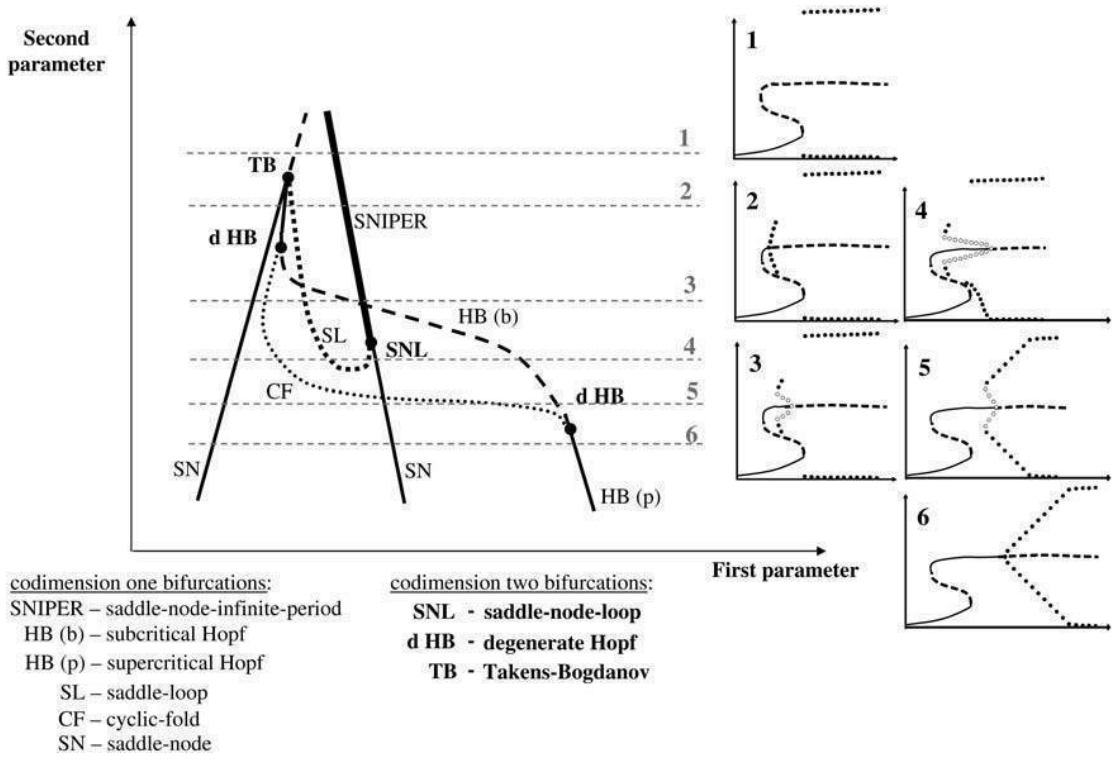

FIGURE 10 An illustrative (hypothetical) two-parameter bifurcation diagram with one-parameter cuts (1–6). See Table 2 for the nomenclature of codimension-one and codimension -two bifurcation points.

To progress further in the cell cycle, these sizer-controlled cells must grow large enough to surpass the critical size at the SNIPER bifurcation. In the oscillator mechanism, rapidly growing cells persist in the limit cycle regime (with cell mass always greater than the critical size at the SNIPER bifurcation), finding a specific combination of average size and average limit-cycle period such that IDT = MDT. In the oscillator regime, cells are unable to arrest in G1 or G2 phase because they are too large. To arrest, they must undergo one or more divisions, without intervening mass doubling, so that they become small enough to be caught by a stable steady state, or the SNIPER bifurcation point must be shifted to a larger size (by a surveillance mechanism), to arrest the cells in G1 or G2.

One-parameter bifurcations diagrams succinctly capture the dependence of the cell cycle engine (Cdk/CycB activity) on cell growth and division (cell mass changes). By superimposing cell cycle trajectories on the one-parameter bifurcation diagram, we have shown how SNIPER bifurcations orchestrate the balance between cell growth and progression through the chromosome replication cycle. In a two-parameter bifurcation diagram, we suppress the display of Cdk/CycB activity (i.e., the state of the engine) and use the second dimension to display a genetic characteristic of the control system (i.e., the level of expression of a gene, from zero, to normal, to overexpression). On the two-parameter diagram we see how the orchestrating SNIPER bifurcations change in response to mutations, and consequently how the phenotype of the organism (viability/inviability and cell size) depends on its genotype. The two-parameter bifurcation diagram can be used not only to obtain an overview of known phenotypes but also to predict potentially unusual phenotypes of cells with intermediate levels of gene expression.

Our model is freely available to interested users in three forms. From the web site (69) one can download .ode and .set files for use with the free software XPP-AUT. From an .ode file one can easily generate FORTRAN or C++ subroutines, or port the model to Matlab or Mathematica. Secondly, one can download an SBML version of the model from the same web site for use with any software that reads this standard format. Thirdly, we have introduced the model and all the mutant scenarios discussed in this article into JigCell, our problem-solving environment for biological network modeling (95–97). The parameter sets in the JigCell version of budding yeast and fission yeast are slightly different from the parameter sets presented in this article. The revised parameter values give better fits to the phenotypic details of yeast mutants. JigCell is especially suited to this sort of parameter twiddling to optimize the fit of a model to experimental details.

APPENDIX: A DYNAMICAL PERSPECTIVE ON MOLECULAR CELL BIOLOGY

A molecular regulatory network, such as Fig. 1, is a set of chemical and physical processes taking place within a living cell. The temporal changes driven by these processes can be described, at least in a first approximation, by a set of ordinary differential equations derived according to the standard principles of biophysical chemistry (36). Each differential equation describes the rate of change of a single time-varying component of the network (gene, protein, or metabolite—the state variables of the network) in terms of fundamental processes like transcription, translation, degradation, phosphorylation, dephosphorylation, binding, and dissociation. The rate of each step is determined by the current values of the state variables and by numerical values assigned to rate constants, binding constants, Michaelis constants, etc. (collectively referred to as parameters).

Given specific values for the parameters and initial conditions (state variables at time = 0), the differential equations determine how the regulatory network will evolve in time. The direction and speed of this change can be represented by a vector field in a multidimensional state space (Fig. 9 A). A numerical simulation moves through state space always tangent to the vector field. Steady states are points in state space where the vector field is zero. If the vector field close to a steady state points back toward the steady state in all directions (Fig. 9 B), then the steady state is (locally) stable; if the vector field points away from the steady state in any direction (near the open circles in Fig. 9, A and C), the steady state is unstable. If the vector field supports a closed loop (Fig. 9 C), then the system oscillates on this periodic orbit, also called a limit cycle. The stability of a limit cycle is defined analogously to steady states. Stable steady states and stable limit cycles are called attractors of the dynamical system. To every attractor is associated a domain of attraction, consisting of all points of state space from which the system will go to that attractor.

As parameters of the system are changed, the number and stability of steady states and periodic orbits may change, e.g., going from Fig. 9, *A* to *B*, or from Fig. 9, *B* to *C*. Parameter values where such changes occur are called bifurcation points (98,99). At a bifurcation point, the system can gain or lose a stable attractor, or undergo an exchange of stabilities. In the case of the cell cycle, we associate different cell cycle phases to different attractors of the Cdk-regulatory system, and transitions between cell cycle phases to bifurcations of the dynamical system (37).

To visualize bifurcations graphically, one plots on the ordinate a representative variable of the dynamical system, as an indicator of the system's state, and on the abscissa, a particular parameter whose changes can induce the bifurcation (Fig. 9 *D*). It is fruitful to think of changes to the parameter as a signal imposed on the control system, and the stable attractors (steady states and oscillations) as the response of the network (100). For the cell cycle control system, the clear choice of dynamic variable is the activity of Cdk1/CycB (the activity of this complex is small in G1, modest in S/G2, and large in M phase). As bifurcation parameter, we choose cell mass because we consider growth to be the primary driving force for progression through the cell cycle. For each fixed value of cell mass, we compute all steady-state and oscillatory solutions (stable and unstable) of the Cdk-regulatory network, and we plot these solutions on a one-parameter bifurcation diagram (Fig. 9 *D*).

Following standard conventions, we plot steady-state solutions by lines: solid for stable steady states and dashed for unstable. For limit cycles, we plot two loci: one for the maximum and one for the minimum value of Cdk1/CycB activity on the periodic solution, denoting stable limit cycles with solid circles and unstable with open circles. A locus of steady states can fold back on itself at a saddle-node (SN) bifurcation point (where a stable steady state—a node—and an unstable steady state—a saddle—come together and annihilate one another). Between the two SN bifurcation points in Fig. 9 *D*, the control system is bistable (coexistence of two stable steady states, which we might call OFF and ON). To the left and right of SN2 in Fig. 9 *D*, the state space looks like Fig. 9, *A* and *B*, respectively. A locus of steady-state solutions can also lose stability at a Hopf bifurcation (HB) point, from which there arises a family of small amplitude, stable limit cycle solutions (Fig. 9 *D*). A Hopf bifurcation converts state space Fig. 9 *B* into Fig. 9 *C*. For experimental verification of these dynamical properties of the cell cycle control system in frog eggs, see recent articles by Sha et al. (94) and Pomerening et al. (63,101).

Positive feedback is often associated with bistability of a control system. For example, if X activates Y and Y activates X, then the system may persist in a stable ''OFF'' state (X low and Y low) or in a stable ''ON'' state (X high

TABLE 2 Definitions and examples of codimension-one and -two bifurcations

Codimension-one bifurcations

Full name	Abbreviation	From/to	To/from	1D example
Saddle-node	SN	3 steady states	1 steady state	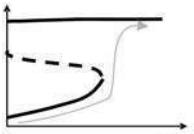
Supercritical Hopf	HBsup	1 stable steady state	Unstable steady state + small amplitude, stable limit cycle	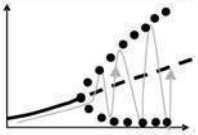
Subcritical Hopf	HBsub	1 unstable steady state	Stable steady state + small amplitude, unstable limit cycle	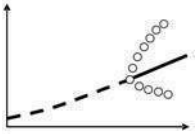
Cyclic-fold	CF	No oscillatory solutions	1 stable oscillation + 1 unstable oscillation	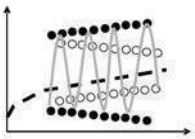
Saddle-node infinite-period	SNIPER	3 steady states	Unstable steady state + large amplitude oscillation	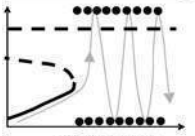
Saddle-loop	SL	Unstable steady state (saddle)	Unstable steady state + large amplitude oscillation	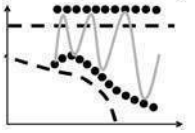

Codimension-two bifurcations

Full name	Abbreviation	From/to	To/from	1D example	2D example
Saddle-node loop	SNL	SN + SL	SNIPER	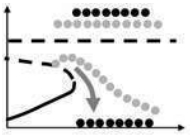	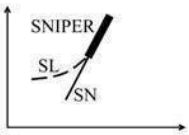
Degenerate Hopf	dHB	HBsup	HBsub + CF	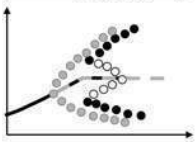	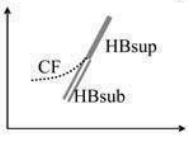
Takens-Bogdanov	TB	SN + HB + SL	SN	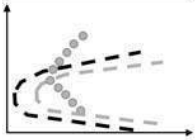	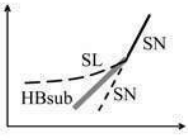
CUSP	CUSP	Bistability (2 SN)	Monostability	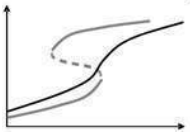	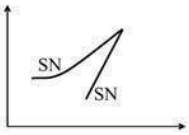

and Y high). Similarly, if X inhibits Y and Y inhibits X (double-negative feedback), the system may also persist in either of two stable steady states (X high and Y low, or X low and Y high). Typically, bistability is observed over a range of parameter values ($k_{SN1} < k < k_{SN2}$). Negative feedback (X activates Y, which activates Z, which inhibits X) may lead to sustained oscillations of X, Y, and Z, for appropriate choices of reaction kinetics and rate constants. These oscillations typically arise by a Hopf bifurcation, with a stable steady state for $k < k_{HB}$ giving way to stable oscillations for $k > k_{HB}$.

In Table 2 we provide a catalog of common codimension-one bifurcations (bifurcations that can be located, in principle, by changing a single parameter of the system). From a one-parameter bifurcation diagram, properly interpreted, one can reconstruct the vector field (see lines *A*, *B*, and *C* in Fig. 9 *D*), which is the mathematical equivalent of the molecular wiring diagram. There are only a small number of common codimension-one bifurcations (see Table 2); hence, there are only a few fundamental signal-response relationships from which a cell must accomplish all the complex signal processing it requires. Of special interest to this article is the SNIPER bifurcation, which is a special type of SN bifurcation point: after annihilation of the saddle and node, the remaining steady state is unstable and surrounded by a stable limit cycle of large amplitude. At the SN bifurcation point, the period of the limit cycle is infinite (SNIPER = saddle-node infinite-period). As the bifurcation parameter pulls away from the SNIPER point, the period of the limit cycle decreases precipitously (see, e.g., Fig. 6).

To continue this process of abstraction, we go from a one-parameter bifurcation diagram to a two-parameter bifurcation diagram (Fig. 10). As the two parameters change simultaneously, we follow loci of codimension-one bifurcation points in the two-parameter plane. For example, the one-parameter diagram in Fig. 9 *D* corresponds to a value of the second parameter at level 6 in Fig. 10. As the value of the second parameter increases, we track SN1 and SN2 along fold lines in the two-parameter plane. Between these two fold lines the control system is bistable. We also track the HB point in the two-parameter diagram for increasing values of the second parameter. We find that, at characteristic points in the two-parameter plane, marked by heavy ''dots'' in Fig. 10, there is a change in some qualitative feature of the codimension-one bifurcations. Because two parameters must be adjusted simultaneously to locate these ''dots'', they are called codimension-two bifurcation points. In Fig. 10 (and Table 2) we illustrate the three most common codimension-two bifurcations: degenerate Hopf (dHB), saddle-node-loop (SNL), and Takens-Bagdanov (TB). From a two-parameter bifurcation diagram, properly interpreted, one can reconstruct a sequence of one-parameter bifurcation diagrams (see lines *1–6* in Fig. 10), which are the qualitatively different signal-response characteristics of the control system. There are only a small number of generic codimension-two bifurcations; hence, there are limited ways by which one signal-response curve can morph into another. These constraints place subtle restrictions on the genetic basis of cell physiology.

In the one-parameter bifurcation diagram, we choose as the primary bifurcation parameter some physiologically relevant quantity (the ''signal'') that is inducing a change in behavior (the ''response'') of the molecular regulatory system. In the two-parameter diagram, we propose to use the second parameter as an indicator of a genetic characteristic of the cell (the level of expression of a particular gene, above and below the wild-type value) with bearing on the signal-response curve. In this format, the two-parameter bifurcation diagram provides a highly condensed summary of the dynamical links from a controlling gene to its physiological outcome (its phenotypes). The two-parameter diagram captures the sequence of dynamically distinct changes that must occur in carrying phenotype of a wild-type cell to the observed phenotypes of deletion mutants (at one extreme) and overexpression mutants (at the other extreme). In between, there may be novel, physiologically distinct phenotypes that could not be anticipated by intuition alone. Examples of this analysis are provided in Figs. 3 and 4, in the Supplementary Material, and on our website.

For alternative explanations of bifurcation diagrams, one may consult the appendix to Borisuk and Tyson (33) or the textbooks by Strogatz (99) or Kaplan and Glass (102).

SUPPLEMENTARY MATERIAL

An online supplement to this article can be found by visiting BJ Online at http://www.biophysj.org.

We thank Jason Zwolak for help with the Supplementary Material and Akos Sveiczer for useful discussions.

This research was supported by grants from Defense Advanced Research Project Agency (AFRL F30602-02-0572), the James S. McDonnell Foundation (21002050), and the European Commission (COMBIO, LSHG-CT-503568). A.C-N. is a Bolyai fellow of the Hungarian Academy of Sciences.

REFERENCES

1. Rupes, I. 2002. Checking cell size in yeast. *Trends Genet.* 18:479–485.
2. Sveiczer, A., B. Novak, and J. M. Mitchison. 1996. The size control of fission yeast revisited. *J. Cell Sci.* 109:2947–2957.
3. Nurse, P. 1994. Ordering S phase and M phase in the cell cycle. *Cell.* 79:547–550.
4. Hartwell, L. H., and T. A. Weinert. 1989. Checkpoints: controls that ensure the order of cell cycle events. *Science.* 246:629–634.
5. Nasmyth, K. 1996. Viewpoint: putting the cell cycle in order. *Science.* 274:1643–1645.
6. Tyson, J. J. 1985. The coordination of cell growth and division—intertional or incidental. *Bioessays.* 2:72–77.
7. Kastan, M. B., and J. Bartek. 2004. Cell-cycle checkpoints and cancer. *Nature.* 432:316–323.
8. Cross, F. R., V. Archambault, M. Miller, and M. Klovstad. 2002. Testing a mathematical model for the yeast cell cycle. *Mol. Biol. Cell.* 13:52–70.
9. Nurse, P. 1992. Eukaryotic cell-cycle control. *Biochem. Soc. Trans.* 20:239–242.
10. Nurse, P. 1990. Universal control mechanism regulating onset of M-phase. *Nature.* 344:503–508.
11. Bray, D. 1995. Protein molecules as computational elements in living cells. *Nature.* 376:307–312.
12. Aguda, B. D. 1999. A quantitative analysis of the kinetics of the G2 DNA damage checkpoint system. *Proc. Natl. Acad. Sci. USA.* 96: 11352–11357.
13. Aguda, B. D. 1999. Instabilities in phosphorylation-dephosphorylation cascades and cell cycle checkpoints. *Oncogene.* 18:2846–2851.
14. Chen, K. C., A. Csikasz-Nagy, B. Gyorffy, J. Val, B. Novak, and J. J. Tyson. 2000. Kinetic analysis of a molecular model of the budding yeast cell cycle. *Mol. Biol. Cell.* 11:369–391.
15. Chen, K. C., L. Calzone, A. Csikasz-Nagy, F. R. Cross, B. Novak, and J. J. Tyson. 2004. Integrative analysis of cell cycle control in budding yeast. *Mol. Biol. Cell.* 15:3841–3862.
16. Goldbeter, A. 1991. A minimal cascade model for the mitotic oscillator involving cyclin and cdc2 kinase. *Proc. Natl. Acad. Sci. USA.* 88:9107–9111.
17. Gonze, D., and A. Goldbeter. 2001. A model for a network of phosphorylation-dephosphorylation cycles displaying the dynamics of dominoes and clocks. *J. Theor. Biol.* 210:167–186.
18. Novak, B., and J. J. Tyson. 1993. Numerical analysis of a comprehensive model of M-phase control in *Xenopus* oocyte extracts and intact embryos. *J. Cell Sci.* 106:1153–1168.
19. Novak, B., and J. J. Tyson. 1995. Quantitative analysis of a molecular model of mitotic control in fission yeast. *J. Theor. Biol.* 173:283–305.
20. Obeyesekere, M. N., J. R. Herbert, and S. O. Zimmerman. 1995. A model of the G1 phase of the cell cycle incorporating cyclinE/cdk2 complex and retinoblastoma protein. *Oncogene.* 11:1199–1205.
21. Obeyesekere, M. N., E. Tecarro, and G. Lozano. 2004. Model predictions of MDM2 mediated cell regulation. *Cell Cycle.* 3:655–661.

22. Qu, Z. L., J. N. Weiss, and W. R. MacLellan. 2003. Regulation of the mammalian cell cycle: a model of the G(1)-to-S transition. *Am. J. Physiol. Cell Physiol.* 284:C349–C364.
23. Qu, Z. L., J. N. Weiss, and W. R. MacLellan. 2004. Coordination of cell growth and cell division: a mathematical modeling study. *J. Cell Sci.* 117:4199–4207.
24. Steuer, R. 2004. Effects of stochasticity in models of the cell cycle: from quantized cycle times to noise-induced oscillations. *J. Theor. Biol.* 228:293–301.
25. Sveiczer, A., A. Csikasz-Nagy, B. Gyorffy, J. J. Tyson, and B. Novak. 2000. Modeling the fission yeast cell cycle: quantized cycle times in *wee1*$^{-}$*cdc25*Δ mutant cells. *Proc. Natl. Acad. Sci. USA.* 97:7865–7870.
26. Swat, M., A. Kel, and H. Herzel. 2004. Bifurcation analysis of the regulatory modules of the mammalian G(1)/S transition. *Bioinformatics.* 20:1506–1511.
27. Thron, C. D. 1991. Mathematical analysis of a model of the mitotic clock. *Science.* 254:122–123.
28. Thron, C. D. 1997. Bistable biochemical switching and the control of the events of the cell cycle. *Oncogene.* 15:317–325.
29. Tyson, J. J. 1991. Modeling the cell division cycle: cdc2 and cyclin interactions. *Proc. Natl. Acad. Sci. USA.* 88:7328–7332.
30. Cross, F. R. 2003. Two redundant oscillatory mechanisms in the yeast cell cycle. *Dev. Cell.* 4:741–752.
31. Marlovits, G., C. J. Tyson, B. Novak, and J. J. Tyson. 1998. Modeling M-phase control in *Xenopus* oocyte extracts: the surveillance mechanism for unreplicated DNA. *Biophys. Chem.* 72:169–184.
32. Zwolak, J. W., J. J. Tyson, and L. T. Watson. 2005. Globally optimized parameters for a model of mitotic control in frog egg extracts. *IEE Proc. Syst. Biol.* 152:81–92.
33. Borisuk, M. T., and J. J. Tyson. 1998. Bifurcation analysis of a model of mitotic control in frog eggs. *J. Theor. Biol.* 195:69–85.
34. Battogtokh, D., and J. J. Tyson. 2004. Bifurcation analysis of a model of the budding yeast cell cycle. *Chaos.* 14:653–661.
35. Novak, B., Z. Pataki, A. Ciliberto, and J. J. Tyson. 2001. Mathematical model of the cell division cycle of fission yeast. *Chaos.* 11:277–286.
36. Tyson, J. J., K. Chen, and B. Novak. 2001. Network dynamics and cell physiology. *Nat. Rev. Mol. Cell Biol.* 2:908–916.
37. Tyson, J. J., A. Csikasz-Nagy, and B. Novak. 2002. The dynamics of cell cycle regulation. *Bioessays.* 24:1095–1109.
38. Qu, Z. L., W. R. MacLellan, and J. N. Weiss. 2003. Dynamics of the cell cycle: checkpoints, sizers, and timers. *Biophys. J.* 85:3600–3611.
39. Novak, B., and J. J. Tyson. 1997. Modeling the control of DNA replication in fission yeast. *Proc. Natl. Acad. Sci. USA.* 94:9147–9152.
40. Novak, B., A. Csikasz-Nagy, B. Gyorffy, K. Chen, and J. J. Tyson. 1998. Mathematical model of the fission yeast cell cycle with checkpoint controls at the G1/S, G2/M and metaphase/anaphase transitions. *Biophys. Chem.* 72:185–200.
41. Novak, B., and J. J. Tyson. 2004. A model for restriction point control of the mammalian cell cycle. *J. Theor. Biol.* 230:563–579.
42. XPP/XPPAUT. 2005. http://www.math.pitt.edu/~bard/xpp/xpp.html. [Online.].
43. Generic Cell Cycle Model. 2006. http://mpf.biol.vt.edu/research/generic_model/main/pp/. [Online.].
44. Giot, L., J. S. Bader, C. Brouwer, A. Chaudhuri, B. Kuang, Y. Li, Y. L. Hao, C. E. Ooi, B. Godwin, E. Vitols, G. Vijayadamodar, P. Pochart, et al. 2003. A protein interaction map of Drosophila melanogaster. *Science.* 302:1727–1736.
45. Kohn, K. W. 1999. Molecular interaction map of the mammalian cell cycle control and DNA repair systems. *Mol. Biol. Cell.* 10:2703–2734.
46. Schwikowski, B., P. Uetz, and S. Fields. 2000. A network of protein-protein interactions in yeast. *Nat. Biotechnol.* 18:1257–1261.
47. Uetz, P., L. Giot, G. Cagney, T. A. Mansfield, R. S. Judson, J. R. Knight, D. Lockshon, V. Narayan, M. Srinivasan, P. Pochart, A. Qureshi-Emili, Y. Li, B. Godwin, et al. 2000. A comprehensive analysis of protein-protein interactions in Saccharomyces cerevisiae. *Nature.* 403:623–627.
48. Uetz, P., and M. J. Pankratz. 2004. Protein interaction maps on the fly. *Nat. Biotechnol.* 22:43–44.
49. Fantes, P., and P. Nurse. 1977. Control of cell size at division in fission yeast by a growth-modulated size control over nuclear division. *Exp. Cell Res.* 107:377–386.
50. Johnston, G. C., C. W. Ehrhardt, A. Lorincz, and B. L. A. Carter. 1979. Regulation of cell size in the yeast *Saccharomyces cerevisiae*. *J. Bacteriol.* 137:1–5.
51. Jorgensen, P., and M. Tyers. 2004. How cells coordinate growth and division. *Curr. Biol.* 14:R1014–R1027.
52. Nurse, P. 1975. Genetic control of cell size at cell division in yeast. *Nature.* 256:547–551.
53. Dolznig, H., F. Grebien, T. Sauer, H. Beug, and E. W. Mullner. 2004. Evidence for a size-sensing mechanism in animal cells. *Nat. Cell Biol.* 6:899–905.
54. Killander, D., and A. Zetterberg. 1965. A quantitative cytochemical investigation of the relationship between cell mass and initiation of DNA synthesis in mouse fibroblast in vitro. *Exp. Cell Res.* 40:12–20.
55. Zetterberg, A., and O. Larsson. 1995. Cell cycle progression and cell growth in mammalian cells: kinetic aspects of transition events. *In* Cell cycle Control. C. Hutchison and D. M. Glover, editors. Oxford University Press. Oxford, UK. 206–227.
56. Baserga, R. 1984. Growth in size and cell DNA replication. *Exp. Cell Res.* 151:1–4.
57. Conlon, I., and M. Raff. 2003. Differences in the way a mammalian cell and yeast cells coordinate cell growth and cell-cycle progression. *J. Biol.* 2:7.
58. Murray, A. W., and M. W. Kirschner. 1989. Cyclin synthesis drives the early embryonic cell cycle. *Nature.* 339:275–280.
59. Solomon, M. J., M. Glotzer, T. H. Lee, M. Philippe, and M. W. Kirschner. 1990. Cyclin activation of p34^{cdc2}. *Cell.* 63:1013–1024.
60. Futcher, B. 1996. Cyclins and the wiring of the yeast cell cycle. *Yeast.* 12:1635–1646.
61. Yang, L., Z. Han, W. Robb Maclellan, J. N. Weiss, and Z. Qu. 2006. Linking cell division to cell growth in a spatiotemporal model of the cell cycle. *J. Theor. Biol.* In press.
62. Moreno, S., and P. Nurse. 1994. Regulation of progression through the G1 phase of the cell cycle by the *rum1*$^{+}$ gene. *Nature.* 367:236–242.
63. Pomerening, J. R., S. Y. Kim, and J. E. Ferrell Jr. 2005. Systems-level dissection of the cell-cycle oscillator: bypassing positive feedback produces damped oscillations. *Cell.* 122:565–578.
64. Ayte, J., C. Schweitzer, P. Zarzov, P. Nurse, and J. A. DeCaprio. 2001. Feedback regulation of the MBF transcription factor by cyclin Cig2. *Nat. Cell Biol.* 3:1043–1050.
65. Benito, J., C. Martin-Castellanos, and S. Moreno. 1998. Regulation of the G1 phase of the cell cycle by periodic stabilization and degradation of the p25rum1 CDK inhibitor. *EMBO J.* 17:482–497.
66. Hayles, J., D. Fisher, A. Woollard, and P. Nurse. 1994. Temporal order of S phase and mitosis in fission yeast is determined by the state of the p34^{cdc2} -mitotic B cyclin complex. *Cell.* 78:813–822.
67. Parisi, T., A. R. Beck, N. Rougier, T. McNeil, L. Lucian, Z. Werb, and B. Amati. 2003. Cyclins E1 and E2 are required for endoreplication in placental trophoblast giant cells. *EMBO J.* 22:4794–4803.
68. Nurse, P., P. Thuriaux, and K. Nasmyth. 1976. Genetic control of the cell division cycle in the fission yeast *Schizosaccharomyces pombe*. *Mol. Gen. Genet.* 146:167–178.
69. Computational Cell Biology at Virginia Tech. 2005. http://mpf.biol.vt.edu/. [Online.].
70. Tyson, J. J. 1983. Unstable activator models for size control of the cell cycle. *J. Theor. Biol.* 104:617–631.
71. Tyers, M. 2004. Cell cycle goes global. *Curr. Opin. Cell Biol.* 16:602–613.

72. Schwob, E., T. Bohm, M. D. Mendenhall, and K. Nasmyth. 1994. The B-type cyclin kinase inhibitor $p40^{sic1}$ controls the G1 to S transition in *S. cerevisiae*. *Cell.* 79:233–244.
73. Visintin, R., S. Prinz, and A. Amon. 1997. *CDC20* and *CDH1*: a family of substrate-specific activators of APC-dependent proteolysis. *Science.* 278:460–463.
74. Zachariae, W., M. Schwab, K. Nasmyth, and W. Seufert. 1998. Control of cyclin ubiquitination by CDK-regulated binding of Hct1 to the anaphase promoting complex. *Science.* 282:1721–1724.
75. Sethi, N., M. C. Monteagudo, D. Koshland, E. Hogan, and D. J. Burke. 1991. The CDC20 gene product of *Saccharomyces cerevisiae*, a beta-transducin homolog, is required for a subset of microtubule-dependent cellular processes. *Mol. Cell. Biol.* 11:5592–5602.
76. Fitzpatrick, P. J., J. H. Toyn, J. B. Millar, and L. H. Johnston. 1998. DNA replication is completed in *Saccharomyces cerevisiae* cells that lack functional Cdc14, a dual-specificity protein phosphatase. *Mol. Gen. Genet.* 258:437–441.
77. Visintin, R., K. Craig, E. S. Hwang, S. Prinz, M. Tyers, and A. Amon. 1998. The phosphatase Cdc14 triggers mitotic exit by reversal of Cdk-dependent phosphorylation. *Mol. Cell.* 2:709–718.
78. Rudner, A., and A. Murray. 2000. Phosphorylation by Cdc28 activates the Cdc20-dependent activity of the anaphase promoting complex. *J. Cell Biol.* 149:1377–1390.
79. Irniger, S., M. Baumer, and G. H. Braus. 2000. Glucose and Ras activity influence the ubiquitin ligases APC/C and SCF in Saccharomyces cerevisiae. *Genetics.* 154:1509–1521.
80. Wasch, R., and F. Cross. 2002. APC-dependent proteolysis of the mitotic cyclin Clb2 is essential for mitotic exit. *Nature.* 418:556–562.
81. Lew, D. J. 2003. The morphogenesis checkpoint: how yeast cells watch their figures. *Curr. Opin. Cell Biol.* 15:648–653.
82. Kellogg, D. R. 2003. Wee1-dependent mechanisms required for coordination of cell growth and cell division. *J. Cell Sci.* 116:4883–4890.
83. Ciliberto, A., B. Novak, and J. J. Tyson. 2003. Mathematical model of the morphogenesis checkpoint in budding yeast. *J. Cell Biol.* 163: 1243–1254.
84. Aguda, B. D., and Y. Tang. 1999. The kinetic origins of the restriction point in the mammalian cell cycle. *Cell Prolif.* 32:321–335.
85. Obeyesekere, M. N., E. S. Knudsen, J. Y. Wang, and S. O. Zimmerman. 1997. A mathematical model of the regulation of the G1 phase of Rb+/+ and Rb−/− mouse embryonic fibroblasts and an osteosarcoma cell line. *Cell Prolif.* 30:171–194.
86. Kozar, K., M. A. Ciemerych, V. I. Rebel, H. Shigematsu, A. Zagozdon, E. Sicinska, Y. Geng, Q. Y. Yu, S. Bhattacharya, R. T. Bronson, K. Akashi, and P. Sicinski. 2004. Mouse development and cell proliferation in the absence of D-cyclins. *Cell.* 118: 477–491.
87. Geng, Y., Q. Y. Yu, E. Sicinska, M. Das, J. E. Schneider, S. Bhattacharya, W. M. Rideout, R. T. Bronson, H. Gardner, and P. Sicinski. 2003. Cyclin E ablation in the mouse. *Cell.* 114:431–443.
88. Malumbres, M., R. Sotillo, D. Santamaria, J. Galan, A. Cerezo, S. Ortega, P. Dubus, and M. Barbacid. 2004. Mammalian cells cycle without the D-type cyclin-dependent kinases Cdk4 and Cdk6. *Cell.* 118:493–504.
89. Ortega, S., I. Prieto, J. Odajima, A. Martin, P. Dubus, R. Sotillo, J. L. Barbero, M. Malumbres, and M. Barbacid. 2003. Cyclin-dependent kinase 2 is essential for meiosis but not for mitotic cell division in mice. *Nat. Genet.* 35:25–31.
90. Dirick, L., T. Bohm, and K. Nasmyth. 1995. Roles and regulation of Cln/Cdc28 kinases at the start of the cell cycle of *Saccharomyces cerevisiae*. *EMBO J.* 14:4803–4813.
91. Richardson, H. E., C. Wittenberg, F. Cross, and S. I. Reed. 1989. An essential G1 function for cyclin-like proteins in yeast. *Cell.* 59:1127–1133.
92. Chow, J. P. H., W. Y. Siu, H. T. B. Ho, K. H. T. Ma, C. C. Ho, and R. Y. C. Poon. 2003. Differential contribution of inhibitory phosphorylation of CDC2 and CDK2 for unperturbed cell cycle control and DNA integrity checkpoints. *J. Biol. Chem.* 278:40815–40828.
93. Hanahan, D., and R. A. Weinberg. 2000. The hallmarks of cancer. *Cell.* 100:57–70.
94. Sha, W., J. Moore, K. Chen, A. D. Lassaletta, C.-S. Yi, J. J. Tyson, and J. C. Sible. 2003. Hysteresis drives cell-cycle transitions in *Xenopus laevis* egg extracts. *Proc. Natl. Acad. Sci. USA.* 100: 975–980.
95. Allen, N. A., L. Calzone, K. C. Chen, A. Ciliberto, N. Ramakrishnan, C. A. Shaffer, J. C. Sible, J. J. Tyson, M. T. Vass, L. T. Watson, and J. W. Zwolak. 2003. Modeling regulatory networks at Virginia Tech. *OMICS.* 7:285–299.
96. Vass, M., N. Allen, C. A. Shaffer, N. Ramakrishnan, L. T. Watson, and J. J. Tyson. 2004. The JigCell model builder and run manager. *Bioinformatics.* 20:3680–3681.
97. JigCell Project. 2005. http://jigcell.biol.vt.edu/. [Online.].
98. Kuznetsov, Y. A. 1995. Elements of Applied Bifurcation Theory. Springer Verlag, New York.
99. Strogatz, S. H. 1994. Nonlinear Dynamics and Chaos. Addison-Wesley, Reading, MA.
100. Tyson, J. J., K. C. Chen, and B. Novak. 2003. Sniffers, buzzers, toggles, and blinkers: dynamics of regulatory and signaling pathways in the cell. *Curr. Opin. Cell Biol.* 15:221–231.
101. Pomerening, J. R., E. D. Sontag, and J. E. Ferrell Jr. 2003. Building a cell cycle oscillator: hysteresis and bistability in the activation of Cdc2. *Nat. Cell Biol.* 5:346–351.
102. Kaplan, D., and L. Glass. 1995. Understanding Nonlinear Dynamics, Chapter 5. Springer-Verlag, New York.

dc_836_14

7.2 Számítógépes modellanalízis az emlős sejtek napi ritmus és a sejtciklus kapcsoltságára

Zámborszky J., Hong CI. & **Csikász-Nagy A.** (2007) Computational Analysis of Mammalian Cell Division Gated by a Circadian Clock: Quantized Cell Cycles and Cell Size Control. *J Biol Rhythms*, **22:** 542-53. **Impakt faktor: 4.211**

Computational Analysis of Mammalian Cell Division Gated by a Circadian Clock: Quantized Cell Cycles and Cell Size Control

Judit Zámborszky,[*,1,2] Christian I. Hong,[†,1] and Attila Csikász Nagy[*,2,3]

[*]*Materials Structure and Modeling Research Group of the Hungarian Academy of Sciences and Department of Applied Biotechnology and Food Science, Budapest University of Technology and Economics, Budapest, Hungary,* [†]*Department of Genetics, Dartmouth Medical School, Hanover, New Hampshire*

Abstract Cell cycle and circadian rhythms are conserved from cyanobacteria to humans with robust cyclic features. Recently, molecular links between these two cyclic processes have been discovered. Core clock transcription factors, Bmal1 and Clock (Clk), directly regulate Wee1 kinase, which inhibits entry into the mitosis. We investigate the effect of this connection on the timing of mammalian cell cycle processes with computational modeling tools. We connect a minimal model of circadian rhythms, which consists of transcription–translation feedback loops, with a modified mammalian cell cycle model from Novak and Tyson (2004). As we vary the mass doubling time (MDT) of the cell cycle, stochastic simulations reveal quantized cell cycles when the activity of Wee1 is influenced by clock components. The quantized cell cycles disappear in the absence of coupling or when the strength of this link is reduced. More intriguingly, our simulations indicate that the circadian clock triggers critical size control in the mammalian cell cycle. A periodic brake on the cell cycle progress via Wee1 enforces size control when the MDT is quite different from the circadian period. No size control is observed in the absence of coupling. The issue of size control in the mammalian system is debatable, whereas it is well established in yeast. It is possible that the size control is more readily observed in cell lines that contain circadian rhythms, since not all cell types have a circadian clock. This would be analogous to an ultradian clock intertwined with quantized cell cycles (and possibly cell size control) in yeast. We present the first coupled model between the mammalian cell cycle and circadian rhythms that reveals quantized cell cycles and cell size control influenced by the clock.

Key words cell cycle, circadian clock, size control, quantized cycles, mathematical modeling, mammalian, stochastic, simulation

A fundamental attribute of a cell is its ability to divide and multiply. The cell cycle executes a precise control mechanism with multiple checkpoints for proper cell division. Its oscillatory dynamics are extensively studied from yeasts to mammals (Nurse, 2000). Although not as essential as cell cycle for viability, the

1. These authors contributed equally to this work.

2. Present address: The Microsoft Research–University of Trento Centre for Computational and Systems Biology, Piazza Manci 17, Povo (Trento), 38100, Italy.

3. To whom all correspondence should be addressed: Attila Csikász Nagy, The Microsoft Research–University of Trento Centre for Computational and Systems Biology, Piazza Manci 17, Povo (Trento), 38100, Italy; email: csikasz@cosbi.eu.

JOURNAL OF BIOLOGICAL RHYTHMS, Vol. 22 No. 6, December 2007 542-553
DOI: 10.1177/0748730407307225

existence of a circadian clock can be observed from cyanobacteria to humans (Dunlap, 1999; Matsuo et al., 2003; Vanselow et al., 2006). In most cases, conserved transcription–translation negative feedback loop (TTFL) is a foundation of robust oscillations in clock mechanisms (Dunlap, 1999). Both the cell cycle and circadian clock are robust oscillatory systems (Chen et al., 2004; Forger and Peskin, 2005; Gonze et al., 2002; Hong et al., 2007; Morohashi et al., 2002). Their properties, however, are significantly different. The most distinct differences are temperature and nutrient compensations. The period of the circadian clock is relatively invariant over a physiologically relevant range in temperature, whereas the cell cycle or mass doubling time is greatly influenced by temperature and/or nutrient conditions (i.e., cell cycle time decreases as a function of temperature, leading to a Q_{10} [rate change with increase of 10 ºC of temperature] of about 3, whereas Q_{10} of a circadian period is close to 1; Tsuchiya et al., 2003). On the other hand, all eukaryotic cell cycles have multiple checkpoints that ensure the proper progress of the cell cycle, but it is still unknown whether checkpoints exist for the biological clock. In any case, the harmonious progress of the cell cycle and circadian rhythms is necessary for the well-being of organisms as malfunctions in the cell cycle and/or clock can lead to tumorigenesis (Fu et al., 2002; Kastan and Bartek, 2004).

The molecular regulatory mechanisms of the cell division cycle are fundamentally identical in all eukaryotes (Nurse, 1990). Although multicellular organisms proliferate only when permitted by specific growth factors, the key enzymes of the cell cycle are functionally conserved across different eukaryotes (Csikasz-Nagy et al., 2006). The key transitions of the cell cycle are regulated by Cyclin-dependent kinases (Cdks) bound to their regulatory Cyclin (Cyc) partners. Four crucial Cdk/Cyc complexes (Cdc2/CycB, Cdk2/CycA, Cdk2/CycE, and Cdk4/CycD) and their regulated sequential functions are necessary for proper mammalian cell cycle progress. Their orders of appearance are meticulously controlled by inhibitors (Rb, p27Kip1), transcription factors (E2F, Mcm), and degradation factors (p55Cdc/APC, Cdh1/APC; Sherr, 1996). We would also like to emphasize the fact that in HeLa cells, the inhibitory kinase Wee1 plays a crucial role in regulating Cdc2 activity and the entry into mitosis, as it does in fission yeast (Chow et al., 2003). Most of this regulatory network of the cell cycle has been mathematically analyzed by Novak and Tyson (2004).

Yeast cells have to reach a critical size for proper cell division. This active size control mechanism prevents yeasts from delayed or premature cell division, resulting in imbalanced cell mass population (Rupes, 2002; Sveiczer et al., 1996). The existence of cell size control is controversial in mammalian cells (Conlon and Raff, 2003; Grebien et al., 2005; Sveiczer et al., 2004; Wells, 2002). In cultured mouse fibroblasts, smaller newborn cells take longer to enter the S-phase compared to larger cells at birth, which indicates a possible cell size checkpoint as in *Saccharomyces cerevisiae* (Johnston et al., 1979; Killander and Zetterberg, 1965). On the other hand, recent findings from Rat Schwann cells suggest absence of size control (i.e., small cells took several cell divisions to reach their typical size; Conlon et al., 2001). This discrepancy is suggested partly because of differences in growth rates: linear vs. exponential. Recently, however, this hypothesis was challenged with results of different cell types readjusting their size in the next cycle, even when the "linear mode" was observed (Dolznig et al., 2004). With our computational modeling, we propose that periodic influences of the circadian clock on cell cycle contribute to the cell size control mechanism regardless of growth type differences.

In mammalian systems, the central clock is located in the suprachiasmatic nucleus (SCN) situated in the hypothalamus. Neurons in the SCN display synchronized endogenous clocks (Yamaguchi et al., 2003), receive input information (i.e., light, temperature, etc.), and transmit output signals. The clock is also present in peripheral tissues (i.e., fibroblast, liver, bone marrow, etc.). Peripheral clocks in both mouse and rat-1 fibroblast cells in culture, however, do not communicate with each other, resulting in desynchronization of the clock as a population (Welsh et al., 2004). Nevertheless, identical components are present in both peripheral tissues and in the SCN neurons. The details of the mammalian clock are complex, with an autoregulatory network of TTFLs. Mammalian *mPer1* and *mPer2* genes are activated by heterodimeric bHLH-PAS transcription factors Bmal1:Clk. The *mPers* are translated and form complexes with mCry1 and mCry2 proteins. The complexes are translocated into the nucleus and inhibit the activity of the Bmal1:Clk heterodimeric transcription factors. This is a nutshell of the time-delayed negative feedback mechanism that generates a robust oscillation of about 24 h. Posttranscriptional and translational regulations of mPers, mCrys, and Bmal1:Clk add multiple layers of complexity in the system (Hardin, 2004).

Earlier studies from the late 1950s to the 1980s indicate that cell divisions in Euglena, Tetrahymena, and Gonyaulax occur only at particular times of the circadian cycle (Edmunds, 1974a, 1974b; Sweeney

and Hastings, 1958). Gated cell division cycle is also observed in some cyanobacteria, with average doubling times less than 24 h (Mori et al., 1996). These data indicate gating of the cell cycle by the clock. Although there has been physiological evidence suggesting circadian-gated cell cycle for more than 4 decades, the molecular link between cell cycle and the clock remained in a black box until recently. Matsuo and his colleagues showed that a cell cycle regulator, *wee1*, is directly regulated by clock components via *wee1*'s E-box elements in mammalian cells (Matsuo et al., 2003). Wee1 phosphorylates Cdc2/CyclinB (Cdk1/CycB) complex and inhibits the entry into mitosis from G2. This regulation is reflected in partial hepatectomy (PH) experiments showing that PH performed at different zeitgeber times (ZT0 vs. ZT8) resulted in similar timing of entry into the S-phases but showed an 8-h delay in the entry of M-phase from the ZT0 PH liver (Matsuo et al., 2003). Wee1 and its kinase activity peaked during the dark phase (~ ZT 16–20) after the PH, and *wee1* mRNA peaked at ZT 8. A high level of Wee1 activity determines the duration of the G2-phase, and it has to drop before cells enter into the M-phase. Intrigued by these results, we present the first coupled mathematical model of mammalian cell cycle and circadian clock with Wee1 as a coupling factor.

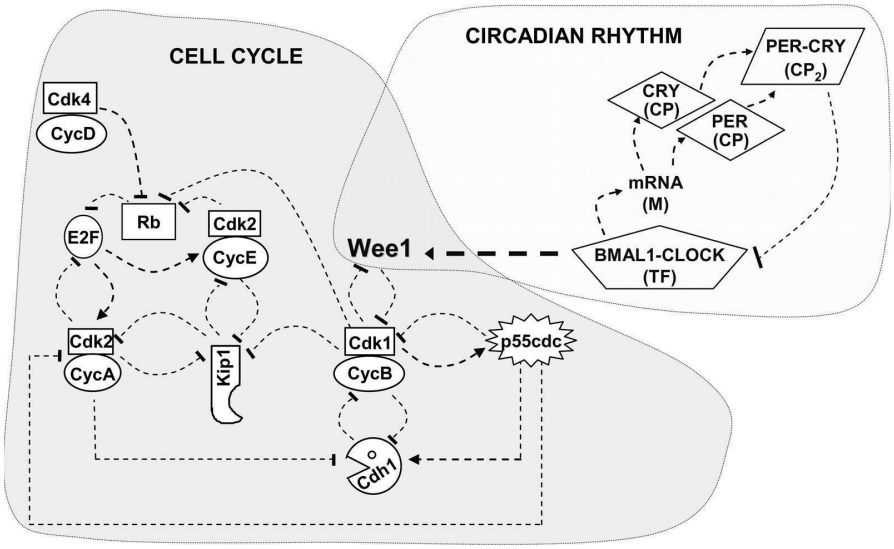

Figure 1. Interaction map of the mammalian cell cycle and circadian clock networks. The cell cycle module is coupled with a simplified circadian clock module via Wee1 (bold dashed arrow). Lines with arrowheads indicate activations (or association of clock protein complex [CP_2]), and lines with ⊣ mean inhibitions.

Our model results in (1) quantized cell cycles and (2) cell size control when the mass doubling time (MDT) deviates from 24 h in our stochastic simulations. Quantized cell cycles in mammalian cell lines were first reported by Robert R. Klevecz in 1976 (Klevecz, 1976). In the 1980s, David Lloyd and his colleagues identified quantized cell cycles in lower eukaryotes and demonstrated with mathematical modeling that ultradian pulses created quantized cell cycles (Lloyd and Kippert, 1987; Lloyd and Volkov, 1990). Although quantized cell cycles were shown both in yeast and mammals (Klevecz, 1976; Sveiczer et al., 1999), a clock-regulated quantized mammalian cell cycle with a known molecular link has never been addressed. More interestingly, our simulations show that the clock-influenced cell cycle via Wee1 triggers cell size control. The cell size control becomes apparent when the clock enforces circadian regulation on Wee1 when the MDT differs greatly from 24 h.

MODELING METHODS

Our purpose is not to address a comprehensive mammalian circadian rhythm model. For simplicity's sake, we want to have a minimal but robust oscillator that generates an endogenous cycle enforcing a periodic influence on the cell cycle. Hence, we built a simplified version of a 4-variable mammalian circadian clock model (Fig. 1) that consists of transcription factors (*TF*: Bmal1 and Clk), clock message (*M: mPer* or *mCry* mRNA), clock protein (*CP*: mPer or mCry), and a dimer complex of clock proteins (CP_2; see Appendix A). For the simplicity of the model, we assume that mPer and mCry are the same species. Therefore, CP_2 represents combinations of mPer/mPer, mPer/mCry, and mCry/mCry dimers. This assumption will be relaxed in our future work when we study a more comprehensive model of circadian clock. We also assume that the CP_2 are more stable than the *CP*, which introduces an autocatalytic positive feedback in the system (Tyson et al., 1999). The *CP* is activated by the *TF*, and the *TF* is inhibited by the

CP_2, which closes the negative feedback loop. Our simplified clock model shows robust endogenous oscillations with a period of 24 h (top panel of Fig. 2).

For our cell cycle model, we adapted Novak and Tyson's mammalian model (2004), which focuses on restriction point control. They simulated "transient inhibition of growth" in mammalian cells upon cycloheximide treatment and its removal (Zetterberg and Larsson, 1995), with in-depth descriptions of cell growth and the *Cdk* regulatory system. This model, however, did not focus on Wee1 and G2/M transition because of an already complicated molecular network with 4 different Cdk/Cyclin complexes. We introduce a Wee1 and Cdc25 regulatory module emphasizing the G2/M transition into the Novak and Tyson (2004) mammalian model. The Wee1 and Cdc25 module regulates the activity of Cdc2/CycB for proper progress of the cell cycle into mitosis. In addition to the basal transcriptional activity of Wee1, we introduce another level of transcriptional activity of *Wee1* that is directly regulated by clock components, Bmal1:Clk (Fig. 1). This connection creates a link between the cell cycle and circadian clock in which periodic regulation of Wee1 is modulated by the clock (Appendix B). The cell cycle model shows robust oscillations with an MDT determined by different growth rates in the absence of a connection with the clock module (i.e., coupling factor $[k_{w5}''] = 0$). Multiple runs of stochastic simulations with different combinations of coupling strength (Appendix C) at different mass doubling times of the cell cycle are executed. For stochastic simulations, we introduce noise into the cell cycle regulatory equations by rewriting the cell cycle model as Langevin-type equations with multiplicative noise (Steuer, 2004; van Kampen, 1981):

$$\frac{d}{dt}x_i = f_i[\ldots] + w_i(t)\sqrt{2 \cdot D_i \cdot x_i}$$

where $f_i[\ldots]$ means the original deterministic equation, $w_i(t)$ is Gaussian white noise with 0 mean and unit variance, and D_i is the noise amplitude. For simplicity, we kept the noise amplitude constant (0.005) for all variables. This number was set by matching the coefficient of variation (CV) of simulated uncoupled cell cycle length (at MDT = 24 h) to experimentally observed CV = 10% (Tyson, 1985). We do not introduce stochasticity in the circadian clock module because its sensitivity to noise may not reflect a truly robust clock mechanism, being an overly simplified version of a

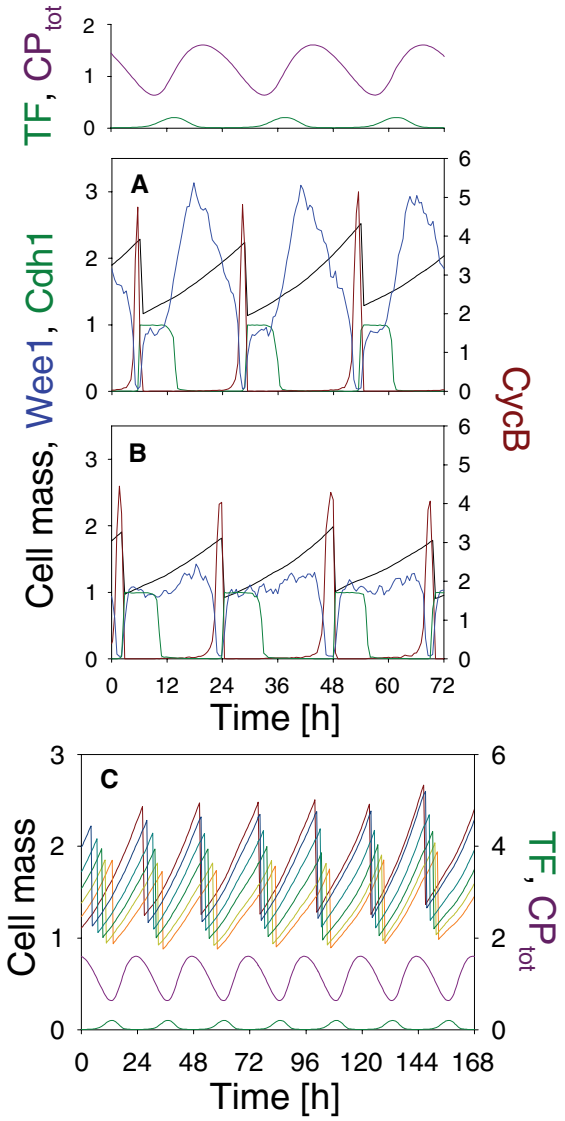

Figure 2. Simulation of the coupled mammalian and circadian clock modules with the mass doubling time (MDT) = 24 h. (A, B) Simulations start at 0 h at the minima of active transcription factor (*TF*; upper panel). Strong circadian coupling induces high peaks of Wee1 (A), while weak circadian influence creates minor changes in Wee1 (B). The zero coupling resembles the results of weak coupling (not shown). Variables are color coded in the *y*-axis of the graph. (C) Gated cell division timing by the circadian clock. Simulations are initiated from different cell cycle stages (4-h intervals), while the circadian clock is always initiated from 0 h at the trough of active *TF* (~ ZT12). After several cycles, cell divisions are synchronized to late night/early morning (high total amount of clock proteins, or CP_{tot}) independent of initial conditions of the cell cycle.

clock model. In this article, we only concentrate on the unidirectional effect of the clock on cell cycle. We discuss the possibility of cross-talk between the cell cycle

and circadian rhythms below. We also keep the cell growth equation deterministic because we cannot take into account the fluctuations in the complex process of cell growth in the current model. Differential equations are solved and analyzed with the software tool XPP-AUT (Ermentrout, 2002). Readers can find our XPPAUT readable ODE files and the description of rate constants of our model on our Web site (http://www.cellcycle.bme.hu/).

We run multiple stochastic simulations for the cell cycle time distribution histograms and related figures (Fig. 4–7). For each simulation, we calculate 50 consecutive cell cycles. We assume that interactions between individual cells are weak and single cells behave independently. In such a case, the investigation of multiple cycles of an individual cell is equivalent to the analysis of a cell population at a given time. This is supported in cell culture systems (i.e., NIH3T3) in which cells do not communicate with each other in terms of the clock.

RESULTS

Circadian regulation of Wee1 results in quantized cell cycles. For initial simulations, it seems natural to start with the MDT of 24 h. The cell cycle synchronizes with the circadian clock regardless of its initial conditions, with an MDT at 24 h (Fig. 2C). A stronger coupling (large k_{w5}'') ensures tighter G2 regulation by inducing high levels of Wee1 (Fig. 2A). As a result, cell division locks into a particular phase of the circadian rhythm (Fig. 2C). Our result is in agreement with the findings that cell divisions frequently occur right after the circadian night (in which mPer and mCry are still high; Hardin, 2004) in different mammalian cell types (Bjarnason et al., 2001).

The MDT of mammalian cell culture varies greatly depending on cell types and growth conditions (i.e., temperature, nutrients, etc.). Hence, we changed the MDT from 16 to 28 h in our simulations and observed the cell cycle time profile over multiple runs of cell division cycles with different coupling strengths. A strong coupling ($k_{w5}'' = 2\ h^{-1}$) results in uneven distribution of cell cycle time (Fig. 3). A periodic influence on *wee1* transcription imposes a delay in G2, depending on the timing of Bmal1:Clk and Wee1 oscillations. Differences in endogenous periods between the 24-h clock and the MDT generate some cycles to entrain close to 24 h and other cycles to be either shorter or longer than 24 h, depending on the MDT (Fig. 3). For example, when the MDT is 20 h, the circadian clock entrains the cell cycle close to 24 h until the birth mass gets too large, which forces a cell to divide with a shorter cycle time even before the rise of Bmal1:Clk and Wee1 (Fig. 3B). This pattern repeats itself every 6 cell cycles at MDT = 20 h or 28 h and every third at MDT = 16 h (Fig. 3A–C). Similar repetitions cannot be observed with weak coupling in our stochastic simulations ($k_{w5}'' = 0.25\ h^{-1}$; Fig. 3D-F). In the absence of any coupling factor ($k_{w5}'' = 0\ h^{-1}$), the two oscillators run with their endogenous periods independently of each other (not shown). The observed pattern with strong coupling is dictated by the least common multiple of the 24-h period and the MDT (Fig. 5C, 5D). This "mode-locking" behavior of two oscillators results in quantized cell cycle times at different MDTs with strong coupling. Figure 4A–C represents histograms with multiple peaks of cell cycle time at MDT = 16, 20, and 28 h, with strong coupling. These multimodal cell cycle distributions show a resemblance to previous experimental results (Klevecz, 1976; Nagoshi et al., 2004). Quantitative comparisons, however, cannot be achieved, because of lack of experimental details. We wish to pursue this in our future work. Weak coupling results in normal distributions of cell cycle times (Fig. 4D–F). Further stochastic simulations are performed with randomly chosen MDTs to investigate cell cycle time across MDTs. This simulation allows us to visualize the distribution patterns of cell cycle time with both strong and weak couplings across a large range of MDTs. Similarly, as shown in Figure 4, the strong coupling results in quantized cycles, whereas the weak coupling reflects normal distribution cycle times from the stochastic modeling (Fig. 5A, 5B). As the MDT deviates from 24 h, the clock-enforced cell cycle goes through repeated cycles of "mode-locking," which create large deviations in cell cycle time. Analysis of the variations in cell cycle time and cell mass agree with experimental data.

The quantized cell cycles with compensatory shorter or longer cell cycle times create smaller or larger cell mass influenced by the circadian clock. Periodic influence of the clock reduces the effect of noise and synchronizes the cell cycle when the MDT is close to 24 h. As the MDT deviates from 24 h, the clock-enforced cell cycle goes through repeated cycles of "mode-locking," which create large deviations of cell cycle time to compensate for differences in cell mass. To measure these deviations, the coefficients of variation (CV = [standard deviation/mean] × 100 [%]) of cell cycle time and cell mass are calculated from 50 cell

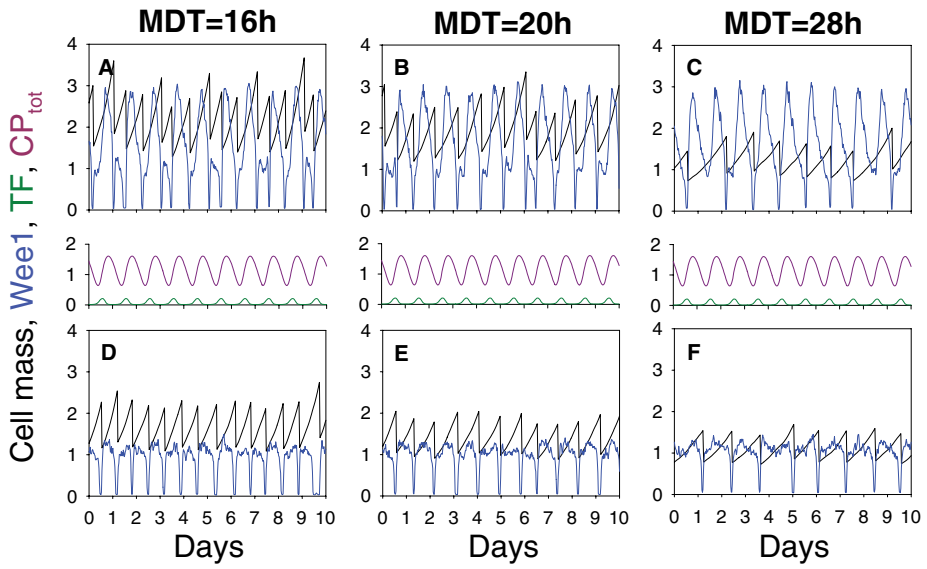

Figure 3. Clock-influenced cell cycle results in uneven distribution of cell cycle time. (A), (B), and (C) represent cell cycle simulations with strong coupling rate ($k_{w5}'' = 2\ h^{-1}$) and the mass doubling time (MDT) at 16 h, 20 h, and 28 h, respectively. Clock-regulated Wee1 (blue) results in variations in sizes and cell cycle times at different MDTs. The black line represents cell mass, which grows exponentially and divides by a factor of 2. Such large deviations are not observed with weak coupling ($k_{w5}'' = 0.25\ h^{-1}$) at MDTs 16 h, 20 h, and 28 h (D–F). The middle panels show a robust 24-h endogenous period of CP_{tot} (purple) and transcription factor (*TF*; green) at various MDTs.

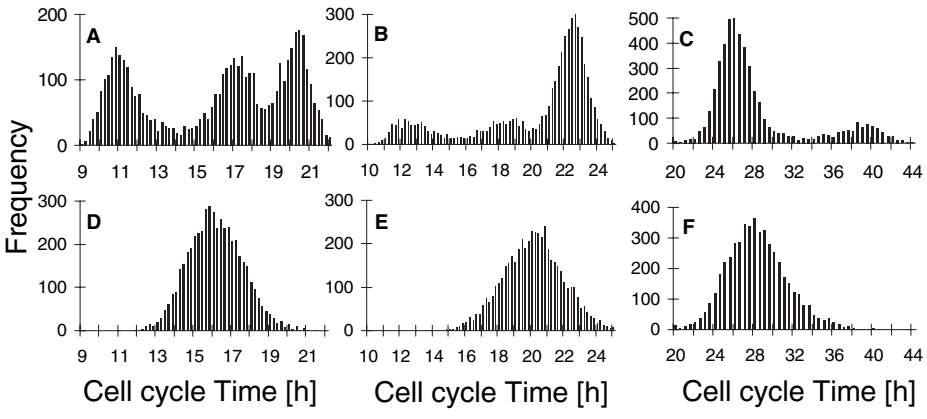

Figure 4. Histogram of cell cycle time distribution at 3 different mass doubling times (MDTs). The *y*-axis represents number of cells going through cell division with a particular cell cycle time. Strong coupling results in multimodal distribution of cell cycle times (A–C), while weak coupling results in normal distribution (D–F) at indicated MDTs (16 h, 20 h, and 28 h). Five thousand cell cycles are analyzed for each plot, which is calculated from 100 simulation runs with 50 consecutive cell cycles.

cycle simulations each, with randomly generated MDTs (Fig. 6). With strong coupling, our simulations show that populations of cells reflect a unique relationship between 2 CVs: the CV of cycle time is roughly twice the CV of cell mass at division, which is in agreement with experimental results (Tyson, 1985; Fig. 6).

The circadian clock contributes to the regulation of cell size control. Cell size control is apparent when smaller or larger cells at birth undergo different durations of growth to reach the critical size for proper cell cycle progression. In other words, it would take less time for large cells at birth to reach the critical cell mass than smaller cells. Experimentally, this phenomenon is reflected by negative correlation (slope of about –1) of net growth throughout the cycle ($mass_{\Delta}$ = mass at division–birth mass) and birth mass ($mass_0$; Sveiczer et al., 1996). To investigate the existence of size control in our model, we studied the relationship between $mass_{\Delta}$ as a function of $mass_0$ from our stochastic simulations of 50 cell cycles each at different MDTs (Fig. 7A, 7B).[1] Cell mass varies greatly depending on different MDTs, as is experimentally shown in yeast (i.e.,

1. We acknowledge that in mammalian system, it is difficult to measure $mass_{\Delta}$ as a function of $mass_0$ because of technical limitations, as it was done in fission yeast. With computational simulations, however, this can be easily measured. This is one of the advantages of computational modeling.

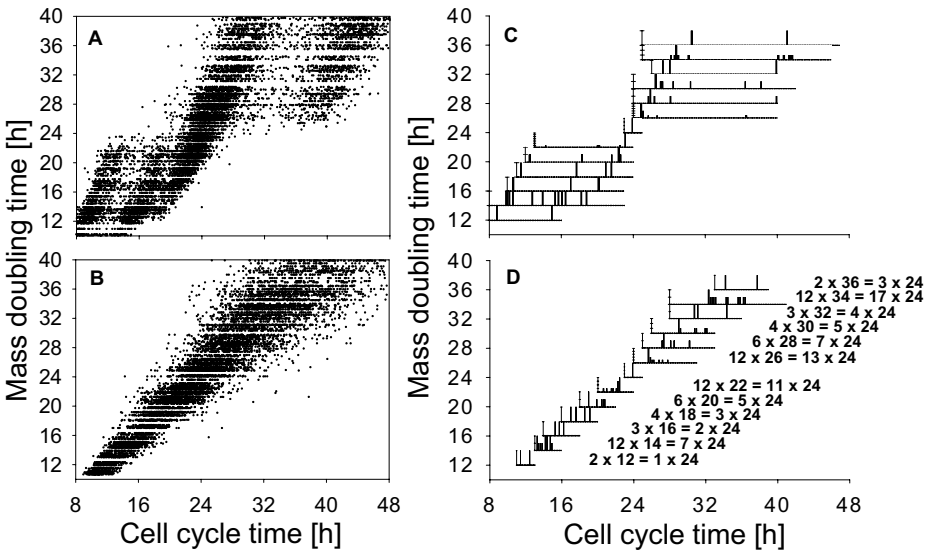

Figure 5. Mode-locked distribution of cell cycle time as a function of mass doubling time (MDT). (A) A cluster of quantized cell cycle populations is observed with a strong coupling in a large range of MDTs. (B) Weak coupling results in normal distribution of cell cycle time (CT) in various MDTs, with the average CT ≈ MDT. About 250 simulation runs are performed in various MDTs, and each simulation calculated 50 cell cycles. (C, D) Deterministic simulations of both strong (C) and weak (D) coupling cause mode-locking. The pattern of cell cycle time repeats with the least common multiple (noted on panel D) of the circadian-imposed 24 h and the MDT. The degree of separation between different cell cycle lengths, however, is very different from strong vs. weak couplings. The weak coupling results in normal distribution of cell cycle time even with mode-locking behavior. The abscissa of each histogram is vertically shifted to the MDT value that is used for the given simulation. Histograms describe distributions of cell cycle lengths depending on periodic repeat sequences. In the deterministic case with zero coupling, we get a simple peak at each MDT at a cycle time = MDT (not shown).

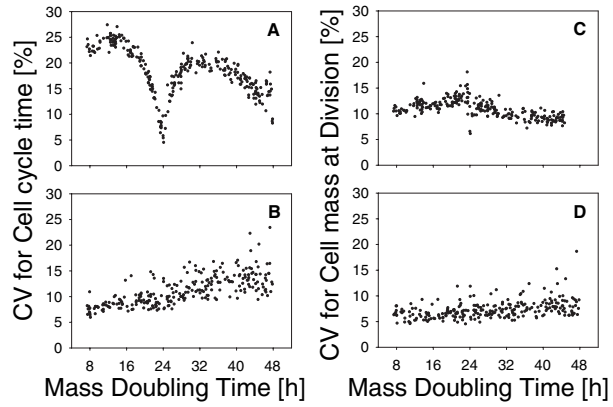

Figure 6. Coefficients of variation of cell cycle time and cell mass as a function of mass doubling time (MDT) at different coupling strengths. Coefficients of variation (CV) of cell cycle length (A, B) and cell mass at division (C, D) are calculated. The CV for cell cycle length is small at a MDT close to 24 h but is large at other MDTs because of the strong influence of the circadian clock (A) compared to the weakly coupled (B) case. The CV for division mass is higher in the strong coupling case (C) than the weak coupling case (D). The CV of cycle time is roughly twice the CV of cell mass at division, which is in agreement with experimental results (Tyson, 1985). Results from zero coupling are identical to the weak coupling data (not shown).

critical cell mass of a cell depends on growth conditions leading to larger cells with rich nutrients [Johnston et al., 1979]). Hence, we categorize our results according to the MDTs. To our surprise, we observe negative correlations with a strong coupling factor in distinct populations of cells when the data are sorted according to the MDTs (Fig. 7A).

The slopes of regression lines (from the previous calculations) as a function of MDT provide relationships between cell size control and different coupling factors (Fig. 7C, 7D). Our stochastic simulations show that weak coupling of the clock with the cell cycle results in no clear correlation between the $mass_{\Delta}$ and the $mass_{0}$ (Fig. 7D). Our simulations with zero coupling are identical to those of weak coupling (not shown). However, we see a general trend of decrease in the slope of regression lines with increasing MDTs because of the innate properties of the cell cycle module as proposed in previous work (Csikasz-Nagy et al., 2006). On the other hand, the strong coupling results in both positive and negative slopes of regression lines, depending on the MDT (Fig. 7C). With strong coupling, cell size control is apparent (slope about –1) when the MDT is either significantly shorter or longer than 24 h. This is because of compensatory cycles in which very large or very small cells undergo short or long cell cycles, as seen in Figure 3 (therefore resulting in quantized cell cycles). The compensatory cycles (hence, resulting cell size control) become apparent when cells experience significant changes in their cell cycle regulatory dynamics by the clock. In other words, the periodic influence of the clock on Wee1 expression perturbs cell cycle dynamics, resulting in cells that are either too large or too small when the MDTs are significantly different from the clock period length. This, in turn, triggers cell size control. Positive slopes of regression lines are observed when the MDTs are close to 24 h, because of "rare" compensatory cycles resulting in loss or gain of cell mass depending on the MDT. For

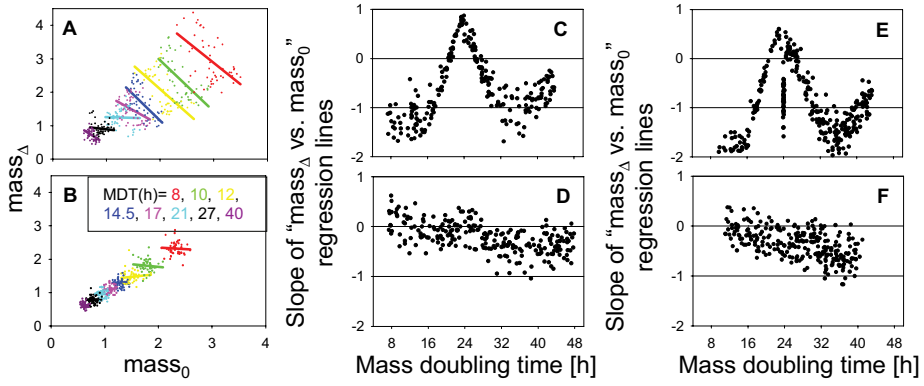

Figure 7. Analysis of critical mass control. (A, B) Growth from cell birth to division (mass$_\Delta$) is plotted as a function of birth mass (mass$_0$) for multiple simulations at different mass doubling times (MDTs). Data points are color coded and clustered according to particular MDTs. Cell size control is reflected when there is a negative correlation (slope of about –1) between mass$_\Delta$ and mass$_0$. Strong coupling results in strict size control when cell masses are either large or small but no apparent correlation at intermediate cell masses (A). Weak coupling (B) shows no clear size control. About 250 simulation runs are calculated at different MDTs. For clear representation, not all data points are displayed on panels (A) and (B), and the legends for both panels are inserted on panel (B). (C, D) Slopes of linear regression lines from (A, B) are plotted as a function of the MDT. Strong coupling results in strict mass control (slope about –1) when the MDTs are either much shorter or longer than 24 h, but size control is not observed when the MDT is close to 24 h (C). Weak coupling shows no apparent mass control (D). (E, F) Similar results are shown with linear growth rate. For these simulations, we change the equation of cell growth by eliminating the mass from the right-hand side of dCycB/dt. Unique slope of regression lines of mass$_\Delta$ vs. mass$_0$ plots are observed with strong coupling as a function of MDT (E), as seen with exponential growth rate (C). The MDT is calculated from the average cell cycle time of 50 cycles.

example, at MDT = 23.8 h, the circadian rhythm synchronizes cell cycles to 24 h. This extra 0.2 h of growth results in a larger mass of individual cells with each additional cell cycle because of exponential growth, until cells undergo compensatory cycles resulting in smaller cells. MDTs of about 20 h and 28 h result in no apparent size control as a consequence of cells constantly losing and gaining cell mass as a population, which balances the slope to zero. Similar results are shown with linear growth rate (Fig. 7E, 7F).

DISCUSSION

Since the early discoveries of circadian clock–gated cell cycles in lower eukaryotes (Edmunds, 1974a, 1974b; Sweeney and Hastings, 1958), numerous molecular findings that connect the cell cycle and circadian clock are now being addressed (Fu et al., 2002; Matsuo et al., 2003). Preliminary screening has shown that there are multiple cell cycle components that oscillate with a period of about 24 h in mouse liver (i.e., CycB1, p55^{Cdc}, Cdc2, CycD1, etc.; Fu et al., 2002; Matsuo et al., 2003). Among many candidates, Wee1 stood out as a strong link based on several facts: (1) both *wee1* mRNA and Wee1 protein cycle with a period of about 24 h, (2) both Wee1 protein and its relative kinase activity showed about 24-h cycles with a delay of 8 h in their peak levels and kinase activities of the PH samples at ZT0 compared to the PH samples at ZT8, and (3) the *wee1* gene contains E-boxes in the 5′ flanking region, where Bmal1:Clk directly regulates *wee1* transcription (Matsuo et al., 2003). We acknowledge that there may be other coupling factors in addition to Wee1 at different checkpoints in the progress of the cell cycle. Furthermore, recent research indicates that this connection may be bidirectional rather than unidirectional. The cell cycle kinase Chk2 phosphorylates a core clock component (i.e., FRQ in *Neurospora crassa* and mPer1 in mice), resulting in DNA damage–dependent reset of the clock (Gery et al., 2006; Pregueiro et al., 2006). The detail of this pathway is still unknown. What we present here, however, is an initiative of computational analysis with a unidirectional link from the circadian clock to the cell cycle via Wee1. In our future computational analysis, we plan to address the following issues: (1) simulations of multiple coupling factors in various checkpoints in cell cycles, (2) use of a comprehensive model of mammalian clock model, (3) effects of cell cycle inhibitors and changes in growth factor levels in the presence of the circadian clock, aimed at better "chronotherapy" (Gardner, 2002; Mormont and Levi, 2003), and (4) cross talk between the cell cycle and circadian clock. At the present moment, we introduce the first coupled mammalian cell cycle and circadian clock model with molecular profiles of both components (Fig. 2–3).

Based on our computational analysis, we report quantized cell cycles when *wee1* transcription is strongly influenced by the circadian clock. This occurs from a "mode-lock" phenomenon that creates various periodic repetitions of cell division cycles with different MDTs. Recently, the mode-lock behavior of cell cycles via periodic external influences (circadian clock in our case) was also studied with a deterministic yeast

cell cycle model (Cross and Siggia, 2005). The authors found that periodically induced Cln2 or Cln3 transcription led to the "mode-locking" of cell division cycles. Based on recent discoveries of a genomewide ultradian respiratory cycle in yeast (Klevecz et al., 2004), it would be interesting to study possible players in this respiratory cycle that may affect the cell division cycle and whether those components influence the cell cycle via Cln2 or Cln3. This in turn may result in quantized cell cycles in yeast. Our results can be tested in both yeast and mammalian cell culture systems. For example, one can compare cell cycle distributions as a function of MDT (our Fig. 5) in the presence and absence of coupling factors (i.e., knock-down of *wee1* in mammalian system) or clock (i.e., knock-out of ultradian clock in yeast [Klevecz et al., 2004] or circadian clock in mammals [Okamura, 2004]).

It is important to note that in 2000, Sveiczer and colleagues mathematically modeled quantized cell cycles in fission yeast double mutant (*wee1^{ts}cdc25*Δ) without assuming ultradian influences (Sveiczer et al., 2000). This double mutant's molecular phenotype (low Wee1 and no Cdc25) abrogates the positive feedback of Cdc2/Cdc13 via Cdc25. In the absence of positive feedback, the system loses bistability and is pushed into a stable oscillatory region with a period much shorter than the MDT (Csikasz-Nagy et al., 2006). In other words, there is a collision of 2 different periods: the MDT and the period set by a stable oscillator. This results in variations in the timing of mitosis entry, which creates quantized cell cycles. This model is significantly different from our model and others (Lloyd and Kippert, 1987) because no external influence (i.e., ultradian cycle) is required to generate quantized cell cycles for the *wee1^{ts}cdc25*Δ double mutant. It will be important to investigate different profiles of quantized cell cycles in both the presence and absence of ultradian cyclic influences in this double mutant. This will enlighten us as to whether an ultradian clock in fission yeast plays a role in cell cycle regulation of the *wee1^{ts}cdc25*Δ double mutant.

In yeast, cell size checkpoints seem to occur at various points along the cell cycle progression. *S. cerevisiae* inspects its size at the G1/S transition, and *Schizosaccharomyces pombe* requires a critical cell size before entry into mitosis (Rupes, 2002). In mammals, however, different results arise from different cell types (Conlon and Raff, 2003; Grebien et al., 2005; Sveiczer et al., 2004; Wells, 2002). For more than 40 years, the existence of cell size control in mammalian cells has been a controversial topic. Here, we report that in mathematical simulations, strong circadian clock regulation on *wee1* transcription triggers cell size control at different MDTs. Cell size control is observed during specific ranges of MDTs when the circadian clock induces periodic perturbations that force the cell cycle out of homeostasis from its dictated MDTs. There is no evidence of mass control with either weak or zero coupling strengths. Qualitatively similar behaviors are observed with both exponential and linear growth types (Fig. 7). In our model, circadian influences on Wee1 introduce cell size control at the G2/M transition. It is possible that there may be additional cell size control at the G1/S transition in the mammalian system as in budding yeast (Rupes, 2002). Interestingly, mammalian cell types that demonstrate cell size control also feature circadian rhythms (i.e., mouse fibroblast [Nagoshi et al., 2004; Tsuchiya et al., 2003] and bone marrow containing erythroid [Chen et al., 2000]), whereas there is no precedent for a functional circadian clock in Rat Schwann cells (where no critical size control has been reported; Conlon et al., 2001) to our knowledge. We acknowledge that the cell size control mechanism may be a complex network within cell cycle regulation. Our simulations suggest that the clock may play an important role in cell size control via Wee1, depending on the MDT. We propose to test quantized cell cycles and cell size control in several ways: (1) observe cell size distribution at different MDTs in mouse fibroblasts that pertain to clock in absence and presence of coupling factors (i.e., Wee1) and (2) if it is feasible, create an inducible system in Rat Schwann cells that creates circadian pulsatile induction of Wee1 and observe the distribution of cell size as a function of the MDT.

APPENDIX A
DIFFERENTIAL EQUATIONS OF THE SIMPLIFIED CIRCADIAN RHYTHM MODULE FOR MAMMALIAN CELLS

Messenger RNA of the clock proteins and Wee1:

$$\frac{d}{dt}M = k_{ms}\frac{TF^n}{J^n + TF^n} - k_{md}M \tag{1}$$

Monomer clock proteins (mPer or mCry):

$$\frac{d}{dt}CP = k_{cps}M - k_{cpd}CP - 2k_aCP^2 + 2k_dCP_2 - k_{p1}\frac{CP}{J_p + CP_{tot}} \tag{2}$$

Dimer form of clock proteins (mPer/mPer, mPer/mCry, or mCry/mCry):

$$\frac{d}{dt}CP_2 = k_a CP^2 - k_d CP_2 - k_{cp2d} CP_2 + k_{icd} IC - k_{ica} CP_2 \cdot TF - k_{p2} \frac{CP_2}{J_p + CP_{tot}} \quad (3)$$

Transcription factor (Bmal1:Clk) of the clock proteins' mRNA:

$$\frac{d}{dt}TF = k_{cp2d} IC + k_{icd} IC - k_{ica} TF \cdot CP_2 + k_{p2} \frac{IC}{J_p + CP_{tot}} \quad (4)$$

Inactive complex of clock dimers and transcription factor:

$$IC = TF_{tot} - TF \quad (5)$$

Total amount of clock proteins:

$$CP_{tot} = CP + 2CP_2 + 2IC$$

Rate constants (h^{-1}):
$k_{ms} = 1$, $k_{md} = 0.1$, $k_{cps} = 0.5$, $k_{cpd} = 0.525$, $k_a = 100$, $k_d = 0.01$, $k_{cp2d} = 0.0525$, $k_{icd} = 0.01$, $k_{ica} = 20$, $k_{p1} = 10$, $k_{p2} = 0.1$

Dimensionless constants:
$TF_{tot} = 0.5$, $Jp = 0.05$, $J = 0.3$, $n = 2$

APPENDIX B
DIFFERENTIAL EQUATIONS FOR THE EXTENSION OF THE NOVAK AND TYSON MODEL (2004)

Extensions to the equation of Cdk1/CycB:

$$\frac{d}{dt}CycB = eps \cdot \left(k_1' + \frac{k_1 \cdot (CycB/J_1)^2}{1 + (CycB/J_1)^2} \right) \cdot mass - V2 \cdot CycB + (k_{cdc25}' + k_{cdc25}'' \cdot Cdc25a) \cdot CycBP - (k_{wee1}' + k_{Wee1}'' \cdot Wee1) \cdot CycB \quad (6)$$

Phosphorylated form of Cdk1/CycB:

$$\frac{d}{dt}CycBP = (k_{wee1}' + k_{wee1}'' Wee1) \cdot CycB - (k_{cdc25}' + k_{cdc25}'' \cdot Cdc25a) \cdot CycBP - V2 \cdot CycBP \quad (7)$$

Active form of Wee1 kinase:

$$\frac{d}{dt}Wee1 = (k_{w5}' + k_{w5}'' \cdot M) - \frac{(k_{w2}' + k_{w2}'' \cdot CycB) \cdot Wee1}{J_{w2} + Wee1} + k_{w1} \frac{Wee1P}{J_{w1} + Wee1P} - k_{w6} \cdot Wee1 \quad (8)$$

Inactive form of Wee1:

$$\frac{d}{dt}Wee1P = \frac{(k_{w2}' + k_{w2}'' \cdot CycB) \cdot Wee1}{J_{w2} + Wee1} - k_{w1} \frac{Wee1P}{J_{w1} + Wee1P} - k_{wd} \cdot Wee1P \quad (9)$$

Active form of Cdc25:

$$\frac{d}{dt}Cdc25a = \frac{(k_{c3}' + k_{c3}'' \cdot CycB) \cdot (1 - Cdc25a)}{J_{c3} + (1 - Cdc25a)} - \frac{k_{c4} \cdot Cdc25a}{J_{c4} + Cdc25a} \quad (10)$$

The cell divides (mass is halved) when CycB crosses 0.2 from the above.

Rate constants (h^{-1}):
$k_{cdc25}' = 0.05$, $k_{cdc25}'' = 10$, $k_{c3}' = 0.1$, $k_{c3}'' = 1$, $k_{c4} = 0.4$, $k_{w1} = 0.4$, $k_{wee1}' = 0.08$, $k_{wee1}'' = 10$, $k_{w2}' = 0.2$, $k_{w2}'' = 2$, $k_{w6} = 1$, $k_{wd} = 1$, (k_{w5}' and k_{w5}'' in Appendix C)

Dimensionless constants:
$J_{c3} = 0.05$, $J_{c4} = 0.05$, $J_{w2} = 0.2$, $J_{w1} = 0.2$

The rest of the parameters are same as in the Novak–Tyson model (Novak and Tyson, 2004).

APPENDIX C
THE VALUES OF THE COUPLING PARAMETERS[a]

	k_{w5}' (h^{-1})	k_{w5}'' (h^{-1})
"Zero" coupling	1.00	0.00
"Weak" coupling	1.00	0.25
"Strong" coupling	0.25	2.00

a. To keep the average cell size similar, we assume the cell cycle has stronger influence on Wee1 when it is weakly dependent on the circadian clock. Wee1 levels have large influence on cell size, and we want to simulate normal distribution of cell size.

ACKNOWLEDGEMENTS

We are grateful for discussions and useful comments from J. J. Tyson, B. Novak, J. C. Dunlap, J. J. Loros, A. Sveiczer, L. Calzone, and K. Chen. This research was supported by the OTKA (F-60414), The Microsoft Research–University of Trento Centre for Computational and Systems Biology (FIRB project RBPR0523C3) to ACN, the European Commission (COMBIO: LSHG-CT-2004-503568 to Bela Novak), the National Academies Keck Futures Initiative

Signaling Grant (CIH), and the NIH (GM34985 and MH44651 to Jay C. Dunlap).

REFERENCES

Bjarnason GA, Jordan RC, Wood PA, Li Q, Lincoln DW, Sothern RB, Hrushesky WJ, and Ben-David Y (2001) Circadian expression of clock genes in human oral mucosa and skin: association with specific cell-cycle phases. Am J Pathol 158:1793-1801.

Chen KC, Calzone L, Csikasz-Nagy A, Cross FR, Novak B, and Tyson JJ (2004) Integrative analysis of cell cycle control in budding yeast. Mol Biol Cell 15:3841-3862.

Chen YG, Mantalaris A, Bourne P, Keng P, and Wu JH (2000) Expression of mPer1 and mPer2, two mammalian clock genes, in murine bone marrow. Biochem Biophys Res Commun 276:724-728.

Chow JPH, Siu WY, Ho HTB, Ma KHT, Ho CC, and Poon RYC (2003) Differential contribution of inhibitory phosphorylation of CDC2 and CDK2 for unperturbed cell cycle control and DNA integrity checkpoints. J Biol Chem 278:40815-40828.

Conlon I and Raff M (2003) Differences in the way a mammalian cell and yeast cells coordinate cell growth and cell-cycle progression. J Biol 2:7.

Conlon IJ, Dunn GA, Mudge AW, and Raff MC (2001) Extracellular control of cell size. Nat Cell Biol 3:918-921.

Cross FR and Siggia ED (2005) Mode locking the cell cycle. Phys Rev E Stat Nonlin Soft Matter Phys 72:021910.

Csikasz-Nagy A, Battogtokh D, Chen KC, Novak B, and Tyson JJ (2006) Analysis of a generic model of eukaryotic cell-cycle regulation. Biophys J 90:4361-4379.

Dolznig H, Grebien F, Sauer T, Beug H, and Mullner EW (2004) Evidence for a size-sensing mechanism in animal cells. Nat Cell Biol 6:899-905.

Dunlap JC (1999) Molecular bases for circadian clocks. Cell 96:271-290.

Edmunds LN Jr (1974a) Circadian clock control of the cell developmental cycle in synchronized cultures of Euglena. In *Mechanisms of Regulation of Plant Growth*, RL Bieleski, AR Ferguson, and MM Cresswell, eds, pp 287-297, The Royal Society of New Zealand, Wellington.

Edmunds LN Jr (1974b) Phasing effects of light on cell division in exponentially increasing cultures of Tetrahymena grown at low temperatures. Exp Cell Res 83:367-379.

Ermentrout B (2002) *Simulating, Analyzing, and Animating Dynamical Systems*, SIAM, Philadelphia.

Forger DB and Peskin CS (2005) Stochastic simulation of the mammalian circadian clock. Proc Natl Acad Sci U S A 102:321-324.

Fu L, Pelicano H, Liu J, Huang P, and Lee C (2002) The circadian gene Period2 plays an important role in tumor suppression and DNA damage response in vivo. Cell 111:41-50.

Gardner SN (2002) Cell cycle phase-specific chemotherapy: computational methods for guiding treatment. Cell Cycle 1:369-374.

Gery S, Komatsu N, Baldjyan L, Yu A, Koo D, and Koeffler HP (2006) The circadian gene per1 plays an important role in cell growth and DNA damage control in human cancer cells. Mol Cell 22:375-382.

Gonze D, Halloy J, and Goldbeter A (2002) Robustness of circadian rhythms with respect to molecular noise. Proc Natl Acad Sci U S A 99:673-678.

Grebien F, Dolznig H, Beug H, and Mullner EW (2005) Cell size control: new evidence for a general mechanism. Cell Cycle 4:418-421.

Hardin PE (2004) Transcription regulation within the circadian clock: the E-box and beyond. J Biol Rhythms 19:348-360.

Hong CI, Conrad E, and Tyson JJ (2007) A proposal for robust temperature compensation of circadian rhythms. Proc Natl Acad Sci U S A 104:1195-1200.

Johnston GC, Ehrhardt CW, Lorincz A, and Carter BLA (1979) Regulation of cell size in the yeast *Saccharomyces cerevisiae*. J Bacteriol 137:1-5.

Kastan MB and Bartek J (2004) Cell-cycle checkpoints and cancer. Nature 432:316-323.

Killander D and Zetterberg A (1965) A quantitative cytochemical investigation of the relationship between cell mass and initiation of DNA synthesis in mouse fibroblast in vitro. Exp Cell Res 40:12-20.

Klevecz RR (1976) Quantized generation time in mammalian cells as an expression of the cellular clock. Proc Natl Acad Sci U S A 73:4012-4016.

Klevecz RR, Bolen J, Forrest G, and Murray DB (2004) A genomewide oscillation in transcription gates DNA replication and cell cycle. Proc Natl Acad Sci U S A 101:1200-1205.

Lloyd D and Kippert F (1987) A temperature-compensated ultradian clock explains temperature-dependent quantal cell cycle times. Symp Soc Exp Biol 41:135-155.

Lloyd D and Volkov EI (1990) Quantized cell cycle times: interaction between a relaxation oscillator and ultradian clock pulses. Biosystems 23:305-310.

Matsuo T, Yamaguchi S, Mitsui S, Emi A, Shimoda F, and Okamura H (2003) Control mechanism of the circadian clock for timing of cell division in vivo. Science 302:255-259.

Mori T, Binder B, and Johnson CH (1996) Circadian gating of cell division in cyanobacteria growing with average doubling times of less than 24 hours. Proc Natl Acad Sci U S A 93:10183-10188.

Mormont MC and Levi F (2003) Cancer chronotherapy: principles, applications, and perspectives. Cancer 97:155-169.

Morohashi M, Winn AE, Borisuk MT, Bolouri H, Doyle J, and Kitano H (2002) Robustness as a measure of plausibility in models of biochemical networks. J Theor Biol 216:19-30.

Nagoshi E, Saini C, Bauer C, Laroche T, Naef F, and Schibler U (2004) Circadian gene expression in individual fibroblasts: cell-autonomous and self-sustained oscillators pass time to daughter cells. Cell 119:693-705.

Novak B and Tyson JJ (2004) A model for restriction point control of the mammalian cell cycle. J Theor Biol 230:563-579.

Nurse P (1990) Universal control mechanism regulating onset of M-phase. Nature 344:503-508.

Nurse P (2000) A long twentieth century of the cell cycle and beyond. Cell 100:71-78.

Okamura H (2004) Clock genes in cell clocks: roles, actions, and mysteries. J Biol Rhythms 19:388-399.

Pregueiro AM, Liu Q, Baker CL, Dunlap JC, and Loros JJ (2006) The Neurospora checkpoint kinase 2: a regulatory link between the circadian and cell cycles. Science 313:644-649.

Rupes I (2002) Checking cell size in yeast. Trends Genet 18:479-485.

Sherr CJ (1996) Cancer cell cycles. Science 274:1672-1677.

Steuer R (2004) Effects of stochasticity in models of the cell cycle: from quantized cycle times to noise-induced oscillations. J Theor Biol 228:293-301.

Sveiczer A, Csikasz-Nagy A, Gyorffy B, Tyson JJ, and Novak B (2000) Modeling the fission yeast cell cycle: quantized cycle times in wee1- cdc25Delta mutant cells. Proc Natl Acad Sci U S A 97:7865-7870.

Sveiczer A, Novak B, and Mitchison JM (1996) The size control of fission yeast revisited. J Cell Sci 109:2947-2957.

Sveiczer A, Novak B, and Mitchison JM (1999) Mitotic control in the absence of cdc25 mitotic inducer in fission yeast. J Cell Sci 112:1085-1092.

Sveiczer A, Novak B, and Mitchison JM (2004) Size control in growing yeast and mammalian cells. Theoretical Biology and Medical Modelling 1:12.

Sweeney BM and Hastings J (1958) Rhythmic cell division in populations of Gonyaulax polyedra. J Protozool 5:217-224.

Tsuchiya Y, Akashi M, and Nishida E (2003) Temperature compensation and temperature resetting of circadian rhythms in mammalian cultured fibroblasts. Genes Cells 8:713-720.

Tyson JJ (1985) The coordination of cell growth and division—intentional or incidental? Bioessays 2:72-77.

Tyson JJ, Hong CI, Thron CD, and Novak B (1999) A simple model of circadian rhythms based on dimerization and proteolysis of PER and TIM. Biophys J 77:2411-2417.

van Kampen NG (1981) *Stochastic Processes in Physics and Chemistry*, North-Holland Publishing Company, Amsterdam.

Vanselow K, Vanselow JT, Westermark PO, Reischl S, Maier B, Korte T, Herrmann A, Herzel H, Schlosser A, and Kramer A (2006) Differential effects of PER2 phosphorylation: molecular basis for the human familial advanced sleep phase syndrome (FASPS). Genes Dev 20:2660-2672.

Wells W (2002) Does size matter? J Cell Biol 158:1156-1159.

Welsh DK, Yoo SH, Liu AC, Takahashi JS, and Kay SA (2004) Bioluminescence imaging of individual fibroblasts reveals persistent, independently phased circadian rhythms of clock gene expression. Curr Biol 14:2289-2295.

Yamaguchi S, Isejima H, Matsuo T, Okura R, Yagita K, Kobayashi M, and Okamura H (2003) Synchronization of cellular clocks in the suprachiasmatic nucleus. Science 302:1408-1412.

Zetterberg A and Larsson O (1995) Cell cycle progression and growth in mammalian cells: kinetic aspects of transition events. In *Cell Cycle Control*, C Hutchison and DM Glover, eds, pp 206-227, Oxford University Press, Oxford, UK.

dc_836_14

7.3 A hasadó élesztő növekedési zónáinak szabályozása a sejtciklus alatt

Csikász-Nagy A., Győrffy B., Alt W., Tyson J.J. & Novák, B. (2008) Spatial controls for growth zone formation during the fission yeast cell cycle. *Yeast*, **25:** 59–69.

Impakt faktor: 2.622

Yeast
Yeast 2008; **25**: 59–69.
Published online 24 October 2007 in Wiley InterScience
(www.interscience.wiley.com) **DOI:** 10.1002/yea.1571

Research Article

Spatial controls for growth zone formation during the fission yeast cell cycle

Attila Csikász-Nagy[1,2], Béla Győrffy[1], Wolfgang Alt[3], John J. Tyson[4] and Béla Novák[1,5]*

[1] *Materials Structure and Modelling Research Group of the Hungarian Academy of Sciences and Department of Applied Biotechnology and Food Science, Budapest University of Technology and Economics, Gellért tér 4, H-1521 Budapest, Hungary*
[2] *The Microsoft Research-University of Trento Centre for Computational and Systems Biology, Piazza Manci 17, Povo, Trento 38100, Italy*
[3] *Department of Theoretical Biology, Mathematics and Natural Science Faculty, University of Bonn, Kirschallee 1, 53115 Bonn, Germany*
[4] *Department of Biological Sciences, Virginia Polytechnic Institute and State University, Blacksburg, VA 24061-0406, USA*
[5] *Oxford Centre for Integrative Systems Biology, University of Oxford, South Parks Road, Oxford OX1 3QU, UK*

*Correspondence to:
Béla Novák, Oxford Centre for Integrative Systems Biology, University of Oxford, South Parks Road, Oxford OX1 3QU, UK.
E-mail:
bela.novak@bioch.ox.ac.uk

Received: 17 April 2007
Accepted: 18 September 2007

Abstract

Because of its regular shape, fission yeast is becoming an increasingly important organism in the study of cellular morphogenesis. Genetic experiments with mutants and drug treatment studies with wild-type cells have revealed the importance of microtubules in controlling new growth zone formation. It is believed that microtubules exert this role by delivering to cell ends a 'dynamic landmark' protein, tea1p, which promotes actin polymerization and growth zone formation. Here we present a simple model for fission yeast morphogenesis that describes the interplay between these two cytoskeletal elements. An essential assumption of the model is that actin polymerization is a self-reinforcing process: filamentous actin promotes its own formation from globular actin subunits via regulatory molecules. In our model, microtubules stimulate actin polymerization by delivering a component of the autocatalytic actin-assembly feedback loop (not by delivering a *de novo* inducer of actin polymerization). We show that the model captures all the characteristic features of polarized growth in fission yeast during normal mitotic cycles. We categorize the types of growth patterns that can exist in the model and show that they correspond to the major classes of morphogenetic mutants (monopolar, orb, banana and tea). Based on these results, we propose that fission yeast cells have specific size ranges in which they can exhibit two or more different stable patterns of growth. Copyright © 2007 John Wiley & Sons, Ltd.

Keywords: mathematical modelling; pattern formation; reaction–diffusion–convection equation; actin polymerization; microtubules

Introduction

A fundamental goal of present-day molecular cell biology is to understand how asymmetry (polarity) is generated at the cellular level. One well-defined example of cellular asymmetry is polarized growth. Fission yeast, *Schizosaccharomyces pombe*, proved to be an excellent model organism for the study of cellular morphogenesis because of its regular cylindrical shape (Chang, 2001; Hayles and Nurse, 2001). Growth of wild-type fission yeast cells is always polarized, but it changes in a characteristic way during the cell cycle (Mitchison and Nurse, 1985). A newly born wild-type cell initiates polarized growth at one end only (monopolar growth), which is always the 'old end' (not the end produced by the latest cell division). Later, in phase G_2 of the cell cycle, cells switch to bipolar growth by activating cell growth at their 'new end' [new end take-off (NETO); Mitchison and Nurse, 1985]. Finally, at mitosis, growth ceases at both ends and the cell makes a septum at its midline.

All instances of polarized cell growth are associated with localized actin polymerization (Marks and Hyams, 1985). Just as in budding yeast, F-actin forms two types of structures — cables and patches. In budding yeast, the site of polarized actin formation, which results in bud formation, is independent of microtubules (Irazoqui and Lew, 2004). In contrast, in fission yeast, many genetic experiments and drug treatment studies suggest that localization of actin polymerization and polarized growth is controlled by interphase microtubules (Mata and Nurse, 1997; Sawin and Nurse, 1998; Verde *et al*., 1995). During most of the cell cycle, microtubules form an antiparallel array along the long axis of the cell, having their plus ends at cell tips. This arrangement of microtubules is explained by their localized catastrophes at cell tips (Brunner and Nurse, 2000). Microtubular motors (such as tea2p) deliver proteins along microtubules, which are abruptly released when the microtubules undergo catastrophe at cell tips (Browning *et al*., 2000). As a consequence of this microtubular transport (convection), these cargo molecules become concentrated around the plus ends of the microtubules, i.e. at the cell tips. Tea1p, the first protein discovered with this property (Behrens and Nurse, 2002; Mata and Nurse, 1997), is a cell end marker for fission yeast, because it appears at both cell ends early in the cycle (even at the new end, before it starts to grow).

Tea1p can be found at cell ends in a large complex (called a polarisome) with one of the fission yeast actin-nucleator formins (for3p), together with tea4p (tea1p — for3p linker), bud6p and sla2p (actin-binding proteins) and possibly some other polarization regulator molecules, such as mod5p, pom1p, tea3p (Arellano *et al*., 2002; Bahler and Pringle, 1998; Castagnetti *et al*., 2005; Feierbach and Chang, 2001; Glynn *et al*., 2001; Martin *et al*., 2005; Niccoli *et al*., 2003; Snaith *et al*., 2005; Snaith and Sawin, 2003). Even more, the localization of most (if not all) of these molecules is tea1p-dependent, and some of these molecules are responsible for the formation of actin cables, which are thought to drive localized cell growth. This suggests that tea1p is the molecule that 'couples' microtubules to the actin cytoskeleton and new growth zone formation.

However, neither microtubules nor tea1p are required for the establishment and maintenance of polarized growth. *tea1Δ* mutants show polarized growth (Mata and Nurse, 1997), but they have only one growth zone (NETO defect), which in a few cells is perpendicular to the long axis (forming T-shaped, branched cells). The fact that tea1p is not required for polarized growth, but seems to be associated with normal localization of polarized growth, has been explained by assuming that tea1p is a dynamically distributed landmark protein (Hayles and Nurse, 2001). Landmark proteins, whether dynamic or historic, determine the site of polarized growth but are not required for the growth process itself. Historic landmarks, as in budding yeast, are laid down at specific positions during one cell cycle to determine sites of polarized growth in the next cell cycle (Irazoqui and Lew, 2004). Historic landmarks are not repositioned over time. What are called dynamic landmarks, on the other hand, are laid down by dynamic processes of convection and diffusion, and can be repositioned in response to changing conditions.

Our aim in this article is to provide a conceptual framework for understanding how the interaction between microtubules and actin filaments determines features of polarized growth in fission yeast cells. We present a simple mathematical model that takes into account tea1p transport to cell tips and autocatalysis in actin polymerization. The model can simulate growth pattern changes for drug treatments that interfere with microtubules and actin polymerization. The model predicts the coexistence of different growth patterns at particular cell sizes, and this coexistence can be revealed by perturbation of stable growth zones.

Materials and methods

Our system of partial differential equations can be solved numerically by dividing the cell into small compartments ($i = 1, 2, \ldots, n$) of length h. We found that 40 compartments gave a sufficiently fine resolution for our simulations. The length of a newborn cell is 8 μm, so initially $h = 0.2$ μm (for $n = 40$). Total cell length is simply $L = n \cdot h$, and we assume that the rate of increase of cell length is exponential and new cell wall material is produced in each compartment:

$$\frac{dh}{dt} = \mu \cdot h \qquad (1)$$

DOI: 10.1002/yea

We chose $\mu = 0.004621\ \text{min}^{-1}$ in order to have a mass doubling time of 150 min.

There are other ways to handle the discretization of growth in a reaction–diffusion system (Crampin *et al*., 2002; Murray, 2003) but, because the length change in our simulations is not extreme and the cell wall material incorporated at the cell tips is produced everywhere inside the cell, our treatment by uniform compartmentalization is adequate.

Let y_i be the concentration of component Y in the ith compartment; then the diffusion term is approximated by the standard central difference scheme:

$$\frac{\partial^2 y_i}{\partial x^2} \cong \frac{y_{i+1} - 2 \cdot y_i + y_{i-1}}{h^2} \tag{2}$$

At the ends of the cell, we set $y_0 = y_1$ and $y_{n+1} = y_n$ in order to model no-flux boundary conditions. Convection of U is approximated by the standard upstream difference scheme:

$$v_u \frac{\partial u_i}{\partial x} \cong v_u \frac{u_j - u_i}{h} \tag{3}$$

In interphase cells, the microtubules are arranged so that $j = i - 1$ for the right half of the cell, and $j = i + 1$ for the left half. A more detailed explanation of the equations and simulations can be found on our webpage (**http://www.cellcycle.bme.hu/morphopaper/**).

The range of stability of computed growth patterns was determined as follows: a simulation was initiated from a particular stable pattern and cell length was continuously and slowly increased (or decreased) until the recorded stable growth pattern disappeared.

Results

Microtubule-created convection field provides a dynamic landmark

If polarized growth is initiated by polarized landmark molecules, then how do the landmarks became asymmetrically distributed in a cell? In the case of a dynamic landmark, such as tea1p, the answer to this question requires an understanding of how microtubule plus ends get concentrated at cell tips. We do not want to deal here with this problem. Instead, we assume that microtubules find cell ends and, as a consequence, set up a convection field for molecules such as tea1p. For dynamic landmark protein U ('unspecified'; perhaps tea1p) that is freely diffusing in the cytoplasm (diffusion constant D_u) and also transported along microtubules (with velocity v_u), the concentration $u(x, t)$ changes in space and time according to a reaction–diffusion–convection equation:

$$\frac{\partial u}{\partial t} = (k_{su} - k_{du} u) + D_u \frac{\partial^2 u}{\partial x^2} + v_u \cdot \frac{\partial u}{\partial x} - \frac{u}{h} \frac{\partial h}{\partial t} \tag{4}$$

In words, the time rate of change of concentration = chemical reaction rates + diffusion + convection − dilution. Because fission yeast cells have a regular cylindrical shape, we can reduce the problem to one spatial dimension. We will discretize total cell length L into n small boxes of length h. The last term in equation 4 represents dilution of chemical concentrations as the cell grows. We assume that the rate of synthesis of U is constant (k_{su}) and degradation follows first-order kinetics.

Spontaneous symmetry breaking

Since a growth zone can be formed even without microtubules or tea1p, fission yeast cells must have an underlying mechanism to initiate polarized growth. Two extreme possibilities can be foreseen. In the absence of tea1p or microtubules, cells may use historical landmarks (as do budding yeast cells) or they may rely on spontaneous symmetry-breaking mechanisms (as do budding yeast mutants, when the genes encoding historical landmark proteins are deleted) (Chant and Herskowitz, 1991). Whatever the mechanism of this tea1p- and microtubule-independent polarized growth, it must provide an explanation for the low penetrance of these phenotypes (most of the cells have normal shape and only few of them are branched). The historical landmark hypothesis cannot explain the existence of branched cells, because the middle of the cell has no previous growth history. Therefore, to address these issues, we consider the possibility that a spontaneous symmetry-breaking mechanism is operating in *tea1Δ* mutants.

In budding yeast there is strong experimental evidence for such a mechanism, which results in random bud-site selection (Chant and Herskowitz, 1991; Wedlich-Soldner *et al*., 2003). According to

theoretical studies on pattern formation, positive feedback is a necessary requirement for spontaneous symmetry breaking in reaction–diffusion systems (Meinhardt and Gierer, 2000). Experiments with budding yeast suggest that more than one such a positive feedback mechanism may be operating (Wedlich-Soldner *et al.*, 2003). One mechanism works upstream of actin polymerization, on Cdc42 activation, and it requires the Bem1 scaffold protein (Irazoqui and Lew, 2004). The other positive feedback involves actin cable formation and an increase in Cdc42 level at the site of polarization (Wedlich-Soldner *et al.*, 2003). A second necessary requirement for spontaneous symmetry breaking is that the positive feedback produces a fast-diffusing inhibitor (activator–inhibitor model) or consumes a fast-diffusing substrate (substrate-depletion model) (Meinhardt, 1995).

Although the polarity-determining molecules are conserved between the two yeasts, the exact mechanisms for generating polarity are not certain in either of them (Chang and Peter, 2003; Sohrmann and Peter, 2003). We use two generic equations to describe this pattern formation system. We assume that a rapidly diffusing substrate (G) is converted into a slowly diffusing polymer (F) by an autocatalytic reaction (positive feedback). We assume that the concentrations, $G(x,t)$ and $F(x,t)$, change in an infinitesimal volume of the cell according to the following reaction–diffusion equations:

$$\frac{\partial G}{\partial t} = (k_s - k_d G - (k_3' + k_3'' F^2) \cdot G + k_4 F) + D_G \frac{\partial^2 G}{\partial x^2} - \frac{G}{h}\frac{\partial h}{\partial t} \quad (5)$$

$$\frac{\partial F}{\partial t} = ((k_3' + k_3'' F^2) \cdot G - k_4 F - k_d F) + D_F \frac{\partial^2 F}{\partial x^2} - \frac{F}{h}\frac{\partial h}{\partial t} \quad (6)$$

We are purposefully vague about the identities of G and F, but perfectly reasonable candidates are G-actin monomers and F-actin filaments. In equations 5 and 6, k_3' represents the rate of *de novo* polymerization, and k_3'' is the rate constant for the autocatalytic step, which we assume to be quadratically dependent on F (more-than-linear rate of autocatalysis is a third requirement for spontaneous symmetry breaking in reaction–diffusion models of this sort).

Although the transport coefficients of G actin and tea1p can be estimated from experiments (see Table 1), the rate constants in our model have not been directly measured. We have chosen reasonable values for these constants that are consistent with observed behaviour of growth zones (e.g. NETO characteristics) of wild-type cells. The phenotypes of mutant cells were not used to fit the rate constants.

The effect of landmark on spontaneous pattern formation

Equations 5 and 6 can induce spatial inhomogeneity from an initial homogenous state if the rates of chemical reactions and diffusion satisfy certain conditions (see Meinhardt, 1982; Murray, 2003) and the cell is large enough. However, the exact position of an excitation zone (polarized area) will be dependent on parameter values (diffusion constants and reaction rates).

As mentioned earlier, microtubules in fission yeast deliver a dynamic landmark protein (tea1p) to the end of the cell, where it promotes growth zone formation. The role of tea1p at cell tips is to localize components of the polarisome (bud6p, for3p, sla2p, tea4p) there, with some help from mod5p, tea3p and pom1p (Martin and Chang, 2003). Because of the current lack of comprehensive knowledge of polarisome formation (Feierbach *et al.*, 2004; Sheu *et al.*, 1998), we do not want to go into details of these interactions. We assume that tea1p can regulate actin polymerization (through neglected intermediates). This means that our u variable of equation 4 follows the behaviour of the microtubule-transported protein, tea1p, but also participates in actin polymerization, as for3p (Feierbach and Chang, 2001; Mata and Nurse, 1997).

With this simplification we can easily couple the microtubule-transported effectors with actin polymerization if we introduce u as an activator of polymerization in equations 5 and 6. The first obvious question is: how does the landmark protein influence the actin polymerization mechanism? Two possibilities arise. The joint landmark–polarisome molecule (U) either provides an initial bias by increasing the rate of *de novo* polymerization (k_3'), or it increases the rate of autocatalytic polymerization of F (k_3'').

The case of an initial bias to the pattern formation mechanism is considered in Figure 3A.

DOI: 10.1002/yea

Table 1. Parameters and their effects on growth patterns

Parameter	Description	Effect of decrease			Effect of increase		Experimental facts and comments
		0	10-fold	Two-fold	Two-fold	10-fold	
$k_s = 0.1\ min^{-1}$	Actin synthesis rate	Not growing	Not growing	NETO mutant	Advanced NETO	Advanced NETO	Actin is created in monomer form
$k_d = 0.05\ min^{-1}$	Actin degradation rate	Bipolar	Bipolar	Advanced NETO	NETO mutant	Not growing	Actin is degraded from both forms
$D_g = 120\ \mu m^2/min$	Actin monomer diffusion constant	Orb mutant	Bipolar	Advanced NETO	NETO mutant	NETO mutant	~186 μm^2/ min (McGrath *et al.*, 1998) 6–6000 μm^2/ min, depending on crowding (Dauty and Verkman, 2004)
$D_f = 1\ \mu m^2/min$	Actin filament diffusion constant	NETO mutant	NETO mutant	Delayed NETO	Advanced NETO	Bipolar	Must be much smaller than monomer diffusion
$k_3' = 6\ min^{-1}$	Background polymerization rate	NETO mutant	NETO mutant	Delayed NETO	Advanced NETO	Bipolar	Set to 0 to simulate LatA or LatB treatment
$k_3'' = 8\ min^{-1}$	Autocatalytic polymerization rate	Orb mutant	NETO mutant	Delayed NETO	Advanced NETO	Bipolar	Set to 0 to simulate LatA or LatB treatment
$k_4 = 5\ min^{-1}$	Actin depolymerization rate	Orb mutant	Bipolar	Advanced NETO	NETO mutant	NETO mutant	
$k_{su} = 0.05\ min^{-1}$	*u* Synthesis rate	Orb mutant	NETO mutant	Delayed NETO	Advanced NETO	Bipolar	
$k_{du} = 0.05\ min^{-1}$	*u* Degradation rate	Advanced NETO	Advanced NETO	Advanced NETO	Delayed NETO	NETO mutant	
$v_u = 2\ \mu m/min$	*u* Convection rate	NETO mutant	NETO mutant	Delayed NETO	Advanced NETO	Bipolar	tea I p transport rate: 3.6 ± 1 μm/ min (Behrens and Nurse, 2002)
$D_u = 0.5\ \mu m^2/min$	*u* Diffusion constant	Bipolar	Advanced NETO	Advanced NETO	Delayed NETO	NETO mutant	*u* represents tea I p, but also other members of polarisome, in any case it does not diffuse very rapidly because it binds to immobile structures, either to microtubules or to the polarisome

The concentrations (*G*, *F* and *u*) are dimensionless variables so the rate constants of the reactions are all min^{-1}. The diffusion and convection rates are consistent with experimental results. Protein synthesis is assumed to occur uniformly throughout the cell.
NETO mutant-cannot induce NETO for cell size <15 μm; Orb mutant-actin polymerization becomes isotropic; Bipolar-wide growth zones are initiated at both ends at the size of small newborn cells.

DOI: 10.1002/yea

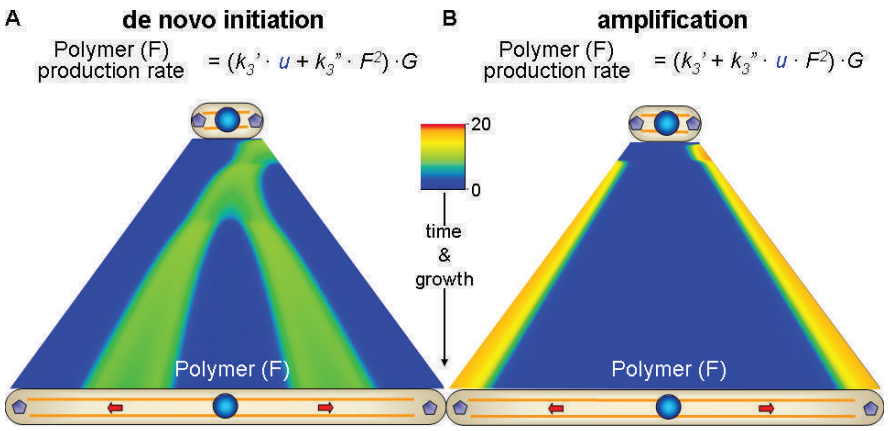

Figure 1. Two possible ways in which a landmark molecule can help F polymerization. (A) The microtubule-transported landmark (U) acts linearly on F polymerization as an initiator of polymerization. F concentration is shown as the length of the cell increases in time. A small perturbation of F at one end initiates polymerization there, but the zone moves away from the tip as the cell grows. (B) As in (A), except that U acts in the positive feedback loop. This assumption gives the correct pattern for fission yeast growth (first at one, later at two ends)

Initially, when the cell is small, we start the simulation with a polymerization zone at only one end of the cell (the 'old' end). As the cell grows, the polymerization zone moves into the middle of the simulated cell and later splits into two internal polymerization zones (simulation details in methods). This phenomenon is typical of substrate-depletion-type reaction–diffusion systems with growth (Crampin *et al.*, 2002; Maini, 1999). The reason for this behaviour is that after polarization has been induced by localized u, the autocatalytic polymerization takes over. The autocatalytic term drives much faster polymerization than the *de novo* term, and so the system adopts the pattern favoured by the autocatalytic reaction. The excitation zone settles in the middle of the cell, where it can most easily collect the uniformly synthesized substrate. As the cell grows, it eventually becomes long enough to accommodate two excitation zones, which divide up the available territory (Figure 1A). Similar patterns are seen in activator–inhibitor models with saturation (Meinhardt, 1995).

If the landmark amplifies the positive feedback (Figure 1B), then the polymerization zone stays at the end of the cell, and as the cell grows a new polymerization zone turns on at the other end, as observed in fission yeast cells. In this case the autocatalytic reactions depend on the U molecules localized at the cell ends. From these results we propose that tea1p-localized polarisome

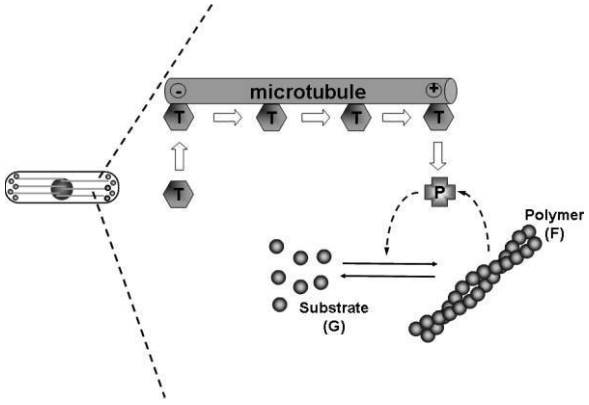

Figure 2. The actin polymerization network in fission yeast. Presumptive landmark proteins T bind to microtubules and are transported to the ends of the cell, where they are released and activate the polarisome (P). P promotes the autocatalytic feedback loop for polymerization, from G to F. In the model, T and P are lumped together as 'unspecified' (U). Both U and G-actin are synthesized from amino acids and degraded into amino acids (not shown)

molecules act inside the positive feedback loop that is responsible for actin polymerization, instead of just promoting *de novo* polymerization of actin.

Figure 2 shows the final model we propose. Microtubules transport tea1p (T) to cell tips, where tea1p recruits other members of the polarisome (P), which acts inside the positive feedback loop that induces actin polymerization. For simplicity, as we described above, T and P are lumped together as $u(x, t)$ in the equations.

Possible growth patterns with landmark transport

After concluding that the microtubule landmark (tea1p) must recruit proteins that amplify the positive feedback loop, we investigated the possible patterns that our model predicts at different cell lengths. By using bidirectional transport of the landmark protein and the above introduced pattern formation mechanism, we could test the possible stable growth patterns of the system (for details, see Materials and methods).

Under normal circumstances, the landmark molecule does not distinguish between the two cell ends: it can be found at both ends at equal concentrations. In this case, only two patterns are evident:

1. F polymer is formed at one end only (monopolar growth).
2. F is formed at both ends (bipolar growth).

There is a region, at very small cell size, where no obvious pattern can be formed. This cell size is too small for symmetry breaking and possibly too small for viability.

We have found that only these two patterns form for a large range of parameter values with the following general rules: (1) the monopolar pattern (F at one end only) is always observable at smaller cell length than the bipolar pattern (F at both ends); (2) the upper length limit of monopolar growth is always larger than the lower limit of bipolar growth. Consequently, the two possible growth patterns always overlap. Parameter values do not change the qualitative picture; they only influence the upper and lower limits of growth patterns.

Small cells have F at one end only because that end collects most of the G molecules in the cell by diffusion, depleting the other end for substrate and thereby preventing F polymerization at the other end. This inhibition is reduced as the cell grows. When G finally reaches a threshold concentration at the new end, F can be formed there as well. Newborn wild-type fission yeast cells start to grow in a monopolar fashion and become bipolar later in the cycle (at NETO). The reaction–diffusion–convection model provides a simple explanation for the critical size requirement of NETO (Mitchison and Nurse, 1985). Once the monopolar cell reaches a critical cell length, the monopolar growth pattern disappears.

However, control of the monopolar-to-bipolar transition (NETO) is actually more complicated because it is influenced by cell cycle stage as well as by cell length (Mitchison and Nurse, 1985). If fission yeast cells are blocked in G_1 or S phase, they grow at one end only, suggesting a cell cycle control over NETO. Remember that the upper and lower limits for growth patterns are dependent on parameter values. Hence, even though G_1-blocked cells have a stable monopolar growth pattern at large cell size, the bipolar growth pattern may still be present in G_1 phase (Figure 3A is still valid qualitatively).

Possible growth patterns without the landmark

According to the consensus picture, tea1p provides the link between microtubules and actin polymerization in controlling fission yeast morphogenesis (Mata and Nurse, 1997). In wild-type cells during interphase, the microtubule plus ends are located at both ends of the cell, and tea1p accumulates at both ends. Consequently, the cell grows at either one or both ends, as discussed above. What happens if the link between microtubules and actin polymerization is broken, as in *tea1Δ* mutants? Remember that in the model we do not distinguish between tea1p and the molecules which are recruited by tea1p (other components of the polarisome); hence, deletion of tea1p can be identified with a lack of U convection ($v_u = 0$). Accordingly we assume that lack of tea1p has a similar effect on polarized growth regulation as disruption of microtubules. This leads to an unpolarized distribution of U in our model, which means equally distributed polarisome concentration in the cell. Without tea1p, the polarisome can still form and help autocatalytic F polarization, but this action is no longer properly localized by the microtubule. Therefore, our model suggests that growth zone formation in *tea1Δ* cells is driven by a spontaneous symmetry-breaking mechanism only.

We simulate both *tea1Δ* and microtubule-defective cells by removing the convection of U from the model, in which case the repertoire of possible patterns increases (Figure 3B, C). Besides monopolar and bipolar F localization, F could be concentrated in the middle of a cell, with either non-growing or growing ends. It is important to mention that the growth zone, which is formed by a

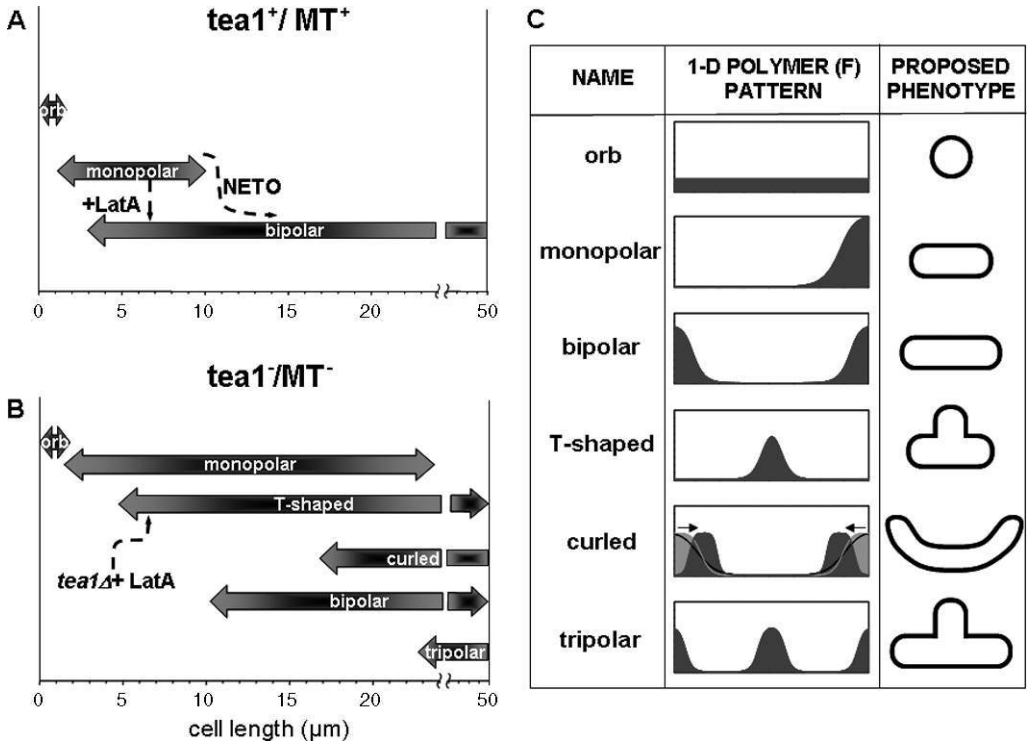

Figure 3. Possible growth patterns. (A) In the presence of microtubules and tea1p ($v_u = 2$ μm/ min) and (B) in the absence of microtubules or in *tea1Δ* mutants ($v_u = 0$ μm/ min). (C) shows examples of the corresponding F polymer distributions to the names used in A and B and also presents the proposed shapes of cells with the given growth pattern. Light grey, black and dark grey curves show the time evolution of growth zones in curled cells

symmetry-breaking mechanism, moves to the middle of the cell very quickly, because the subunit (G) supply is symmetrical from both directions. If F accumulates in the middle of the cell and initiates growth, then a new growth axis is formed and the cell will branch. Observe that small, newborn cells without a landmark can choose between monopolar and T-shaped growth patterns. We conclude that the spontaneous symmetry-breaking hypothesis can explain the coexistence of the two different types of morphologies (straight and branched cells) found in *tea1Δ* cultures. Of course, we cannot exclude the possibility that a historical landmark is operating in fission yeast cells, but this assumption is not required to explain polarity establishment in *tea1Δ* mutants.

Another type of pattern is when the growth zone slowly moves away from cell tips, most possibly leading to curled cell shape formation. As before, the possible regions of existence of these patterns overlap. Notice that the monopolar growth pattern stays stable for much larger cell size, consistent with the fact that *tea1Δ* cells fail to undergo NETO (Verde *et al.*, 1995).

Experimental proofs for pattern coexistence

Is there any evidence that cells in the same phase of the division cycle are able to grow in either a monopolar or bipolar manner? The experiment of Rupes *et al.* (1999) supports the coexistence of growth patterns in G_1 cells. These authors disrupted the monopolar actin network by treatment with latranculin A (LatA) in *cdc10*^{ts} mutant cells blocked at the restrictive temperature in G_1 phase of the cell cycle. After removing the drug, actin repolymerized at both ends of the cell, supporting the notion of coexisting monopolar and bipolar patterns (Figure 3A). The same treatment by LatA on *tea1Δ* cells does not induce NETO (Rupes *et al.*, 1999), as is also the case in the model simulations at the same cell size as before but without convection of u (cf. Figures 3A, B). According to the model, LatA-treated *tea1Δ* cells are able to

DOI: 10.1002/yea

find another stable growth pattern, as they relocalize the growth zone to the middle of the cell and form T-shaped cells (Figure 3B). This happens in 80% of G_1-blocked cells after latranculin B (LatB) treatment (Sawin and Snaith, 2004). Under normal conditions (no LatA treatment), only a few percent of *tea1Δ* cells form branches, which suggests that most cells choose the monopolar growth pattern (Mata and Nurse, 1997). The curled cells proposed by the model can be related to long G_2-blocked cells that start to curl at their tips, or possibly to banana-shaped cells, which are mutated in proteins with unknown microtubule regulatory functions (Verde *et al*., 1995). Tripolar cells are formed if microtubules are disrupted in long G_2-blocked cells (Castagnetti *et al*., 2007); thus, the model system moves from Figure 3A to Figure 3B at large cell mass, and some cells pick up the tripolar growth pattern. These experimental results support the model's prediction of coexistence of growth patterns. Alternative growth patterns switch only if cell length reaches a critical value when stability of a pattern disappears (i.e. at NETO), or if the actin distribution system is perturbed. Without these effects, a stable pattern can persist throughout the cell cycle. Which pattern is adopted depends on the history of the cell. This can be seen in most NETO mutants, where the daughter with the old (previously growing) end initiates growth at this place, but the daughter without the previously growing end polarizes to the new end or mislocalizes and forms T-shaped cells and keeps this growth pattern for the whole cycle (Niccoli *et al*., 2003).

Parameter sensitivity, finding correlation with polarisome mutants

We have tested the model for sensitivity in parameter values over a 100-fold range, as well as setting each parameter in turn to 0 (Table 1). Most interestingly, if we increase the rate of U synthesis (k_{su}) two-fold, the cell cycle position of NETO is advanced (Figure 4), resembling tea1p-for3p fusion protein overexpression, which also leads to advanced NETO (Martin *et al*., 2005). A 10-fold increase of U synthesis creates cells with instantaneous bipolar growth, which might happen in a large percentage of these tea1p-for3p fusion protein-containing cells (Martin *et al*., 2005). On the other hand, two-fold reduction of U synthesis

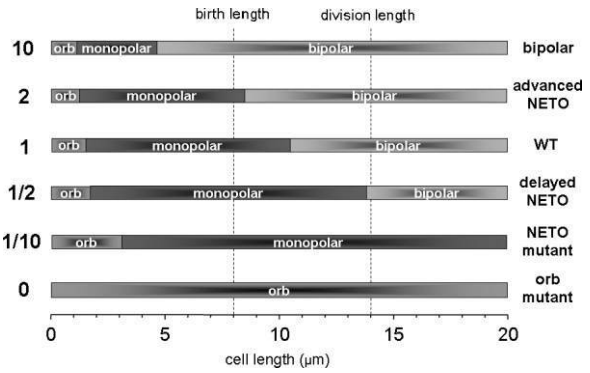

Figure 4. Growth patterns depend on the expression of U. The dependence of growth patterns on cell length as the synthesis rate of U is varied (k_{su} is multiplied by the number stated on the left). Birth and division lengths of wild-type cells are noted, the proposed phenotype in this size regime is given on the right

delays NETO and 10-fold reduction permits only monopolar growth, as in *tea1Δ, tea4Δ* or *for3Δ* cells (Feierbach and Chang, 2001; Martin *et al*., 2005; Mata and Nurse, 1997). If we turn off U synthesis totally, the cell cannot form polarized growth zones and grows spherically (the Orb phenotype). The orb phenotype is observed in triple mutant *tea1Δ bud6Δ for3Δ* cells ('polarisome defective') (Feierbach *et al*., 2004). These results further support the proposed identification of U with the polarisome.

Most other parameter changes lead to shifts in NETO position, but some perturbations result in total loss of polarity (Table 1). The majority of two-fold parameter alterations lead to mild shifts in the cell-cycle position of NETO, and all 10-fold changes retain polarized growth, showing the polarity-establishing system to be quite robust.

Discussion

We have proposed a mechanism for fission yeast morphogenesis based on pattern-forming reactions that combine the ideas of local self-enhancement/long-range inhibition (Gierer and Meinhardt, 1972) and gradient-sensing positional information (Wolpert, 1996). In our model, subunits (G) are condensed into a polymer (F) by a reaction that is quadratically autocatalytic in F (G might possibly be G-actin and F be filamentous actin, but we need not be specific in this identification at the present

stage of modelling). Quite naturally, the subunits are assumed to diffuse more readily than the polymer, and so the system satisfies the conditions to create Turing patterns (Segel and Jackson, 1972; Turing, 1952). However, we propose that the activated zones created by Turing instabilities are positioned by 'landmark' molecules (U) transported on microtubules.

We present numerical simulations of the partial differential equations describing reaction, diffusion and convection of G, F and U. Our calculations suggest that the landmark component acts inside the autocatalytic polymerization loop (if, alternatively, U were to promote *de novo* polymerization of F, then the growth zones do not properly localize to cell tips). With the landmark acting inside the positive feedback loop, we find that monopolar and bipolar growth patterns coexist over a wide range of cell sizes in wild-type cells. If correct localization of the landmark is disturbed (*tea1Δ* mutant or microtubule disruption), then the model admits additional growth patterns, some with growth zones in the middle of the cell. Several of these growth patterns co-exist over a range of cell sizes, showing that the system is multi-stable. Cells can be switched from one growth pattern to another by short perturbations (actin disruption) of the system. We have correlated our simulation results with experimental observations.

With this simple model we can account for many details of polarized growth in wild-type, drug-treated and mutant fission yeast cells. Because the mechanism of localized growth and actin polymerization is not a special phenomenon of fission yeast cells, and because many genes that regulate growth zones are well conserved in evolution (Irazoqui and Lew, 2004; Johnson, 1999; Verde *et al.*, 1998), we believe that our model can help to understand the regulation of polarized cell growth in higher eukaryotes as well.

Acknowledgements

We thank P. Nurse and many earlier and current members of his laboratory, especially J. Hayles, S. Castagnetti and K. Leonhard, for sharing ideas and helping model development. This work was supported by the James S. McDonnell Foundation (Grant No. 21002050), the European Commission (Grant No. YSBN: LSHG-CT-018942) and OTKA (Grant No. F-60414).

References

Arellano M, Niccoli T, Nurse P. 2002. Tea3p is a cell end marker activating polarized growth in *Schizosaccharomyces pombe*. *Curr Biol* **12**: 751–756.

Bahler J, Pringle Jr. 1998. Pom1p, a fission yeast protein kinase that provides positional information for both polarized growth and cytokinesis. *Genes Dev* **12**: 1356–1370.

Behrens R, Nurse P. 2002. Roles of fission yeast tea1p in the localization of polarity factors and in organizing the microtubular cytoskeleton. *J Cell Biol* **157**: 783–793.

Browning H, Hayles J, Mata J, *et al*. 2000. Tea2p is a kinesin-like protein required to generate polarized growth in fission yeast. *J Cell Biol* **151**: 15–28.

Brunner D, Nurse P. 2000. CLIP170-like tip1p spatially organizes microtubular dynamics in fission yeast. *Cell* **102**: 695–704.

Castagnetti S, Behrens R, Nurse P. 2005. End4/Sla2 is involved in establishment of a new growth zone in *Schizosaccharomyces pombe*. *J Cell Sci* **118**: 1843–1850.

Castagnetti S, Novák B, Nurse P. 2007. Microtubules offset growth site from the cell centre in fission yeast. *J Cell Sci* **120**: 2205–2213.

Chang F. 2001. Establishment of a cellular axis in fission yeast. *Trends Genet* **17**: 273–278.

Chang F, Peter M. 2003. Yeasts make their mark. *Nat Cell Biol* **5**: 294–299.

Chant J, Herskowitz I. 1991. Genetic control of bud site selection in yeast by a set of gene products that constitute a morphogenetic pathway. *Cell* **65**: 1203–1212.

Crampin EJ, Hackborn WW, Maini PK. 2002. Pattern formation in reaction–diffusion models with nonuniform domain growth. *Bull Math Biol* **64**: 747–769.

Dauty E, Verkman AS. 2004. Molecular crowding reduces to a similar extent the diffusion of small solutes and macromolecules: measurement by fluorescence correlation spectroscopy. *J Mol Recognit* **17**: 441–447.

Feierbach B, Chang F. 2001. Roles of the fission yeast formin for3p in cell polarity, actin cable formation and symmetric cell division. *Curr Biol* **11**: 1656–1665.

Feierbach B, Verde F, Chang F. 2004. Regulation of a formin complex by the microtubule plus end protein tea1p. *J Cell Biol* **165**: 697–707.

Gierer A, Meinhardt H. 1972. A theory of biological pattern formation. *Kybernetik* **12**: 30–39.

Glynn JM, Lustig RJ, Berlin A, Chang F. 2001. Role of bud6p and tea1p in the interaction between actin and microtubules for the establishment of cell polarity in fission yeast. *Curr Biol* **11**: 836–845.

Hayles J, Nurse P. 2001. A journey into space. *Nat Rev Mol Cell Biol* **2**: 647–656.

Irazoqui JE, Lew DJ. 2004. Polarity establishment in yeast. *J Cell Sci* **117**: 2169–2171.

Johnson DI. 1999. Cdc42: an essential rho-type GTPase controlling eukaryotic cell polarity. *Microbiol Mol Biol Rev* **63**: 54–105.

Maini PK. 1999. Some mathematical models for biological pattern formation. In *On Growth and Form. Spatio-temporal Pattern Formation in Biology*, Chaplain MAJ, Singh GD, McLachalan JC (eds). Wiley: Chichester, UK; 111–128.

Marks J, Hyams JS. 1985. Localisation of F-actin through the cell-division cycle of *Schizosaccharomyces pombe*. *Eur J Cell Biol* **39**: 27–32.

Martin SG, Chang F. 2003. Cell polarity: a new mod(e) of anchoring. *Curr Biol* **13**: R711–713.

Martin SG, McDonald WH, Yates JR III, Chang F. 2005. Tea4p links microtubule plus ends with the formin for3p in the establishment of cell polarity. *Dev Cell* **8**: 479–491.

Mata J, Nurse P. 1997. tea1 and the microtubular cytoskeleton are important for generating global spatial order within the fission yeast cell. *Cell* **89**: 939–949.

McGrath JL, Tardy Y, Dewey CF Jr, Meister JJ, Hartwig JH. 1998. Simultaneous measurements of actin filament turnover, filament fraction, and monomer diffusion in endothelial cells. *Biophys J* **75**: 2070–2078.

Meinhardt H. 1982. *Models of Biological Pattern Formation*. Academic Press: New York.

Meinhardt H. 1995. *The Algorithmic Beauty of the Sea Shells*. Springer-Verlag: Berlin.

Meinhardt H, Gierer A. 2000. Pattern formation by local self-activation and lateral inhibition. *Bioessays* **22**: 753–760.

Mitchison JM, Nurse P. 1985. Growth in cell length in the fission yeast *Schizosaccharomyces pombe*. *J Cell Sci* **75**: 357–376.

Murray JD. 2003. *Mathematical Biology. II: Spatial Models and Biomedical Applications*, 3rd edn. Springer-Verlag: Berlin.

Niccoli T, Arellano M, Nurse P. 2003. Role of Tea1p, Tea3p and Pom1p in the determination of cell ends in *Schizosaccharomyces pombe*. *Yeast* **20**: 1349–1358.

Rupes I, Jia Z, Young PG. 1999. Ssp1 promotes actin depolymerization and is involved in stress response and new end take-off control in fission yeast. *Mol Biol Cell* **10**: 1495–1510.

Sawin KE, Nurse P. 1998. Regulation of cell polarity by microtubules in fission yeast. *J Cell Biol* **142**: 457–471.

Sawin KE, Snaith HA. 2004. Role of microtubules and tea1p in establishment and maintenance of fission yeast cell polarity. *J Cell Sci* **117**: 689–700.

Segel LA, Jackson JL. 1972. Dissipative structure: an explanation and an ecological example. *J Theor Biol* **37**: 545–559.

Sheu Y-J, Santos B, Fortin N, Costigan C, Snyder M. 1998. Spa2p interacts with cell polarity proteins and signaling components involved in yeast cell morphogenesis. *Mol Cell Biol* **18**: 4053–4069.

Snaith HA, Samejima I, Sawin KE. 2005. Multistep and multi-mode cortical anchoring of tea1p at cell tips in fission yeast. *EMBO J* **24**: 3690–3699.

Snaith HA, Sawin KE. 2003. Fission yeast mod5p regulates polarized growth through anchoring of tea1p at cell tips. *Nature* **423**: 647–651.

Sohrmann M, Peter M. 2003. Polarizing without a c(l)ue. *Trends Cell Biol* **13**: 526–533.

Turing A. 1952. The chemical basis of morphogenesis. *Phil Trans R Soc Lond B Biol Sci* **237**: 37–72.

Verde F, Mata J, Nurse P. 1995. Fission yeast cell morphogenesis: identification of new genes and analysis of their role during the cell cycle. *J Cell Biol* **131**: 1529–1538.

Verde F, Wiley DJ, Nurse P. 1998. Fission yeast orb6, a ser/thr protein kinase related to mammalian rho kinase and myotonic dystrophy kinase, is required for maintenance of cell polarity and coordinates cell morphogenesis with the cell cycle. *Proc Natl Acad Sci USA* **95**: 7526–7531.

Wedlich-Soldner R, Altschuler S, Wu L, Li R. 2003. Spontaneous cell polarization through actomyosin-based delivery of the Cdc42 GTPase. *Science* **299**: 1231–1235.

Wolpert L. 1996. One hundred years of positional information. *Trends Genet* **12**: 359–364.

dc_836_14

7.4 Az élesztő sejtciklusának sztochasztikus Petri Net modellje

Mura I., **Csikász-Nagy A.** (2008) Stochastic Petri Net extension of a yeast cell cycle model. *J Theor Biol.* **254 (4)**, 850-60. **Impakt faktor: 2.454**

Journal of Theoretical Biology 254 (2008) 850–860

Contents lists available at ScienceDirect

Journal of Theoretical Biology

journal homepage: www.elsevier.com/locate/yjtbi

Stochastic Petri Net extension of a yeast cell cycle model

Ivan Mura *, Attila Csikász-Nagy

The Microsoft Research - University of Trento, Centre for Computational and Systems Biology, Piazza Manci 17, Povo-Trento I-38100, Italy

ARTICLE INFO

Article history:
Received 31 January 2008
Received in revised form
15 July 2008
Accepted 16 July 2008
Available online 24 July 2008

Keywords:
Systems biology
Cell cycle
SPN
Model comparison
Mathematical modeling
Simulation

ABSTRACT

This paper presents the definition, solution and validation of a stochastic model of the budding yeast cell cycle, based on Stochastic Petri Nets (SPN). A specific family of SPNs is selected for building a stochastic version of a well-established deterministic model. We describe the procedure followed in defining the SPN model from the deterministic ODE model, a procedure that can be largely automated. The validation of the SPN model is conducted with respect to both the results provided by the deterministic one and the experimental results available from literature. The SPN model catches the behavior of the wild type budding yeast cells and a variety of mutants. We show that the stochastic model matches some characteristics of budding yeast cells that cannot be found with the deterministic model. The SPN model fine-tunes the simulation results, enriching the breadth and the quality of its outcome.

1. Introduction

Cell cycle is the collective name for a complex network of coordinated biochemical phenomena that control the reproduction of the basic living unit, the cell. Cells reproduce by dividing themselves into daughter cells, each one endowed with the biochemical machinery that allows them growing and repeating the process (Morgan, 2006). Before committing themselves to reproduction, cells must grow to an appropriate size (Rupes, 2002; Sveiczer et al., 2004). Then, they have to duplicate DNA and segregate the two copies so that each sibling receives one complete copy of it. These tasks are the most delicate ones in the cell cycle, and require the creation of complex structures that ensure the two copies of the cell genome are properly pulled apart.

The cell cycle of an eukaryotic cell can be split into a sequence of phases, namely G1, S, G2, M, where G1 and G2 are two *gap* phases, S is DNA synthesis phase and M is mitosis. By sensing the environmental conditions, and after reaching an adequate mass, a cell can commit itself to start the S phase, a cell cycle transition called *Start*. Once started, the synthesis phase goes irreversibly to completion (Novak et al., 2007). In gap phase G2 the cell ensures the duplication of DNA has completed and checks that the environment is favorable to proceed to the M phase. The mitosis phase is divided in various subphases, which encompass the condensation of chromatin into chromosomes (*prophase*), formation of the mitotic spindle and alignment of the duplicated chromosomes (*prometaphase* and *metaphase*), their separation and movement toward opposite sides of the cell (*anaphase*), partitioning of the two nuclei (*telophase*).

In each phase, specific tasks are accomplished through the activity of biochemical species, among which cyclin dependent kinases (Cdks) play a major role. When bound to a cyclin partner, Cdks are activated and able to make cells to progress along their cycle. Various Cdks and cyclins exist in eukaryotic cells, and each Cdk/cyclin dimer has specific activity. Changes in the concentration of active Cdk/cyclin dimers are responsible for causing the transition from one phase to the subsequent one in the cell cycle. By sensing the internal and environmental conditions through signaling networks, an eukaryotic cell controls the expression of the genes responsible for activation of Cdks, proceeding to the next phase in the cycle only when the current one has been successfully completed (Morgan, 2006).

Higher organisms have a variety of Cdks and cyclins that control the progress of their cell cycle. In the model organism budding yeast *Saccharomyces cerevisiae* only one Cdk is present (called Cdk1 or Cdc28), which can complex with a limited number of cyclins (Cln1-3 and Clb1-6) (Futcher, 1996). Though, the dynamics of the biochemical network controlling the cell cycle of budding yeast follow the same outline as in more complex eukaryotes (Csikász-Nagy et al., 2006). Cell cycle of buddying yeast has been subject to extensive experimental study and computational models have been developed for its regulation (Sible and Tyson, 2007). In particular, the work on deterministic modeling of budding yeast cell cycle conducted by a research

* Corresponding author. Tel.: +39 0461 882825; fax: +39 0461 882814.
E-mail addresses: mura@cosbi.eu (I. Mura), csikasz@cosbi.eu (A. Csikász-Nagy).

0022-5193/$ - see front matter © 2008 Elsevier Ltd. All rights reserved.
doi:10.1016/j.jtbi.2008.07.019

team headed by John Tyson has led to the formulation of comprehensive models, based on ODEs (Chen et al., 2000, 2004).

In recent years, a number of stochastic modeling techniques started to be applied to model biological phenomena (Wilkinson, 2006). We focus in this study on Stochastic Petri Nets (SPNs, hereafter), for which various applications to biology exist in the literature, see for instance (Goss and Peccoud, 1998; Srivastava et al., 2001; Tsavachidou and Liebman, 2002; Nutsch et al., 2005; Peleg et al., 2005). The SPN formalism is based on a discrete state-space modeling approach, hence it has the expressive power to capture the discrete molecular dynamics of the system at a lower level of abstraction than deterministic models. As the number of molecules grows, abstracting discrete number of molecules into continuous concentration levels and representing evolution of dynamics through a system of coupled ODEs provides very accurate representations and also has the advantage of not suffering from the state-space explosion problem that plagues stochastic modeling tools. Moreover, stochastic models are mostly solved via simulation, which may require performing a substantial number of simulation runs to compute statistically relevant results.

There is not yet a precise and agreed upon characterization of modeling problems that are best handled with deterministic or that best suite the stochastic approach. In the literature we find a few stochastic cell cycle models built with stochastic ODE Langevine type equations (Steuer, 2004; Zámborszky et al., 2007), with the Gillespie method (Sabouri-Ghomi et al., 2007) and with stochasticity on transitions (Alt and Tyson, 1987; Sveiczer et al., 2001; Zhang et al., 2006). The main objective and contribution of this paper is to demonstrate that stochastic extensions of deterministic models can be built very easily with exploiting the modeling capabilities of SPNs. We show through a practical case study that the two modeling methods can provide results at different levels of detail. Therefore, the choice on which to use should be guided by the objectives of the modeling and traded against the cost of model solution. We define in the paper a stochastic version, based on SPNs, of an existing deterministic textbook model of budding yeast cell cycle. The deterministic model selected is one produced by Novak and Tyson (2002). The stochastic model is built with a constructive approach that can be largely automated. We present in the paper the comparative evaluation of the results provided by the models built with the two different approaches, and we compare them with experimental data on wild type and mutant budding yeast cells. We show that the stochastic model provides results that support the outcome of the deterministic one, and also can be used to probe into more precise analysis of various characteristics of the biological phenomena under consideration. Such analysis, which is based on the probabilistic nature of the SPN model, cannot obviously be performed with the deterministic model, and is found to better describe some experimental results away from the average behavior.

The rest of this paper is organized as follows. In Section 2 we describe the cell cycle of budding yeast, provide some details about the biochemical network that controls its progress through the various phases and present the deterministic model that is used as a basis for the stochastic modeling. Then, in Section 3.1 we introduce the class of SPNs that are used to build the stochastic model of the system. This stochastic model is defined in Section 3.2, and Section 4 is devoted to its validation, through the comparison of its results with those provided by the deterministic model and experimental data. Finally, conclusions and directions for future work are given in Section 5.

2. The cell cycle regulation of *Saccharomyces cerevisiae*

The budding yeast is a well-studied and understood example of how the cell cycle can be controlled with only one Cdk and a few cyclins (Alberts et al., 2002). We shall focus hereafter on the biochemical machinery that controls Cdks activity in budding yeast, as described in Novak and Tyson (2002).

2.1. Narrative description

In budding yeast *Saccharomyces cerevisiae*, during the G1 phase, the activity of Cdk1 is low because the cyclin transcription is mostly inhibited. Moreover, the produced cyclin proteins are rapidly degraded by the proteasome after ubiquitination by the anaphase-promoting complex (APC). The activity of the APC is regulated by two auxiliary proteins, Cdc20 and Cdh1. When active, these two latter proteins mediate the presentation of various targets (including B-type cyclins) to the APC for ubiquitination (Zachariae and Nasmyth, 1999). In G1 phase, there is abundance of active Cdh1. Furthermore, during G1 the remaining Cdk1/cyclinB dimers are sequestered by Sic1, a stoichiometric Cdk inhibitor, which forms an inactive heterotrimer with Cdk1/cyclin dimers (Schwob et al., 1994).

If the environmental conditions are favorable, as the cell progresses in the G1 phase the mass of cell grows, and this leads to an increased production of Cln3, a cyclin that is resistant to Cdh1 and Sic1. Cln3 can activate the transcription factors SBF/MBF that induce the production of Cln1, Cln2 and Clb5, Clb6. The complexes of Cdk1 and G1 cyclins (Cln1,2,3) together are called *starter kinases*. They are insensitive to Cdh1 and Sic1 and have the effect of mediating the inactivation of both Cdh1 and Sic1, which allows the other cyclins ($Clb1, 2, \ldots, 6$) to start accumulating in the cell. Cln1 and Cln2 induce budding and Clb5 and Clb6 induce DNA replication. The key regulator of entry into M phase is Cdk1/Clb2. Cyclin synthesis is induced and cyclin degradation inhibited throughout the rest of the cell cycle, hence Clb2 concentration increases throughout S, G2 and M phases. High concentration of active Cdk1/Clb2 also has the effect of causing the inactivation of the transcription factors SBF/MBF for the starter kinases, which have already accomplished their role in the cell cycle (Nasmyth, 1996). Moreover, Cdk1/Clb2 also induces the synthesis of the Cdc20 protein (Spellman et. al., 1998).

At the metaphase/anaphase transition, Cdc20 molecules bind to the APC and Cdk1/Clb2 activates them through a signal generated by the mitotic process itself, supposedly through some intermediate enzymes. The active Cdc20 induces the separation of sister chromatides, the degradation of the Clb's and activates the other APC regulation protein, Cdh1. As the Cdk1 activity reverts to low levels, the telophase completes and the cell divides. The synthesis of the APC regulation protein Cdc20 stops as the activity of Cdk1 is lost. The newborn cells are back in G1 phase with low cyclin levels and the process starts again.

2.2. Deterministic mathematical model of budding yeast cell cycle

We present in this section the deterministic model proposed in Novak and Tyson (2002) for capturing the biochemical dynamics of the cell cycle in budding yeast. The picture in Fig. 1 shows a pictorial representation of the synthesis/degradation and activation/deactivation processes of the various chemical species described in the previous section. In Fig. 1, the budding yeast Cdk1 is called Cdk and the stoichiometric inhibitor Sic1 is represented by CKI. Cdk/CycB represents the active dimers of Cdk1/Clb's and CKI/Cdk/CycB the inactive trimer Sic1/Cdk1/Clb's. The transcription factors SBF/MBF are collectively represented by species TF,

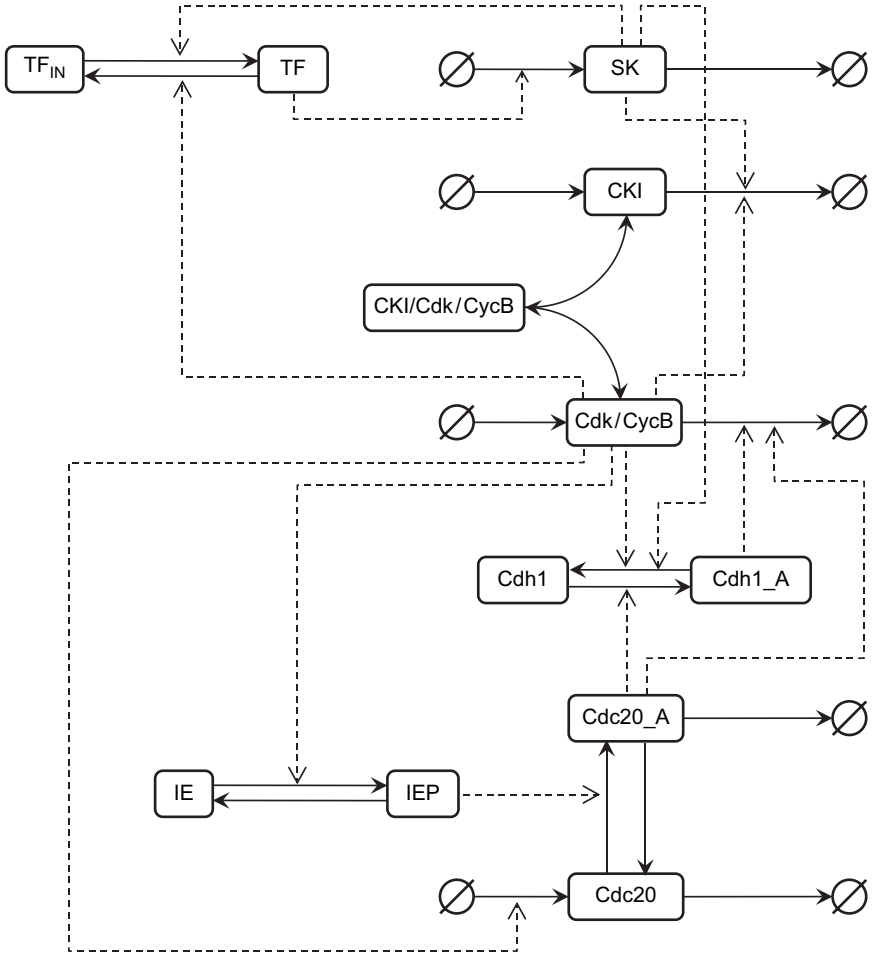

Fig. 1. Graphical representation of cell cycle engine, a slightly revised and more detailed one from that shown in Novak and Tyson (2002, p. 270). It shows the biochemical species involved in the cell cycle, and depicts the main reactions. Solid lines represent link reactants and reaction products, dashed lines represent the mediation effect that some species have on reactions. Notation $\oslash\rightarrow$ represents a synthesis process, $\rightarrow\oslash$ represents a degradation process.

the starter kinases (Cdk1/Cln's dimers) are represented by species SK, and finally the intermediate enzymes that mediate APC activation are represented by species IE. It is worthwhile observing that the synthesis and degradation processes of Cdk are not included in the model, as its concentration is assumed to be constant throughout the cell cycle and in excess with respect to the available cyclin partners. Also, it is assumed that the concentration of Cdk1/Clb's is always in equilibrium with the Clb's and Cdk1 concentration, and the same is assumed for Sic1/Cdk/Clb's trimers.

Novak and Tyson (2002) model the above system with 8 ODEs in their book chapter. Also, an additional ordinary differential equation models cellular growth, as several terms in the other equations depend on the cell mass. They also provide rules for cell division, which is triggered when the activity of Cdk/CycB, expressed by the product $m \cdot [Cdk/CycB]$ falls below an assigned threshold (0.1, in this model) during telophase. In their model, which we report below, cells are assumed to divide equally at the end of mitosis, a simplification of the asymmetric division of budding yeast cells.

$$\frac{\mathrm{d}}{\mathrm{d}t}m = \mu m(1 - m/m^*) \tag{1}$$

$$\frac{\mathrm{d}}{\mathrm{d}t}[CycB_T] = k_1 - (k_2' + k_2''[Cdh1_A] + k_2'''[Cdc20_A])[CycB_T] \tag{2}$$

$$\begin{aligned}\frac{\mathrm{d}}{\mathrm{d}t}[Cdh1_A] = {} & (k_3' + k_3''[Cdc20_A]) \\ & \times(1 - [Cdh1_A])/(J_3 + 1 - [Cdh1_A]) \\ & - (k_4 m[CycB] + k_4'[SK]) \\ & \times[Cdh1_A])/(J_4 + [Cdh1_A])\end{aligned} \tag{3}$$

$$\begin{aligned}\frac{\mathrm{d}}{\mathrm{d}t}[Cdc20_T] = {} & k_5' + k_5''(m[CycB])^n/(J_5^n + (m[CycB])^n) \\ & - k_6[Cdc20_T]\end{aligned} \tag{4}$$

$$\begin{aligned}\frac{\mathrm{d}}{\mathrm{d}t}[Cdc20_A] = {} & (k_7[IEP]([Cdc20_T] - [Cdc20_A]))/(J_7 + [Cdc20_T] \\ & - [Cdc20_A]) - k_8[Cdc20_A]/(J_8 + [Cdc20_A]) \\ & - k_6[Cdc20_A]\end{aligned} \tag{5}$$

$$\frac{\mathrm{d}}{\mathrm{d}t}[IEP] = k_9 m[CycB](1 - [IEP]) - k_{10}[IEP] \tag{6}$$

$$\frac{\mathrm{d}}{\mathrm{d}t}[CKI_T] = k_{11} - (k_{12}' + k_{12}''[SK] + k_{12}'''m[CycB])[CKI_T] \tag{7}$$

$$\frac{\mathrm{d}}{\mathrm{d}t}[SK] = k_{13}' + k_{13}''[TF] - k_{14}[SK] \tag{8}$$

$$\frac{d}{dt}[TF] = (k'_{15}m + k''_{15}[SK])(1-[TF])/(J_{15}+1-[TF]) - (k'_{16}+k''_{16}m[CycB])[TF])/(J_{16}+[TF]) \quad (9)$$

The variable $[CycB]$ in the equations above expresses the concentration of the active dimer *Cdk/CycB*. Because it is assumed that the concentration of the dimer is always in equilibrium with that of $CycB_T$ and CKI_T, $[CycB]$ is algebraically expressed as follows:

$$[CycB] = [CycB_T] - \frac{2[CycB_T][CKI_T]}{\Sigma + \sqrt{\Sigma^2 - 4[CycB_T][CKI_T]}}$$

where $\Sigma = [CycB_T] + [CKI_T] + K_{eq}^{-1}$. The ODE model is completed with a set of values for the rate constants and the other numerical parameters (see Novak and Tyson, 2002, p. 273), not reported here for the sake of brevity.

It is important to notice the different levels of abstraction (elementary and non-elementary reactions) included in the deterministic model above. From zero order up to Michaelis–Menten and high order *Hill* functions, many different type of terms can be found in the right hand sides of the differential equations. This variable level of abstraction has important implications on the selection of the modeling formalism that can be applied to define a stochastic extension of this same model. Indeed, such an extension requires the support of a stochastic modeling formalism that allows representing rates of non-elementary reactions, a task that can be easily accomplished by using SPN models.

3. Stochastic modeling of *Saccharomyces cerevisiae* cell cycle

3.1. The SPN modeling formalism

Stochastic Petri Nets (SPNs) is a modeling formalism that accounts for randomness of event occurrence times. Competition for resources, simultaneous progress of independent processes and synchronization of multiple flows make them suitable for representing networks of biochemical transformations (Wilkinson, 2006).

Being an abstract modeling formalism, SPNs by themselves do not refer to any specific aspect of the biological domain, but rather a meaning has to be associated by the modeler to places, tokens and transitions. In the context of biological phenomena, the classical interpretation of Petri net elements is the following one:

- Places represent chemical species or more complex biological entities as well, such as ribosomes, receptors, genes.
- Tokens inside a place (the marking of the place) model the number of molecules of the species or of the entities represented by the place. Tokens are anonymous entities that do not carry any qualifying information, and thus the molecule or the biological entity they represent changes as they move from a place to another. Tokens are not always graphically depicted, apart from those cases in which there are a few of them.
- Transitions represent biochemical reactions. The rate of a transition represents the speed at which a reaction occurs. If the number of tokens in the input places allows for multiple reactions to proceed concurrently, the rate of the transition is multiplied by the number of the reactions, which is indeed quite a simple way of modeling chemical reactions obeying the mass-action law.
- Arcs (arrows linking places to transitions and transitions to places) represent the flow of biochemical transformations, from reactants to reactions and from reactions to products. The cardinality of an arc is an integer number that represents the number of tokens that flow through it, which has a direct biological interpretation in terms of reaction stoichiometry.

A number of syntactical extensions have been proposed for including higher levels constructs into SPNs, so to model complex systems in a compact way. Marking-dependent enabling conditions (also called *guards*) on transitions and marking-dependent cardinality arcs and firing rates are all unambiguous shorthand notations for representing in the SPN formalism behaviors that would otherwise require additional graphical elements. We shall make use of such extended notation for the purposes of our modeling. Various families of SPNs exist that match the features of the modeling formalism we will be using in the following, e.g. Stochastic Activity Networks (Peccoud et al., 2007) and Stochastic Reward Nets (Ciardo et al., 1989).

3.2. The SPN model

In this section, we explain the constructive approach through which we build the SPN model of budding yeast cell cycle, which is shown in Fig. 3. The rationale behind our approach is to use the same abstractions as the ones adopted in the deterministic model to define an easy to understand mapping process from ODEs into SPN elements.

Let us consider for instance the ordinary differential equation (3), which we write below in a slightly expanded form for the sake of clarity:

$$\frac{d}{dt}[Cdh1_A] = k'_3(1-[Cdh1_A])/(J_3+1-[Cdh1_A]) \quad (10)$$
$$+ k''_3[Cdc20_A](1-[Cdh1_A])/(J_3+1-[Cdh1_A]) \quad (11)$$
$$- k_4 m[CycB][Cdh1_A]/(J_4+[Cdh1_A]) \quad (12)$$
$$- k'_4[SK]/(J_4+[Cdh1_A]) \quad (13)$$

This equation is describing the time-dependent evolution of the concentration of active molecules of species Cdh1 (which we denoted as $Cdh1_A$). Differential equation (3) is describing four possible reactions; the first 2, which correspond to terms (10) and (11), transform inactive molecules into active ones, and the other 2, which correspond to terms. (12) and (13), model the opposite transformation. Notice that $1-[Cdh1_A]$ is equivalent to $[Cdh1_I]$ because there is neither creation nor degradation of Cdh1 molecules, and their total concentration is 1.

The SPN model for this part of the biochemical network is shown in Fig. 2. It includes one place, named $Cdh1_A$, containing tokens that represent the active molecules of Cdh1, and one place named $Cdh1_I$ containing tokens that represent the inactive molecules of Cdh1. In fact, because the two forms of the Cdh1 biochemical species behave differently in the cell cycle regulation, we consider them as two distinct species. To model the four reactions, the SPN model includes four transitions that move tokens between places $Cdh1_A$ and $Cdh1_I$, which for the sake of an easy correspondence we named t'_3, t''_3, t_4 and t'_4 to match the corresponding rate constants k'_3, k''_3, k_4 and k'_4 in the ODE terms (10)–(13).

The first term (10) is a Michaelis–Menten type of enzymatic reaction occurring at a rate $k'_3(1-[Cdh1_A])/(J_3+1-[Cdh1_A])$, which can also be rewritten as $k'_3[Cdh1_I]/(J_3+[Cdh1_I])$. Because in the continuous deterministic model the reaction rate is an algebraic function of the concentration of inactive Cdh1, in the discrete stochastic model built with the SPNs the firing rate of transition t'_3 will be defined as a function of the number of molecules of inactive Cdh1, that is the number of tokens in place $Cdh1_I$.

Let #X denote the marking of place X, which represents in the SPN model the number of molecules of chemical species X, and let α be the scalar constant defined as $\alpha = (N_A 10^{-6} V)^{-1}$, where N_A is Avogadro's number and V is the average volume of budding yeast *Saccharomyces cerevisiae* cell nucleus. Constant α is a scaling factor that accounts for mapping a concentration (expressed in μM) into an equivalent number of molecules in the fixed volume of cell nucleus, assumed to be equal to 2% of 42 fL, the average wild type budding yeast cell volume, as per Jorgensen et al. (2002). The conversion factor α^{-1} accounts for about 505 molecules in the cell per μM. This value may be low for some species, for instance cyclins, as shown in Cross et al. (2002). However, for the sake of simplicity, we consistently use this same value of α^{-1} to scale the concentration of all biochemical species in the definition of the SPN model, same as in Gonze et al. (2002), to keep the same ratios among concentrations as in the deterministic model, leaving to a future modeling work the goal of a more accurate representation of the abundance of species. Hence, the firing rate of transition t_3', which we denote by $f_{t_3'}(\#Cdh1_I)$, is as follows: $f_{t_3'}(\#Cdh1_I) = k_3' \#Cdh1_I/(J_3 + \alpha \#Cdh1_I)$.

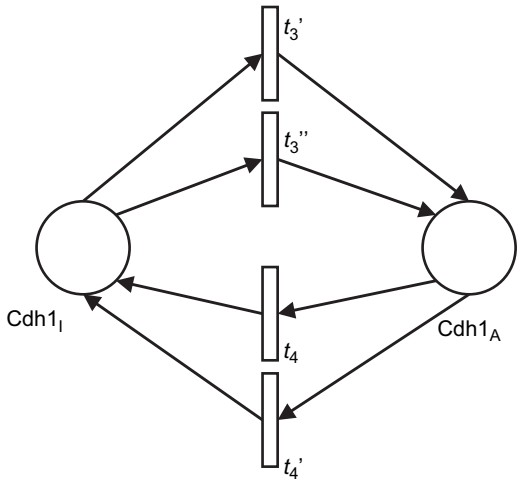

Fig. 2. SPN model corresponding to differential equation (3). SPN notation is as follows: ○ denotes a place, ▯ denotes a timed transition whose firing times are exponentially distributed. Tokens contained into places are not graphically shown.

Let us now consider the term (11), which can be equivalently rewritten as $k_3''[Cdc20_A][Cdh1_I]/(J_3 + [Cdh1_I])$. This expression tells that a reaction of activation exists for Cdh1, which is enzymatically driven by the active molecules of species Cdc20. Transition t_3'' in Fig. 3 represents this reaction in the SPN model. Its firing rate is a function of the marking of the model, in particular of the number of active molecules of Cdc20 and of the number of inactive molecules of Cdh1, and is defined as follows: $f_{t_3''}(\#Cdc20_A, \#Cdh1_I) = k_3'' \alpha \#Cdc20_A \#Cdh1_I/(J_3 + \alpha \#Cdh1_I)$.

Similarly, we can model all the reactions that are described by the system of differential equations in Novak and Tyson (2002), thus obtaining the SPN model shown in Fig. 3. It is important to remark that, although the net graphically appears composed by disjoint subnets, the mediation effect that species have on reactions is properly accounted for in the transition rates of the model. It is exactly this feature of SPNs that makes possible such a simple one-to-one translation, from the terms of the differential equations (reactions in the deterministic model) into the transitions of the stochastic model. The possibility of defining general rate functions of transitions allows building a stochastic model at an analogous level of abstraction as the one adopted in the deterministic one.

The specification of the SPN model is to be completed with the rate functions of transitions and the guards associated to them. Guards are boolean conditions that, when not satisfied, prevent transitions from firing. In the model in Fig. 3, the guards are used to disable the firing of transitions when their firing rate becomes null. This information is provided in Table 1. The species *Cdk/CycB*

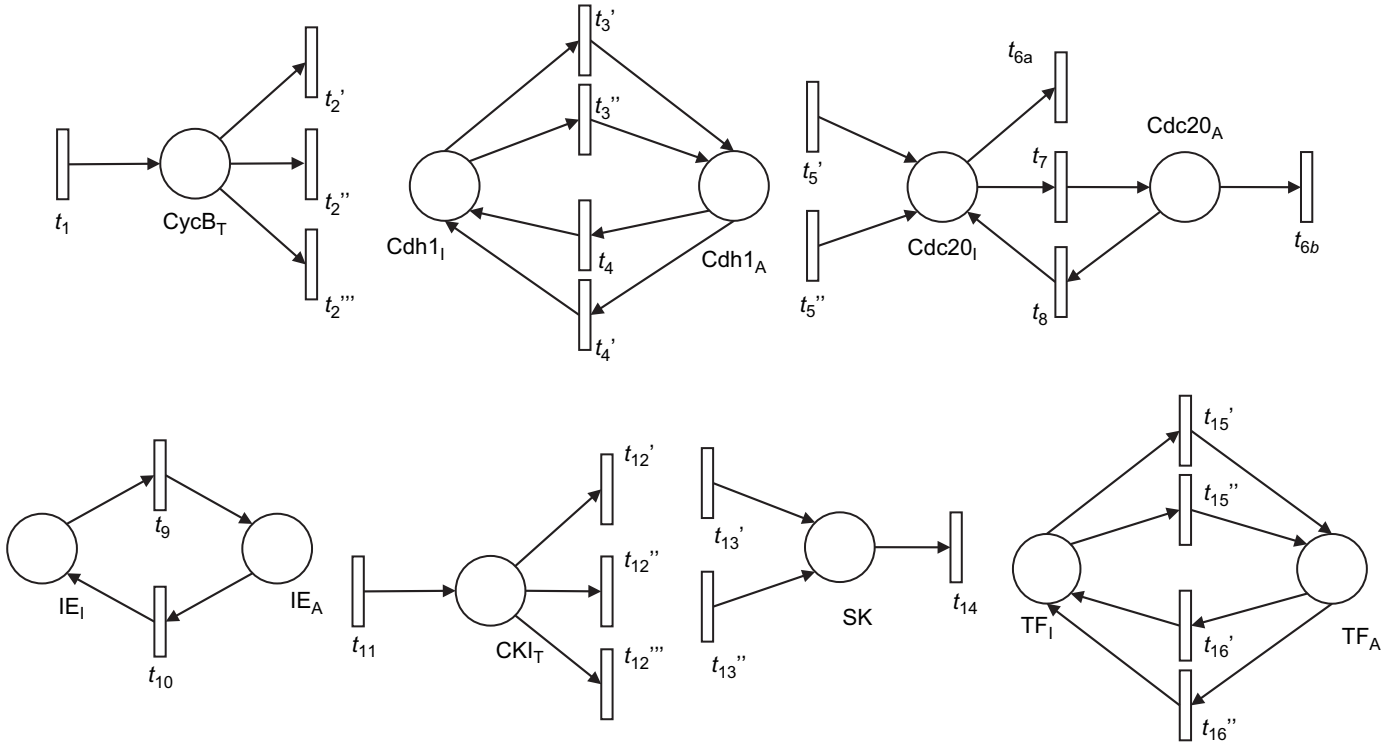

Fig. 3. SPN model of budding yeast cell cycle. The model has one place for each of the biochemical species, considering both the active (places with index A) and inactive forms (places with index I), and one transition for each possible reaction.

Table 1
Mapping between terms of the deterministic model and the SPN transitions

Eq.	Term	Transition	Rate function	Guard
(2)	k_1	t_1	$k_1\alpha^{-1}$	–
	$-k'_2[CycB_T]$	t'_2	$k'_2\#CycB_T$	–
	$-k''_2[Cdh1_A][CycB_T]$	t''_2	$k''_2\#Cdh1_A\#CycB_T\alpha$	$\#Cdh1_A>0$
	$-k'''_2[Cdc20_A][CycB_T]$	t'''_2	$k'''_2\#Cdc20_A\#CycB_T\alpha$	$\#Cdc20_A>0$
(3)	$\frac{k'_3(1-[Cdh1_A])}{(J_3+1)-[Cdh1_A]}$	t'_3	$\frac{k'_3\#Cdh1_I}{J_3+\#Cdh1_I\alpha}$	–
	$\frac{k''_3[Cdc20_A](1-[Cdh1_A])}{(J_3+1)-[Cdh1_A]}$	t''_3	$\frac{k''_3\#Cdc20_A\#Cdh1_I\alpha}{J_3+\#Cdh1_I\alpha}$	$\#Cdc20_A>0$
	$-\frac{k_4m[CycB][Cdh1_A]}{J_4+[Cdh1_A]}$	t_4	$\frac{k_4mCycB\#Cdh1_A}{J_4+\#Cdh1_A\alpha}$	$CycB>0$
	$-\frac{k'_4[SK]}{J_4+[Cdh1_A]}$	t'_4	$\frac{k'_4\#SK}{J_4+\#Cdh1_A\alpha}$	$\#SK>0$
(4)	k'_5	t'_5	$k'_5\alpha^{-1}$	–
	$k''_5\frac{(m[CycB])^n}{J_5^n+(m[CycB])^n}$	t''_5	$k''_5\frac{(m[CycB])^n}{J_5^n+(m[CycB])^n}$	$CycB>0$
	$-k_6[Cdc20_T]$	t_{6a}	$k_6\#Cdc20_I$	–
(5)	$\frac{k_7[IEP]([Cdc20_T]-[Cdc20_A])}{J_7+[Cdc20_T]-[Cdc20_A]}$	t_7	$\frac{k_7\#IE_A\#Cdc20_I\alpha}{J_7+\#Cdc20_I\alpha}$	$\#IE_A>0$
	$-\frac{k_8[Cdc20_A]}{J_8+[Cdc20_A]}$	t_8	$-\frac{k_8\#Cdc20_A}{J_8+\#Cdc20_A\alpha}$	–
	$-k_6[Cdc20_A]$	t_{6b}	$k_6\#Cdc20_A$	–
(6)	$k_9m[CycB](1-[IEP])$	t_9	$k_9mCycB\#IE_I$	$CycB>0$
	$-k_{10}[IEP]$	t_{10}	$-k_{10}\#IE_A$	–
(7)	k_{11}	t_{11}	$k_{11}\alpha^{-1}$	–
	$-k'_{12}[CKI_T]$	t'_{12}	$k'_{12}\#CKI_T$	–
	$-k''_{12}[SK][CKI_T]$	t''_{12}	$k''_{12}\#SK\#CKI_T\alpha$	$\#SK>0$
	$-k'''_{12}m[CycB][CKI_T]$	t'''_{12}	$k'''_{12}mCycB\#CKI_T$	$CycB>0$
(8)	k'_{13}	t'_{13}	$k'_{13}\alpha^{-1}$	–
	$k''_{13}[TF]$	t''_{13}	$k''_{13}\#TF_A$	$\#TF>0$
	$-k_{14}[SK]$	T_{14}	$k_{14}\#SK$	–
(9)	$\frac{k'_{15}m(1-[TF])}{J_{15}+1-[TF]}$	t'_{15}	$\frac{k'_{15}m\#TF_I}{J_{15}+\#TF_I\alpha}$	–
	$\frac{k''_{15}[SK](1-[TF])}{J_{15}+1-[TF]}$	t''_{15}	$\frac{k''_{15}\#SK\#TF_I\alpha}{J_{15}+\#TF_I\alpha}$	$\#SK>0$
	$-\frac{k'_{16}[TF]}{J_{16}+[TF]}$	t'_{16}	$-\frac{k'_{16}\#TF_A}{J_{16}+\#TF_A\alpha}$	–
	$-\frac{k''_{16}m[CycB][TF]}{J_{16}+[TF]}$	t''_{16}	$-\frac{k''_{16}mCycB\#TF_A}{J_{16}+\#TF_A\alpha}$	$CycB>0$

is not explicitly represented in the SPN model; same as in Novak and Tyson (2002) it is assumed that the concentration of the dimer is always in equilibrium with that of $CycB_T$ and CKI_T. Therefore, *CycB* is algebraically expressed in the SPN model as follows:

$$CycB=\alpha\#CycB_T-\frac{2\alpha^2\#CycB_T\#CKI_T}{\Sigma+\sqrt{\Sigma^2-4\alpha^2\#CycB_T\#CKI_T}}$$

where $\Sigma=\alpha\#CycB_T+\alpha\#CKI_T+K_{eq}^{-1}$.

Translating the ordinary differential equation (1) provided for cell mass growth in Novak and Tyson (2002) into the stochastic model requires a different process. Indeed, that equation does not have a counterpart in terms of a discrete number of molecules. Therefore, an SPN subnet in which the mass is represented by a continuous number of tokens[1] is included in the SPN model. This subnet is shown in Fig. 4. Each firing of transition *growth* causes an increase in the marking of place *Mass* of a fixed quantity

[1] Places containing continuous number of tokens are a specific feature of the Möbius tool (Peccoud et al., 2007).

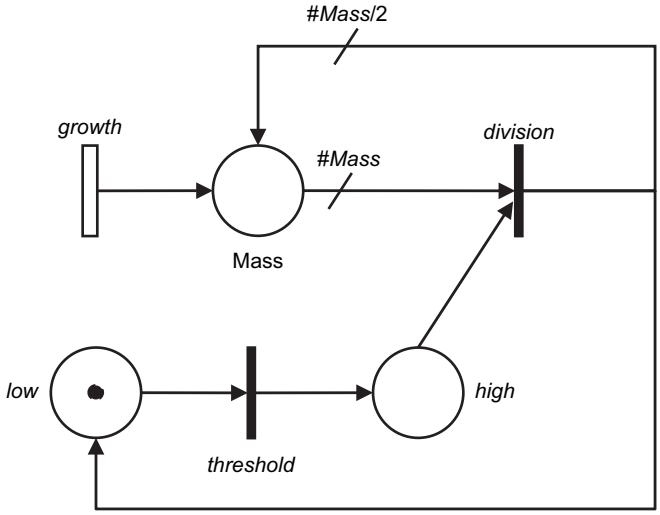

Fig. 4. SPN subnet modeling mass growth a cell division. SPN additional notation is as follows: | is an instantaneous transition firing in 0 time, arcs cut by a small mark have variable cardinality.

Table 2
Specification of transition attributes of the SPN subnet modeling mass growth and cell division

Transition	Rate function	Guard
Growth	$\frac{\mu}{\delta}\#m(1-\#m/m^*)$	–
Threshold	∞	$\#MassCycB>0.2$
Division	∞	$\#MassCycB<0.1$

$\delta=0.005$. The firing rate of *growth* is itself dependent of the marking of place *Mass*, thus reproducing the exponential growth described by Eq. (1).

The subnet in Fig. 4 also checks the condition for which the cell divides. First of all, the marking dependent guard $m\cdot CycB>0.2$ is assigned to the immediate transition *threshold*, which when satisfied causes the transition to fire immediately (zero delay). This firing removes the token initially assigned to place *low* and puts one token in place *high*, representing the fact that the activity of Cdks has reached a level that allows the cell to leave the interphase and enter mitosis. The exit from mitosis is modeled through the marking-dependent guard $m\cdot CycB<0.1$ assigned to transition *division*. When the condition is satisfied, *division* fires immediately (zero delay). The two conditions assigned to transition *threshold* and *division* check whether Cdk/CycB activity first reached a critical high activity and later dropped to a critical low activity, which is the condition for proper cell division (Csikász-Nagy et al., 2007). The firing of *division* removes the tokens contained in place *Mass* (through a marking-dependent weight on the connecting arc) and puts half of them back into *Mass* (through another marking-dependent arc). This halving of the marking of place *Mass* models the cell division. The firing of transition *division* also removes the token contained in place *high* and inserts one token back into place *low*, to reset the subnet for another cell cycle. The firing rates and guards assigned to the transitions of the subnet in Fig. 4 are provided in Table 2.

The overall SPN model is composed by the subnets in Figs. 3 and 4 plus the transition specification reported in Tables 1 and 2. This model has been implemented into the Möbius tool (Peccoud et al., 2007), which supports the adopted modeling formalism and allows for graphical model definition and for solution via simulation. The initial state of the model, i.e. the number of

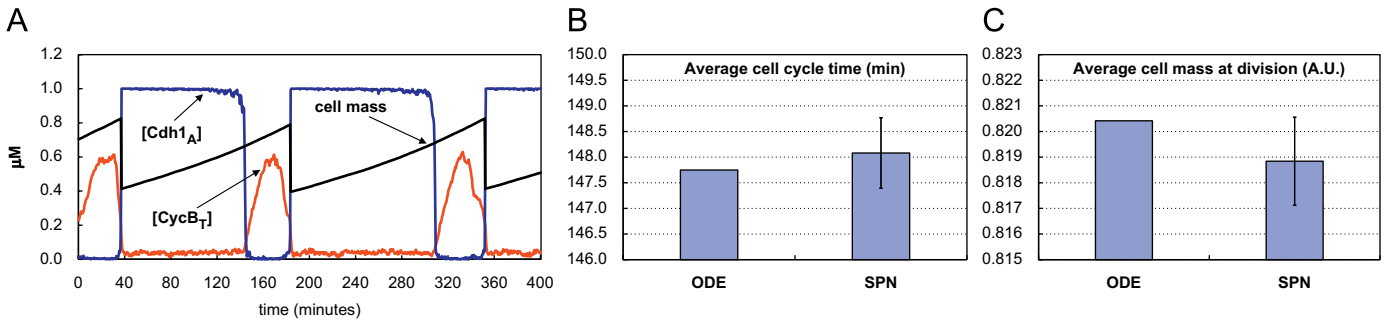

Fig. 5. Stochastic model results for wild type budding yeast cells. (A) single run of SPN simulation results, started with the same initial state as the one applied to the ODE system of equations in Novak and Tyson (2002). Simulation runs with different seeds of the pseudo-random number generator only show minor stochastic fluctuation in cell cycle duration. Comparison of average cycle time duration (B) and average cell mass at division (C) statistics from the deterministic and the SPN model. A simulation experiment consisting of 1000 runs, each using a disjoint sequence of pseudo-random numbers, was used to evaluate the average cycle time duration and the average mass at cell division time.

tokens in each place, has been selected to match the concentrations of the species and the mass size of the yeast cell used in Novak and Tyson (2002). The Möbius produced documentation of the model as well as an export of the SPN model, which can be imported into the tool for reproducing the results presented in this paper, can be found in the on-line supplemental material.

It is important to observe that the SPN model defined as explained above is not completely specifying the dynamics of the system in terms of elementary biochemical reactions, as it would be required for instance for a Gillespie stochastic simulation (Gillespie, 1977). In fact, the same abstractions used in the deterministic model, i.e., Hill functions, Michaelis–Menten enzymatic reactions, which account for a high-level mathematical representation of biochemical sub-networks (possibly not known at the lowest level of detail), are incorporated in the form of rate-dependent functions in the SPN model. The rate dependent functions define the reaction propensities of the stochastic model. We assume in our work that the *fundamental hypothesis* of Gillespie, i.e. each reaction time is a random variable following a negative exponential distribution with rate equal to the value of the propensity function (Gillespie, 1977), is verified for the biological system we are modeling. If this hypothesis is valid, a stochastic characterization of the reaction times as negatively distributed random variables is an accurate modeling choice, as proved by Gillespie (1977). When, as in our case, a model includes non-elementary biological transformations for which details of the elementary kinetics are not known, approximations may be introduced. In some modeling studies, even though non-elementary Michaelis–Menten type of reactions (Rao and Arkin, 2003) and gene transcription reactions (Goutsias, 2005) were considered, the applicability of the fundamental hypothesis was mathematically assessed, and in some others dealing with the circadian rhythm this same hypothesis was experimentally verified in silico (Gonze et al., 2002). In our case, because the SPN model we are proposing is including many non-elementary reactions, a careful validation is required to check the effects of the approximations introduced, a fundamental task to which we will devote most of the rest of this paper.

4. Validation of the stochastic model

In this section we compare the results of SPN model solution with the results provided by the deterministic model and with those obtained via real experiments, with the purpose of validating the stochastic version. To do this, we solved the SPN model and the system of ODEs for the wild type budding yeast and for a set of mutants that can be easily modeled with simple changes in the two models. A vast repertoire of budding yeast mutant strains have been generated by deletion of genes or specific sequence regions and overexpression of proteins that are involved in the cell cycle. It is worthwhile to remark that using the deterministic model results to validate the average behavior of the SPN model is indeed a correct procedure. In fact, even though the two models are built using the same amount of biological information, their dynamics are quite different from each other.

4.1. Wild type budding yeast cells

The results obtained from the simulation of the SPN model are shown in Fig. 5. We used the arbitrary unit concentrations defined by Novak and Tyson (2002) as micromolar units. For visual purposes the protein numbers have been rescaled to concentrations for all plots, by using the equivalence $[X] = \alpha \cdot \#X$ where $[X]$ and $\#X$ are the concentration and the number of molecules of species X, respectively. The simulated time-courses in Fig. 5A match those obtained with the ODE solution, shown in Novak and Tyson (2002).

We compare the results obtained with the stochastic model against the values obtained from the deterministic model in Fig. 5B, C. The SPN model provides an average duration of the cell cycle of about 148.08 (min) with a standard deviation of 10.67, which gives a coefficient of variation (defined as the ratio between standard deviation and average value) of 7.28%, and an average cell size at division time of about 0.819 (arbitrary units) with a standard deviation of 0.01455, which gives a coefficient of variation of 1.78%. These results indicate that the variability in cycle time duration is larger than the one in cell size, as reported from experimental observations in Tyson (1985). For the results computed through the simulation of the SPN model, Fig. 5 also shows the confidence interval computed from the observations. The confidence intervals were computed at the 95% level of confidence. For both results, the relative width of the confidence interval is less than 1%. As it can be observed, there is a close match between the results of the two models, and the ODE results falls within the confidence interval obtained via stochastic simulations.

Möbius (version 2.1.2) simulations of the SPN model were run on a standard WinXP desktop machine equipped with 2GB of RAM. Simulation of 1000 min of the wild type yeast cell cycle requires approximately 50 s per run. Simulating the models of yeast mutants described in the following sections is slightly quicker, as the considered mutations turn out in a reduction of the number of reactions.

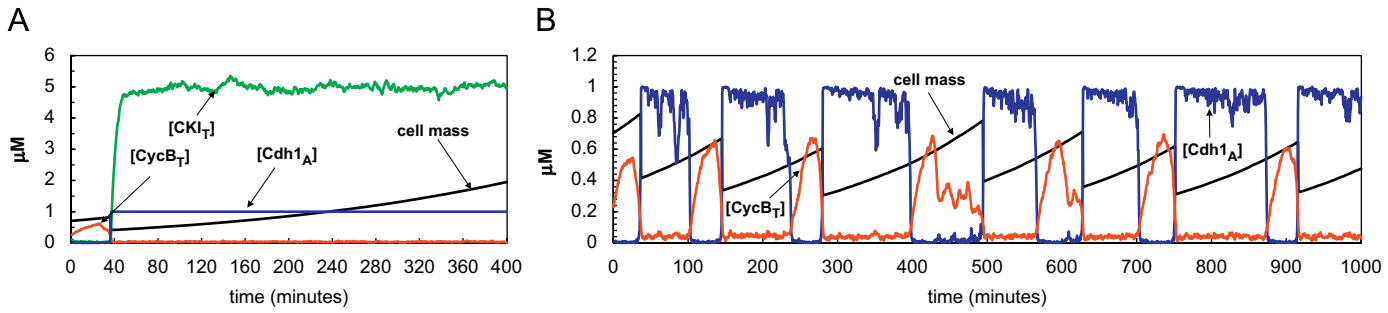

Fig. 6. Stochastic model results for the $cln1\Delta, cln2\Delta, cln3\Delta$ mutant. Example time courses (A) as obtained from a single simulation run of the stochastic model. Stochastic model results for the $cln1\Delta, cln2\Delta, cln3\Delta, sic1\Delta$ mutant (B).

4.2. Removal of the starter kinases

Let us now consider the mutant of budding yeast obtained by deleting all the starter kinases $cln1, cln2, cln3$, collectively modeled by species SK in both the deterministic and stochastic models. Because in the models SK is responsible for starting the series of biochemical processes that drive the cell from G1 to S phase, the $cln1\Delta, cln2\Delta, cln3\Delta$ triple mutant cells are not able to start DNA replication and block in G1 phase (Richardson et al., 1989).

Allowing for such a mutation in the ODE and SPN models is straightforwardly accomplished by simply setting parameters k'_{13} and k''_{13} to 0. In the ODE simulation results (Novak and Tyson, 2002), cells are able to complete mitosis once, because the initial condition sets the state of the system past the S phase, when the Cln's (SK in the models) have already accomplished their role and thus are not necessary anymore. However, in the subsequent cell cycle, the lack of SK blocks the mutant in G1, as nothing can induce the destruction of the Cdk/CycB stoichiometric inhibitor Sic1 (CKI in the models) and the activity of Cdh1. Consequently, the total concentration of CycB stays very low and what is available in the cell is bound with CKI and thus inactive, the typical condition of the G1 phase.

We show in Fig. 6A the stochastic model simulation results. The match with the result provided by the deterministic model is very accurate. The first mitosis is completed and then the cell blocks in G1 (in 100% of the 1000 simulation runs executed).

4.3. Rescue of the lethal phenotype of triple cln^- deletion

Because one of the main consequences of SK activity is to cause the degradation of the Cdk/CycB stoichiometric inhibitor CKI, it is interesting to look at a double mutant in which both SK and CKI are deleted. Indeed, in a mutant $cln1\Delta, cln2\Delta, cln3\Delta, sic1\Delta$ it is not obvious whether the cell would stop in G1 phase, or the active CycB cyclin may raise to a level that overrides the activity of Cdh1 thus making the cell able to enter S phase.

The ODE model (Novak and Tyson, 2002) matches the experimental observation that deletion of Sic1 can rescue the triple cln^- mutant phenotype (Tyers, 1996). Fig. 6B shows the results obtained with one simulation run of the SPN model. The results of the stochastic model also suggest the viability of this double mutant, with an appreciable increase in the variability of the cell cycle duration. It also shows that some cycles are delayed in M phase with high CycB activity, which might correlate with the sick phenotype of this strain (Tyers, 1996).

4.4. Removal of the Cdk stoichiometric inhibitor

We further investigate this sick behavior in the SPN simulations by looking at the $sic1\Delta$ mutant cells. We show in Fig. 7A the results provided by the deterministic model of the mutant, where we set parameter $k_{11} = 0$ to simulate $sic1\Delta$. The ODE results indicate the viability of the mutant, which fits the experimental observations (Schneider et al., 1996). Cdh1 alone is enough to stabilize the G1 phase in those cells.

The simulation output of the SPN model somewhat resembles the results of the deterministic one, as it can be seen from Fig. 7B. Though, it can be observed from the simulated time course that the cell cycle in this mutant shows relevant irregularities, with high variability in its length. Moreover, the mutant appears to have problems in degrading CycB, which leads to a prolonged M phase. On the other hand, some other cycles show a very regular pattern of oscillations, matching the one returned by the deterministic model in Fig. 7A. So we can conclude that removal of Sic1 causes problems in simulation with noise. It is important to mention that delayed cell cycles have been experimentally observed for this mutant, as the $sic1\Delta$ strain shows "sick" phenotype cells (Nugroho and Mendenhall, 1994).

We conducted a simulation experiments to compute a few statistics for the cell cycle of $sic1\Delta$ cells. We computed first of all the average values of cell cycle duration and of the cell mass in a population of asynchronous cells (by sampling this measure randomly along the cell cycle), and compared them against the deterministic results provided by the ODEs, as shown in Fig. 7C, D. As it can be observed, the results provided by the two methods are in agreement at this level.

Then, we also looked at the spread of the observation for the cell mass. The estimated average values of the cell mass is of about 0.59 for the wild type with a standard deviation 0.0167, corresponding to a coefficient of variation of 2.83%. However, for $Sic1\Delta$ mutant cells the average value is around 0.47 and the standard deviation 0.0543, which gives a coefficient of variation of about 11.55%, thus showing the spread of the cell mass distribution is quite different in the two modeled organisms. Indeed, as it can be seen from Fig. 7E, the distribution of the mass of the mutant exhibits a much higher variability, in agreement with the experimental observations (compare Nugroho and Mendenhall, 1994, Fig. 6). Thus, the stochastic model reveals the "sick" non robust phenotype of $sic1\Delta$ cells, which could not be revealed by the deterministic model.

4.5. A mutant with nutritional level sensitive viability

Experimental results show that the $Clb2db\Delta, clb5\Delta$ mutant is viable, but only under those circumstances that slow down its growth rate (Cross, 2003). These two cyclins are collectively modeled by species CycB in the models considered in this study. We can represent these two mutations as follows:

- the deletion of cyclin Clb2 destruction box is modeled by removing the ability of active Cdc20 to degrade CycB, by

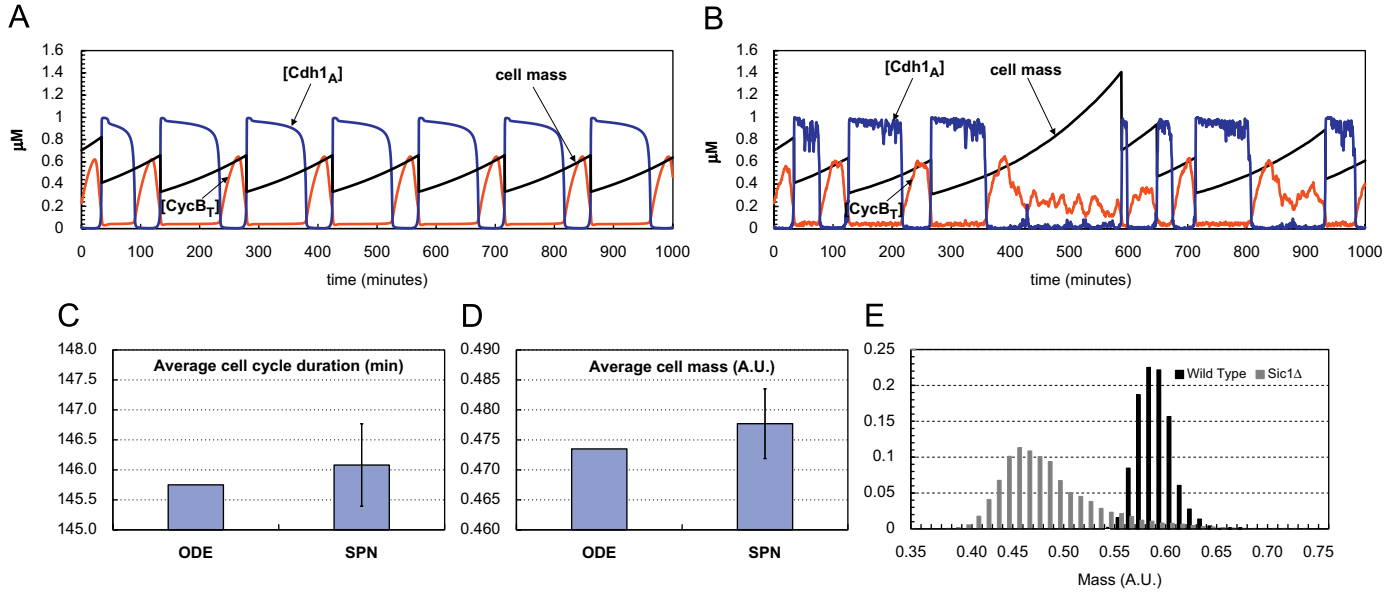

Fig. 7. Deterministic and stochastic model results for the *sic1Δ* mutant, (A) and (B), respectively. Comparison of deterministic values and statistics from stochastic model for the average cell cycle duration (C) and average cell mass in an asynchronous population (D) of *sic1Δ* mutant. Two thousand runs of simulation were used to compute the statistics, with 95% confidence level of results. Distribution of average cell mass for asynchronous populations of *sic1Δ* mutant and of wild type cells (E).

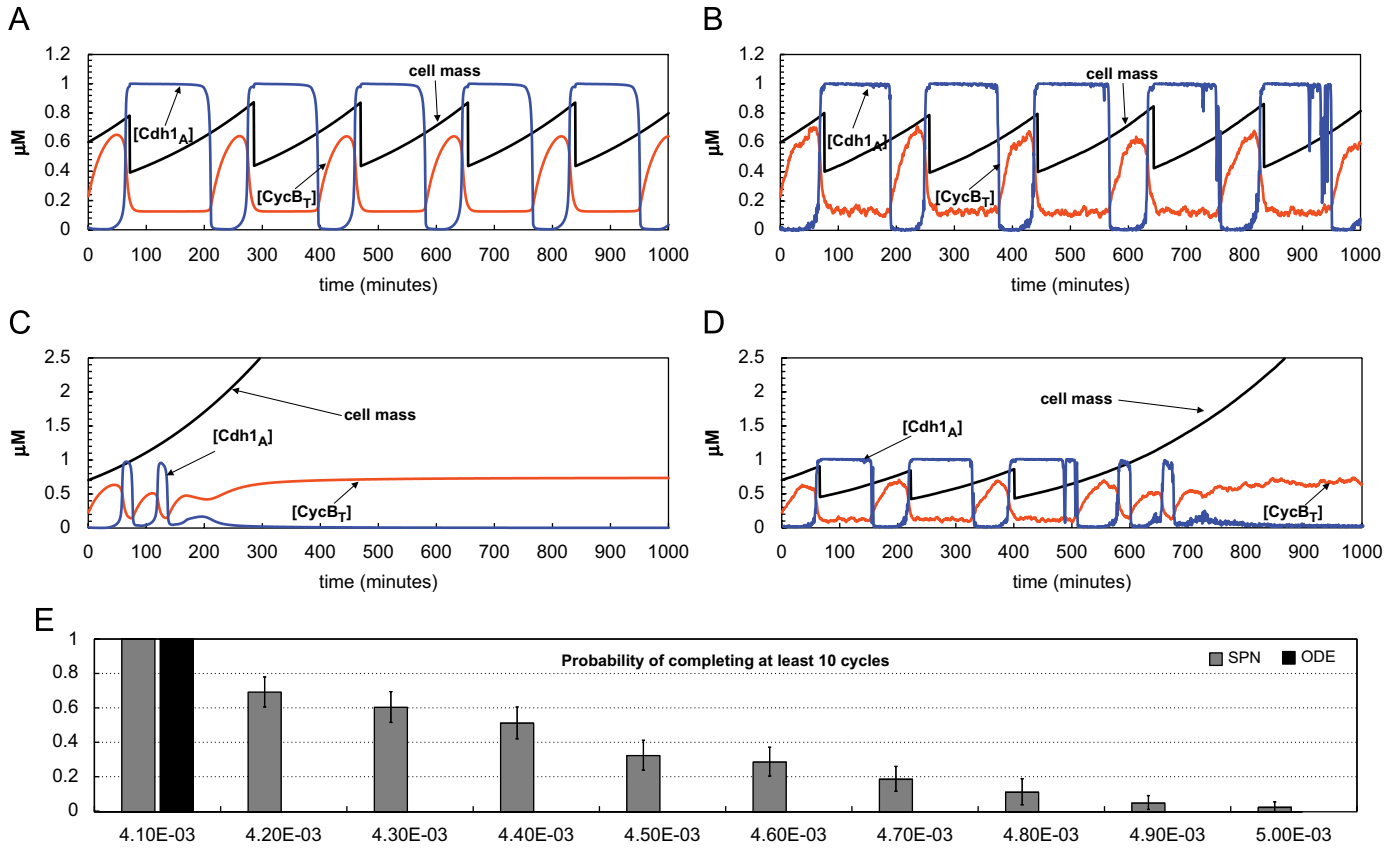

Fig. 8. Deterministic and stochastic model results for the *Clb2dbΔ, clb5Δ* mutant, (A) and (B), respectively, with growth rate $\mu = 0.004$. Deterministic model results for the *Clb2dbΔ, clb5Δ* mutant (C), and stochastic model results for the same mutant, with growth rate $\mu = 0.0043$ (D); The mutant cell can complete three cell cycles in the stochastic model before dying. (E) Probability of having at least 10 replications of a mutant with varying the growth rate.

setting parameter $k_2'' = 0$, and by reducing the degradation rate of CycB by active Cdh1, by setting parameter $k_2''' = 0.2$ (residual Cdh1 activity remains because of the KEN box on Clb2) (Wäsch and Cross, 2002);

- the deletion of cyclin Clb5 is modeled by reducing the production rate of CycB, by setting parameter $k_1 = 0.03$.

The deterministic model results for this mutant are shown in Fig. 8A, and correctly indicate its viability in poor growth conditions, i.e. growth rate $\mu = 0.004$ (here and in the following the time unit of the growth rate is min^{-1}). Fig. 8B shows the results obtained from the SPN model of the mutant with the same growth rate $\mu = 0.004$. As it can be observed,

the time courses returned by the two models match very well.

It is interesting to observe that the deterministic model is also able to fit the lethality of the mutation in glucose (growth rate $\mu = 0.005$). Actually, the transition from dead to viable for the ODE model is at $\mu \approx 0.0041$, and the model cannot predict any intermediate situation. For instance, Fig. 8C shows the solution of the deterministic model for a growth rate $\mu = 0.0043$, which indicates lethality of the mutation. However, it is reasonable to expect a continuous transition as the growth rate varies in the interval [0.004, 0.005], with some mutant cells having a limited survivability for values of the growth rate inside the interval. If in a population of mutant cells each of them is able to complete a sufficient number of cells cycles before dying, a small colony may develop, even if its overall growth would be slow. Such small colonies have been experimentally observed for various other mutants as well (Cross, 2003). We show in Fig. 8D the results provided by the stochastic model for a run using the growth rate value $\mu = 0.0043$, in which the cell was able to complete some cycles before reaching a state that does not allow it to survive further.

We conducted an in-silico experiment to evaluate the probability that the progeny of a single mutant cell would be able to divide at least 10 times before dying (forming a small colony), with varying the growth rate within the interval [0.0041, 0.005]. For each value of the growth rate, mutant cells were simulated over a time window [0–2000] min. The metric of interest was estimated as the ratio between the number of runs in which cells completed at least 10 cycles and the total number of runs, 1000 in these experiments. The results of the simulation are shown in the chart in Fig. 8E, together with their confidence intervals. Also, that same probability is shown for the result provided by the ODE model, obviously jumping from one to zero as μ is increased over the critical value 0.0041.

The results in Fig. 8E clearly show that colonies of the mutant may exist for values of the growth rate higher than the threshold value 0.0041, which sets the upper limit for the viability of the mutant in the ODE model. Thus we present that stochastic simulations can be important to check the "partial" viability of some mutants that are at the border between life and death. Similar nutrition sensitive mutants (Cross, 2003) were simulated in a much more complex model (Csikász-Nagy et al., 2006). It would be interesting to see their behavior in a more detailed SPN model.

5. Conclusions and future work

This paper presents the results of a stochastic modeling of the cell cycle of budding yeast cells. A well-established deterministic model, based on ODEs (Novak and Tyson, 2002), has been taken as the starting point for constructing a Stochastic Petri Net (SPN) model of the cell cycle biochemical machinery. The SPN model was built with adopting the same abstractions captured by the deterministic model. A simple and largely automatable procedure for mapping ODEs into SPN constructs has been presented through its application to the model definition process.

The resulting SPN model has been described, and then its validation conducted, with a comparison of the results obtained via simulation against the results provided by the deterministic model as well as with reference to experimental results. The validation encompassed the wild type and various mutants of budding yeast.

The validation showed a general agreement between the results of the two methods. We demonstrated how the stochastic version of the model can, however provide deeper insights about the cell cycle of the modeled organisms, as it allows a statistic characterization of cell cycle parameters such as duration and average cellular mass. In some circumstances, for instance when cells may die after completing a few cell cycles, the SPN model better reproduces the experimentally observed cell phenotype of small colony formation. Hence, with SPNs we can simulate cell behaviors beyond the average one. This could have been done by Langevine equations as well, but that would not allow dealing correctly with the small number of molecules in some phases the cell cycle. Indeed, when the abundance of molecules is low, an added Wiener noise may result in negative numbers which need to be scaled to meaningful values, thus changing in an artificial way the stochastic properties of the fluctuation process.

It is important to notice that a gap exists between the variability in the outcome of the SPN model and the one observed experimentally. For instance, the coefficient of variation computed from the SPN results for wild type yeast cells is 7.28% for cell cycle duration, 1.78% for cell mass at division and 2.83% for average cell mass in an asynchronous population, whereas the typical values found in experiments are about 10% for cell cycle length and 5% for mass, see for instance Tyson (1985). The reason for such reduced variation has to be explained taking into consideration the approximations introduced in defining the model. First of all, as we already pointed out, the model is still using various abstractions of biochemical elementary reactions that are represented by the Michaelis–Menten and Hill functions rendered via deterministic marking-dependent rate functions. We may expect such abstractions to result in a lower variability with respect to the one that would be obtained with a model fully capturing the elementary biochemical reactions that compose the cell cycle network. On the other hand, the limited amount of molecules accounted for by our choice of the scaling factor α^{-1} (505 molecules in the cell per μM) compared to a few thousands (Cross et al., 2002) may yield to a larger molecular noise, thus contributing to increase the variability of the species concentrations and ultimately that of the measures of interest. Moreover, it must be considered that the SPN model considers a precise and even division between mother and daughter cells, thus lacking the noise on the asymmetric division of *Saccharomyces cerevisiae* yeast cells. This modeling assumption limits the variability in both cell cycle duration and cell mass.

Therefore, we intend in our future research to alleviate such limitations of the work presented in this paper, by considering, besides the effects of intrinsic noise of molecular fluctuation, sources of extrinsic noise such as randomness in cell division and non-symmetrical division of budding yeast cells. Moreover, we also intend to watch in more detail at the measured molecule numbers of cell cycle regulatory proteins (Cross et al., 2002) and at precise measurements of budding yeast *Saccharomyces cerevisiae* cell nucleus size (Jorgensen et al., 2007).

Finally, more detailed deterministic models of the cell cycle in budding yeast are available in the literature, which include molecules other than the ones we considered in this paper. In our future work we also plan to extend the stochastic modeling by looking at the information contained in these models (Chen et al., 2000, 2004; Barberis et al., 2007; Toth et al., 2007). Furthermore, we can enrich the model with the explicit representation of the various checkpoints (Hartwell and Weinert, 1989; Ciliberto et al., 2003). These checkpoints are controlled by a number of signaling pathways that ensure the completion of various step of the cell cycle, such as DNA replication, bud formation, complete formation of the mitotic spindle, alignment of chromosomes. Hence, the explicit modeling of checkpoints provides the interface point in the cell cycle to include detailed models of those pathways, an activity that we shall tackle in our future work.

Acknowledgements

The authors are grateful to John J. Tyson for the useful comments on the preliminary version of this manuscript. They also acknowledge support from the Italian research fund FIRB (project RBPR0523C3) and from the Hungarian research fund OTKA (F 60414).

Appendix A. Supplementary data

Supplementary data associated with this article can be found in the online version at 10.1016/j.jtbi.2008.07.019

References

Alberts, B., Johnson, A., Lewis, J., Raff, M., Roberts, K., Walter, P., 2002. Molecular Biology of the Cell. Garland Sciences, New York.
Alt, W., Tyson, J.J., 1987. A stochastic model of cell division (with application to fission yeast). Math. Biosci. 84, 159–187.
Barberis, M., Klipp, E., Vanoni, M., Alberghina, L., 2007. Cell size at S phase initiation: an emergent property of the G1/S network. PLoS Comput. Biol. 3 (4), e64.
Chen, K.C., Csikász-Nagy, A., Gyorffy, B., Val, J., Novak, B., Tyson, J.J., 2000. Kinetic analysis of a molecular model of the budding yeast cell cycle. Mol. Biol. Cell 11, 369–391.
Chen, K.C., Calzone, L., Csikász-Nagy, A., Cross, F.R., Novak, B., Tyson, J.J., 2004. Integrative analysis of cell cycle control in budding yeast. Mol. Biol. Cell 15, 3841–3862.
Ciardo, G., Muppala, J.K., Trivedi, K.S., 1989. SPNP: stochastic Petri net package. In: International Workshop on Petri Nets and Performance Models (PNPM'89), pp. 142–151.
Ciliberto, A., Novak, B., Tyson, J.J., 2003. Mathematical model of the morphogenesis checkpoint in budding yeast. J. Cell Biol. 163 (6), 1243–1254.
Cross, F.R., 2003. Two redundant oscillatory mechanisms in the yeast cell cycle. Dev. Cell 4, 741–752.
Cross, F.R., Archambault, V., Miller, M., Klovstad, M., 2002. Testing a mathematical model for the yeast cell cycle. Mol. Biol. Cell 13, 52–70.
Csikász-Nagy, A., Battogtokh, D., Chen, K.C., Novak, B., Tyson, J.J., 2006. Analysis of a generic model of eukaryotic cell-cycle regulation. Biophys. J. 90, 4361–4379.
Csikász-Nagy, A., Kapuy, O., Gyorffy, B., Tyson, J.J., Novak, B., 2007. Modeling the septation initiation network (SIN) in fission yeast cells. Curr. Genet. 51, 245–255.
Futcher, B., 1996. Cyclins and the wiring of the yeast cell cycle. Yeast 12, 1635–1646 doi:10.1002/(SICI)1097-0061(199612)12:16<1635::AID-YEA83>3.0.CO;2-O.
Gillespie, G.T., 1977. Exact stochastic simulation of coupled chemical reactions. J. Phys. Chem. 81 (25), 2340–2361.
Gonze, D., Halloy, J., Goldbeter, A., 2002. Deterministic Versus Stochastic Models for Circadian Rhythms. J. Biol. Phys. 28, 637–653.
Goss, P.J.E., Peccoud, J., 1998. Quantitative modeling of stochastic systems in molecular biology by using stochastic Petri nets. Proc. Natl. Acad. Sci. USA 95, 6750–6755.
Goutsias, J., 2005. Quasiequilibrium approximation of fast reaction kinetics in stochastic biochemical systems. J. Chem. Phys. 122 (8), 184102.
Hartwell, L.H., Weinert, T.A., 1989. Checkpoints: controls that ensure the order of cell cycle events. Science 246, 629–634.
Jorgensen, P., Nishikawa, J.L., Breitkreutz, B.-J., Tyers, M., 2002. Systematic identification of pathways that couple cell growth and division in yeast. Science 297, 395–400.
Jorgensen, P., Edgington, N.P., Schneider, B.L., Rupeš, I., Tyers, M., Futcher, B., 2007. The size of the nucleus increases as yeast cells grow. Mol. Biol. Cell 18, 3523–3532.
Morgan, D.O., 2006. The Cell Cycle: Principles of Control. New Science Press.
Nasmyth, K., 1996. At the heart of the budding yeast cell cycle. Trends Genet. 12, 405–412.
Novak, B., Tyson, J.J., 2002. Cell Cycle Controls. In: Fall, C.P., et al. (Eds.), Computational Cell Biology. Springer, Berlin, pp. 261–284.
Novak, B., Tyson, J.J., Gyorffy, B., Csikász-Nagy, A., 2007. Irreversible cell-cycle transitions are due to systems-level feedback. Nature Cell. Biol. 9, 724–728.
Nugroho, T.T., Mendenhall, M.D., 1994. An inhibitor of yeast cyclin-dependent protein kinase plays an important role in ensuring the genomic integrity of daughter cells. Mol. Biol. Cell 14, 3320–3328.
Nutsch, T., Oesterhelt, D., Gilles, E.D., Marwan, W, 2005. A quantitative model of the switch cycle of an archaeal flagellar motor and its sensory control. Biophys. J. 89 (4), 2307–2323.
Peccoud, J., Courtney, T., Sanders, W.H., 2007. Möbius: an integrated discrete-event modeling environment. Bioinformatics, doi:10.1093/bioinformatics/btm517.
Peleg, M., Rubin, D., Altman, R.B., 2005. Using Petri net tools to study properties and dynamics of biological systems. J. Am. Med. Inf. Assoc. 12, 181–199.
Rao, C.V., Arkin, A.P., 2003. Stochastic chemical kinetics and the quasi-steady-state assumption: application to the Gillespie algorithm. J. Chem. Phys. 118 (11), 4999–5010.
Richardson, H., Wittenberg, C., Cross, F.R., Reed, S.I., 1989. An essential G1 function for cyclin-like proteins in yeast. Cell 59, 1127–1133.
Rupes, I., 2002. Checking cell size in yeast. Trends Genet. 18, 479–485.
Sabouri-Ghomi, M., Ciliberto, A., Kar, S., Novak, B., Tyson, J.J., 2007. Antagonism and bistability in protein interaction networks. J. Theor. Biol.
Schneider, B.L., Yang, Q.-H., Futcher, A.B., 1996. Linkage of replication to start by the Cdk inhibitor Sic1. Science 27, 560–562.
Schwob, E., Böhm, T., Mendenhall, M.D., Nasmyth, K., 1994. The B-type cyclin kinase inhibitor $p40^{SIC1}$ controls the G1 to S transition in S. cerevisiae. Cell 79 (2), 233–244.
Sible, J.C., Tyson, J.J., 2007. Mathematical modeling as a tool for investigating cell cycle control networks. Methods 41, 238–247.
Spellman, P.T., Sherlock, G., Zhang, M.Q., Iyer, V.R., Anders, K., Eisen, M.B., Brown, P.O., Botstein, D., Futcher, B., 1998. Comprehensive identification of cell cycle-regulated genes of the yeast *Saccharomyces cerevisiae* by microarray hybridization. Mol. Cell Biol. 9, 3273–3297.
Srivastava, R., Peterson, M.S., Bentley, W.E., 2001. Stochastic kinetic analysis of *Escherichia coli* stress circuit using σ_{32} targeted antisense. Biotechnol. Bioeng. 75 (1), 120–129.
Steuer, R., 2004. Effects of stochasticity in models of the cell cycle: from quantized cycle times to noise-induced oscillations. J. Theor. Biol. 228, 293–301.
Sveiczer, A., Tyson, J.J., Novak, B., 2001. A stochastic, molecular model of the fission yeast cell cycle: role of the nucleocytoplasmic ratio in cycle time regulation. Biophys. Chem. 92, 1–15.
Sveiczer, A., Novak, B., Mitchison, J.M., 2004. Size control in growing yeast and mammalian cells. Theor. Biol. Med. Model. 1, 12.
Toth, A., Queralt, E., Uhlmann, F., Novak, B., 2007. Mitotic exit in two dimensions. J. Theor. Biol. 248, 560–573.
Tsavachidou, D., Liebman, M.N., 2002. Modeling and simulation of pathways in menopause. J. Am. Med. Inf. Assoc. 9, 461–471.
Tyers, M., 1996. The cyclin-dependent kinase inhibitor $p40^{SIC1}$ imposes the requirement for Cln G1 cyclin function at start. Proc. Natl. Acad. Sci. USA 93, 7772–7776.
Tyson, J.J., 1985. The coordination of cell growth and division—intentional or incidental? BioEssays 2 (2), 72–77.
Wäsch, R., Cross, F.R., 2002. APC-dependent proteolysis of the mitotic cyclin Clb2 is essential for mitotic exit. Nature 418, 556–562.
Wilkinson, D.J., 2006. Stochastic Modelling for Systems Biology. Chapman & Hall, CRC, London.
Zachariae, W., Nasmyth, K., 1999. Whose end is destruction: cell division and the anaphase-promoting complex. Genes Dev. 13, 2039–2058.
Zámborszky, J., Hong, C.I., Csikász-Nagy, A., 2007. Computational analysis of mammalian cell division gated by a circadian clock: quantized cell cycles and cell size control. J. Biol. Rhythms 22, 542–553.
Zhang, Y., Qian, M., Ouyang, Q., Deng, M., Li, F., Tanga, C., 2006. Stochastic model of yeast cell-cycle network. Physica D 219 (1), 35–39.

dc_836_14

7.5 Sejtciklus reguláció előrecsatolásos hurkokkal

Csikász-Nagy A., Kapuy O., Toth A., Pal C., Jensen, L.J. Uhlmann, F. Tyson, J.J. & Novák B. (2009) Cell cycle regulation by feed-forward loops coupling transcription and phosphorylation. *Mol Sys Biol* **5**:236 **Impakt faktor: 12.125**

Molecular Systems Biology 5; Article number 236; doi:10.1038/msb.2008.73
Citation: ***Molecular Systems Biology*** **5:236**

www.molecularsystemsbiology.com

molecular systems biology

REPORT

Cell cycle regulation by feed-forward loops coupling transcription and phosphorylation

Attila Csikász-Nagy[1,*], Orsolya Kapuy[2,3], Attila Tóth[3], Csaba Pál[1,4], Lars Juhl Jensen[5,6], Frank Uhlmann[7], John J Tyson[8] and Béla Novák[2,3,*]

[1] The Microsoft Research—University of Trento Centre for Computational and Systems Biology, Povo (Trento), Italy, [2] Department of Biochemistry, Oxford Centre for Integrative Systems Biology, University of Oxford, Oxford, UK, [3] Department of Applied Biotechnology and Food Science, Budapest University of Technology and Economics, Budapest, Hungary, [4] Systems Biology Unit, Institute of Biochemistry, Biological Research Center, Szeged, Hungary, [5] European Molecular Biology Laboratory, Heidelberg, Germany, [6] Novo Nordisk Foundation Center for Protein Research, University of Copenhagen, Copenhagen, Denmark, [7] Chromosome Segregation Laboratory, Cancer Research UK London Research Institute, London, UK and [8] Department of Biological Sciences and Virginia Bioinformatics Institute, Virginia Polytechnic Institute & State University, Blacksburg, VA, USA
* Corresponding authors. A Csikász-Nagy, The Microsoft Research—University of Trento Centre for Computational and Systems Biology, Piazza Manci 17, Trento 38100, Italy. Tel.: +39 046 188 2824; Fax: +39 046 188 2814; E-mail: csikasz@cosbi.eu or B Novák, Oxford Centre for Integrative Systems Biology, Department of Biochemistry, University of Oxford, South Parks Road, Oxford OX1 3QU, UK. Tel.: +44 1865 613216; Fax: +44 1865 613213; E-mail: bela.novak@bioch.ox.ac.uk

Received 30.9.08; accepted 4.12.08

The eukaryotic cell cycle requires precise temporal coordination of the activities of hundreds of 'executor' proteins (EPs) involved in cell growth and division. Cyclin-dependent protein kinases (Cdks) play central roles in regulating the production, activation, inactivation and destruction of these EPs. From genome-scale data sets of budding yeast, we identify 126 EPs that are regulated by Cdk1 both through direct phosphorylation of the EP and through phosphorylation of the transcription factors that control expression of the EP, so that each of these EPs is regulated by a feed-forward loop (FFL) from Cdk1. By mathematical modelling, we show that such FFLs can activate EPs at different phases of the cell cycle depending of the effective signs (+ or −) of the regulatory steps of the FFL. We provide several case studies of EPs that are controlled by FFLs exactly as our models predict. The signal-transduction properties of FFLs allow one (or a few) Cdk signal(s) to drive a host of cell cycle responses in correct temporal sequence.
Molecular Systems Biology 20 January 2009; doi:10.1038/msb.2008.73
Subject Categories: simulation and data analysis; cell cycle
Keywords: budding yeast; cell cycle; DNA replication; feed-forward loop

Introduction

A eukaryotic cell's progression through G1, S, G2 and M phases of the cell replication division cycle is orchestrated by large-amplitude fluctuations in Cyclin-dependent protein kinase (Cdk) activities that are generated by a series of coupled positive and negative feedback loops (Novak *et al*, 2007; Holt *et al*, 2008; Skotheim *et al*, 2008; Tyson and Novak, 2008). Cdk signals are transduced into appropriate cell cycle responses by specific executor proteins (EPs) (Sutani *et al*, 1999; Tanaka *et al*, 2007a) (Box 1). For example, cell division is controlled by Cdk1 phosphorylation of components of a signalling pathway called the 'mitotic exit network' in budding yeast and the 'septation initiation network' in fission yeast (Bardin and Amon, 2001). Recently, we showed (Csikasz-Nagy *et al*, 2007) that the septation initiation network has the characteristic topology of a feed-forward loop (FFL): the high level of Cdk1–cyclin B in mitosis activates proteins that function early in the network (sensors) and inactivates proteins that function late in the network (executors). High Cdk1 activity primes the septation initiation network, but the network cannot 'fire' until Cdk1 activity falls and releases the inhibitory arm. A similar FFL controls the onset of DNA synthesis, according to the 'licensing factor' hypothesis (Blow, 1993). Recognizing the roles of FFLs in executing DNA synthesis and cell division, we hypothesized that FFLs might be common motifs in transmitting signals from Cdk1–cyclin master regulatory complexes to target proteins that execute cell cycle events.

Cdk1 substrates are potential EPs, as are proteins that are periodically expressed during the cell cycle (Spellman *et al*,

Box 1 Cdk signal transduction by feed-forward loops

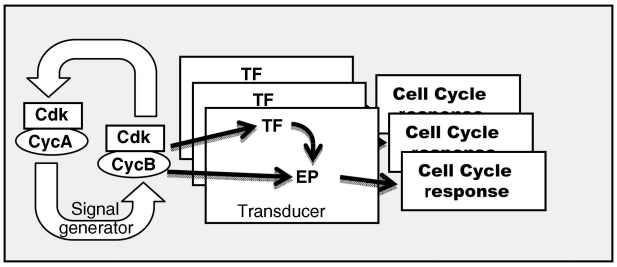

Feed-forward loops, involving a Cdk substrate executor protein (EP) and its transcription factor (TF), are proposed to function as transducers between cell cycle regulatory signals (periodic fluctuations in Cdk activity) and cell cycle responses, such as initiation of DNA synthesis or cell division.

1998; Jensen *et al*, 2006). Intriguingly, proteins that are periodically expressed during the cell cycle are often Cdk substrates (Ubersax *et al*, 2003; Jensen *et al*, 2006). Furthermore, the transcription factors (TFs) that drive cell cycle-dependent gene expression must be cell cycle-regulated themselves, and it is reasonable to suspect that at least some of them are phosphorylated by Cdks. Wherever this is the case, the Cdk–TF–EP trio are involved in an FFL (Box 1). Owing to large-scale experimental screens in budding yeast (*Saccharomyces cerevisiae*) for targets of Cdk1 (Ubersax *et al*, 2003; Loog and Morgan, 2005), as well as for cell cycle TFs (Lee *et al*, 2002), it is possible to systematically test this hypothesis at the genome-wide scale.

Results and discussion

To this end, we classified all the 4691 verified protein-coding genes of the budding yeast genome into 6 non-overlapping network topologies (Figure 1A) based on whether or not the encoded protein has been reported to be a Cdk1 substrate, whether or not TFs of the gene are known and whether or not at least one TF is a Cdk1 target. We identified 126 genes involved in an FFL, that is the encoded protein is a Cdk1 target and at least one TF is a Cdk1 target. Of these 126 genes involved in FFLs, 68 (54%) are found to be periodically expressed during the cell cycle, whereas only 13 would be expected by chance ($P<10^{-28}$). None of the other regulatory motifs shows a comparably high ratio of periodically expressed genes (Figure 1A; Supplementary Table S1). Thus, it is clear that a strong predictor of cell cycle periodicity is the involvement of a gene in an FFL regulatory motif. This observation suggests that the 68 periodically transcribed, FFL-regulated proteins (Supplementary Table S2) may indeed be key cell cycle EPs.

To provide further support for this assertion, we show that cell cycle-related functions are significantly over-represented among the proteins involved in FFLs. We checked the distribution of proteins with cell cycle (and related) MIPS functional category annotations (Ruepp *et al*, 2004; Guldener *et al*, 2005) among the proteins of the different regulatory topologies established on Figure 1A. We found that FFL-regulated proteins are significantly over-represented among most gene classes with cell cycle functions (Figure 1B; Supplementary Table S3). The converse statement is also true: cell cycle functions are over-represented among the terms associated with FFL-regulated proteins (Supplementary Table S4). Thus, we conclude that FFLs are indeed important transducers of Cdk 'signals' to cell cycle 'responses' (Box 1). The other regulatory topology with high over-representation of cell cycle-related functions is the small group of 'only Cdk'-regulated genes. If our conclusion is correct, then, once the TFs for these genes are discovered, most of these EPs will fall disproportionately into the FFL-regulated group.

If cell cycle EPs are indeed significantly associated with FFL-regulatory topologies, then we must ask what possible function(s) these signal-transduction pathways play in orchestrating progression through the cell cycle. The function of an FFL depends on the signs of the three links of the motif ($\pm\ \pm/\pm$). The first sign ($+$ for activation or $-$ for inhibition) indicates the effect of Cdk-mediated phosphorylation on the activity of TF, and the second sign indicates whether the active form of TF upregulates or downregulates gene expression. The product of these two signs indicates the net effect (activation or inhibition) of the 'long arm' of the FFL on EP activity. The third sign indicates whether direct phosphorylation of EP by Cdk activates the protein or inhibits it. The eight possible sign combinations can be divided into two classes (Mangan and Alon, 2003): coherent FFLs, ($\pm\ \pm/+$) and ($\mp\ \pm/-$) with the same effective signs on the long and short arms and incoherent FFLs, ($\pm\ \pm/-$) and ($\mp\ \pm/+$) with opposite signs. Coherent FFLs have noise-filtering properties (Mangan *et al*, 2003): ($\pm\ \pm/+$) EPs would be active only when Cdk activity is sustained at a high level (in S + G2 + M phase), and ($\mp\ \pm/-$) EPs would be active only when Cdk1 activity is absent for a prolonged period of time (in G1 phase). Incoherent FFLs have rich signal response capabilities (Tyson *et al*, 2003; Csikasz-Nagy and Soyer, 2008; Kaplan *et al*, 2008). Of particular relevance here, they may respond only to sufficiently strong bursts of a signal: a ($\mp\ \pm/+$) EP is activated transiently when Cdk activity rises after a prolonged period of low Cdk activity (at the G1/S transition), and a ($\pm\ \pm/-$) EP is activated transiently when Cdk activity falls after a prolonged period of high Cdk1 activity (at the M/G1 transition). We propose that many of the FFL-regulated proteins identified by our bioinformatics survey of the yeast genome/proteome play exactly these roles in the yeast cell cycle.

To see how FFLs might regulate cell cycle events, we first study their dynamics from a theoretical perspective. We model the eight FFL motifs using ordinary differential equations for phosphorylation reactions and delay differential equations for changes in EP concentrations (Figure 2A; Supplementary Table S5). To implement a single transient activation of EPs per cell cycle, the direct arm of the FFL is expected to have a lower phosphorylation threshold and operate on a faster timescale than the indirect arm. These timescale differences arise naturally in a phosphorylation-transcription FFL: direct phosphorylation of an EP by Cdk happens within seconds, but phosphorylation of its TF has a delayed effect on production of the EP (timescale ~ minutes) (Adelman *et al*, 2002).

Simulation results of the model are shown in Figure 2B. In this figure, we plot (in black) a typical trajectory of

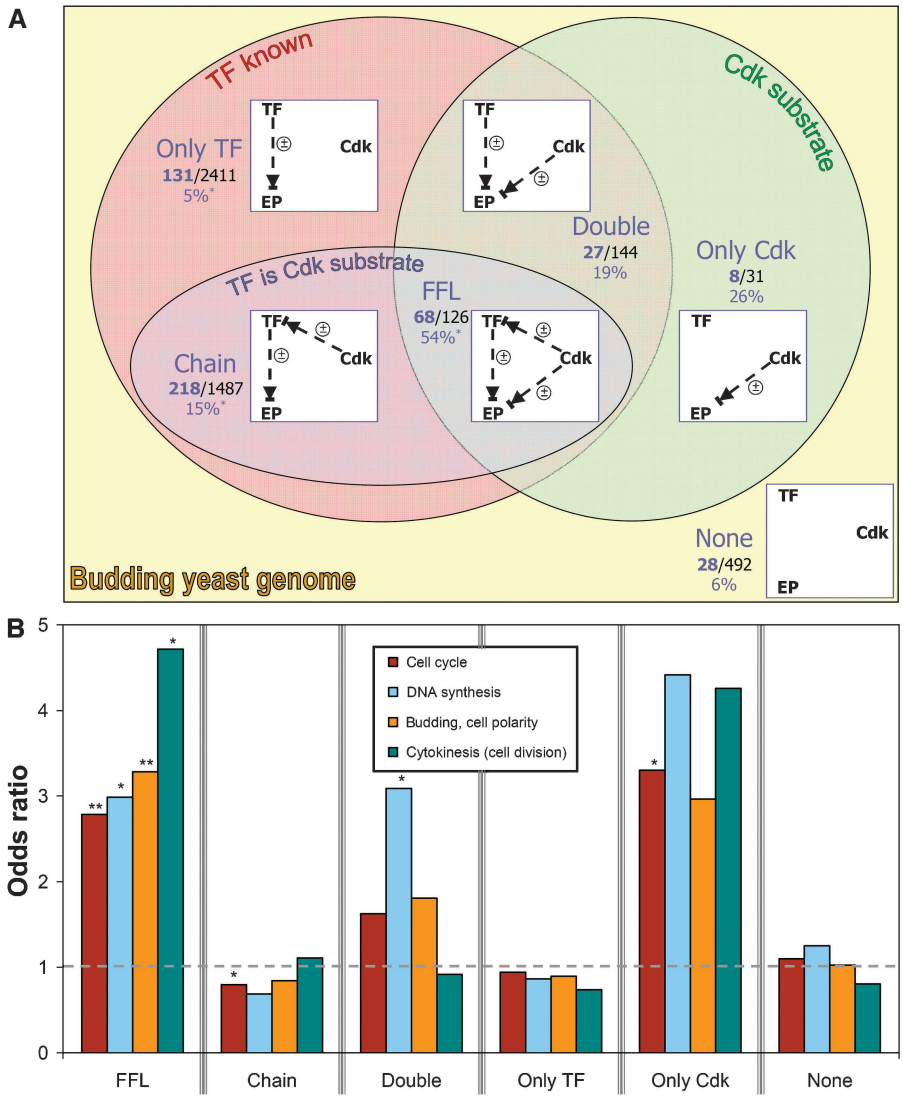

Figure 1 FFL-regulated proteins are over-represented among both periodically transcribed genes and cell cycle-related genes. (**A**) All verified ORFs of the budding yeast genome were distributed into groups by the topology of their regulation by Cdk (Cdk1) and transcription factors. For each group, we report the number of periodically transcribed/total proteins. For details, see Supplementary Table S1. (**B**) Odds ratios (observed/expected) of finding a gene with a certain type of regulation (as explained on (A)) to be found with an MIPS functional category term given by the colour code in the legend. For detailed statistics, see Supplementary Table S3. On all six panels, a single star denotes those cases where the probability of random appearance (according to a binomial distribution) is less than 10^{-3}, and two stars denotes a probability less than 10^{-6}. The dashed line indicates an expected odds ratio of 1.

Cdk1–cyclin B during the budding yeast cell cycle. We think of this trajectory as the 'signal generator' and the FFLs as 'signal transducers' (Box 1). Cdk1–cyclin B activity begins to rise at the G1/S transition, peaks in mitosis and falls rapidly as cells exit mitosis and return to G1 phase. As expected, the coherent FFLs, $(-\ +/-)$ and $(+\ +/+)$, drive sustained EP activity in G1 phase (yellow curve) and in S + G2 + M phase (red curve), respectively. The incoherent FFLs drive bursts of EP activity at the G1/S transition (blue curve: $(-\ +/+)$ FFL) and at the M/G1 transition (green curve: $(+\ +/-)$ FFL). Coherent FFLs ensure the proper temporal appearance of G1-specific and of (S + G2 + M)-specific proteins. Incoherent FFLs convert the periodic rise and fall of Cdk activity into a strict alternation of S-phase entry and M-phase exit, the two transitions that must occur once and only once during each cell cycle to ensure proper duplication and separation of the cell's genetic material.

Next, we use diverse evidences to predict, in some cases, the signs of the regulatory effects in our FFL motifs (Supplementary Table S6). From these predictions, we could identify 59 FFLs involving 46 EPs for which the signs of all three links may be proposed (Supplementary Table S7). We found examples of all eight types of FFLs, including some important regulators whose times of appearance in the cell cycle match the predictions of our theory (Figure 2B). In Figure 3, we show examples of an $(-\ +/-)$ FFL controlling a G1 protein, Sic1 (Knapp *et al*, 1996), an $(+\ +/+)$ FFL controlling a mitotic protein, Cdc5 (Zhu *et al*, 2000), an $(+\ +/-)$ FFL controlling a cell division protein, Dbf2 (Visintin and Amon, 2001) and an $(-\ +/+)$ FFL controlling an S-phase initiator, Sld2 (Tanaka

et al, 2007a). In the case of Sld2, our database search revealed 'only Cdk' regulation (with periodic gene expression). However, Ash1 has been proposed (Teixeira *et al*, 2006) as a potential TF for Sld2. If our theory of signal transduction is correct, then, as Sld2 is an S-phase initiator, the FFL should be (− +/+) and Ash1 is predicted to be an activator of *SLD2* expression. This prediction fits recent experimental results on the role and regulation of Sld2 at S-phase initiation (Tanaka *et al*, 2007b; Zegerman and Diffley, 2007) as well its protein fluctuation profile (not shown) (Masumoto *et al*, 2002).

The eight basic FFLs that we have described theoretically are clearly oversimplifications of the signal-transduction schemes operating in real cells. For example, the case of Sld2 (Figure 3C) illustrates that FFLs may be overlapping and even contradictory. Sld2 contains PEST sequences (Supplementary Table S6), which suggests that, after Sld2 is activated by Cdk1 (Zegerman and Diffley, 2007; Tanaka *et al*, 2007b), it is phosphorylated by Cdk1 on a different site that induces its degradation, giving two overlapping, contradictory FFLs. Similar overlapping FFLs might operate for other initiators of DNA replication, such as MCM proteins and Cdc6. (Our methods may be insufficient to identify an early, transient activation of these proteins by Cdk1 before they are degraded.) The case of Cln3 (Figure 3E) suggests that interlocked FFLs may be employed to achieve more complex regulatory effects.

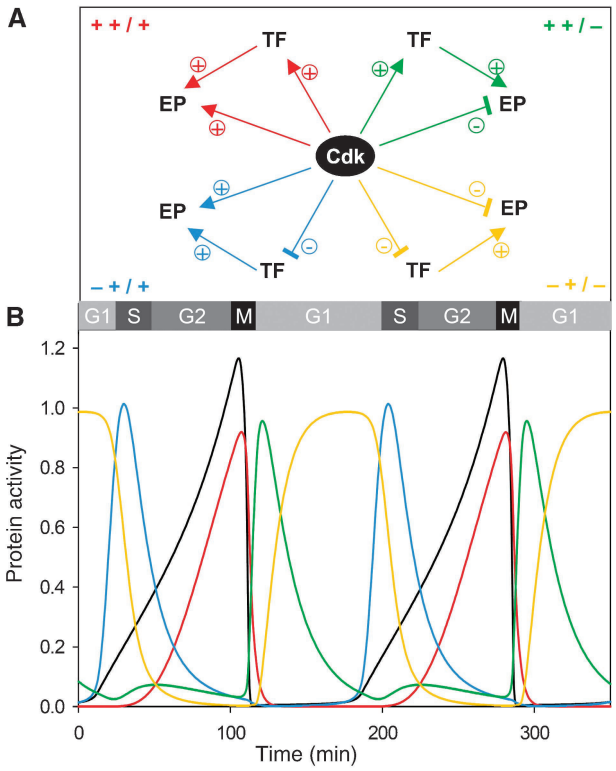

Figure 2 Four feed-forward loops can regulate the cell cycle. We limit our attention here to the case of upregulation of transcription by TF; for the case of downregulation, see the Supplementary information. (**A**) Four different types of FFL, for the case where TF upregulates synthesis of EP. Arrows with + or − represent activation or inhibition, respectively. (**B**) Computer simulations of equations (Supplementary Table S5) describing the interactions diagrammed above. Black line: Cdk activity; coloured lines: EP activities for FFL motifs of same colour in (A). Proposed borders of cell cycle phases are also indicated.

Sic1 (Figure 3D) presents an example where an FFL is composed with a double-negative feedback loop, because Sic1 is a well-known inhibitor of Cdk1-Clb in budding yeast (Schwob *et al*, 1994). The double-negative (=positive) feedback loop functions as a switch, flipping on (Cdk1-Clb activity high) at start and off (Cdk1-Clb activity low) at mitotic exit (Chen *et al*, 2004). By embedding the double-negative feedback loop within a coherent FFL, the switch is made more robust. This feature has been demonstrated recently by removing all Cdk phosphorylation sites from Sic1 (Cross *et al*, 2007), i.e. by removing one leg of the FFL, which made the two transitions less robust. In passing, we note that Sic1 is not an inhibitor of Cdk1-Cln, so the Cln-dependent kinases do indeed control Sic1 by a simple coherent FFL.

Cdc5 (Figure 3A) presents a similar example because of its multiple downstream targets, including proteins such as Cdc25, Wee1 and cyclin B involved in activating Cdk1 at the transition into mitosis (Barr *et al*, 2004). Activation of Cdk1 by Cdc5 turns the coherent FFL into a pair of interlocked positive feedback loops, which may be important in stabilizing M phase. However, it is not clear that this feedback loop is operational in budding yeast, where the functional homologues of Cdc25 and Wee1 do not play such a strong role in mitotic entry.

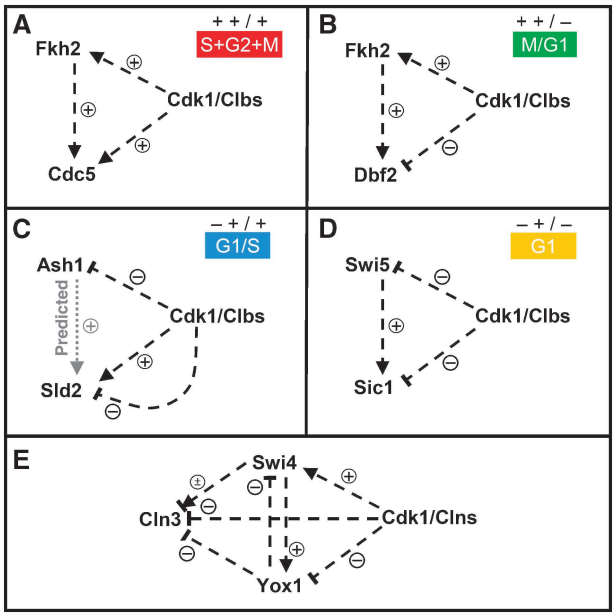

Figure 3 Examples of FFLs coupling transcriptional and post-translational controls. Interaction signs (±) are predicted by the rules presented in Supplementary Table S6. (**A**) Both the mitotic polo kinase (Cdc5) and its transcriptional activator (Fkh2) are phosphorylated and presumably activated by Cdk1 (bound to B-type cyclins). (**B**) The mitotic exit initiator Dbf2 shares the same transcription factor (Fkh2) with Cdc5, but Dbf2 appears to be inhibited by Cdk1. Dbf2 has a PEST sequence (Rechsteiner and Rogers, 1996) and its phosphoprotein cannot be detected (Chi *et al*, 2007), suggesting that Cdk1 phosphorylation of Dbf2 induces its degradation. (**C**) The DNA replication inducer Sld2 is phosphorylated and activated by Cdk1 (Tanaka *et al*, 2007b; Zegerman *et al*, 2007). Although there is no documented TF associated with Sld2, Ash1 has been proposed to regulate *SLD2* expression (Teixeira *et al*, 2006). Our model predicts that Ash1 upregulates production of Sld2. (**D**) The G1 stabilizer, Sic1, is inhibited by Cdk directly and through its TF, Swi5 (Knapp *et al*, 1996). (**E**) An example of a complex embedding of FFLs. Further details and other examples in Supplementary Table S7.

We have associated coherent FFLs with EPs that are continually expressed either in G1 phase (when Cdk activity is low) or in S + G2 + M phase (when Cdk activity is high). Consulting Figure 1A, we might conclude that 'only Cdk' and 'chain' topologies can serve these purposes equally well. But theory suggests that coherent FFLs are more robust signal transducers than the single-arm topologies (Mangan and Alon, 2003).

In the case of incoherent FFLs, robustness is not the only advantage: the two regulatory arms are needed to achieve transient activation of the EP. Incoherent FFLs are activated only for a short period of the cell cycle to induce downstream events (DNA replication, budding and cell division) in the correct order. Our analysis revealed that most known FFLs in budding yeast cells are playing roles in these events (Figure 1B) and indeed most examples we predict are incoherent FFLs (Supplementary Table S7). Furthermore, we found examples of DNA replication initiators and cell division inducers that are under direct control of incoherent FFLs (Figure 3B and C).

Altogether, these examples suggest that the eight basic FFLs play important roles in converting periodic Cdk oscillations into a correct temporal sequence of events in the cell cycle, but that these FFLs are often involved in more complex network topologies.

Conclusion

In all eukaryotic organisms that have been studied in detail, there appear to be two or more Cdk–cyclin pairs that play crucial roles in coordinating cell cycle events. Each one may have its own suite of EPs, probably activated by FFLs. Nonetheless, in fission yeast, a single periodic Cdk–cyclin activity is sufficient to drive all events of the mitotic cell cycle in a viable temporal sequence (Fisher and Nurse, 1996). Our simulation (Figure 2B) shows, in principle, how one Cdk–cyclin pair, utilizing the four basic FFL motifs, can drive G1- and G2-specific proteins and can trigger S-phase entry and M-phase exit in an alternating manner. We imagine that the last common ancestor of present-day eukaryotic cells relied on a single Cdk–cyclin control signal, and that FFLs played a crucial role in converting this single oscillatory signal into coordinated events of a eukaryotic-style cell cycle.

We conclude that the idealized view (Box 1) of FFLs as transducers of periodic Cdk signals provides a reasonable scenario for the evolution of cell cycle controls in early eukaryotes and has merit even now as a 'first approximation' of the temporal organization of cell cycle events. In present day organisms, FFLs may be involved in more complex regulatory topologies that exploit and modify their intrinsic dynamical potentials. Nonetheless, incoherent FFLs are still intimately involved in the initiation of DNA synthesis and cell division at the G1/S and M/G1 transitions of budding yeast.

Materials and methods

Bioinformatics analysis

Cdk1 substrates were obtained from two large-scale screens (Ubersax *et al*, 2003; Loog and Morgan, 2005). TFs and their targets were downloaded from the YEASTRACT database (Teixeira *et al*, 2006). As many TFs act in complexes, we say that a TF complex is a Cdk1 substrate if at least one of its components is phosphorylated by Cdk1. In total, 600 periodic proteins were identified by de Lichtenberg *et al* (2005). MIPS FunCat annotations of genes were downloaded from the CYGD database (Guldener *et al*, 2005). In the Supplementary information, more details are given on determining the signs of TF–EP connections and of the effect of Cdk1-mediated protein phosphorylations.

Model construction

We wrote differential equations (Supplementary Table S4) for the rates of change of concentrations of the active forms of TFs and EPs. If Cdk1 directly activates the EP, then we plot the active form of EP only. For cases where Cdk1 inactivates the EP, we assume that phosphorylation induces degradation, thus phosphorylated EP is rapidly degraded, and we plot the total amount of EP as it represents the total active form. Parameters were chosen to get unique EP peaks at different phases of the cell cycle. The Cdk1 time course was generated from a minimal model of the Cdk regulatory system, comparable to (Tyson and Novak, 2001).

Supplementary information

Supplementary information is available at the *Molecular Systems Biology* website (www.nature.com/msb).

Acknowledgements

We thank Fredrick R Cross for stimulating discussions and Orkun S Soyer for a critical reading of the paper. This study was supported by grants from Hungarian Scientific Research Fund (OTKA-F60414), Italian Ministry of University and Research Project FIRB (RBPR0523C3) (AC-N), European Research Council (202591) (CP), the European Commission (YSBN and FP7: 201142), the National Institutes of Health (5R01GM079207) and the James S McDonnell Foundation (21002050) (BN and JJT).

Conflict of interest

The authors declare that they have no conflict of interest.

References

Adelman K, La Porta A, Santangelo TJ, Lis JT, Roberts JW, Wang MD (2002) Single molecule analysis of RNA polymerase elongation reveals uniform kinetic behavior. *Proc Natl Acad Sci USA* **99:** 13538–13543

Bardin AJ, Amon A (2001) MEN and SIN: what's the difference? *Nat Rev Mol Cell Biol* **2:** 815–826

Barr FA, Sillje HH, Nigg EA (2004) Polo-like kinases and the orchestration of cell division. *Nat Rev Mol Cell Biol* **5:** 429–440

Blow JJ (1993) Preventing re-replication of DNA in a single cell cycle: evidence for a replication licensing factor. *J Cell Biol* **122:** 993–1002

Chen KC, Calzone L, Csikasz-Nagy A, Cross FR, Novak B, Tyson JJ (2004) Integrative analysis of cell cycle control in budding yeast. *Mol Biol Cell* **15:** 3841–3862

Chi A, Huttenhower C, Geer LY, Coon JJ, Syka JE, Bai DL, Shabanowitz J, Burke DJ, Troyanskaya OG, Hunt DF (2007) Analysis of phosphorylation sites on proteins from *Saccharomyces cerevisiae* by electron transfer dissociation (ETD) mass spectrometry. *Proc Natl Acad Sci USA* **104:** 2193–2198

Cross FR, Schroeder L, Bean JM (2007) Phosphorylation of the Sic1 inhibitor of B-type cyclins in *Saccharomyces cerevisiae* is not essential but contributes to cell cycle robustness. *Genetics* **176:** 1541–1555

Csikasz-Nagy A, Kapuy O, Gyorffy B, Tyson JJ, Novak B (2007) Modeling the septation initiation network (SIN) in fission yeast cells. *Curr Genet* **51:** 245–255

Csikasz-Nagy A, Soyer OS (2008) Adaptive dynamics with a single two-state protein. *J R Soc Interface* **5** (Suppl 1)**:** S41–S47

de Lichtenberg U, Jensen LJ, Brunak S, Bork P (2005) Dynamic complex formation during the yeast cell cycle. *Science* **307:** 724–727

Fisher DL, Nurse P (1996) A single fission yeast mitotic cyclin B $p34^{cdc2}$ kinase promotes both S-phase and mitosis in the absence of G1 cyclins. *EMBO J* **15:** 850–860

Guldener U, Munsterkotter M, Kastenmuller G, Strack N, van Helden J, Lemer C, Richelles J, Wodak SJ, Garcia-Martinez J, Perez-Ortin JE, Michael H, Kaps A, Talla E, Dujon B, Andre B, Souciet JL, De Montigny J, Bon E, Gaillardin C, Mewes HW (2005) CYGD: the Comprehensive Yeast Genome Database. *Nucleic Acids Res* **33:** D364–D368

Holt LJ, Krutchinsky AN, Morgan DO (2008) Positive feedback sharpens the anaphase switch. *Nature* **454:** 353–357

Jensen LJ, Jensen TS, de Lichtenberg U, Brunak S, Bork P (2006) Co-evolution of transcriptional and post-translational cell-cycle regulation. *Nature* **443:** 594–597

Kaplan S, Bren A, Dekel E, Alon U (2008) The incoherent feed-forward loop can generate non-monotonic input functions for genes. *Mol Syst Biol* **4:** 203

Knapp D, Bhoite L, Stillman DJ, Nasmyth K (1996) The transcription factor Swi5 regulates expression of the cyclin kinase inhibitor p40Sic1. *Mol Cell Biol* **16:** 5701–5707

Lee TI, Rinaldi NJ, Robert F, Odom DT, Bar-Joseph Z, Gerber GK, Hannett NM, Harbison CT, Thompson CM, Simon I, Zeitlinger J, Jennings EG, Murray HL, Gordon DB, Ren B, Wyrick JJ, Tagne JB, Volkert TL, Fraenkel E, Gifford DK *et al* (2002) Transcriptional regulatory networks in *Saccharomyces cerevisiae*. *Science* **298:** 799–804

Loog M, Morgan DO (2005) Cyclin specificity in the phosphorylation of cyclin-dependent kinase substrates. *Nature* **434:** 104–108

Mangan S, Alon U (2003) Structure and function of the feed-forward loop network motif. *Proc Natl Acad Sci USA* **100:** 11980–11985

Mangan S, Zaslaver A, Alon U (2003) The coherent feedforward loop serves as a sign-sensitive delay element in transcription networks. *J Mol Biol* **334:** 197–204

Masumoto H, Muramatsu S, Kamimura Y, Araki H (2002) S-Cdk-dependent phosphorylation of Sld2 essential for chromosomal DNA replication in budding yeast. *Nature* **415:** 651–655

Novak B, Tyson JJ, Gyorffy B, Csikasz-Nagy A (2007) Irreversible cell-cycle transitions are due to systems-level feedback. *Nat Cell Biol* **9:** 724–728

Rechsteiner M, Rogers SW (1996) PEST sequences and regulation by proteolysis. *Trends Biochem Sci* **21:** 267–271

Ruepp A, Zollner A, Maier D, Albermann K, Hani J, Mokrejs M, Tetko I, Guldener U, Mannhaupt G, Munsterkotter M, Mewes HW (2004) The FunCat, a functional annotation scheme for systematic classification of proteins from whole genomes. *Nucleic Acids Res* **32:** 5539–5545

Schwob E, Bohm T, Mendenhall MD, Nasmyth K (1994) The B-type cyclin kinase inhibitor $p40^{sic1}$ controls the G1 to S transition in *S. cerevisiae*. *Cell* **79:** 233–244

Skotheim JM, Di Talia S, Siggia ED, Cross FR (2008) Positive feedback of G1 cyclins ensures coherent cell cycle entry. *Nature* **454:** 291–296

Spellman PT, Sherlock G, Zhang MQ, Iyer VR, Anders K, Eisen MB, Brown PO, Botstein D, Futcher B (1998) Comprehensive identification of cell cycle-regulated genes of the yeast *Saccharomyces cerevisiae* by microarray hybridization. *Mol Biol Cell* **9:** 3273–3297

Sutani T, Yuasa T, Tomonaga T, Dohmae N, Takio K, Yanagida M (1999) Fission yeast condensin complex: essential roles of non-SMC subunits for condensation and Cdc2 phosphorylation of Cut3/SMC4. *Genes Dev* **13:** 2271–2283

Tanaka S, Tak YS, Araki H (2007a) The role of CDK in the initiation step of DNA replication in eukaryotes. *Cell Div* **2:** 16

Tanaka S, Umemori T, Hirai K, Muramatsu S, Kamimura Y, Araki H (2007b) CDK-dependent phosphorylation of Sld2 and Sld3 initiates DNA replication in budding yeast. *Nature* **445:** 328–332

Teixeira MC, Monteiro P, Jain P, Tenreiro S, Fernandes AR, Mira NP, Alenquer M, Freitas AT, Oliveira AL, Sa-Correia I (2006) The YEASTRACT database: a tool for the analysis of transcription regulatory associations in *Saccharomyces cerevisiae*. *Nucleic Acids Res* **34:** D446–D451

Tyson JJ, Chen KC, Novak B (2003) Sniffers, buzzers, toggles, and blinkers: dynamics of regulatory and signaling pathways in the cell. *Curr Opin Cell Biol* **15:** 221–231

Tyson JJ, Novak B (2001) Regulation of the eukaryotic cell cycle: molecular antagonism, hysteresis and irreversible transitions. J Theor Biol **210:** 249–263

Tyson JJ, Novak B (2008) Temporal organization of the cell cycle. *Curr Biol* **18:** R759–R768

Ubersax JA, Woodbury EL, Quang PN, Paraz M, Blethrow JD, Shah K, Shokat KM, Morgan DO (2003) Targets of the cyclin-dependent kinase Cdk1. *Nature* **425:** 859–864

Visintin R, Amon A (2001) Regulation of the mitotic exit protein kinases Cdc15 and Dbf2. *Mol Biol Cell* **12:** 2961–2974

Zegerman P, Diffley JF (2007) Phosphorylation of Sld2 and Sld3 by cyclin-dependent kinases promotes DNA replication in budding yeast. *Nature* **445:** 281–285

Zhu G, Spellman PT, Volpe T, Brown PO, Botstein D, Davis TN, Futcher B (2000) Two yeast forkhead genes regulate the cell cycle and pseudohyphal growth. *Nature* **406:** 90–94

dc_836_14

7.6 DNS-károsodás hatása a napi ritmusra

Hong CI., Zámborszky J. & **Csikász-Nagy A.** (2009) Minimum Criteria for DNA Damage-Induced Phase Advances in Circadian Rhythms. *PLoS Comput Biol.***5(5):**e1000384

Impakt faktor: 5.759

OPEN ACCESS Freely available online PLoS COMPUTATIONAL BIOLOGY

Minimum Criteria for DNA Damage-Induced Phase Advances in Circadian Rhythms

Christian I. Hong[1☯], Judit Zámborszky[2☯], Attila Csikász-Nagy[2*]

1 Department of Genetics, Dartmouth Medical School, Hanover, New Hampshire, United States of America, **2** The Microsoft Research–University of Trento Centre for Computational and Systems Biology, Povo (Trento), Italy

Abstract

Robust oscillatory behaviors are common features of circadian and cell cycle rhythms. These cyclic processes, however, behave distinctively in terms of their periods and phases in response to external influences such as light, temperature, nutrients, etc. Nevertheless, several links have been found between these two oscillators. Cell division cycles gated by the circadian clock have been observed since the late 1950s. On the other hand, ionizing radiation (IR) treatments cause cells to undergo a DNA damage response, which leads to phase shifts (mostly advances) in circadian rhythms. Circadian gating of the cell cycle can be attributed to the cell cycle inhibitor kinase Wee1 (which is regulated by the heterodimeric circadian clock transcription factor, BMAL1/CLK), and possibly in conjunction with other cell cycle components that are known to be regulated by the circadian clock (i.e., c-Myc and cyclin D1). It has also been shown that DNA damage-induced activation of the cell cycle regulator, Chk2, leads to phosphorylation and destruction of a circadian clock component (i.e., PER1 in *Mus* or FRQ in *Neurospora crassa*). However, the molecular mechanism underlying how DNA damage causes predominantly phase advances in the circadian clock remains unknown. In order to address this question, we employ mathematical modeling to simulate different phase response curves (PRCs) from either dexamethasone (Dex) or IR treatment experiments. Dex is known to synchronize circadian rhythms in cell culture and may generate both phase advances and delays. We observe unique phase responses with minimum delays of the circadian clock upon DNA damage when two criteria are met: (1) existence of an autocatalytic positive feedback mechanism in addition to the time-delayed negative feedback loop in the clock system and (2) Chk2-dependent phosphorylation and degradation of PERs that are not bound to BMAL1/CLK.

Citation: Hong CI, Zámborszky J, Csikász-Nagy A (2009) Minimum Criteria for DNA Damage-Induced Phase Advances in Circadian Rhythms. PLoS Comput Biol 5(5): e1000384. doi:10.1371/journal.pcbi.1000384

Editor: Herbert M. Sauro, University of Washington, United States of America

Received December 19, 2008; **Accepted** April 7, 2009; **Published** May 8, 2009

Funding: This research was supported by the Italian Ministry of University and Research Project FIRB (RBPR0523C3) and the Hungarian Scientific Research Fund OTKA (F-60414). The funders had no role in study design, data collection and analysis, decision to publish, or preparation of the manuscript.

Competing Interests: The authors have declared that no competing interests exist.

* E-mail: csikasz@cosbi.eu

☯ These authors contributed equally to this work.

Introduction

Circadian rhythms are periodic physiological events that recur about every 24 hours. The importance of circadian rhythms is well recognized in many different organisms' survival as well as in human physiology. Misregulations in circadian rhythms may lead to different conditions such as depression, familial advanced sleep phase syndrome (FASPS), delayed sleep phase syndrome (DSPS), or insomnia, which largely impact our society [1,2]. Recent studies indicate higher incidents of cancer in clock defective individuals [3,4] and chronic jet-lag is associated with higher mortality rate in aged mice as well as faster growth of tumor [5,6]

The molecular mechanism of circadian rhythms began to become clear beginning with the discovery of the *period* (*per*) gene in *Drosophila melanogaster* in 1971 [7], and the *frequency* (*frq*) gene in *Neurospora crassa* in 1973 [8]. Through analysis of the genetic variants of these genes, pieces of the clock's mechanism could be described. The consensus idea is that it involves interlocked feedback loops largely based on a transcription-translation related time-delayed negative feedback loop [9]. Most of the genes encoding proteins involved in the mechanism of circadian rhythms have been found simply by screens aimed at cataloging the components or by analysis of the regulation of the components. Several studies of mathematical modeling and systems approaches helped further understanding of circadian rhythms in various organisms [10–14].

One of the defining properties of circadian rhythms is the ability to phase shift upon a stimulus from external cues. This property allows organisms to adapt efficiently to the external environment. For example, a person traveling east to Europe from the U.S. will experience a jet-lag in the process to adapt advanced phase. Even a brief pulse of light may cause phase advances or delays depending on the timing and influence of the pulse [15]. It is intuitive to assume that a phase shifting agent will create both phase advances and delays depending on the timing and strength of the pulse by uniformly affecting molecular pathways in the circadian system [16]. It has been observed that 2 h treatments of Rat-1 fibroblasts with dexamethasone (Dex) result in large advances and delays (Type 0 resetting of the phase), possibly by inducing transcription of both *rPer1* and *rPer2* [17,18]. This Dex-dependent PRC is also observed in the NIH3T3-Bmal1-Luc-1 cells [19]. If the Dex-dependent induction of *Per* transcripts causes both phase advances and delays, we would also predict that DNA damage-dependent phosphoryla-

Author Summary

Molecular components and mechanisms that connect cell cycle and circadian rhythms are important for the well-being of an organism. Cell cycle machinery regulates the progress of cell growth and division while the circadian rhythm network generates an ~24 h time-keeping mechanism that regulates the daily processes of an organism (i.e. metabolism, bowel movements, body temperature, etc.). It is observed that cell divisions usually occur during a certain time window of a day, which indicated that there are circadian-gated cell divisions. Moreover, it's been shown that mice are more prone to develop cancer when certain clock genes are mutated resulting in an arrhythmic clock. Recently, a cell cycle checkpoint regulator, Chk2, was identified as a component that influences a core clock component and creates mostly phase advances (i.e., jet lags due to traveling east) in circadian rhythms upon DNA damage. This phase response with minimum delays is an unexpected result, and the molecular mechanism behind this phenomenon remains unknown. Our computational analyses of a mathematical model reveal two molecular criteria that account for the experimentally observed phase responses of the circadian clock upon DNA damage. These results demonstrate how circadian clock regulation by cell cycle checkpoint controllers provides another layer of complexity for efficient DNA damage responses.

tion and degradation of PERs by Chk2 [20,21] would result in similar PRCs. Recent findings indicate that this prediction is wrong [18,21]. Upon experiencing DNA damage, the cell cycle machinery influences the circadian clock in such a way that creates predominantly phase advances in Rat-1 fibroblasts and mice [18], as well as in *Neurospora crassa* [21]. These data strongly suggest that there is a conserved pathway across different species that affects the phase of the clock after DNA damage, and involves physical interactions of ATM and/or Chk2 with a core clock component (i.e. PER1 or FRQ) [18,20,21]. This interaction leads to phosphorylation of PER1 and FRQ [21,22]. The molecular mechanism for this unique phenomenon, however, remains unexplained.

In this paper, we explore the minimum criteria in the molecular network of circadian rhythms that simulate the above PRCs with tools of computational modeling. Theoretically, a time-delayed negative feedback is sufficient to create robust oscillations. Both cell cycle and circadian rhythms, however, contain both negative and positive feedbacks in their wiring networks. Positive feedback mechanisms are essential for proper eukaryotic cell divisions [23] whereas their roles in circadian rhythms remain elusive. Recently, Tsai and colleagues indicated that a general function of positive feedbacks in different networks is to create tunable robustness in the system [24]. In our study, we address two questions 1) what is a molecular mechanism that accounts for Chk2-dependent PRC in circadian rhythms?, and 2) is the positive feedback mechanism necessary for the observed PRC? In the conditions that we have tested, we discovered that we can only simulate the Chk2-dependent PRC with predominantly phase advances when Chk2 only affects PERs that are not bound to BMAL1/CLK in the presence of an autocatalytic positive feedback mechanism. Both conditions are required for proper simulations. Our study is the only in silico experiment to indicate the necessity of an autocatalytic positive feedback mechanism in simulating specific phenotype in the circadian system.

Results

Chk2-dependent differential degradation of PER creates predominantly phase advances upon DNA damage

We explored our simple mammalian circadian clock model (Fig. 1) from our previous work [25] to investigate whether we can simulate different PRCs from the Dex and IR treatment experiments [17,18]. Note that an autocatalytic positive feedback mechanism is already embedded in our model [12,26]. Based on the experimental data, we added the following in our previous model: 1) Dex increases the transcripts of *Per* but not *Bmal1* [18], and 2) Chk2 phosphorylates PERs and facilitates their degradation upon DNA damage [20,21]. Our simulations show that the Dex-dependent increase of *Per* messages creates both Type 0 (as shown in the experiment, strong resetting of the phase) and Type 1 PRCs (weak resetting of the phase) depending on the strength (concentration) of the Dex treatments (Fig. 2A). It is, however, not trivial to simulate a PRC with mostly phase advances reproducing the phenotype from the IR treatment experiments [18]. We observe a PRC with large advances and delays if we follow the simplest possible assumption that DNA damage induces Chk2-dependent phosphorylation and degradation of all forms of PER (monomer, dimer, and complex with BMAL1/CLK) (Fig 1 and Fig 2B). Through in silico experiments, however, we observe minimum phase delays as seen in experiments [18,21] only when Chk2 does not affect the PER that is in a complex with BMAL1/CLK (i.e. due to conformational changes of PER upon complex formation) (Fig. 2B). In other words, Chk2 prematurely degrades PERs that are not bound to BMAL1/CLK to advance the clock, while allowing continued repression of BMAL1/CLK by not degrading the PERs that are in complex with BMAL1/CLK

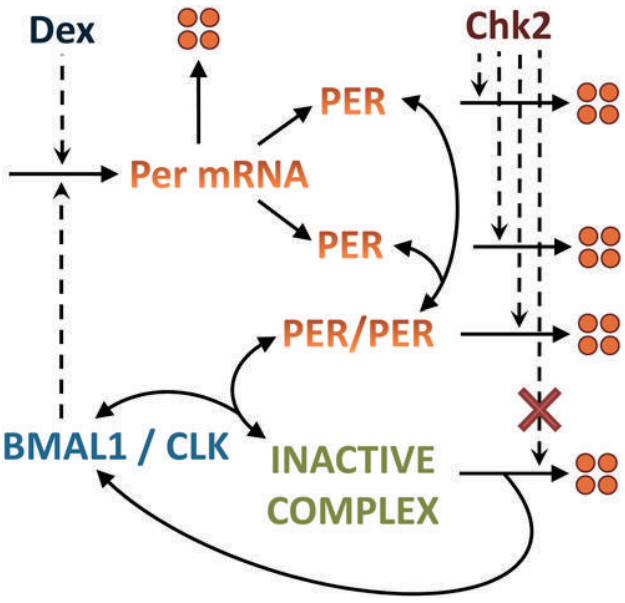

Figure 1. Molecular wiring diagram of the simple circadian clock network. For simplicity of the model, we only deal with PER protein, and treat PER1, PER2, and PER3 as same proteins. We assume that PERs exist in monomers, dimers, and complex with the BMAL1/CLK. We also assume that the BMAL1/CLK is inactive when bound to PER forming a negative feedback loop. A pulse of Dex activates the transcription of *Per* in addition to the BMAL1/CLK. Chk2 does not affect the PERs that are bound to the BMAL1/CLK, which accounts for the unique phase response upon DNA damage.
doi:10.1371/journal.pcbi.1000384.g001

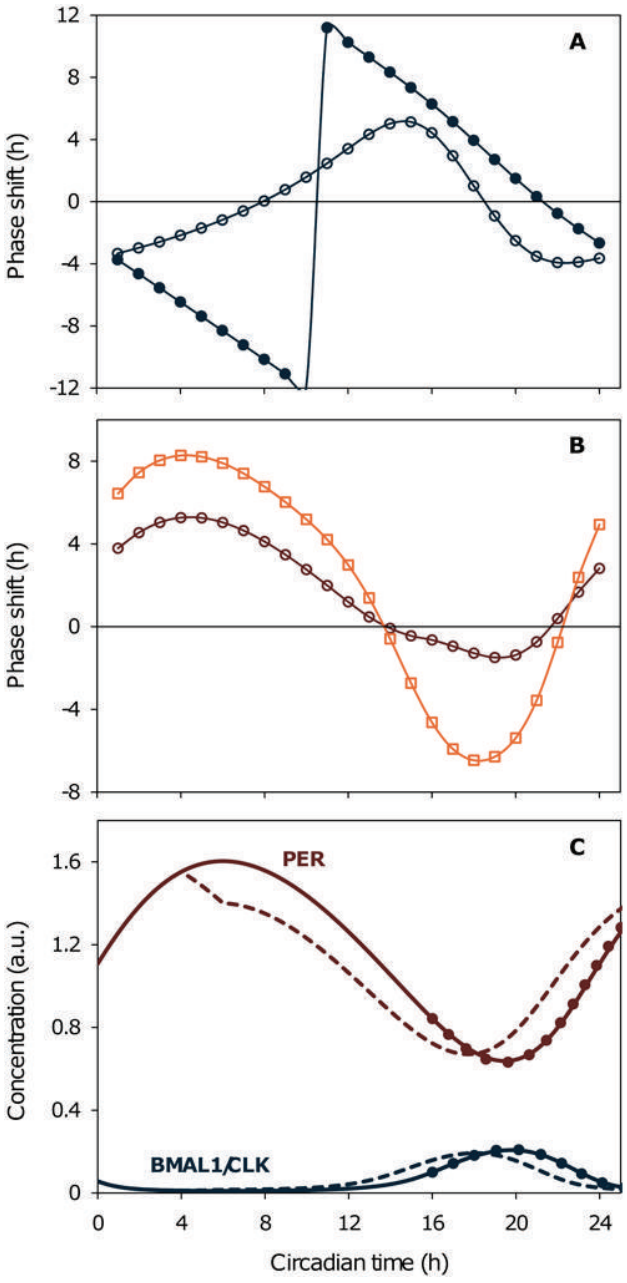

Figure 2. In silico Dex and IR treated experiments. (A) Strong pulses of Dex generate Type 0 PRC (filled circles; strong resetting of the circadian clock to the new phase which does not depend on the old phase) whereas weak pulses of Dex generates Type 1 PRC (blank circles; weak resetting of the phase where the new phase changes as a function of the old phase). (B) Large advances and delays are observed when Chk2 is assumed to affect all forms of PERs including the complex with BMAL1/CLK (orange squares). Chk2-dependent phase advances and minimum delays of the circadian clock are observed only if Chk2 does not affect the PERs that are in complex with BMAL1/CLK (red circles). (C) DNA damage-induced Chk2 activation causes phase advances of circadian clock. Solid lines represent endogenous profiles of PER and BMAL1/CLK. Dashed lines indicate PER (red - CP_{total}) and BMAL1/CLK (blue - *TF*) in response to a 2 h IR treatment at simulation hour 4 and dots represent the results after the same 2 hr treatment at hour 16 (hour 0 corresponds to the peak of PER monomers (*CP*)).
doi:10.1371/journal.pcbi.1000384.g002

(Fig. 2C). This prolonged repression on BMAL1/CLK creates small delays when Chk2 affects PERs around their minima as observed in experiments [18,21].

It is interesting to note that an inhibition of CKIε, another kinase that is known to phosphorylate PER, generates a PRC with only delays [27]. This PRC is qualitatively different than the PRC after DNA damage as there are no advances. We can simulate a mirror image of the PRC with mostly advances, which creates mostly delays, by reducing the rates for Chk2-dependent phosphorylations (not shown). Our data, however, is qualitatively different as we do see small advances whereas Badura and colleagues did not observe any advances [27]. This difference are possibly due to the following reasons: 1) Badura et al. administered a CKIε inhibitor not as a pulse (there was no removal of the drug after administration), and 2) it is possible that Chk2 and CKIε results in different types of phosphorylations which can lead to different consequences. We plan to further investigate this with an extended version of circadian clock module.

An autocatalytic positive feedback mechanism is required for the observed PRC

Our simple model is adapted from Tyson and colleagues' earlier paper where both negative and positive feedbacks play essential roles in creating a robust oscillator [12,26]. The autocatalytic positive feedback mechanism in the model arises from different stabilities between PER monomers vs. PER complexes. Based on molecular data from *Drosophila* system [28–31], we assume that PER monomers are more susceptible to degradation than PER in complexes (i.e. PER/PER, PER/CRY, etc.). This creates autocatalytic PER dynamics as PER stabilizes itself by forming complexes. To date, this is the only circadian rhythm model that employs an essential positive feedback mechanism that is necessary to maintain a robust oscillator [32]. Hence, we wondered whether the incorporated essential positive feedback is required (or disposable) in simulating the unique PRCs upon DNA damage.

In order to test our hypothesis, we removed the autocatalysis in the model by assuming no stability differences between PER monomers and complexes. Then, we re-parameterized the system to rescue oscillations (see materials and methods). Note that we had to use a Hill-coefficient = 4 for highly cooperative negative feedback in order to rescue oscillations in our four-variable model in the absence of the autocatalytic positive feedback mechanism. To our surprise, we were not able to generate the unique PRC with predominantly phase advances upon DNA damage even by assuming differential phosphorylation and degradation of PER monomers vs. PER complexes with BMAL1/CLK (lane 2, Table 1).

We wondered whether above conclusions from our simple model can be generalized to a more comprehensive model with distinct wiring network. Hence, we tested Leloup and Goldbeter's mammalian model [33,34]. They used four sets of parameters in order to investigate possible functions of multiple feedback loops in the circadian system. For our purposes, we concentrated in parameter sets 1 and 3. In the parameter set 1, robust oscillations of their model can arise from two different time-delayed negative feedback loops: PER-driven and PER/CRY-independent BMAL1/CLK-driven negative feedback loops. For this parameter set, they can generate an oscillator based on BMAL1/CLK-driven negative feedback loop in the absence of the PER-driven negative feedback loop. In the parameter set 3, they disabled the BMAL1/CLK-driven negative feedback loop making the system a PER/CRY-dependent single negative feedback oscillator. We did not explore parameter sets 2 and 4 because PER is not required for oscillations in parameter sets 2 and 4. The wiring network of

Table 1. Theoretical requirements for the experimentally observed DNA damage-induced PRCs with small delays in circadian clock models.

Model	Positive feedback	Ratio of maximum advance and maximum delay
Simple model	Yes	3.54
Simple model, positive feedback removed	No	0.77
Leloup and Goldbeter set 1	No	0.57
Leloup and Goldbeter set 3	No	1.11
Leloup and Goldbeter set 1 with positive feedback	Yes	0.71
Leloup and Goldbeter set 3 with positive feedback	Yes	2.47

We removed the autocatalytic positive feedback from our simple model and added positive feedback into the Leloup and Goldbeter's model as discussed in the text. In all cases, we checked the maxima and minima from PRCs after the Chk2-dependent degradations of PER. In the last column, we report the ratio of these values (larger value indicates most advance with least delay). See text for analysis and Table S1 for detailed results. In all cases we assume that Chk2 acts only on the free forms of PER.
doi:10.1371/journal.pcbi.1000384.t001

Leloup and Goldbeter's model is significantly different from our model which consists of an intertwined dynamics between an essential autocatalytic positive feedback and time-delayed negative feedback [12,32].

We incorporated Chk2-induced degradation of PER molecules that are not bound to BMAL1/CLK in the Leloup and Goldbeter's model. Then, we tested Chk-2-dependent differential degradation of PER as in our simple model. Our simulations indicate that we see both TYPE 1 and TYPE 0 PRC depending on the strength of Chk2, but we do not observe asymmetric PRCs with mostly advances (lane 3 and 4, Table 1). These results show that the differential effect of Chk2-dependent degradation of PER complexes is not enough to create the observed DNA-damage induced PRCs with the innate wiring of the Leloup and Goldbeter's model.

Our next step was to introduce an autocatalytic positive feedback mechanism in the Leloup and Goldbeter's model and investigate its role in reproducing the asymmetric PRC upon DNA-damage. First, we added an autocatalytic positive feedback in the parameter set 1 of Leloup and Goldbeter's model in a similar way as in our simple model. PER complexes are assumed to be more stable than PER monomers. To our surprise, we were not able to generate the PRCs with predominantly phase advances with differential degradations of PER complexes by Chk2 even with an added autocatalytic positive feedback mechanism (lane 5, Table 1). We wondered whether this was due to the PER-independent BMAL1/CLK-driven negative feedback loop which is built in the parameter set 1. Hence, we tested the parameter set 3 which consists of the PER-driven single negative feedback. Interestingly, we were able to simulate the observed asymmetric PRC with predominantly phase advances as we have observed in our simple model only when both the autocatalytic positive feedback and the differential effect of Chk2 on PERs were implemented in the absence of BMAL1/CLK-driven negative feedback loop (lane 6, Table 1). This suggests that there exists an important dynamical relationship between negative feedback loops and an autocatalytic positive feedback mechanism.

Discussion

What are the implications of DNA damage-induced phase responses of the circadian clock to the cell cycle? We hypothesize that cells utilize various pathways for different timing events in response to DNA damage. The Chk2 kinase directly inhibits the progress of the cell cycle by phosphorylating and removing Cdc25C (a phosphatase that is antagonistic to Wee1 which activates cell proliferation) from the nucleus [35]. Moreover, the cell cycle machinery also employs Chk2 in order to provide an additional mechanism that helps to delay the cell cycle progress for extended time by indirectly increasing the level of Wee1 via the circadian network. We believe that the above sequential roles of Chk2 maximize the efficiency of DNA damage-induced delay. With our model, we show that premature degradation of PER, resulting in phase advances, causes early activation of BMAL1 (Fig 2C). This creates an early transcriptional activation of the Wee1 (G2 inhibitor of the cell cycle) during the upcoming circadian cycle, which delays the cell cycle in the G2 phase. If the DNA damage-response induces large phase delays, it will generate a short-lived, transient increase of BMAL1, but a long delay in the activation of Wee1 by BMAL1/CLK for the upcoming circadian cycle. This late activation of Wee1 is probably not a desired result for an efficient DNA damage response.

Our model is simple and intuitive, and yet predicts a molecular mechanism that is responsible for the observed PRC. Our in silico experiments elucidate a molecular mechanism that accounts for Chk2-dependent phase advances and minimum delays of the circadian clock upon DNA damage. It seems counterintuitive to assume that Chk2 does not affect the PER that is in a complex with BMAL1/CLK. This may appear to prolong the repression on BMAL1, which will delay the activation of Wee1. However, due to the cyclic nature of the circadian clock, our simulations suggest that these unique Chk2-dependent phase responses are the best strategy for inducing large and prolonged induction of Wee1 by BMAL1/CLK, allowing extended time for the cell cycle to repair problems upon DNA damage. We propose that the cell cycle network is ingeniously wired with the circadian clock for an optimal response upon DNA damage. Previously, experimentalists showed that the functional circadian clock is important for optimum response to the chemotherapeutic agent cyclophosphamide or γ radiation [4,36]. For example, reduced apoptosis is observed in m*Per2* deficient mice compared to wild-type mice upon γ radiation, which resulted in tumorigenesis [4]. Based on these works, it can be assumed that DNA damage response is more efficient when the circadian clock is intact. We do not know, however, how the efficiency of DNA damage response is affected by the circadian clock. Hence, we suggest testing the efficiency of DNA damage response in the presence and absence of the circadian clock in both in cell culture (i.e. wild-type vs. cry^{ko}) as well as in vivo.

Another intriguing finding is the importance of the autocatalytic positive feedback mechanism in simulating the observed PRC upon DNA damage. Our simple model is adapted from Tyson and

colleagues which implemented both negative and positive feedback mechanisms [12,32]. DNA damage-induced PRCs with predominantly advances are lost upon removal of the positive feedback even with the differential degradation of PERs by Chk2. This observation is extended to the Leloup and Goldbeter's model [33,34]. We tested four different combinations of positive and negative feedback loops with two different sets of parameters (Table 1). Our findings confirm that the autocatalytic positive feedback mechanism is required to simulate DNA damage-induced PRCs. Our results elucidate three important points: (1) the role of the autocatalytic positive mechanism in the circadian system, (2) the wiring of different negative feedback loops, and (3) the interplay between positive and negative feedbacks in response to DNA damage. We acknowledge that there are multiple feedback loops in the circadian system [9]. Therefore, it is essential to develop a more comprehensive model accounting detailed dynamics of different negative feedback loops in the clock network. Furthermore, it is important to experimentally verify autocatalytic positive feedback mechanisms in the context of circadian rhythms, the nonlinearity of negative feedback loops, and the possible interplay between the positive and negative feedback loops in the circadian clock.

Materials and Methods

Circadian rhythm model

Our objective is to create a simple mammalian circadian clock model that accounts for different phase response curves (PRCs) observed from various experiments [17,18,21]. For simplicity of the model, we only deal with PER protein and treat PER1, PER2, and PER3 as same proteins. CRY proteins (CRY1 and CRY2) are also part of core clock components that negatively regulate BMAL1/CLK. We do not consider, however, CRY proteins in this model for two reasons: (1) simplicity of the model, and (2) it is not yet known whether Chk2 phosphorylates and triggers degradation of CRY proteins as mPER1. We will include the function of CRY proteins in our future work. We assume that PERs exist in monomers (Clock Protein, CP), dimers (Clock Protein, CP_2), and complex with the BMAL1/CLK (Transcription Factor, TF). We imagine that the BMAL1/CLK is inactive when bound to PER (Inactive Complex, IC) creating a negative feedback. We treat CLK as a parameter in the system since it does not cycle [37]. We also assume that the CP_2 is more stable than the CP, which introduces a positive feedback in the system [12]. Dex induces the transcription of *Per* message (Message, M) [18], and DNA damage-activated Chk2 promotes phosphorylation and degradation of PERs [20,21]. We use same equations and parameter values from our previous publication [25] other than the newly added effects of Dex or Chk2.

Differential equations of the simplified circadian rhythm model for mammalian cells

Messenger RNA of the clock proteins (*Per* mRNA):

$$\frac{d}{dt}M = Dex + k_{ms}\frac{TF^n}{J^n + TF^n} - k_{md}M \tag{1}$$

Monomer clock proteins (PER):

$$\begin{aligned}\frac{d}{dt}CP &= k_{cps}M - k_{cpd}CP - 2k_aCP^2 \\ &+ 2k_dCP_2 - k_{p1}\frac{CP}{J_p + CP_{tot}} - Chk2\cdot CP\end{aligned} \tag{2}$$

Dimer form of clock proteins (PER/PER):

$$\begin{aligned}\frac{d}{dt}CP_2 &= k_aCP^2 - k_dCP_2 - k_{cp2d}CP_2 + k_{icd}IC \\ &- k_{ica}CP_2\cdot TF - k_{p2}\frac{CP_2}{J_p + CP_{tot}} - Chk2\cdot CP_2\end{aligned} \tag{3}$$

Transcription factor (BMAL1/CLK):

$$\begin{aligned}\frac{d}{dt}TF &= k_{cp2d}IC + k_{icd}IC - k_{ica}TF\cdot CP_2 \\ &+ k_{p2}\frac{IC}{J_p + CP_{tot}} + Chk2c\cdot IC\end{aligned} \tag{4}$$

Inactive complex of clock dimers and transcription factor:

$$IC = TF_{tot} - TF \tag{5}$$

Total amount of clock proteins (PER on Fig. 2):

$$CP_{tot} = CP + 2CP_2 + 2IC \tag{6}$$

Rate constants (h^{-1}):

$$\begin{aligned}&k_{ms} = 1,\ k_{md} = 0.1,\ k_{cps} = 0.5,\ k_{cpd} = 0.525,\\ &k_a = 100,\ k_d = 0.01,\ k_{cp2d} = 0.0525,\ k_{icd} = 0.01,\\ &k_{ica} = 20,\ k_{p1} = 10,\ k_{p2} = 0.1,\ Dex = 0,\ Chk2 = 0,\ Chk2_c = 0\end{aligned}$$

Dimensionless constants:

$$TF_{tot} = 0.5,\ J_p = 0.05,\ J = 0.3,\ n = 2$$

All protein concentrations in the model are expressed in arbitrary units (au) because, for the most part, we do not know the actual concentrations of most circadian proteins in the cell. All rate constants capture only the timescales of processes (rate constant units are in h^{-1}).

Simulation of Dex and IR treatments

(1) Strong resetting (type 0 PRC) of circadian period by Dex treatment (2 h pulse):

$$Dex = 9,\ Chk2 = Chk2_c = 0$$

(2) Weak resetting (type 1 PRC) of circadian period by Dex treatment (2 h pulse):

$$Dex = 0.05,\ Chk2 = Chk2_c = 0$$

(3) Chk2 affects degradation of all forms of PER, including inactive complex (*IC*) of transcription factor BMAL1/CLK (*TF*) and PER dimers (2 h treatment).

$$Dex = 0,\ Chk2 = 0.2,\ Chk2_c = 0.05$$

(4) Chk2 only affects degradation of PER monomers and dimers (2 h treatment).

$$Dex = 0,\ Chk2 = 0.2,\ Chk2_c = 0$$

Removal of the positive feedback mechanism from Zámborszky et al. [25]

Various parameters of the model of Zámborszky et al. [25] have been changed in order to remove the originally existing positive feedback from the system. The equations are the same as presented above. Many parameters were changed to create a robust circadian rhythm with approx 24 h period. Changed parameters: Rate constants (h-1): $k_{ms} = 0.5$, $k_{md} = 0.045$, $k_{cps} = 10$, $k_{cpd} = 0.0001$, $k_a = 100$, $k_d = 0.001$, $k_{cp2d} = 0.0001$, $k_{icd} = 0.001$, $k_{ica} = 4$, $k_{p1} = 1.97$, $k_{p2} = 1.97$. Dimensionless constants: $TF_{tot} = 1$, $J_p = 0.05$, $J = 0.4$, $n = 4$.

Simulation of IR treatments in the Leloup and Goldbeter's model [33,34]

The Chk2 induces degradation of PER monomers and PER-CRY dimers but not PER proteins that are in complex with BMAL1/CLK. To achieve this we replaced the original V_{phos} term by $(V_{phos}+V_{Chk2})$ in the original Leloup and Goldbeter models [33,34]. In simulations we used $V_{Chk2} = 1$ to simulate the effect of IR pulse treatment.

Addition of a positive feedback mechanism to the Leloup and Goldbeter's model [33,34]

We increased the nonspecific degradation rate constant for destruction of nonphosphorylated PER monomers in the cytosol from 0.01 to 0.3, while keeping the background degradation rates of PER/PER dimers and PER/CRY complexes at the original 0.01 level. In this way PER has a positive influence on itself by forming complexes. This creates a similar autocatalytic positive feedback mechanism as the one we used in Zámborszky et al. [25].

Computer simulations

We used XPP-AUT computer program [38] of G. Bard Ermentrout (freely available at http://www.math.pitt.edu/~bard/xpp/xpp.html) for simulations and analysis of our model. The ODE file of our model is available as online supplementary material of this article (see Text S1). The SBML version of the model is also downloadable from the BioModels Database (http://www.ebi.ac.uk/biomodels-main/) [39], as MODEL7984093336. For each simulation, we calculated the phase differences between unperturbed and perturbed systems after 10 days (10 circadian cycles). Treatments were induced at each circadian hour.

Supporting Information

Table S1 Detailed results of the positive feedback necessity analysis of Table 1.
Found at: doi:10.1371/journal.pcbi.1000384.s001 (0.03 MB DOC)

Text S1 Readers can simulate this model by the XPP-AUT computer program, freely available at http://www.math.pitt.edu/~bard/xpp/xpp.html
Found at: doi:10.1371/journal.pcbi.1000384.s002 (0.00 MB TXT)

Author Contributions

Conceived and designed the experiments: CIH ACN. Performed the experiments: CIH JZ. Analyzed the data: CIH JZ ACN. Wrote the paper: CIH ACN.

References

1. Ko CH, Takahashi JS (2006) Molecular components of the mammalian circadian clock. Hum Mol Genet 15(Spec No 2): R271–R277.
2. Leloup JC, Goldbeter A (2008) Modeling the circadian clock: from molecular mechanism to physiological disorders. Bioessays 30: 590–600.
3. Sahar S, Sassone-Corsi P (2007) Circadian clock and breast cancer: a molecular link. Cell Cycle 6: 1329–1331.
4. Fu L, Pelicano H, Liu J, Huang P, Lee C (2002) The circadian gene Period2 plays an important role in tumor suppression and DNA damage response in vivo. Cell 111: 41–50.
5. Davidson AJ, Sellix MT, Daniel J, Yamazaki S, Menaker M, et al. (2006) Chronic jet-lag increases mortality in aged mice. Curr Biol 16: R914–R916.
6. Filipski E, Delaunay F, King VM, Wu MW, Claustrat B, et al. (2004) Effects of chronic jet lag on tumor progression in mice. Cancer Res 64: 7879–7885.
7. Konopka RJ, Benzer S (1971) Clock Mutants of *Drosophila melanogaster*. Proc Natl Acad Sci U S A 68: 2112–2116.
8. Feldman JF, Hoyle MN (1973) Isolation of circadian clock mutants of *Neurospora crassa*. Genetics 75: 605–613.
9. Dunlap JC, Loros JJ, Colot HV, Mehra A, Belden WJ, et al. (2007) A circadian clock in *Neurospora*: how genes and proteins cooperate to produce a sustained, entrainable, and compensated biological oscillator with a period of about a day. Cold Spring Harb Symp Quant Biol 72: 57–68.
10. Gallego M, Eide EJ, Woolf MF, Virshup DM, Forger DB (2006) An opposite role for tau in circadian rhythms revealed by mathematical modeling. Proc Natl Acad Sci U S A 103: 10618–10623.
11. Gonze D, Halloy J, Goldbeter A (2002) Robustness of circadian rhythms with respect to molecular noise. Proc Natl Acad Sci U S A 99: 673–678.
12. Hong CI, Conrad ED, Tyson JJ (2007) A proposal for robust temperature compensation of circadian rhythms. Proc Natl Acad Sci U S A 104: 1195–1200.
13. Locke JC, Kozma-Bognar L, Gould PD, Feher B, Kevei E, et al. (2006) Experimental validation of a predicted feedback loop in the multi-oscillator clock of *Arabidopsis thaliana*. Mol Syst Biol 2: 59.
14. Ueda HR (2007) Systems biology of mammalian circadian clocks. Cold Spring Harb Symp Quant Biol 72: 365–380.
15. Pittendrigh CS (1975) Circadian Clocks: What are They? In: Hastings JW, Schweiger H-G, eds (1975) The Molecular Basis of Circadian Rhythms. Berlin: Abakon Verlagsgesellschaft. pp 11–48.
16. Myers MP, Wager-Smith K, Rothenfluh-Hilfiker A, Young MW (1996) Light-induced degradation of TIMELESS and entrainment of the *Drosophila* circadian clock. Science 271: 1736.
17. Izumo M, Sato TR, Straume M, Johnson CH (2006) Quantitative analyses of circadian gene expression in mammalian cell cultures. PLoS Comput Biol 2: e136. doi:10.1371/journal.pcbi.0020136.
18. Oklejewicz M, Destici E, Tamanini F, Hut RA, Janssens R, et al. (2008) Phase resetting of the mammalian circadian clock by DNA damage. Curr Biol 18: 286–291.
19. Nagoshi E, Saini C, Bauer C, Laroche T, Naef F, et al. (2004) Circadian gene expression in individual fibroblasts: cell-autonomous and self-sustained oscillators pass time to daughter cells. Cell 119: 693–705.
20. Gery S, Komatsu N, Baldjyan L, Yu A, Koo D, et al. (2006) The circadian gene per1 plays an important role in cell growth and DNA damage control in human cancer cells. Mol Cell 22: 375–382.
21. Pregueiro AM, Liu Q, Baker CL, Dunlap JC, Loros JJ (2006) The *Neurospora* checkpoint kinase 2: a regulatory link between the circadian and cell cycles. Science 313: 644–649.
22. Matsuoka S, Ballif BA, Smogorzewska A, McDonald ER III, Hurov KE, et al. (2007) ATM and ATR substrate analysis reveals extensive protein networks responsive to DNA damage. Science 316: 1160–1166.
23. Novak B, Tyson JJ, Gyorffy B, Csikasz-Nagy A (2007) Irreversible cell-cycle transitions are due to systems-level feedback. Nat Cell Biol 9: 724–728.
24. Tsai TY, Choi YS, Ma W, Pomerening JR, Tang C, et al. (2008) Robust, tunable biological oscillations from interlinked positive and negative feedback loops. Science 321: 126–129.
25. Zamborszky J, Hong CI, Csikasz Nagy A (2007) Computational analysis of mammalian cell division gated by a circadian clock: quantized cell cycles and cell size control. J Biol Rhythms 22: 542–553.
26. Tyson JJ, Hong CI, Thron CD, Novak B (1999) A simple model of circadian rhythms based on dimerization and proteolysis of PER and TIM. Biophys J 77: 2411–2417.
27. Badura L, Swanson T, Adamowicz W, Adams J, Cianfrogna J, et al. (2007) An inhibitor of casein kinase I epsilon induces phase delays in circadian rhythms under free-running and entrained conditions. J Pharmacol Exp Ther 322: 730–738.

28. Huang ZJ, Curtin KD, Rosbash M (1995) PER protein interactions and temperature compensation of a circadian clock in *Drosophila*. Science 267: 1169–1172.
29. Kloss B, Price JL, Saez L, Blau J, Rothenfluh A, et al. (1998) The *Drosophila* clock gene *double-time* encodes a protein closely related to human casein kinase Iε. Cell 94: 97–107.
30. Ko HW, Jiang J, Edery I (2002) Role for Slimb in the degradation of *Drosophila* Period protein phosphorylated by Doubletime. Nature 420: 673–678.
31. Price JL, Blau J, Rothenfluh A, Young MW (1998) *double-time* is a novel *Drosophila* clock gene that regulates PERIOD protein accumulation. Cell 94: 83–95.
32. Tyson JJ, Hong CI, Thron CD, Novak B (1999) A simple model of circadian rhythms based on dimerization and proteolysis of PER and TIM. Biophys J 77: 2411–2417.
33. Leloup J, Goldbeter A (2003) Toward a detailed computational model for the mammalian circadian clock. Proc Natl Acad Sci U S A 100: 7051–7056.
34. Leloup JC, Goldbeter A (2004) Modeling the mammalian circadian clock: sensitivity analysis and multiplicity of oscillatory mechanisms. J Theor Biol 230: 541–562.
35. Matsuoka S, Huang M, Elledge SJ (1998) Linkage of ATM to cell cycle regulation by the Chk2 protein kinase. Science 282: 1893–1897.
36. Gorbacheva VY, Kondratov RV, Zhang R, Cherukuri S, Gudkov AV, et al. (2005) Circadian sensitivity to the chemotherapeutic agent cyclophosphamide depends on the functional status of the CLOCK/BMAL1 transactivation complex. Proc Natl Acad Sci U S A 102: 3407–3412.
37. Shearman LP, Sriram S, Weaver DR, Maywood ES, Chaves I, et al. (2000) Interacting molecular loops in the mammalian circadian clock. Science 288: 1013–1019.
38. Ermentrout B (2002) Simulating, Analyzing, and Animating Dynamical Systems. Dongarra JJ, ed. Philadelphia: SIAM.
39. Le Novere N, Bornstein B, Broicher A, Courtot M, Donizelli M, et al. (2006) BioModels Database: a free, centralized database of curated, published, quantitative kinetic models of biochemical and cellular systems. Nucleic Acids Res 34: D689–D691.

dc_836_14

7.7 A sejtciklusátmenetek transzkripciós kontrollja

Romanel A., Cardelli L., Jensen LJ., **Csikász-Nagy A.** (2012) Transcriptional regulation is a major controller of cell cycle transition dynamics. *PLoS One* **7:** e29716

Impakt faktor: 3.730

OPEN ACCESS Freely available online

PLoS one

Transcriptional Regulation Is a Major Controller of Cell Cycle Transition Dynamics

Alessandro Romanel[1¤], Lars Juhl Jensen[2], Luca Cardelli[3], Attila Csikász-Nagy[1]*

1 The Microsoft Research-University of Trento Centre for Computational and Systems Biology, Trento, Italy, **2** Novo Nordisk Foundation Center for Protein Research, University of Copenhagen, Copenhagen, Denmark, **3** Microsoft Research Cambridge, Cambridge, United Kingdom

Abstract

DNA replication, mitosis and mitotic exit are critical transitions of the cell cycle which normally occur only once per cycle. A universal control mechanism was proposed for the regulation of mitotic entry in which Cdk helps its own activation through two positive feedback loops. Recent discoveries in various organisms showed the importance of positive feedbacks in other transitions as well. Here we investigate if a universal control system with transcriptional regulation(s) and post-translational positive feedback(s) can be proposed for the regulation of all cell cycle transitions. Through computational modeling, we analyze the transition dynamics in all possible combinations of transcriptional and post-translational regulations. We find that some combinations lead to 'sloppy' transitions, while others give very precise control. The periodic transcriptional regulation through the activator or the inhibitor leads to radically different dynamics. Experimental evidence shows that in cell cycle transitions of organisms investigated for cell cycle dependent periodic transcription, only the inhibitor OR the activator is under cyclic control and never both of them. Based on these observations, we propose two transcriptional control modes of cell cycle regulation that either STOP or let the cycle GO in case of a transcriptional failure. We discuss the biological relevance of such differences.

Citation: Romanel A, Jensen LJ, Cardelli L, Csikász-Nagy A (2012) Transcriptional Regulation Is a Major Controller of Cell Cycle Transition Dynamics. PLoS ONE 7(1): e29716. doi:10.1371/journal.pone.0029716

Editor: Shree Ram Singh, National Cancer Institute, United States of America

Received October 13, 2011; **Accepted** December 1, 2011; **Published** January 6, 2012

Funding: The work carried out in this study was in part supported by the Italian Research Fund FIRB (RBPR0523C3) and the Novo Nordisk Foundation Center for Protein Research. The funders had no role in study design, data collection and analysis, decision to publish, or preparation of the manuscript.

Competing Interests: LC is employed by Microsoft Research and ACN is employed by The Microsoft Research-University of Trento Centre for Computational Systems Biology. There are no patents, products in development or marketed products to declare. This does not alter the authors' adherence to all the PLoS ONE policies on sharing data and materials.

* E-mail: csikasz@cosbi.eu

¤ Current address: Centre for Integrative Biology, University of Trento, Trento, Italy

Introduction

The cell division cycle is controlled by a complex regulatory network that ensures the proper order and timing of DNA replication, mitosis and division of cells [1]. The core regulators are cyclin dependent kinases (Cdks) that periodically get activated by cyclins. These cyclins and many other cell cycle regulators are under periodic transcriptional regulation [2], and it has been recently shown that these transcriptional waves continue even if cyclins are perturbed [3]. Still, the critical cell cycle transitions of G1/S, G2/M and M/G1 are all controlled by significant changes in Cdk activity and only one Cdk/cyclin complex is enough to drive the cell cycle [4]. It was proposed that cell cycle transitions are controlled by positive feedback loops [5,6] making the transitions work as irreversible switches [7,8]. The G2/M transition has been extensively studied in frog eggs and in fission yeast cells and a picture emerged, in which Cdk activity is inhibited by Wee1 and activated by Cdc25 [9]. It has been shown that Cdk can post-translationally activate its activator, Cdc25 and inhibit its inhibitor, Wee1 [10]. Both of these effects create positive feedback loops that can lead to bistability - when the system can be in either one of two distinct steady states. Such bistability has been observed experimentally by showing a higher critical cyclin level to activate Cdk than the cyclin level needed to keep Cdk active, proving the system is bistable between the two critical cyclin levels [11,12]. Furthermore, importance of the positive feedback for proper cell cycle regulation has also been proven in frog egg extracts [13]. Additional results in other organisms underlined the important role of the two positive feedback loops in the G2/M cell cycle transition [10,14–16]. Mathematical and computational modeling further facilitated cell cycle research [17–19] and theoretical investigations of the feedback loops concluded that the joint effect of the two positive feedback loops can make the transitions even more robust [20]. Furthermore, it has been shown that the effects of the two loops (pure positive and double negative) are not totally equivalent [21,22].

Already in 1990, Paul Nurse proposed that the control of G2/M transition is universal among eukaryotes [9]. Recent results support this idea [10,15,16] and extend it to the other cell cycle transitions [5,6]. Indeed, further studies found that the G1/S transition is also controlled by positive feedback loop in budding yeast [23–25] and similar importance of positive feedbacks on the M/G1 transition were also discovered [26,27]. Here we expand the universality concept and study a generic cell cycle transition regulatory system. Through computational modeling we investigate the dynamical differences between models with different transcriptional and post-translational control modes. Specifically, we analyze the transition dynamics in systems with periodic transcription of the activator or inhibitor, with single or double positive feedbacks and with cell cycle checkpoints acting on

activators or inhibitors. We find that the effect of periodic transcriptional regulation on the activator or the inhibitor has the major impact on the dynamics.

Results

Paul Nurse proposed that the control mechanism of G2/M transition is universal [9], here we investigate if the same picture holds true for all cell cycle transition regulatory modules. The unified cell cycle transition control system consists of an activator and an inhibitor, which control the activity of a transition regulator protein (TR on Fig. 1). The active form of the transition regulator (TR*) can activate its activator and/or inhibit its inhibitor – closing one or two positive feedback loops (PFB). All three components of this network could be transcriptionally regulated during the cell cycle, by various transcription factors (TFs on Fig. 1). A third layer of control on the system could come from checkpoints of the cell cycle (ChP), which ensure that a transition occurs only after an earlier cell cycle event has properly finished [1,28]. These checkpoint signals stop the cell cycle transitions either by inhibiting the activator or activating the inhibitor [29], thus making it harder for the active transition regulator to turn on its positive feedback loops (Fig. 1). This wiring diagram consists of all possible transcriptional and post-translational regulatory interactions proposed for the cell cycle transition modules. Thus, Figure 1 presents all the well understood regulatory mechanisms that affect the dynamics of cell cycle transitions. For the detailed molecular mechanism of the proposed activation-inhibition steps, consult File S1.

Literature data on regulation of cell cycle transitions

The universal G2/M control proposed by Nurse [9], fits this picture with Cdk/cyclins as transition regulators and Cdc25-Wee1 as the activator-inhibitor pair. Similar models have been proposed for the regulation of G1/S and M/G1 transitions, with the common pattern of the existence of one or more positive feedback loops [6]. Another common feature between transitions is that the activator-inhibitor pair often acts post-translationally, controlling the phosphorylation state of the transition regulator. In Table 1, we collected cell cycle transition regulators and their activators and inhibitors that are wired – fully or partially – in the generic way, presented in figure 1. Note that we do not investigate slower time scale regulations where a transition regulator is controlled by an activator or inhibitor which acts on its synthesis or degradation rate. We rather focus on cell cycle transitions where positive feedback works on the post-translational level. As table 1 shows, in fission and budding yeast and in humans all three cell cycle transitions have post-translational positive feedback loop control. Other crucial cell cycle events are also regulated by positive feedback loops [30,31], but here we focus only on the mentioned three major cell cycle transitions.

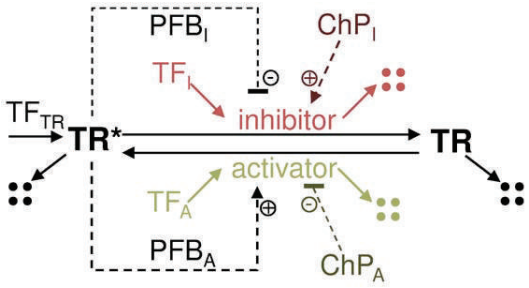

Figure 1. Regulation of a generic cell cycle transition regulator (TR) protein. TR, its activator and inhibitor all can be transcriptionally regulated (by TF_{TR}, TF_A and TF_I respectively) as well as both the activator and inhibitor can be controlled by checkpoints (ChP_A and ChP_I respectively). Active form of the transition regulator (TR*) might activate its activator and/or inhibit its inhibitor, forming two positive feedback loops (PFB_A and PFB_I). (Note that inhibiting an inhibitor is a positive effect leading to a double-negative = positive feedback loop). Solid lines represent reactions, dashed lines show regulatory effects. Positive feedbacks work on the post-translational level and catalyzed reactions have a non-catalyzed background rate, details for each individual reaction can be found in File S1.
doi:10.1371/journal.pone.0029716.g001

Our literature survey of Table 1 shows that two positive feedback loops were discovered in most organisms for G2/M transition regulations, but for some other transitions we find evidence for the existence of only one feedback loop. In these cases, we do not see a clear preference for positive feedback either through the activator or the inhibitor. Similar observations can be made on the effects of checkpoints on transitions: the most investigated G2/M transition has evidence for checkpoint signals affecting both inhibitors and activators, while in many other cases only one of the controllers is regulated by checkpoint signals – again without a clear preference towards activators or inhibitors. Based on theoretical analysis [20], one would think that the safest way to regulate cell cycle transitions is to use two feedback loops and have checkpoints which affect both regulators. Below we investigate if the lack of experimental evidence for the existence of an arrow on Figure 1 could have any biological importance.

It is important to notice in Table 1 that in all cases only one of the controllers (inhibitor or activator) of TR is expressed periodically during the cell cycle (noted with bold letters in Table 1). Again, we do not see a preference of transcriptional regulation of the activator or inhibitor in a database of high-throughput studies in numerous organisms [2]. The lack of evidence for a regulatory effect is not equal to evidence of the lack of such regulation; we might have incomplete knowledge of the systems, but it may also be that such variation in regulation is real and leads to biologically important dynamical differences.

Comparing regulatory modes by computational modeling

To reveal if variation in the regulation can cause difference in the dynamics of cell-cycle transitions, we created a computational model of the generic network shown in Figure 1. We investigate *in silico* how the dynamic properties of the system are changing if one of the feedback loops is removed, how checkpoints can delay transitions and how the transcriptional control of the activator and inhibitor influences the dynamics. Furthermore, we test how reliably these transitions together with a negative feedback loop can give periodic oscillations – as expected from a robust cell cycle control system [13,18].

We converted the regulatory network of Figure 1 into a computational model, using the BlenX programming language, which provides a framework that combines modular modeling and stochastic simulation capabilities [32]. Specifically, we created 24 models representing all combinations of: positive feedback on activator, inhibitor or both; transcription factor on activator or inhibitor; and checkpoint not induced, acting on activator or on inhibitor or on both. We assumed nonlinear enzymatic interactions (as do others [33]) between inhibitor/activator and their substrates. Although, the dynamics of the system would not change even if we were to use multisite phosphorylation to enhance nonlinearity of the feedback loops [21,22].

Table 1. Cell cycle transition regulation in various organisms.

Transition	Organism	TR	Inhibitor	Activator	ChP	PFB
G2/M	**Fission yeast**	Cdc2/**Cdc13**	Wee1	**Cdc25**	**B**	**B**
	Budding yeast	Cdc28/**Clb2**	**Swe1**	Mih1	**I**	**B**
	Fly	Cdk1/CyclinB	Wee1, Myt1	**String**	**B**	**I**
	Frog	Cdc2/CyclinB	Wee1, Myt1	Cdc25	**B**	**B**
	Human	**Cdc2/CcnB1,2**	Wee1hu **Myt1**	hCdc25c	**B**	**B**
M/G1	**Budding yeast**	Cdh1, **Sic1**	Cdc28/**Clb2**	Cdc14	**A**	**I**
		***Pds1**^{Inh}*	*Cdc14*$^{\#}$	*Cdc28/**Clb2***$^{\#}$	***I***	***I***
	Fission yeast	Wee1, (**Cdc25** inactivation)	Cdc2/**Cdc13**	Clp1	**A**	**I**
	Human	Wee1hu, (hCdc25c inactivation)	**Cdc2/CcnB1,2**	Cdc14A or PP2A	**A**	**B**
		Cdh1	**Cdc2/CcnB1,2**	Cdc14A	**A**	**I**
G1/S	**Budding yeast**	***Whi5**^{Inh}*	*Cdc28/**Cln1,2,3***	*Cdc14*	***I***	***I***
	Fission yeast	Cdc2/**Cig2**	**Mik1**	Pyp3	**I**	**A**
	Human	Cdk2/Cyc**E**,A	Wee1hu	**hCdc25a**	**A**	**A**
		Rb1^{Inh}	*Cdk6/CycD Cdk2/**CycE***	*PP1*	***I***	***I***

Cell cycle transition regulatory modules that resemble (in part or whole) the structure of Figure 1 were collected, together with the known information about periodic transcription, the existence of checkpoint and positive feedback regulation. Checkpoint regulation (ChP) and positive feedback loop (PFB) notation: **A**- acting through activator, **I** - through inhibitor, **B**- through both of them. **Bold** letters note genes that are periodically expressed during the cell cycle [2]. Note that all regulations are by phosphorylation - dephosphorylation reactions, with activators being phosphatases and inhibitors being kinases, except two reverse systems, noted by $^{\#}$.
^{Inh} superscript and italic letters for the whole row means the TR is an inhibitor of the cell cycle transition, thus all effects on it are acting with reverse sign to the transition, furthermore an inhibitor of such a transition inhibitor is an indirect activator of the transition. (Detailed discussion and references for all of these findings can be found in File S1).
doi:10.1371/journal.pone.0029716.t001

Two transcriptional control modes of cell cycle transitions

The major finding as shown in Table 1 is that periodic transcription affects only one of the regulators. We do not see a general trend in which one of them is controlled transcriptionally. If a periodically induced inhibitor fails to be transcribed, but the activator is constantly present, the cell can proceed through the transition without a delay (Fig. 2 lower panels). Transcriptional control of the inhibitor is needed to stop/delay the transition and the default (periodic transcription independent) state of the system is to GO through the transition. This is what we see for the budding yeast G2/M, fission yeast G1/S and for various M/G1 transitions (see table 1 – note that for inhibitors of transitions (italic) the meaning should be reversed, since a GO for a transition inhibitor means STOP for the transition). These transitions are examples that cannot be fully stopped by a cell cycle checkpoint, eventually the cells ''adapt'' and proceed through the transitions, even though the checkpoint signal is still active [34–36]. In the simulations, we see that TR can be activated without a delay if the inhibitor is present in a low amount, as is in this case where the TR turns on its positive feedback loop(s) and keeps the inhibitor in its inactive form (Fig. 2)

If the activator is periodically expressed and the inhibitor is static, a failure in the periodic transcriptional program will inhibit the transition and without a high transcription of the activator it never happens (Fig. 2 upper panels). In this case, the positive feedback loop(s) of TR cannot fire, since the inhibitor is fully active. Without any activator, the TR cannot overcome this inhibition. Thus, the default message is to STOP the cell cycle if the periodic transcription is perturbed. Examples for this type of regulation include the G2/M control of fission yeast and the G1/S control of budding yeast cells (Table 1) in which transitions are blocked when the activators are missing [37,38]. Note that in the case of the budding yeast G1/S control Whi5 is a TR that inhibits the transition and its inhibitor is periodically expressed, which leads to the STOP transcriptional control of the transition.

The above findings suggest that the most important transitions of the cell cycle are regulated by STOP transcriptional control of an activator that can be easily delayed in case of failure. In human cell cycle regulation, we explored the controls of the various forms of Cdc25: direct experiments showed that the level of the mitotic Cdc25c is constant, whereas the other forms are periodic [39]. In the view of the proposed GO and STOP regulations, this would suggest that human G1/S is the major control point with a STOP control and G2/M is less important with a GO control. The regulation of the restriction point transition inhibitor Rb1 also supports the idea that in human cells the G1/S transition is more carefully controlled by transcriptional regulation than the G2/M or M/G1 transitions.

The M/G1 transition is best characterized in budding yeast. The activation of Cdc20 induces a cascade of events that lead to Cdc14 activation [40,41], which serves as the major activator of the irreversible exit of mitosis. The role of positive feedbacks in Sic1, Cdh1 and Pds1 regulation were established in recent years [26,42,43] and the importance of some of these proteins in the irreversibility of the transition was also proved [27]. Cdc14 inhibits the transition inhibitor Pds1 and activates the transition activators Sic1 and Cdh1 and periodically appearing Cdc28/Clb2 acts as an inhibitor of the transition – leading to a GO transcriptional control. Cdc28/Clb2 also affects Cdc14 activity directly [44], the introduction of such crosstalk do not influence our simulation results (not shown), still such feed-forward regulation could help the irreversibility of the transition [45,46].

As we found that most TRs are also periodically expressed during the cell cycle (table 1), we wanted to test how problems in transcriptional waves might influence the systems with the proposed two transcriptional regulatory modes. Stochastic simu-

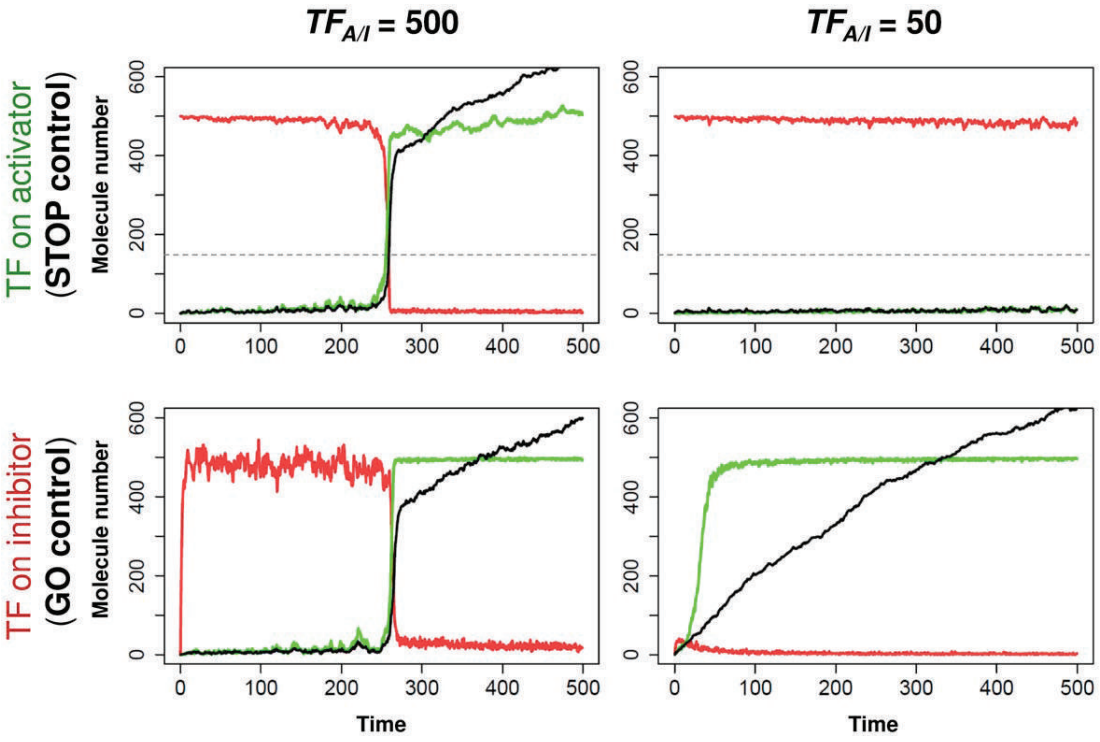

Figure 2. Transcriptional control modes of cell cycle transitions. Computational simulations of the system presented in figure 1 with transcription factor (TF) acting on the activator (upper panels) or on the inhibitor (lower panels) of TR, while the other regulator is assumed to be present in a constant total amount. At time = 0 we turned on the transcription of TR and of the activator or inhibitor with a highly active (left column) or a reduced (10%) activity (right column) of TF_A or TF_I. Plotted are the molecule numbers of the active forms of: activator - green, inhibitor - red, TR* - black. At high TF level the two system behave similarly hitting the presumed TR* threshold (grey dashed line) at the same time, but at reduced transcriptional level they show totally different behavior. (Both positive feedbacks were working during these simulations, removal of one of them does not change the qualitative picture – see File S1). One can notice the elevated noise the transcriptional regulation causes in the activator and inhibitor levels.
doi:10.1371/journal.pone.0029716.g002

lations were initiated from the time point when TR transcription started, and we tested how the timing of the cell cycle transition (time for TR* to hit a critical value) depends on the time when the periodic regulator (activator or inhibitor) transcription is initiated. A delay (positive values on x-scale of Fig. 3) or advance (negative values) in the transcription of the activator compared to transcription of TR, causes less divergence. On the other hand, a bit of a delay in the inhibitor transcriptional induction (GO control) can cause a large advance in the timing of cell cycle transitions (Fig. 3). This difference between the two systems is the result of positive feedback loops which lock the transition controllers in either one of two stable states. In one state, the inhibitor is active, TR is inactive and the activator is inactive. In the other state, TR can turn its loop with the active activator ON causing the inactivation of the inhibitor. In which of the two steady states the system locks depend on the initial state and on the activator and inhibitor levels.

To better see the significance of the positive feedback loops, we characterize the bistability of cell cycle transitions [11,12,24] in the various models with different regulations. Figure 4 shows that the transcriptional STOP and GO controls do not show great differences in bistability - measured by the averages (± standard deviation) of stochastic simulations with slowly increasing or decreasing TR synthesis rate [47]. A small reduction in the bistable regime (thus the robustness of the switch) for GO controlled model however could be observed. Still, we conclude that transcriptional regulation has a minor role in the bistability of cell cycle transitions. Plots shown in figure 4 were created from both positive feedback loops present in the system. In File S1, we show that one positive feedback is enough to create bistability and the bistable regions are quite similar in GO and STOP controlled systems. Still with one positive feedback the bistability is reduced compared to the two loops system [20].

Since our model uses arbitrary parameter values that were selected in order to get a sharp threshold for TR activation (at the same TR synthesis rate – see Fig. 4), we were interested in how robustly these sharp cell cycle transitions are preserved for parameter variations. We find (Fig. 5) that similarly to the results presented above, the model with transcriptional regulation of the activator (STOP control) leads to lower noise for parameter variations compared to systems with transcriptional regulation of the inhibitor (GO control). We see this trend both in the increased spread on the timing of successful transitions and in the decreased percentage of successful transitions as parameter variation increases (dots and solid line respectively on Fig. 5). As the bistability test also suggested above, the presence of both positive feedback loops give a model with the best parameter robustness, but its advantage compared to a single positive feedback system is minimal (File S1). Thus, we conclude that robustness of cell cycle transitions depend most on the modes of transcriptional control as long as at least one strong positive feedback is present in the system.

Next, we test how reliably the various model versions provide a cell cycle transition that can support robust cell cycle oscillations.

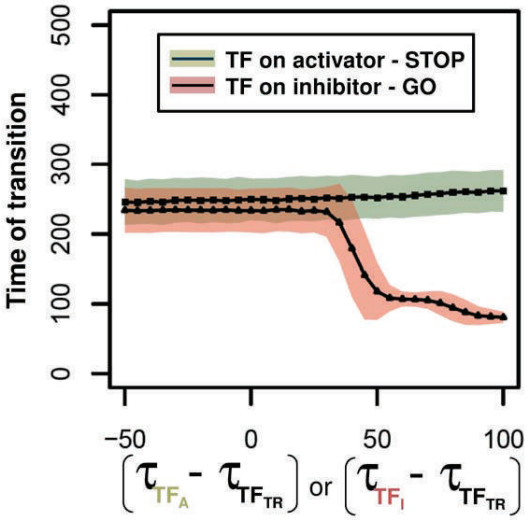

Figure 3. Effects of advance or delay in timing of transcriptional induction of activator or inhibitor. Time for the active form (TR*) to reach a threshold is registered versus the time difference between transcriptional initiation of the activator (green) or inhibitor (red). Rectangles show averages, shaded backgrounds show ± standard deviations from 1000 simulations at a given transcriptional advance (negative values on x-axis) or delay (positive values) compared to TR transcription.
doi:10.1371/journal.pone.0029716.g003

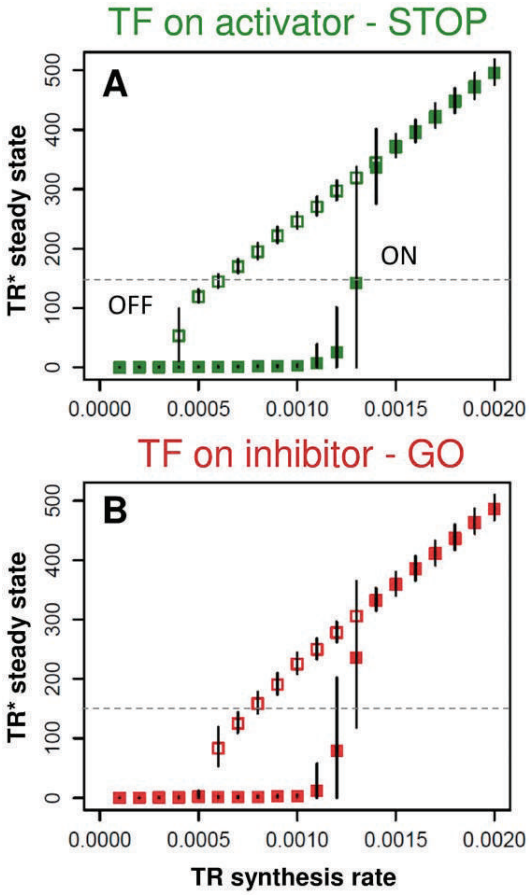

Figure 4. Bistability in cell cycle transitions under various transcriptional control modes. Similarly to experimental investigations of bistability of cell cycle transitions [11,12], here we plot the *in silico* calculated average steady state molecular levels of the active form TR* when its synthesis rate was moved from lower to higher values (filled rectangles) or when it was moved from high to low values (empty rectangles). Error bars show ± standard deviation of 100 simulations at each input values. (**A**) TF_A is active and inhibitor level is constant (STOP control), (**B**) the other way around (GO control). Grey dashed lines show an idealized threshold value, above this level TR* induces the cell cycle transition. When TR synthesis is increasing both models show a sharp ON transition when TR synthesis crosses ~0.0013 (we set the flexible parameters of the models to get this value approximately equal in all cases).
doi:10.1371/journal.pone.0029716.g004

We connected the cell cycle transition models to a minimal negative feedback loop model [48], where a high level of TR* induces its own degradation. Such combination of positive and negative feedback loops is expected to give a robust minimal cell cycle oscillator [13,18,49]. We observe that in the presence of both positive feedback loops, the two transcriptional regulations do not show relevant differences in oscillation robustness, but the combination of transcriptional regulation and positive feedback both acting on the inhibitor cannot provide reliable oscillations (File S1). Thus, we conclude that in the case of absence of positive feedback on the activator, the STOP controlled (TF on activator) cell cycle transitions more reliably provide a robust control in oscillating cell cycles.

As Figure 1 and Table 1 show, checkpoints of the cell cycle can act either by up-regulating the inhibitors or down-regulating the activators or both. We computationally check how the three types of checkpoint signaling can delay the transitions in the various versions of the model. In Figure 6, we plot how long different strength checkpoints can delay cell cycle transitions. In most cases, the STOP control gives a tighter checkpoint block than a GO control, especially in the case when the checkpoint acts only on the inhibitor. Even a strong checkpoint signal on the inhibitor is unable to block the transition in a GO control model (Fig. 6B), while in a STOP control model the same checkpoint strength could be enough to block the transition indefinitely (Fig. 6A). We conclude that systems with checkpoints acting only on the inhibitor and transcriptional control also affecting the inhibitor, cannot give a reliable cell cycle block. This is the case for the budding yeast G2/M control system (Table 1), which can adapt and leak through the morphogenesis checkpoint [36]. If only one of the positive feedbacks is present then the trends are similar: transcription and checkpoint both on inhibitor are ineffective in stopping the transition (File S1), thus major differences by the loss of one feedback cannot be noticed. We conclude that in the case of transcriptional regulation on the inhibitor, the checkpoint should act on the activator or on both regulators in order to give a solid cell cycle block. Cell cycle transitions with transcriptional control of the activator can be better stopped by the checkpoint acting either on the activator or inhibitor.

Discussion

The key regulatory components of the cell cycle were discovered more than 30 years ago [50] and the universal picture that positive feedback loops regulate mitotic entry has gradually emerged [9,18,19,51]. Here we investigated how far this universality holds for all cell cycle transitions in some of the most well studied organisms. Our computational modeling results suggest that there are crucial differences in transition dynamics if periodic transcription acts on the activator or inhibitor of the transition. The exact details of checkpoint and positive feedback regulation are not that

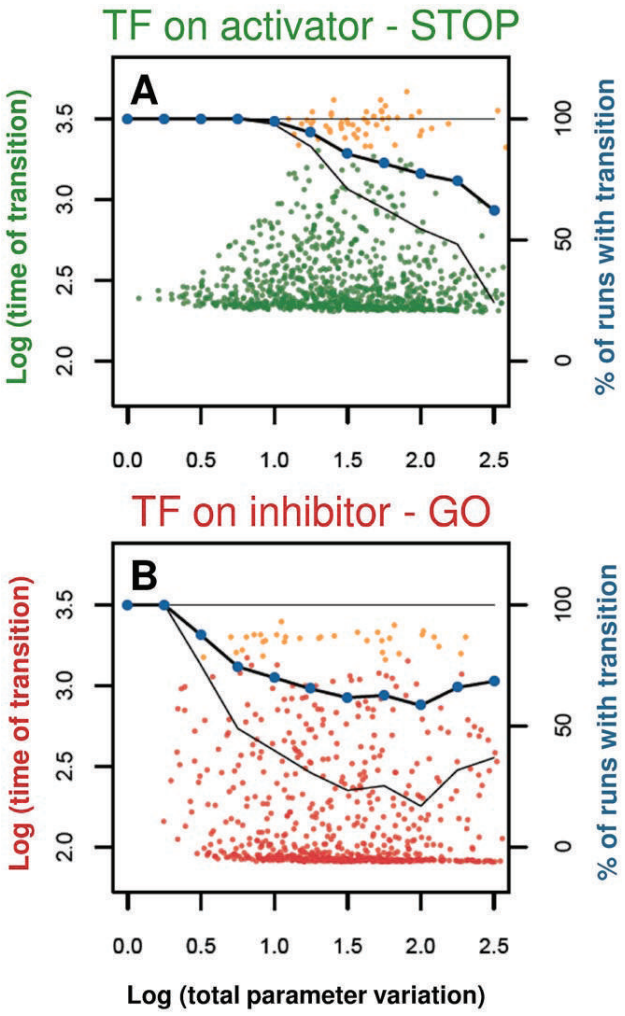

Figure 5. Parameter robustness test of the models. We tested how extrinsic parameter variations in the regulation of the transcriptionally controlled proteins influence the timing of cell cycle transitions. The parameters that control synthesis and degradation of the activator (**A**) or inhibitor (**B**) were randomly sampled (1000 parameter sets) between one tenth and ten times the basal values and the variations in the timing of the transitions are reported versus a measure of parameter variation distance as earlier defined [68]. Each colored dot represents the average of 100 parallel stochastic simulations at a randomly drawn parameter set, orange dots stand for parameter combinations where not all 100 simulations gave successful transitions (TR* hitting the critical value). Connected blue dots give the average percentage of successful transitions, with black lines giving ± standard deviation (corresponding values on the right y-axis).
doi:10.1371/journal.pone.0029716.g005

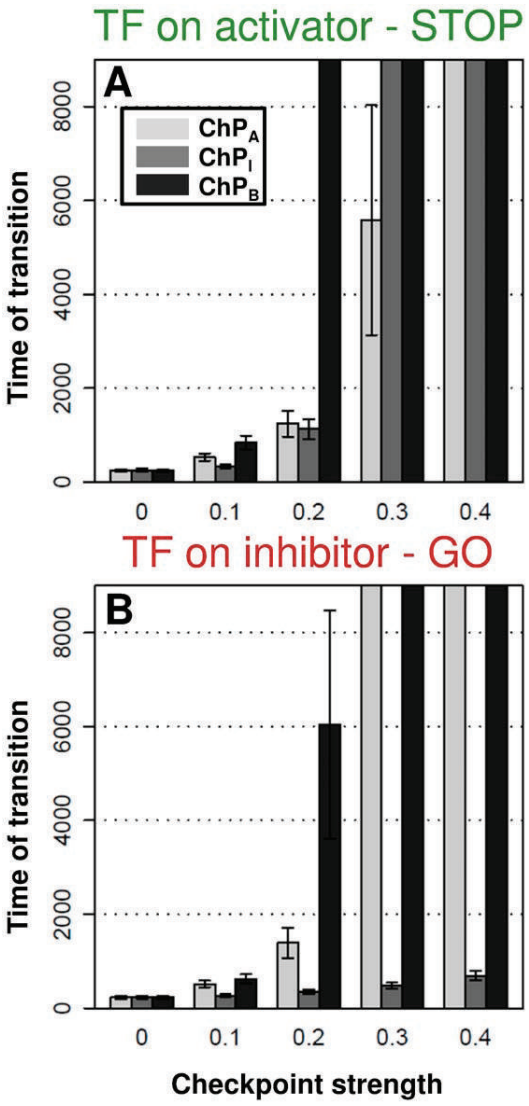

Figure 6. Checkpoint efficiency on various versions of cell cycle transition control models. ChP_A of figure 1 is inhibiting the activator of the TR, while ChP_I moves the inhibitor into a form that is more active in inhibiting TR* [69] and ChP_B labels results when both checkpoints are effective with similar strength (see File S1 for more details). We plot the average times of cell cycle transitions (and with error bars the ± standard deviation) of 1000 stochastic simulations for each model version. Where the columns exceed the plot height, transitions did not occur in >90% of the simulations, so here the checkpoints hold tightly.
doi:10.1371/journal.pone.0029716.g006

crucial for proper cell cycle transitions, still co-existence of the two feedback loops makes the transitions more robust and checkpoints acting on both regulators are more capable of stopping the transitions. Our literature survey shows that there is no evidence for the existence for such double regulations in all investigated organisms at various cell cycle transitions.

The major differences between cell cycle transitions are in the transcriptional regulation of the activator and inhibitor of the transition regulators. In all investigated cases only one is regulated periodically during the cell cycle (Table 1). The computational analysis shows that the transcriptional regulation of the inhibitor leads to a systems that is less robust for transcriptional delays or parameter variations and less responsive for checkpoint controls; furthermore, it is less effective to serve as the regulator of a single transition in a cell cycle oscillator. Thus, we termed this as "GO control", as it is effective in passing through the transition even in the case of a failure. By contrast, "STOP control" is achieved by transcriptional regulation of the activator. This module does not allow the transition to happen in case of a failure and gives a higher robustness of the transition in all investigated tests. Thus, our computational analysis predicts that the most important cell cycle transitions need to be regulated by STOP control. Indeed the G2/M control of fission yeast cells and G1/S control of budding yeast and human cells are under STOP control (Table 1 - also note that a GO control of a transition inhibitor is a STOP signal

for the transition). These are the most crucial control points of the cell cycle of these organisms [1]. On the other hand, some cell cycle transitions are much less carefully controlled by a GO control as we see in some cases (Table 1). Various checkpoints in yeasts and higher eukaryotes can adapt and allow the cells to proceed even in the case of a failure and leave the repair for later times [34,35]. Our analysis suggests that in these cases, a GO transcriptional control works together with a checkpoint working only on the inhibitor. Indeed in the budding yeast G2/M transition and morphogenesis checkpoint is controlled by a checkpoint that acts only on the inhibitor and has a GO transcriptional control [2,36,52].

On the other hand, the most reliable transitions we observe are when both positive feedbacks are working and when checkpoints act on both regulators. One would expect to see this setup for all of the important transitions and indeed for the most investigated G2/M transitions we found all the needed pieces of evidence [20,21]. Maybe we just lack the key experiments from other organisms, but it also could be that evolution found these double regulations too expensive and solved it with a cheaper - although a bit less reliable - system. Our analysis suggests that the most reliable, although more economical solution is the use of the positive feedback through the inhibitor, the checkpoint on the activator together with a STOP transcriptional control on the activator. Some recent evidence supports these findings as the positive feedback loop through the inhibition of the inhibitor was suggested to be the most important for the robustness of the transitions [14,22,53,54] and the activator, Cdc25 was suggested as the major target of the mitotic checkpoint [39,55]. It is also worth noticing that in most cases phosphatases are the activators of TR, which itself is often a kinase, in particular a cyclin-dependent kinase. Importance of phosphatases for M/G1 transition has been already discussed [56], our analysis suggests that they might be generally important for cell cycle transitions.

We collected data in Table 1 from experiments that were indeed performed in the given cell type. During our literature review, we noticed that many papers use results from experiments on other organisms to build their further investigations on different cell types; e.g. considering the effect of frog PP2a on Cdk targets [57] as a starting point of investigations of human cells [58]. Such merging of experimental results from different organisms could lead to a universal picture, but until all experiments are performed on a given organism we cannot be sure if the lack of a link compared to the universal network of figure 1 is a consequence of lack of knowledge or a result of special dynamical or economical constraints.

Following the observation that we did not find a single case in which both regulators are periodically expressed, we further speculate that the periodic transcription of crucial regulators might have been a subject of selection. If either the activator or inhibitor is more often needed in the life cycle of the cell, then this protein might be selected for constant transcription, while proteins with lower demand might keep periodic transcriptional regulation [59–61]. Such thinking suggests that cell cycle transitions that are usually passed quickly are selected for GO transcriptional control while transitions that are halted for longer times are under STOP control. The two yeast systems perfectly fit this picture with budding yeast having GO control in G2/M and STOP at G1/S and fission yeast having it the opposite way, but having its critical transition at G2/M compared to budding yeast with an essential G1/S control.

Following our findings on lack of evidence to support a universal view of all cell cycle transitions, we propose to investigate more carefully if a cell cycle transition regulatory effect is conserved between organisms. We present a unified picture of all possible transcriptional and post-translational controls on cell cycle transition regulators (Fig. 1), but parts of this interaction network might be missing from some of the transition regulatory networks in various organisms. Depending on which part of the system is missing, it can have different effect on transition dynamics. This could be an explanation for the observed differences in the cell cycle regulation of different organism. Indeed, recent results in plants show that the regulatory network interactions greatly differ from the yeast or metazoan systems [62] and even in the yeast there are some opposing ideas about the importance of some of the interactions [63,64]. Such uncertainty in the presence or absence of some regulations might cause a problem in understanding cell cycle regulation. For instance, variations in transcriptional regulation could have a major impact on differentiated mammalian cells, where different cell types in the same organism have different transcriptional profiles [65]. Our results suggest that such transcriptional alterations of cell cycle transition regulators can cause a major change in the dynamics of these transitions.

Methods

In this section, we give a high-level explanation of the methods we used. A more detailed description can be found in File S1.

Model development

We built models of cell cycle transition regulations representing different combinations of three regulatory effects such as transcription, post-translational positive feedback and checkpoint. Transcription factors can act on the activator or on the inhibitor (2 sub-model types); positive feedback can work through the activator, through the inhibitor or both (3 sub-model types) and checkpoints can be absent or act on activator or inhibitor or on both (4 sub-model types). All combinations of these lead to 24 models. In the main text, we mainly discuss the models where both positive feedbacks are active while the models with only one positive feedback are mainly discussed in File S1. Also in File S1, we discuss the extension of the basic 6 models (no checkpoints) by a negative feedback loop.

Model implementation

All the models have been created using the BlenX programming language [32] and simulated by means of the Beta Workbench [66]. BlenX is a language based on process calculi and rule-based paradigms. It is a stochastic language in the sense that the probability and speed of the interactions are specified in the program. In this respect, we solve the models by a stochastic simulator based on an efficient variant of the Gillespie algorithm [67]. In File S1, we provide detailed description of the simulation methods of results presented in the figures 2, 3, 4, 5, 6.

Supporting Information

File S1 Supplementary text containing and extended version of Table 1 with references, details on model development and implementation. Here we also describe simulation methods and details on the main figures of the paper with 7 figures and 7 tables.
(PDF)

Acknowledgments

The authors are thankful to John J. Tyson, Csaba Pal, Orsolya Kapuy and Angela Sanger for their critical reading of an earlier version of the manuscript.

Author Contributions

Conceived and designed the experiments: AR LJJ LC ACN. Performed the experiments: AR ACN. Analyzed the data: AR ACN. Contributed reagents/materials/analysis tools: LJJ LC. Wrote the paper: AR LJJ LC ACN.

References

1. Morgan DO The Cell Cycle: Principles of Control, New Science Press.
2. Gauthier NP, Jensen LJ, Wernersson R, Brunak S, Jensen TS (2010) Cyclebase.org: version 2.0, an updated comprehensive, multi-species repository of cell cycle experiments and derived analysis results. Nucleic Acids Res 38: D699–702.
3. Orlando DA, Lin CY, Bernard A, Wang JY, Socolar JE, et al. (2008) Global control of cell-cycle transcription by coupled CDK and network oscillators. Nature 453: 944–947.
4. Coudreuse D, Nurse P (2010) Driving the cell cycle with a minimal CDK control network. Nature 468: 1074–1079.
5. Kapuy O, He E, Lopez-Aviles S, Uhlmann F, Tyson JJ, et al. (2009) System-level feedbacks control cell cycle progression. FEBS Lett 583: 3992–3998.
6. Novak B, Tyson JJ, Gyorffy B, Csikasz-Nagy A (2007) Irreversible cell-cycle transitions are due to systems-level feedback. Nat Cell Biol 9: 724–728.
7. Ferrell JE, Jr. (2002) Self-perpetuating states in signal transduction: positive feedback, double-negative feedback and bistability. Curr Opin Cell Biol 14: 140–148.
8. Tyson JJ, Chen KC, Novak B (2003) Sniffers, buzzers, toggles and blinkers: dynamics of regulatory and signaling pathways in the cell. Curr Opin Cell Biol 15: 221–231.
9. Nurse P (1990) Universal control mechanism regulating onset of M-phase. Nature 344: 503–508.
10. O'Farrell PH (2001) Triggering the all-or-nothing switch into mitosis. Trends Cell Biol 11: 512–519.
11. Pomerening JR, Sontag ED, Ferrell JE, Jr. (2003) Building a cell cycle oscillator: hysteresis and bistability in the activation of Cdc2. Nat Cell Biol 5: 346–351.
12. Sha W, Moore J, Chen K, Lassaletta AD, Yi CS, et al. (2003) Hysteresis drives cell-cycle transitions in Xenopus laevis egg extracts. Proc Natl Acad Sci U S A 100: 975–980.
13. Pomerening JR, Kim SY, Ferrell JE, Jr. (2005) Systems-level dissection of the cell-cycle oscillator: bypassing positive feedback produces damped oscillations. Cell 122: 565–578.
14. Deibler RW, Kirschner MW (2010) Quantitative reconstitution of mitotic CDK1 activation in somatic cell extracts. Mol Cell 37: 753–767.
15. Lindqvist A, Rodriguez-Bravo V, Medema RH (2009) The decision to enter mitosis: feedback and redundancy in the mitotic entry network. J Cell Biol 185: 193–202.
16. Perry JA, Kornbluth S (2007) Cdc25 and Wee1: analogous opposites? Cell Div 2: 12.
17. Csikasz-Nagy A (2009) Computational systems biology of the cell cycle. Brief Bioinform 10: 424–434.
18. Ferrell JE, Tsai TY, Yang Q (2011) Modeling the Cell Cycle: Why Do Certain Circuits Oscillate? Cell 144: 874–885.
19. Tyson JJ, Novak B (2008) Temporal organization of the cell cycle. Curr Biol 18: R759–R768.
20. Ferrell JE, Jr. (2008) Feedback regulation of opposing enzymes generates robust, all-or-none bistable responses. Curr Biol 18: R244–245.
21. Domingo-Sananes MR, Novak B (2010) Different effects of redundant feedback loops on a bistable switch. Chaos 20: 045120.
22. Trunnell NB, Poon AC, Kim SY, Ferrell JE (2011) Ultrasensitivity in the Regulation of Cdc25C by Cdk1. Molecular cell 41: 263–274.
23. Charvin G, Oikonomou C, Siggia ED, Cross FR (2010) Origin of irreversibility of cell cycle start in budding yeast. PLoS Biol 8: e1000284.
24. Cross FR, Archambault V, Miller M, Klovstad M (2002) Testing a mathematical model of the yeast cell cycle. Mol Biol Cell 13: 52–70.
25. Skotheim JM, Di Talia S, Siggia ED, Cross FR (2008) Positive feedback of G1 cyclins ensures coherent cell cycle entry. Nature 454: 291–296.
26. Holt LJ, Krutchinsky AN, Morgan DO (2008) Positive feedback sharpens the anaphase switch. Nature 454: 353–357.
27. Lopez-Aviles S, Kapuy O, Novak B, Uhlmann F (2009) Irreversibility of mitotic exit is the consequence of systems-level feedback. Nature 459: 592–595.
28. Lukas J, Lukas C, Bartek J (2004) Mammalian cell cycle checkpoints: signalling pathways and their organization in space and time. DNA Repair (Amst) 3: 997–1007.
29. Tyson JJ, Csikasz-Nagy A, Novak B (2002) The dynamics of cell cycle regulation. Bioessays 24: 1095–1109.
30. He E, Kapuy O, Oliveira RA, Uhlmann F, Tyson JJ, et al. (2011) System-level feedbacks make the anaphase switch irreversible. Proc Natl Acad Sci U S A 108: 10016–10021.
31. Pomerening JR (2009) Positive-feedback loops in cell cycle progression. FEBS Lett 583: 3388–3396.
32. Dematté L, Larcher R, Palmisano A, Priami C, Romanel A (2010) Programming Biology in BlenX. In: Choi S, ed. Systems Biology for Signaling Networks. Heidelberg: Springer. pp 777–821.
33. Novak B, Tyson JJ (1993) Numerical analysis of a comprehensive model of M-phase control in Xenopus oocyte extracts and intact embryos. J Cell Sci 106(Pt 4): 1153–1168.
34. Bartek J, Lukas J (2007) DNA damage checkpoints: from initiation to recovery or adaptation. Curr Opin Cell Biol 19: 238–245.
35. Khodjakov A, Rieder CL (2009) The nature of cell-cycle checkpoints: facts and fallacies. J Biol 8: 88.
36. Sia RA, Herald HA, Lew DJ (1996) Cdc28 tyrosine phosphorylation and the morphogenesis checkpoint in budding yeast. Mol Biol Cell 7: 1657–1666.
37. Rupes I (2002) Checking cell size in yeast. Trends Genet 18: 479–485.
38. Sveiczer A, Novak B, Mitchison JM (1996) The size control of fission yeast revisited. J Cell Sci 109(Pt 12): 2947–2957.
39. Donzelli M, Draetta GF (2003) Regulating mammalian checkpoints through Cdc25 inactivation. EMBO Rep 4: 671–677.
40. Shirayama M, Toth A, Galova M, Nasmyth K (1999) APCCdc20 promotes exit from mitosis by destroying the anaphase inhibitor Pds1 and cyclin Clb5. Nature 402: 203–207.
41. Sullivan M, Uhlmann F (2003) A non-proteolytic function of separase links the onset of anaphase to mitotic exit. Nat Cell Biol 5: 249–254.
42. Amon A (1997) Regulation of B-type cyclin proteolysis by Cdc28–associated kinases in budding yeast. The EMBO Journal 16: 2693–2702.
43. Visintin R, Craig K, Hwang ES, Prinz S, Tyers M, et al. (1998) The phosphatase Cdc14 triggers mitotic exit by reversal of Cdk-dependent phosphorylation. Molecular cell 2: 709–718.
44. Azzam R, Chen SL, Shou W, Mah AS, Alexandru G, et al. (2004) Phosphorylation by Cyclin B-Cdk Underlies Release of Mitotic Exit Activator Cdc14 from the Nucleolus. Science 305: 516–519.
45. Csikász-Nagy A, Kapuy O, Győrffy B, Tyson J, Novák B (2007) Modeling the septation initiation network (SIN) in fission yeast cells. Current Genetics 51: 245–255.
46. Csikasz-Nagy A, Kapuy O, Toth A, Pal C, Jensen LJ, et al. (2009) Cell cycle regulation by feed-forward loops coupling transcription and phosphorylation. Mol Syst Biol 5: 236.
47. Csikasz-Nagy A, Cardelli L, Soyer OS (2011) Response dynamics of phosphorelays suggest their potential utility in cell signalling. J R Soc Interface 8: 480–488.
48. Goldbeter A (1991) A minimal cascade model for the mitotic oscillator involving cyclin and cdc2 kinase. Proc Natl Acad Sci U S A 88: 9107–9111.
49. Tsai TY, Choi YS, Ma W, Pomerening JR, Tang C, et al. (2008) Robust, tunable biological oscillations from interlinked positive and negative feedback loops. Science 321: 126–129.
50. Nasmyth K (2001) A Prize for Proliferation. Cell 107: 689–701.
51. Csikasz-Nagy A, Battogtokh D, Chen KC, Novak B, Tyson JJ (2006) Analysis of a generic model of eukaryotic cell-cycle regulation. Biophys J 90: 4361–4379.
52. Sia RA, Bardes ES, Lew DJ (1998) Control of Swe1p degradation by the morphogenesis checkpoint. EMBO J 17: 6678–6688.
53. Enders GH (2010) Gauchos and ochos: a Wee1-Cdk tango regulating mitotic entry. Cell Div 5: 12.
54. Novak B, Kapuy O, Domingo-Sananes MR, Tyson JJ (2010) Regulated protein kinases and phosphatases in cell cycle decisions. Curr Opin Cell Biol 22: 1–8.
55. Boutros R, Lobjois V, Ducommun B (2007) CDC25 phosphatases in cancer cells: key players? Good targets? Nat Rev Cancer 7: 495–507.
56. Wurzenberger C, Gerlich DW (2011) Phosphatases: providing safe passage through mitotic exit. Nat Rev Mol Cell Biol 12: 469–482.
57. Mochida S, Ikeo S, Gannon J, Hunt T (2009) Regulated activity of PP2A-B55[delta] is crucial for controlling entry into and exit from mitosis in Xenopus egg extracts. EMBO J 28: 2777–2785.
58. Burgess A, Vigneron S, Brioudes E, Labbé JC, Lorca T, et al. (2010) Loss of human Greatwall results in G2 arrest and multiple mitotic defects due to deregulation of the cyclin B-Cdc2/PP2A balance. Proc Natl Acad Sci U S A 107: 12564–12569.
59. Alon U (2007) Introduction to systems biology: design principles of biological circuits. Boca RatonFL: Chapman and Hall/CRC Press.
60. Dekel E, Alon U (2005) Optimality and evolutionary tuning of the expression level of a protein. Nature 436: 588–592.
61. Savageau MA (1998) Demand theory of gene regulation. I. Quantitative development of the theory. Genetics 149: 1665–1676.
62. Dissmeyer N, Weimer AK, Veylder LD, Novak B, Schnittger A (2010) The regulatory network of cell-cycle progression is fundamentally different in plants versus yeast or metazoans. Plant Signal Behav 5.
63. Lew DJ, Kornbluth S (1996) Regulatory roles of cyclin dependent kinase phosphorylation in cell cycle control. Curr Opin Cell Biol 8: 795–804.
64. Pal G, Paraz MT, Kellogg DR (2008) Regulation of Mih1/Cdc25 by protein phosphatase 2A and casein kinase 1. J Cell Biol 180: 931–945.
65. Maniatis T, Goodbourn S, Fischer JA (1987) Regulation of inducible and tissue-specific gene expression. Science 236: 1237–1245.

66. Dematte L, Priami C, Romanel A (2008) The Beta Workbench: a computational tool to study the dynamics of biological systems. Brief Bioinform 9: 437–449.
67. Gillespie DT (1977) Exact stochastic simulation of coupled chemical reactions. J Phys Chem 81: 2340–2361.
68. Barkai N, Leibler S (1997) Robustness in simple biochemical networks. Nature 387: 913–917.
69. Ciliberto A, Novak B, Tyson JJ (2003) Mathematical model of the morphogenesis checkpoint in budding yeast. J Cell Biol 163: 1243–1254.

dc_836_14

7.8 A sejtpolaritás és a sejtciklus-szabályozó hálózatok kapcsolatainak vizsgálata

Vaggi F., Dodgson J., Bajpai A., Chessel A., Jordan F., Sato M., Carazo-Salas RE., **Csikász-Nagy A.** (2012) Linkers of cell polarity and cell cycle regulation in the fission yeast protein interaction network. *PLoS Computational Biology* **8(10):** e1002732

Impakt faktor: 4.867

OPEN ACCESS Freely available online

PLOS | COMPUTATIONAL BIOLOGY

Linkers of Cell Polarity and Cell Cycle Regulation in the Fission Yeast Protein Interaction Network

Federico Vaggi[1], James Dodgson[2], Archana Bajpai[1], Anatole Chessel[2], Ferenc Jordán[1], Masamitsu Sato[3], Rafael Edgardo Carazo-Salas[2], Attila Csikász-Nagy[1]*

1 The Microsoft Research-University of Trento Centre for Computational Systems Biology, Rovereto, Italy, **2** The Gurdon Institute, University of Cambridge, Cambridge, United Kingdom, **3** Department of Biophysics and Biochemistry, University of Tokyo, Tokyo, Japan

Abstract

The study of gene and protein interaction networks has improved our understanding of the multiple, systemic levels of regulation found in eukaryotic and prokaryotic organisms. Here we carry out a large-scale analysis of the protein-protein interaction (PPI) network of fission yeast (*Schizosaccharomyces pombe*) and establish a method to identify 'linker' proteins that bridge diverse cellular processes - integrating Gene Ontology and PPI data with network theory measures. We test the method on a highly characterized subset of the genome consisting of proteins controlling the cell cycle, cell polarity and cytokinesis and identify proteins likely to play a key role in controlling the temporal changes in the localization of the polarity machinery. Experimental inspection of one such factor, the polarity-regulating RNB protein Sts5, confirms the prediction that it has a cell cycle dependent regulation. Detailed bibliographic inspection of other predicted 'linkers' also confirms the predictive power of the method. As the method is robust to network perturbations and can successfully predict linker proteins, it provides a powerful tool to study the interplay between different cellular processes.

Citation: Vaggi F, Dodgson J, Bajpai A, Chessel A, Jordán F, et al. (2012) Linkers of Cell Polarity and Cell Cycle Regulation in the Fission Yeast Protein Interaction Network. PLoS Comput Biol 8(10): e1002732. doi:10.1371/journal.pcbi.1002732

Editor: Robert B. Russell, University of Heidelberg, Germany

Received May 1, 2012; **Accepted** August 21, 2012; **Published** October 18, 2012

Funding: The authors gratefully acknowledge support from a Human Frontier Science Program (HFSP) Young Investigator Grant (R.E.C.-S., A.C.-N., M.S.; HFSP RGY0066/2009-C), an European Research Council (ERC) Starting Researcher Investigator Grant (R.E.C.-S.; SYSGRO), a Grant-in-Aid for Young Scientists from the Japan Society for the Promotion of Science (JSPS) (M.S.) and A.C.-N., A.B., F.J. are funded by the Italian Research Fund FIRB (RBPR0523C3). The funders had no role in study design, data collection and analysis, decision to publish, or preparation of the manuscript.

Competing Interests: The authors have declared that no competing interests exist.

* E-mail: csikasz@cosbi.eu

Introduction

The eukaryotic cell cycle is one of the most important and evolutionary conserved processes of cells [1,2]. The cell cycle integrates signals from multiple pathways to control tissue growth and homeostasis in multicellular organisms, as well as reproduction and proliferation in single cell organisms [3]. To ensure cell integrity, the cell cycle regulates and is regulated by other key processes such as DNA replication, cytokinesis and cell growth [4–9]. Disruption of the regulation between the cell cycle and other cellular processes can cause a myriad of cellular pathologies including defects in cell shape, abnormal cell growth and aneuploidy, potentially leading to cancer [10].

With the accumulation of data from high-throughput biology as well as the generalisation of manually curated online databases, we now can mine existing biological networks to make experimentally verifiable predictions about system-wide properties of genes and gene products. In this work, we present a new method to search for proteins that serve as linkers between distinct functional sub-networks. Because of the well-characterized interactions between the cell cycle and other processes in the fission yeast *Schizosaccharomyces pombe*, we focus our analysis on this organism, where these processes have not yet been investigated yet by protein interaction network analysis methods.

The fission yeast - a rod-shaped unicellular eukaryote - is ideally suited to study the relationship between cell cycle and cell polarity regulation, as its highly polarized growth pattern is tightly correlated with cell cycle progression [7,11]. After cytokinesis, newborn *S. pombe* cells resume growth in G1 in a monopolar fashion from their 'old end' - the cell end that existed prior to division - and later in early G2 activate growth at their 'new end' derived from the site of septation, an event termed new-end take-off or NETO [12]. Bipolar growth then continues through G2 until cells reach a critical size, after which cells enter M phase again. At that point cells stop growing [13], mitosis takes place and each cell divides by growing a septum in its middle. Daughter cells resume their cyclic pattern of growth at the ends and division at the middle, a pattern that relies on the cytoskeleton of actin and microtubules and on diverse polarity-regulating proteins ('polarity factors'). Cytokinesis, polarity, and the cell cycle have been extensively studied in fission yeast –using both experiments and mathematical modelling [14–18]. The insights gained from studies in fission yeast often carry over to higher eukaryotes, as the molecular machinery controlling those processes has been highly conserved throughout evolution [1,19,20].

Several proteins have been identified that play important roles connecting these processes in fission yeast. For example, the polarized growth-regulating DYRK kinase Pom1 [21] was recently shown to form a spatial gradient that is used by the cell cycle machinery to sense the length of the cell [17,22,23]. Another link was observed between the morphogenesis-related NDR kinase network (MOR) and the septation initiation network (SIN) [24].

Author Summary

Analysis of protein interaction networks has been of use as a means to grapple with the complexity of the interactome of biological organisms. So far, network based approaches have only been used in a limited number of organisms due to the lack of high-throughput experiments. In this study, we investigate by graph theoretical network analysis approaches the protein-protein interaction network of fission yeast, and present a new network measure, linkerity, that predicts the ability of certain proteins to function as bridges between diverse cellular processes. We apply this linkerity measure to a highly conserved and coupled subset of the fission yeast network, consisting of the proteins that regulate cell cycle, polarized cell growth, and cell division. In depth literature analysis confirms that several proteins identified as linkers of cell polarity regulation are indeed also associated with cell cycle and/or cell division control. Similarly, experimental testing confirms that a mostly uncharacterized polarity regulator identified by the method as an important linker is regulated by the cell cycle, as predicted.

MOR is important for the localization of actin patches to sites of polarized growth, while SIN is responsible for triggering cytokinesis. It was discovered that SIN inhibits the MOR pathway, through inhibition of the Orb6 activator Nak1. MOR itself also interferes with SIN, and this antagonism is required for proper progression through the cell cycle [25,26]. Furthermore, a similar antagonism between the MOR and SIN pathways has also been observed in higher eukaryotes [27,28]. The NETO transition from monopolar to bipolar growth and the switch from polarized growth to actin ring-mediated cell septation are also controlled by the cell cycle [13], thus the cell cycle machinery enforces a major control on both polarized growth and cytokinesis. Although many polarity or cytokinesis regulators contain potential phosphorylation sites for the cell cycle-regulating Cyclin-Dependent Kinases [29] (CDK), the molecular details of these couplings are not well known. In the other direction, if either polarized cell growth or cytokinesis is inhibited, both can send signals to stop the cell cycle [30,31], further underlining that these three functional modules are highly interlinked.

To tackle the interplay between different cellular processes, we utilized a network theory approach. Hitherto, network based approaches have only been used in a limited number of organisms, due to the paucity of genome-wide interaction data available for most species. Recently, however, improvements in automatic experimental annotation, literature mining [32], machine learning [33] and orthology annotations [34], are allowing the use of network approaches in a wider range of organisms. For example, 'meta databases' such as STRING [35,36], benchmark information from multiple sources and provide for each possible interaction a confidence score that reflects the likelihood of a set of proteins of actually interacting. Here, we take advantage of such developments and build on the efforts of the fission yeast community in annotating protein functions [37–39], to establish a new method to identify proteins linking diverse cellular processes, based on integrating Gene Ontology (GO) [40,41] and Protein-Protein Interaction (PPI) data together with network theory based measures. Network-based approaches in biology have been used in the past to identify community structures, study lethality, identify specific regulatory circuits and study hierarchical organization [42]. In particular, the nature of large scale protein-protein interaction networks has recently been under considerable debate with different groups disagreeing about the modularity of networks, as well as the properties of the nodes responsible for bringing together different modules [43–46]. In this work, we sidestep the difficult problem of identifying hierarchical modules in a large, genome-wide network and focus instead on a method to identify proteins that link different cellular processes. To do this, we use the highly characterized sub-genomic network consisting of proteins regulating the cell cycle, cytokinesis, and polarized cell growth in fission yeast. We propose a new network measure, termed 'linkerity', and use it to predict a novel role for a number of proteins as key bridges between these biological processes.

Results

Constructing and validating the fission yeast protein interaction network

We constructed the fission yeast protein-interaction network using data from STRING [35,36] and BioGRID [47]. By applying a cutoff on the confidence score from STRING, we can reject interaction pairs for which there is a limited amount of evidence (see Materials and Methods for details on data in STRING) and use the remaining edges to construct a non-directed and non-weighted network.

We then examined the effects of increasing the cutoff in STRING confidence scores in both the genome-wide interaction dataset of fission yeast and that of the better characterized budding yeast *Saccharomyces cerevisiae* on the network topology. Increasing the cutoff decreased the amount of nodes (Figure 1A) and the edge density (Figure 1B) in the largest component (the connected component in the network containing the highest number of edges and nodes) of both the fission and budding yeast networks (Tables S1, S2). This decrease was less sharp in budding yeast compared to fission yeast due to the extensive amount of genome-wide interaction experiments carried out in the former, increasing the amount of high-confidence interactions. Interestingly, in the 'core' sub-network consisting of proteins involved in cell cycle regulation, polarity and cytokinesis (Figure 2 for fission yeast and Figure S1 for budding yeast), the drop off in the number of nodes and edges was far less significant in both yeasts, suggesting that interaction data for the core fission yeast network tends to be more reliable than interaction data for the rest of the network (Figure 1, red stars versus red dots, also Tables S1, S2, S3, S4). As a more stringent test, we constructed networks for both organisms using only data from BioGRID [47]. BioGRID is a database that only contains data from manually annotated experiments (distinguishing between experiments that show direct physical interaction and genetic interactions). Networks built using the BioGRID physical interaction data also show that the core networks of fission yeast and budding yeast are relatively dense, while the fission yeast organism-wide network is rather sparse (Figure 1). Even with the relatively high coverage of the core (regulation of cell cycle, cytokinesis, polarity) network in fission yeast, it is important to note that fission yeast lacks any genome-wide protein-protein interaction experiments, and as such, several of the interactions predicted by STRING are based on indirect evidence such as genetic interactions, inference from homology, or literature mining [35,36].

As no analysis of the fission yeast network has been previously published, we performed a few checks to verify that our network construction procedure was giving sensible results, and that the data for fission yeast available in STRING was of sufficiently high quality. As a first check, we sought to replicate a number of analyses previously performed with budding yeast (Table 1). At a cutoff of 0.7 (defined by STRING as a 'high confidence'

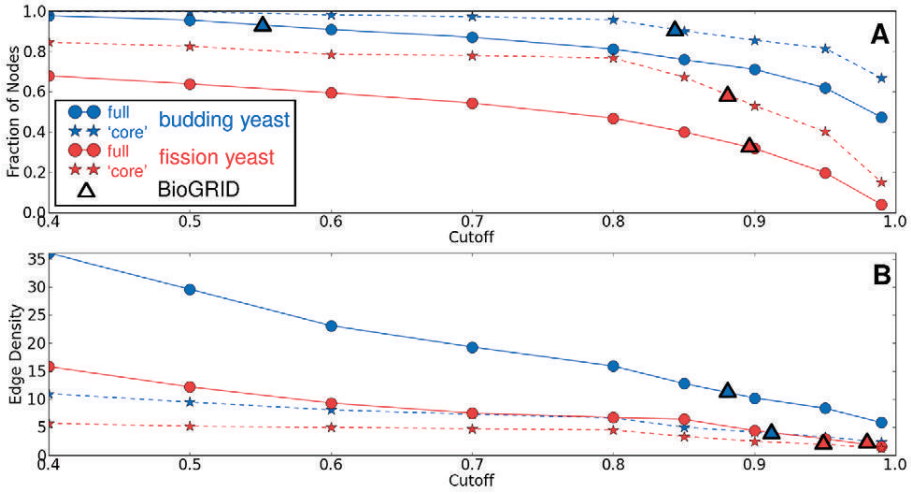

Figure 1. Dependence of network measures on protein-protein interaction data quality. As we increase the minimal accepted confidence (cutoff) for the PPI data of the STRING database, the number of nodes in the largest connected component (**A**) and the network density (**B**) both decrease for all networks. This decrease is faster in fission yeast compared to budding yeast, and faster in the full organism network compared to the core network. Triangles overlaid on each curve show the same network measures for the PPI network based on the BioGRID database, the position on the x-axis of BioGRID data is calculated using linear interpolation to estimate the corresponding cutoff in STRING which would give a similarly-sized network, thus the overlay of the BioGRID data gives an indication how this relates to different cutoff STRING data. As can be seen from the figure panels the fission yeast core network is quite robust to cutoff changes and behaves similarly to the core network of budding yeast cells. This is also true for the core networks based on BioGRID data.
doi:10.1371/journal.pcbi.1002732.g001

threshold), the genome-wide fission yeast network has 2770 nodes with at least one connection and 20432 edges compared to 5477 nodes and 105429 edges found in budding yeast, although they have approximately similar number of proteins. We calculated the degree distribution for the nodes in the network, and observed that, as previously described for numerous other complex networks [48], the fission yeast PPI network has a scale-free distribution (Figure S2). We also repeated analyses done in numerous other studies examining the relationship between network measures and gene deletion lethality [43–45]. As reported for budding yeast, we

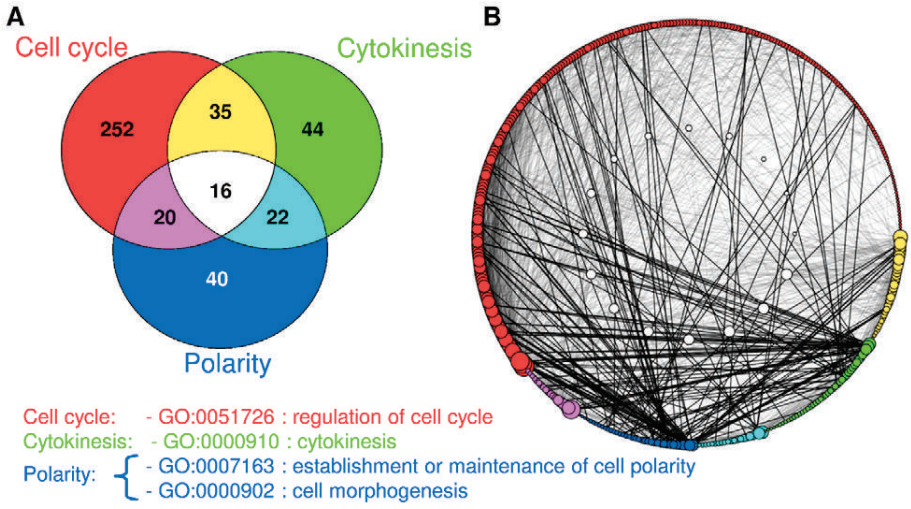

Figure 2. The cell cycle + cytokinesis + polarity = core interaction network of fission yeast proteins. (**A**) Venn diagram showing the overlap among the different Gene Ontology functional groups for the proteins belonging to the core network. Proteins with multiple functional annotations have colours that are the sum of the colours of the individual functional annotations; proteins belonging to all three functional groups are in white. (**B**) Protein-protein interactions inside the fission yeast core network (from the STRING database at cutoff 0.7). Node colours are the same as in panel A. Node size is proportional to the degree of each protein, and node order within a category (clockwise) is also determined by degree. 165 black edges link proteins that do not share functional annotations, while 1869 grey edges link proteins that have at least one common GO annotation (thus white nodes have only grey links). White nodes (nodes belonging to all categories) are shown in the inner circle in the middle of the network.
doi:10.1371/journal.pcbi.1002732.g002

observed that degree (the number of interactions with other proteins) is the best predictor network measure of gene deletion-induced lethality in fission yeast, and that ratio of these essential genes among hubs (the top 20% of proteins by degree) is even higher in fission yeast than in budding yeast (see Text S1).

Since there is no high-throughput genome-wide interaction data available for fission yeast, we tested the possibility that highly investigated proteins might have more interactions. To check this, we tested to see whether the number of abstracts in PubMed discussing a particular protein was correlated with the degree of that protein in the network. The Pearson correlation between the number of PubMed abstracts citing a protein and its degree in the network was 0.13 for budding yeast (p-value$<10^{-19}$) and 0.14 for fission yeast (p-value$<10^{-13}$) (details in Tables S1, S2), suggesting there is no fission yeast-specific bias for proteins with large amounts of publications in STRING networks. However, a large amount of evidence for the fission yeast interactions in STRING is obtained from homology, and specifically from interactions of homologues proteins in budding yeast. As essential genes are more likely to be conserved [49,50] and STRING is more likely to identify homology between highly conserved genes, it is possible that this might introduce a subtle bias making essential genes appear to be more highly connected in virtue of their higher conservation. This is consistent with the observation that a very high percentage of hubs in fission yeast appear to be essential (Text S1).

The core network of regulators of the cell cycle, cell polarity and cytokinesis

The sub-network of all proteins regulating cell cycle, cytokinesis and polarized growth, henceforth, the 'core' network (see Materials and Methods for definitions of exact GO terms used) in fission yeast contains 550 proteins: 384 of those are associated with regulation of cell cycle, 155 with cytokinesis and 139 with polarity. Using a cutoff of 0.7 in STRING, 429 of the total 550 proteins are connected to the largest connected component of the core network. Most of the proteins not in the network have no known interactions, and the second largest connected component contains only 4 proteins, thus we focus only on the interaction network of the largest connected component. There are a high number of proteins with multiple functions in the network (Figure 2A), 16 of them (Alp4, Cdc15, Gsk3, Lsk1, Mor2, Orb6, Pab1, Pmo25, Pom1, Ppb1, Ras1, Scd1, Shk1, Sid2, Tea1, Wsp1) are important for all three cellular processes and 77 have dual functions. The ratio of multifunctional proteins is quite similar to the ratio in the analogous core budding yeast network (Figure S1). Interestingly the budding yeast core network contains less nodes than the fission yeast core network (although it is more densely connected), this could be a consequence of the extensive studies of cytokinesis [19], cell cycle [51] and cell polarity [13] and their careful annotation in fission yeast [37–39], but it also reflects the loss of some of the conserved eukaryotic cell cycle genes from budding yeast [29,52].

The core interaction network contains several interactions between proteins that do not share a GO annotation; however the majority of links (91%) are between proteins which share at least one functional annotation among those under consideration (regulation of cell cycle, cytokinesis, and polarity) (Figure 2B). To probe this, we examined the relationship between the functional annotation of a node and that of its interaction partners. In fission yeast, any protein with a given functional annotation was 11 times (1.9 would be expected randomly, see Figure S3A) more likely to interact with another protein with the same functional annotation than with another protein with different functional annotations (for the budding yeast core network, this ratio was 4.5 vs. 1.06 expected, see Figure S3B). Since fission yeast has more proteins that belong to all three categories (16 in fission yeast versus 6 in budding yeast), we tested to see whether this observed functional modularity was due to their presence. We removed all proteins belonging to all three categories from both networks and repeated the analysis. This did not significantly alter the results as the ratios remained after the removal (10.38 times more likely for fission yeast and 4.16 for budding yeast) suggesting that the functional modularity observed in fission yeast is not caused by the presence of highly connected proteins with multiple annotations, but rather that the fission yeast network is characterized by strong connections between local communities that share functional annotations. It is however important to note that the GO categories 'regulation of cell cycle' and 'cytokinesis' are partially overlapping. In particular 'regulation of cell cycle cytokinesis' is a child term of both 'regulation of cell cycle' and 'cytokinesis'. Even when taking this overlap into account in the analysis, we still observe a high degree of functional modularity in the core networks of both fission and budding yeast (not shown).

We further analyzed this effect using a community detection algorithm, which identifies local communities in a network and allows their overlap – as we have nodes with multiple annotations. We applied the k-clique propagation algorithm [53,54] and examined the communities generated by the method with $k = 4$. While the communities generated by the algorithm do not exactly match the functional annotations, we find that the cliques generated by the algorithm are primarily formed by proteins that share functional annotations (Figure 3A,B). Upon closer examination, the few proteins that do not share a functional annotation with the other members of a clique seem to have related roles: for example, in the 5th clique on Figure 3B, the lone 'non-polarity' protein is Rgf3, which was shown to play an important cell-wall

Table 1. Network statistics and gene essentiality comparison between the two yeasts.

	budding yeast	fission yeast	references
Degree Distribution:	Scale Free	Scale Free	[105]
BC Distribution:	Scale Free	Scale Free	[106]
Network measure most predictive of lethality:	Degree	Degree	[45,107]
% of essential genes in hubs	39	56	[45]
% of essential genes in bottlenecks	31	47	[45]

Quality check of the fission yeast PPI network in comparison to earlier published data on the budding yeast PPI network. Hubs are the top 20% of nodes in the network according to degree. Bottlenecks are the top 20% of nodes in the network according to betweenness centrality (BC).
doi:10.1371/journal.pcbi.1002732.t001

remodeling role downstream of Rho1, one of the key regulators of polarity [55,56] (consult Table S5 for all clique members).

Identification of 'linker' proteins by network analysis

To systematically study proteins linking different cellular processes, we next used a network-based approach aiming to identify proteins that function as 'linkers' between different functional categories (Figure 4A). To do so, we constructed protein-protein interaction networks consisting only of proteins with one of the investigated functional annotations (cell cycle, cytokinesis or polarity regulation). We then calculated the betweenness centrality score for every node in each of these networks and in the merged core network. Betweenness Centrality (BC) measures how often a node is found in the shortest path between pairs of other nodes in the network; intuitively, it can be thought of as a measure of how central a node is in a network. If a node has a low centrality score it is localized at the fringe of a network, while if it has a high score it is localized near the centre. Next we ranked the proteins based on their BC score (in case of a tie, these proteins got their average rank). To ensure that this ranking method is robust even in the presence of imperfect interaction data certainly missing important links, we randomly added 10% extra edges to all the networks 1000 times, and recalculated the ranking of all proteins at each iteration (Figures S4). While the exact ranking of proteins is not very robust to addition of extra edges, if we examine all the proteins in the top 20%, we can observe that most fluctuate out of the top 20% only very rarely, and that we nearly never observe a protein in the top 10% drop out of the top 20%. It is also reassuring that the top of the rankings starts with expected key regulators of each function: the polarity landmark Tea1 [57–59], the actin-regulating Rho GTPase Cdc42 [60,61] and actin (Act1) all came on the top of the polarity list. At the same time Cdc2, Wee1 and Cdc25 [62] are on the top of the cell cycle list (and also on the top of the core list) and the SIN scaffold Cdc11 [63] and the CDK counteracting, SIN activator phosphatase Clp1 [64,65] are leading the cytokinesis ranking (Figure S4 and Table S3).

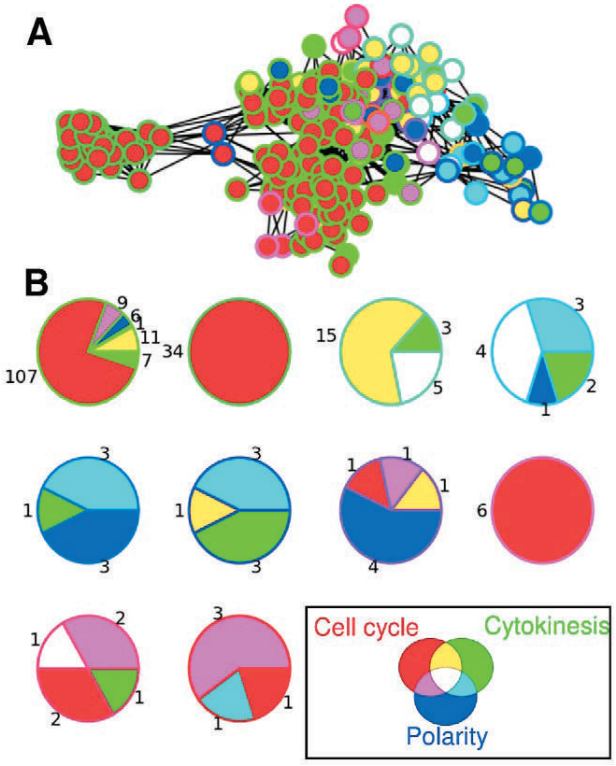

Figure 3. Segregation of functional communities in the core network. A clique propagation algorithm was used to identify locally highly connected communities of the core network. The ten cliques generated by the algorithm segregate in the interaction network if laid out by a force-based algorithm that brings closer together the stronger interacting groups (**A**). Node colour determined by the functional annotation (same as Figure 2, inset on panel B here). Proteins belonging to the same clique share the same border colour. Proteins belonging to the same clique largely share functional annotations. Pie charts show the functional distribution of proteins found in each clique (**B**). Numbers report the number of proteins with the annotations corresponding to the given colour coded annotation (see inset for colours).
doi:10.1371/journal.pcbi.1002732.g003

In the next step we compared the betweenness centrality rank of every protein in a sub-network to its relative rank in the core network. Only proteins that were originally in the sub-network were considered during this ranking based on scores they got for their position in the core network. We then calculated the ratio of the relative rank in the core network and the rank in the sub-network. We termed this calculated value 'linkerity', as this value is high for proteins that are found at the fringe of the network of proteins controlling a given cellular process, but central when considered in the context of a bigger network (Figure 4A):

$$linkerity = \frac{Rank_{sub-network}}{Rank_{core}} \quad (1)$$

Proteins with high linkerity, we hypothesized, are likely to play a crucial role to function as linkers between different cellular processes. Specifically, we focused on the relationship of the polarity network to the rest of the core network to clarify how the cell cycle and the cytokinesis machinery control the temporal changes in the localization of polarized growth zones (top of Table 2, consult Table S3 for the rest of the list). Here, we show the top 10 proteins with the highest linkerity scores. These proteins became far more central when the polarity sub-network was embedded into the core network. Most of these proteins have GO annotations for multiple processes (among the annotations under consideration), thus their linking capacity is not that surprising. Novel linkers of polarity regulation could be those that were not associated with cytokinesis or cell cycle control but gained a high linkerity score in our analysis. The formin For3 [66], the AMP-activated, Snf1-like protein kinase Ssp2 [67,68], the RNB-like protein Sts5 [69] and the MRG family protein Alp13 [70] are examples of proteins that match this. For3 is a well-characterized regulator of Tea1 to Cdc42 signalling [71,72], the other three are less well characterized. The Rho GTPase Rho4 [73] might be also an interesting linker candidate as it has established roles in polarity and cytokinesis regulation, but its exact function is not well characterized and it has no association to cell cycle regulation. Despite this, Rho4 has a central position in the core network that contains 75% cell cycle proteins (Figure 2A), furthermore its expression is cell cycle regulated [74]. The highest linkerity proteins from the cytokinesis and cell cycle regulation networks also contain a number of proteins which are also associated with polarity regulation (Table 2). Scd1, Pom1 and Tea1 are on the top of the cell cycle linkerity list and Pmk1 [75], Shk1 and Tea1 lead the cytokinesis list after Bgs1, which is essential for cell wall synthesis [76], but has no polarity related GO annotation. These are on the edge of the cell cycle regulation or cytokinesis network but became central when they are merged with the polarity

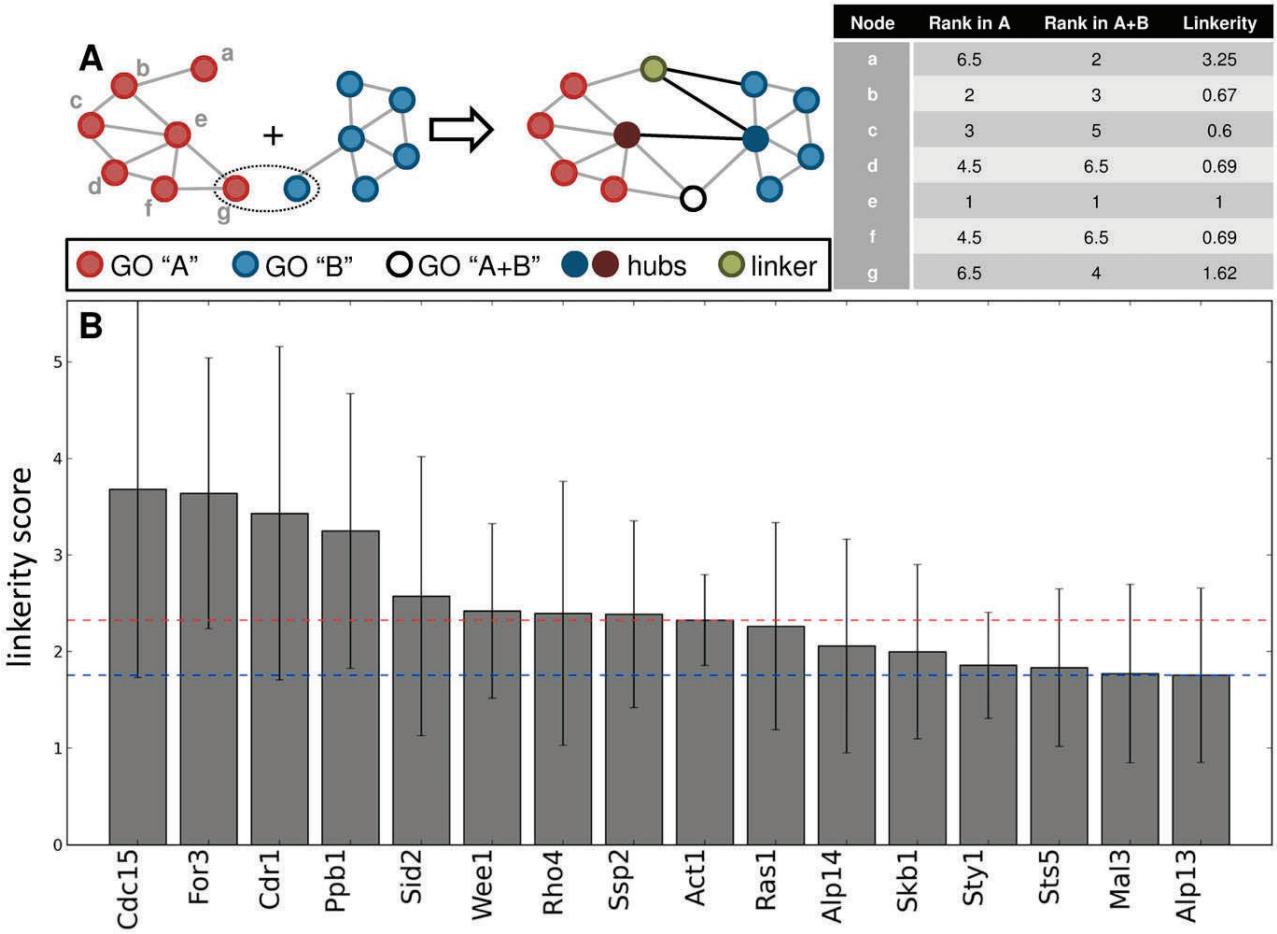

Node	Rank in A	Rank in A+B	Linkerity
a	6.5	2	3.25
b	2	3	0.67
c	3	5	0.6
d	4.5	6.5	0.69
e	1	1	1
f	4.5	6.5	0.69
g	6.5	4	1.62

Figure 4. Concepts of 'linker' protein detection and robustness of the method. (**A**) 'Linker' proteins are found at the edge of a sub-network, but are central in the context of a larger network. Such proteins have low betweenness centrality (BC) score when considered in the context of their sub-network, but have a high BC score in the core network even though they do not have a functional annotation to the other category making up the core network. Black edges indicate edges between proteins that do not share functional annotations, while the other edges are gray. Table on right gives ranks and linkerity measures for all nodes in network 'A' in the same style as Table 2 does. (**B**) Analysis of the robustness of linkerity scores for the polarity network of fission yeast cells. We added 10% extra edges randomly to the network, and computed the linkerity score of all proteins after each iteration. Bars show mean ranking with standard deviation. Blue dashed line indicates cutoff for top 10% and red line marks the top 20% (results of other type of network perturbations are reported in Figure S5).
doi:10.1371/journal.pcbi.1002732.g004

network, thus these can be also considered as linkers. As above for BC scores, we analysed the robustness of linkerity in the presence of imperfect network interaction data: we added or removed 10% of the edges from the core network at random or following a preferential attachment model and calculated linkerity scores for all proteins. Figure 4B reports the average and standard deviation from 500 random networks with 10% extra edge (other cases in Figure S5) for the top linkerity polarity proteins. Importantly the top 10 of the unperturbed list (Table 2) can be found in the top 16 of the list after 10% possible missing links were considered (Figure 4B).

As discussed above, in both fission yeast and budding yeast, we observe a high degree of functional modularity, i.e. proteins tend to interact with proteins that share their functional role. Since linker proteins play a special role in bringing together different cellular processes, we examined whether proteins with high linkerity interacted with proteins with different functional roles at a higher rate than low linkerity proteins. For all the proteins of the core network we calculated the number of its interactors (network neighbours) with cell cycle, cytokinesis and polarity annotations (Table S3). Then for every protein in each functional category (Figure 2) we calculated the ratio of the number of its interactions with proteins with the two other functional annotations to the number of its interactions with proteins with the same functional annotation. We observed that high linkerity is significantly correlated with having a high ratio of heterogeneously annotated neighbours across all functional categories in both yeasts, suggesting that linker proteins do play an important role in bridging proteins from different functional groups (see Text S2 for details).

Sts5 is a novel linker protein bridging cell polarity to cell cycle

Among predicted linker proteins we focused on Sts5, which is known to genetically interact with Ssp2 [69], which itself is likely to be linked with the cell cycle machinery as *ssp2Δ* cells cannot start mitosis when nutrient-starved [77]. Sts5 is an orthologue of budding yeast SSD1 [78] and therefore a candidate translational

Table 2. Top ten proteins with highest Linkerity measures from the three sub-networks.

Protein Name	GO terms	$Rank_{Sub}$	$Rank_{Core}$	Linkerity
Polarity proteins				
Rho4	Pol, Cyt	73.5	8	9.19
For3	Pol	35	5	7
Ssp2	Pol	73.5	19	3.87
Skb1	Pol, CC	38	13	2.92
Sts5	Pol	25	9	2.78
Cdr1	Pol, CC	73.5	29	2.53
Act1	Pol, Cyt	5	2	2.5
Cdc15	Pol, Cyt, CC	57	23	2.48
Alp13	Pol	54	22	2.45
Ppb1	Pol, Cyt, CC	27	12	2.25
Cytokinesis proteins				
Bgs1	Cyt, CC	12	3	4
Pmk1	Pol, Cyt	64	16	4
Shk1	Pol, Cyt, CC	15	4	3.75
Tea1	Pol, Cyt, CC	32	9	3.55
Rho4	Pol, Cyt	17	7	2.43
Pab1	Pol, Cyt, CC	67	29	2.31
Cdc7	Cyt, CC	29	13	2.23
Plo1	Cyt, CC	24	11	2.18
Klp5	Cyt	30	14	2.14
Fin1	Cyt, CC	97	46	2.11
Cell cycle proteins				
Scd1	Pol, Cyt, CC	288	39	7.38
Pom1	Pol, Cyt, CC	184	26	7.08
Tea1	Pol, Cyt, CC	143	25	5.72
Bgs1	Cyt, CC	30	8	3.75
Cdc10	CC	67	18	3.72
Cdc15	Pol, Cyt, CC	179	63	2.84
Cdc13	CC	15	6	2.5
Its3	Cyt, CC	234	94	2.49
Mal3	Pol, CC	123	50	2.46
Pmh1	Pol, Cyt, CC	76	34	2.23

Proteins were ranked according to BC in the polarity/cytokinesis/cell cycle regulation sub-networks ($Rank_{Sub}$ column) as well as in the core network ($Rank_{Core}$ column). Proteins with the same BC score were given the same ranking. In the core network, we considered proteins that also belonged to the investigated sub-network and skipped all other proteins (thus we had three different core network rankings). The cell cycle network gives higher linkerity scores, since it contains more nodes, thus higher ranking jumps are possible. Consult Table S3 for the rest of the lists. Table S4 contains the same data for budding yeast cells. The second column gives the GO annotations of each protein among polarity (Pol), cytokinesis (Cyt) and cell cycle (CC) related GO terms as defined on Figure 2.

doi:10.1371/journal.pcbi.1002732.t002

repressor. It is reported to control actin localisation in interphase and *sts5Δ* was shown to be compensated by mutations in Ssp2. Furthermore, Sts5 mRNA levels were shown to oscillate [74,79]. To examine the interplay between Sts5 and the cell cycle, we tagged the endogenous protein with a triple GFP tag and visualized its localization together with that of mCh-Atb2 (Alpha tubulin 2), which labels microtubules and hence served as a cell cycle stage marker. In interphase cells, Sts5 had a mostly diffuse cytoplasmic localization, however during mitosis it appeared to localize in dotted, cytoplasmic bodies (Figure 5A). The number of Sts5 dots increased throughout mitosis and peaked coinciding with the assembly of the Post Anaphase Array (PPA) of microtubules (Figure 5B). Time-lapse movies of mitotic cells also confirmed that the number of cytoplasmic dots increased until the formation of the PAA and sharply dropped to zero as cells entered interphase (Figure S6). Previous studies of Sts5 [69] showed that it was required for correct cell growth and actin patch localization during interphase. Taken together with our results, this suggests that the cell cycle controls Sts5 activity by gradually sequestering it in cytoplasmic bodies during mitosis.

Discussion

In this work, we have carried out the first network analysis based, large-scale identification of proteins linking various cellular processes in the fission yeast protein-protein interaction network. Although data for fission yeast mostly comes from manually annotated experiments, literature mining and computational inference, the network displays features comparable to those observed in other organisms. We have shown that the relationship between lethality and different network measures holds in fission yeast, and that network based approaches can give meaningful and interesting results even in organisms lacking high-throughput interaction experiments.

Our analysis of the core network of all proteins regulating cell cycle, cytokinesis, and polarized growth revealed a striking degree of functional modularity, which we have found to be highly robust to the deletion of key nodes in the network. This functional modularity was also observed when examining the communities detected by a clique propagation algorithm. Detected communities had very low heterogeneity between the functional annotations of member proteins. We investigated this modularity further by using a network approach to identify linker proteins bridging different functional categories. We propose a new network measure, linkerity, which is the ratio of the ranking by betweennness centrality measures of all the nodes belonging to a given sub-network considered in the sub-network alone and considered in the context of a larger network (Figure 4A). This new network measure does not appear to show strong correlation with other existing network measures (Text S3). Due to the non-linear distribution of betweenness centrality measures in real systems [48], it might be necessary to normalize this linkerity measure in case linkers between large sub-networks are investigated.

We tested this concept on the connections of the polarized cell growth regulatory network to the cytokinesis and cell cycle networks of fission yeast cells. These are highly characterized and strongly interacting networks and the connection between these processes is of high importance in other organisms [7,13,80–82]. We confirmed that many of the highest linkerity scoring proteins in the polarity network were already known to play important roles in multiple processes. Among these the F-BAR protein Cdc15 provide good validation as it was already shown to play a role in switching from polarized growth to cytokinetic-actin ring formation in mitosis [83]. Similarly Skb1 [84] and Cdr1 [17,23] were shown to serve as links between cell cycle and cell polarity. All these proteins shifted from a low ranking in the polarity network to a high rank in the core network (Table 2), and thus their role in polarity regulation might come from the pleotropic behavior of these proteins or from their active role in connecting polarized growth regulation to cell cycle and cytokinesis. We also discovered that the proteins with high linkerity tend to interact

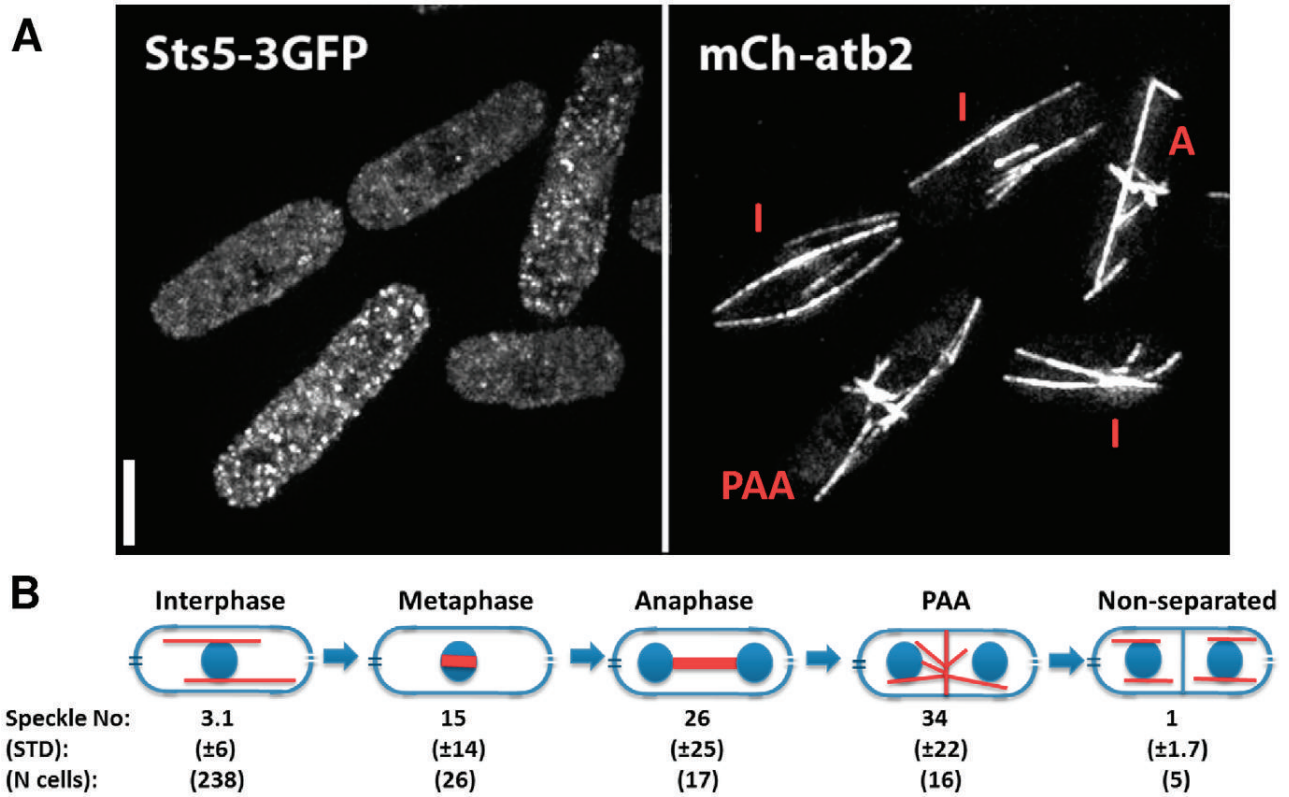

Figure 5. Localization in cells of Sts5 during the cell cycle. (**A**) Imaging of fission yeast cells co-expressing Sts5-3GFP and mCh-atb2 (labelling the different microtubule structures seen through the cell cycle, and hence acting as cell cycle stage indicators). Interphase cells (I) have diffuse Sts5 localization (with a few cytoplasmic speckles) while cells in mitosis (either in anaphase (A) or during the time of the post anaphase array (PAA)) have several Sts5 cytoplasmic dots. Scalebar: 5 μm. (**B**) Population based analysis of cycling cells revealed that at metaphase the number of Sts5 speckles greatly increases and sharply drops during septum formation. Average and standard deviation of number of dots were automatically detected in multiple cells (see Materials and Methods for details).
doi:10.1371/journal.pcbi.1002732.g005

with a more diverse set of proteins than those with low linkerity. This suggests that high linkerity proteins might play a pleiotropic role by linking together different functional processes [85,86].

Sts5 had the second highest ranking in the polarity network among the top ten linkerity proteins (after actin, Act1 that is also essential for cytokinesis). Sts5 is known to play an important role in controlling the localization of the actin machinery to cell ends during interphase, although Sts5 is localized in the cytoplasm [69]. We have shown that Sts5 is localized in cytoplasmic dots during mitosis, but diffuse during interphase, implying that its localization is cell cycle regulated. Growing tip localized polarity proteins change their localization when cells enter mitosis [13,87], but it is not expected from a cytoplasmic protein to localize into clusters in a cell cycle dependent manner. The overall level of Sts5 protein slightly increases upon entry to mitosis (Figure S6), but its activity reaches its lowest level as its accumulation into cytoplasmic dots reaches a peak. This suggests that the cell cycle controls polarity by sequestering Sts5 in and out of cytoplasmic bodies, and the triggered release and sequestration function as switches between polarized cell growth and cytokinesis. The exact nature of those cytoplasmic bodies is still unclear, however the budding yeast Sts5 homologue SSD1 was shown to localize to P-bodies [88], the cytoplasmic centers of mRNA degradation. Interestingly, like Sts5, Ssp2 and the stress pathway kinase Wis4 are also localized into cytoplasmic dots [89] and it was proposed that the stress pathway and Sts5 might act in opposing manner on cell polarity [68]. It will be important in the future to investigate if these proteins co-localize in the observed cytoplasmic dots and how these are exactly controlled by the cell cycle.

Sts5 was previously shown to genetically interact with members of the stress pathway [69]. A number of other kinases associated with stress response (such as Sty1, Skb1, Orb6, Pmk1, Mkh1) have been shown to have defects in NETO [84,89] and many of these appear highly ranked in our linkerity lists (Table 2). Furthermore, the cell end-localized polarity factor Tea4 was also shown to interact with the stress pathway [90]. These make the stress pathway a particularly intriguing target for further analysis in the search for proteins linking cell cycle and polarity, as it may play a special role as a pleiotropy integrator of both internal and external cellular signals in response to different stimuli in fission yeast and also in higher eukaryotes [91,92]. The linkerity analysis of cytokinesis and cell cycle regulatory proteins (bottom parts of Table 2) also give some interesting predictions. For instance the high linkerity of the transcription factor Cdc10 [93] in the cell cycle network suggests its role controlling the transcription of important polarity and cytokinesis genes, especially with key regulators, such as Cdc15, Scd2, Sts5, Rho4 and Sid2 having periodic transcriptional profile [74,79].

While we believe that the method presented here can be applied to other organisms and cellular processes to find linker proteins, different model organisms offer unique advantages and challenges. In this study, we took advantage of the extensive annotation of

proteins by the fission yeast community to define discrete sub-networks, bypassing the very difficult problems involved in defining meaningful 'communities' using purely network based approaches [46,54,94]. While this approach has its advantages, it is important to be aware of any partial overlaps between the used GO terms due to the presence of common child terms. The amount of overlap between child terms is also not consistent across multiple organisms, requiring special care when doing comparisons that involve multiple organisms (for example, the "regulation of cell cycle cytokinesis" is a child term of both "regulation of cell cycle" and "cytokinesis" and it contains 47 proteins in fission yeast, and only 4 proteins in budding yeast). Furthermore, while we have shown that the ranking of proteins within the communities is robust to noise, the actual communities detected by various algorithms as well as the structure of the network are strongly influenced by the granularity and quality of the interaction data used (Text S4 and [95]). In fission yeast, where interaction data is relatively sparse but there is extensive functional annotation, it makes sense to use GO annotations to define functional sub-networks [38]. Very recent network predictions based on machine-learning methods [33] will enable us to perform more careful analysis in this organism as well. Other organisms with larger gene sets will often have a lower annotation coverage [96]; in these cases functional groups in the PPI network need to be identified by community detection algorithms or predefined by the authors [80]. Once such functional groups are established, the described method provides a good means to identify proteins likely to have a role in connecting functional regulatory networks in any organism. Likewise, the defined linkerity measure can be used to identify key linker nodes of sub-networks in any complex network [54,97–99].

Materials and Methods

Bioinformatics data compilation

To obtain a list of proteins associated with specific cellular processes, we used the Gene Ontology (http://www.geneontology.org/) and downloaded all gene products associated with a given term. It is important to note that while 'cytokinesis' (GO:0000910) and 'cell cycle regulation' (GO:0051726) have specific terms that cover all proteins commonly associated with those processes, for polarity *S. pombe* proteins are split between 'establishment or maintenance of cell polarity' (GO:0007163) and 'cell morphogenesis' (GO:0000902). In the analysis, we thus used the umbrella term 'polarity' to include proteins in both of these categories. Data in STRING (http://string-db.org/) is present at different confidence scores. Confidence scores in STRING represent the likelihood of the two proteins actually interacting, and depend on the reliability of the source of the interaction. For example, an interaction that is reported in a single experiment will have a far higher confidence score than an interaction that is inferred through text mining or homology alone. We studied the effect of a cutoff in this confidence score on network size defined as the fraction of all proteins connected with at least one other protein; the main component size defined as the fraction of all proteins connected to the largest component in the network; and the edge fraction defined as the fraction of all edges found, compared to the theoretical maximum. To download the number of PubMed abstracts mentioning the name of a protein in the network, we relied on the Entrez module of the Biopython package (http://biopython.org/wiki/Biopython). Statistical analysis, including calculation of correlations, was carried out using the Statistics module of the SciPy package (http://www.scipy.org/). All network measures were calculated using pre-existing algorithms implemented in NetworkX (http://networkx.lanl.gov/). For community structure detection we used the k-clique propagation algorithm originally described in [53], and implemented in NetworkX [100]. Packages were packaged in the Enthought Python Distribution courtesy of Enthought (http://www.enthought.com/).

Network analysis workflow

The pipeline used to create the networks was:

1. We connected to the MySQL Gene Ontology database using custom python scripts, and downloaded all proteins associated with a given biological process.
2. We took all proteins downloaded and used them to query STRING, downloading all the information about protein-protein interactions in PSI-MI-TAB format. It is important to note that STRING and Gene Ontology sometimes identify the same gene by a different name, therefore special care was taken to use consistent nomenclature.
3. We parsed the PSI-MI-TAB file and transformed it into a NetworkX graph, which we could then study using both algorithms built into NetworkX as well as custom scripts.

We repeated the analysis described in the main text using networks obtained from BioGRID. In that case, instead of using STRING in step 2 we parsed the full network of a given organism from a PSI-MI-TAB file available for download on the BioGRID website, then extracted the sub-graph containing the nodes obtained in step 1 and edges of physical interactions stored in the database. The results presented are based on the state of all databases on 13 March 2012. The calculated network measures, PubMed citations and all presented numerical results are detailed in the Excel files of Tables S1, S2, S3, S4.

All Python scripts used to download data from databases as well as for analysis are available upon request.

Strains and strain construction

The *S. pombe* strain used in this study was MH123 (*h- sts5-3GFP-L-nat Z2-mCh-atb2-hph leu1 ura4 ade6-M216 his7*). Conventional PCR-based gene targeting methods for *S. pombe* were used for gene tagging [101–103].

Live microscopy cell imaging

Prior to imaging, *S. pombe* strains were grown at 32°C in yeast extract with supplements (YES) (*5*) to exponential growth. Aliquots of 300 ml cells were mounted onto 1.5 coverslip glass-bottomed plastic dishes (MatTek; P35G-1.5-14-C) pre-coated with 10 ml 1 mg/ml lectin (Sigma; L1395 and Patricell Ltd; L-1301-25) that had been allowed to air dry. After a 30-minute incubation, cells unbound to the lectin-coated glass were removed by washing with minimal medium (EMM) [101–103] and the bound cells were kept in a final suspension of 1 ml EMM.

Imaging was performed with both: an OMX microscope (Applied Precision) in conventional resolution mode, with an Olympus UPlanSapo ×100 oil immersion lens (NA1.4) and 1.512 RI immersion oil (Applied Precision); and a DeltaVision microscope (Applied Precision), comprising an Olympus 1×71 widefield microscope, an Olympus UPlanSapo ×100 oil immersion lens (NA1.4) and an Photometrics CoolSNAP HQ^2 camera. For analysis of Sts5-3GFP speckle number, stacks were taken at 0.4 um apart for 16 focal planes on the Deltavision microscope. Time lapses were taken for single focal planes at ten-minute intervals on the DeltaVision microscope.

Automated analysis of Sts5-3GFP speckle number

Cells within microscopy image fields were automatically segmented from the transmitted light channel using an algorithm developed in-house and coded in Matlab. For each cell, the cell-cycle stage was determined manually by looking at the mCh-Atb2 channel.Sts5-GFP speckles were detected using the spot detection module of the ICY software (http://icy.bioimageanalysis.org/; [104]

Supporting Information

Figure S1 The cell cycle + cytokinesis + polarity = core interaction network of budding yeast proteins. (**A**) Venn diagram showing the overlap among the different Gene Ontology functional groups in the proteins present in the core network of budding yeast. Proteins with multiple functional annotations have colours that are the sum of the colours of the individual functional annotations, proteins belonging to all three functional groups are in white. (**B**) Protein-protein interaction in the budding yeast core network (from the STRING database at cutoff 0.7). Node colour same as in panel A. Node size is proportional to degree of the protein, and node order within a category (clockwise) is also determined by degree. 469 Black edges link proteins that do not share functional annotations, while 2146 grey edges link proteins that have at least one common GO annotation (thus white nodes have only grey links). White nodes (nodes belonging to all categories) are shown in the inner circle in the middle of the network.
(PDF)

Figure S2 Scale free distribution of networks. We calculated the degree of every node in the largest connected component of the genomwide network for both fission yeast (**A**) and budding yeast (**B**). We then calculated a histogram for frequency of degree (with number of bins equal to the maximum degree observed in the network) and plotted log(frequency) vs log(degree). Best fits to $\log(P(k)) \sim \log(ck^{-\gamma})$ were calculated using a least square minimization algorithm from scipy (http://www.scipy.org/).
(PDF)

Figure S3 Functional modularity in the core networks. To calculate how much the functional modularity (the ratio of interactions between nodes with a shared GO category versus interactions between nodes with no GO category in common) observed for the core network of budding and fission yeast deviated from a random network, we kept all the category labels for all the nodes, but rewired the network either completely at random (**A**, **C**), or using a method that preserves degree-distribution (**B**, **D**) [108]. To rewire the networks at random, we removed every edge from the network then added an edge between any two nodes chosen at random until the total amount of edges in the network was equal to the original amount. To preserve degree distribution of the networks, we performed a double edge swap across the network. We picked two existing edges at random between nodes (**u,v**) and (**x,y**). We then added an edge between (**u,x**) and (**y,v**) and removed the original edge. Red arrows indicate the observed ratio for the core network, the distributions represent 1000 different random networks and their functional modularity.
(PDF)

Figure S4 Robustness analysis for the betweenness centrality ranking for polarity, cytokinesis and cell cycle networks in fission yeast. We analysed the robustness of ranking proteins by BC centrality in the presence of imperfect network interaction data. We added 10% extra edges at random to the network, calculated BC for every node after adding the edges, and ranked all the proteins. We calculated the mean and standard deviation for the rank of every protein in the network after repeating the procedure 1000 times. We normalized the rank of all proteins (Rank/number of nodes) and plotted the top 20% of nodes and their mean and standard deviation. The blue dotted line represents the cutoff for top 10% nodes, and the red dotted line represents the cutoff for top 20% of nodes. **A**, **B**, **C** are the top 20% proteins of regulation of cell cycle, cytokinesis and polarity of fission yeast.
(PDF)

Figure S5 Robustness analysis of linkerity of proteins in the fission yeast polarity network. We systematically analysed the robustness of linkerity in the presence of imperfect network interaction data. We added 10% edges preferentially to nodes with high degree (**A**) or removed 10% edges at random (**B**) to the core network. In the preferential attachment model, the probability P that a given node N had of gaining an edge was directly proportional to its degree $P(N) \sim Degree(N)$. In the random model $P(N) \sim k$ where k is a constant. Probabilities were normalized to increase or decrease the total edges of the network by 10%. We calculated the mean and standard deviation for the betweenness centrality of every protein belonging to the polarity sub-network after repeating the procedure 1000 times. We plotted the top 20% of nodes and their mean and standard deviation. The blue dotted line represents the cutoff for top 10% nodes, and the red dotted line represents the cutoff for top 20% of nodes.
(PDF)

Figure S6 Time-lapse analysis of Sts5 localization in fission yeast cells. Microtubules are visualized using mCherry labeled tubulin (Atb2) to identify cell cycle stage (**A** and **B** right column and Sts5-3GFP is visualized on the left). As the cell cycle progresses, Sts5 starts to accumulate into cytoplasmic dots, which then rapidly disappear upon septum formation. **C** is an automatic quantification of the amount of cytoplasmic dots in cells at different stages of the cell cycle.
(PDF)

Table S1 Analysis of the genome-wide fission yeast network. See detailed description under Table S2.
(XLS)

Table S2 Analysis of the genome-wide budding yeast network. Tabulated file (in .xls format) containing network measures for all protein in the largest connected component of the genome-wide network of fission (S1) and budding (S2) yeast. Columns include: **Common name:** Common name. **Systematic name:** Systematic name (for fission yeast), GO database ID (for budding yeast) **Description:** Brief description of known protein activity. **PubMed count:** Number of abstracts discussing that particular protein in fission yeast available in PubMed. **Lethality: E** (Essential) If deletion of the gene causes lethality, **V** (Viable) otherwise. **Scores**: Betweenness Centrality and Degree scores for the protein in the network using either STRING interaction data (at increasing cutoffs, 0.4, 0.7, 0.9) or data from BioGRID (only the physical protein-protein interaction data). Genes with no entry at a given cutoff have no other interactions with any proteins in the network.
(XLS)

Table S3 Analysis of the core fission yeast network. See detailed description under Table S4.
(XLS)

Table S4 Analysis of the core budding yeast network. Tabulated file (in .xls format) containing network measures for all protein in the core network of fission (S3) and budding (S4) yeast. Columns include: **Common name:** Common name. **Systematic name:** Systematic name (for fission yeast), GO database ID (for budding yeast) **Description:** Brief description of known protein activity. **PubMed count:** Number of abstracts discussing that particular protein in fission yeast available in PubMed. **Lethality: E** (Essential) If deletion of the gene causes lethality, **V** (Viable) otherwise. **GO Categories:** Which of the three categories (Cytokinesis (**CY**), Polarity (**P**), Cell Cycle (**CC**)) does the protein belong too? **Scores**: Betweenness Centrality and Degree scores and ranks for all the sub-networks the protein belongs to, as well as the core network. In the sub-network, betweenness rank ($Rank_{sub\text{-}network}$) is calculated by ranking all the proteins from highest to lowest according to their betweenness. In the core network, the betweenness rank ($Rank_{core}$) is calculated only between proteins that are found in the original sub-network. To avoid artifacts due to the presence of multiple proteins with 0 betweenness, we assign consecutive proteins with the exact same score have the same rank, which is simply defined as the average of their ranking [109]. For example: in a network of 6 proteins [**A**, **B**, **C**, **D**, **E**, **F**], with BC values of [10, 10, 7, 5, 5, 5], the ranking would be: [(**A**, 1.5), (**B**, 1.5), (**C**, 3), (**D**, 5), (**E**, 5), (**F**, 5)] **Linkerity**: Linkerity calculated for all the categories as given in Equation 1. Note that the linkerity for a protein that doesn't shift in rank is 1 by definition.
(XLS)

Table S5 All members of the cliques identified on Figure 3B. List of all proteins belonging to the cliques described in Figure 3. Clique 1 corresponds to the top left clique in Figure 3B, with cliques increasing moving from left to right.
(PDF)

Text S1 Predicting essentiality by network measures in fission and budding yeast.
(PDF)

Text S2 Analysis of the neighbors of high linkerity proteins.
(PDF)

Text S3 Correlation between linkerity and other network measures.
(PDF)

Text S4 Linkerity at various network confidences.
(PDF)

Acknowledgments

The authors are thankful to L.J. Jensen, V. Wood, J. Bahler, H. Moriya, K. Nakano, M. Toya, J. Pines, M. Godinho Ferreira, T. Surrey, J. Howard, A. Ciliberto, C. Pal, A. Sveiczer, C. Bakal and the Carazo-Salas, Csikasz-Nagy and Sato groups for help and comments

Author Contributions

Conceived and designed the experiments: FV RECS ACN. Performed the experiments: FV JD AC. Analyzed the data: FV AB AC ACN. Contributed reagents/materials/analysis tools: AB FJ MS. Wrote the paper: FV RECS ACN.

References

1. Nurse P (1990) Universal control mechanism regulating onset of M-phase. Nature 344: 503–508. doi:10.1038/344503a0.
2. Nurse P (2002) Cyclin dependent kinases and cell cycle control (nobel lecture). Chembiochem 3: 596–603. doi:10.1002/1439-7633(20020703)3:7<596::AID-CBIC596>3.0.CO;2-U.
3. Morgan DO (2006) The Cell Cycle: Principles of Control. New Science Press, Ltd.
4. Enoch T, Carr AM, Nurse P (1992) Fission yeast genes involved in coupling mitosis to completion of DNA replication. Genes Dev 6: 2035–2046. doi:10.1101/gad.6.11.2035.
5. Lacroix B, Maddox AS (2012) Cytokinesis, ploidy and aneuploidy. J Pathol 226: 338–351. doi:10.1002/path.3013.
6. Diffley JFX (2011) Quality control in the initiation of eukaryotic DNA replication. Phil Trans R Soc Lond B Biol Sci 366: 3545–3553. doi:10.1098/rstb.2011.0073.
7. Martin SG (2009) Geometric control of the cell cycle. Cell Cycle 8: 3643–3647.
8. Verde F, Mata J, Nurse P (1995) Fission yeast cell morphogenesis: identification of new genes and analysis of their role during the cell cycle. J Cell Biol 131: 1529–1538.
9. Kellogg DR (2003) Wee1-dependent mechanisms required for coordination of cell growth and cell division. J Cell Sci 116: 4883–4890. doi:10.1242/jcs.00908.
10. Wilson PD (1997) Epithelial cell polarity and disease. Am J Physiol 272: F434–42.
11. Mitchison JM (1990) The fission yeast, Schizosaccharomyces pombe. Bioessays 12: 189–191. doi:10.1002/bies.950120409.
12. Mitchison JM, Nurse P (1985) Growth in cell length in the fission yeast Schizosaccharomyces pombe. J Cell Sci 75: 357–376.
13. Hayles J, Nurse P (2001) A journey into space. Nat Rev Mol Cell Biol 2: 647–656. doi:10.1038/35089520.
14. Vavylonis D, Wu J-Q, Hao S, Shaughnessy BO, Pollard TD, et al. (2007) Assembly mechanism of the contractile ring for cytokinesis by fission yeast. Science 319: 97–100. doi:10.1126/science.1151086.
15. Wu J-Q, Sirotkin V, Kovar DR, Lord M, Beltzner CC, et al. (2006) Assembly of the cytokinetic contractile ring from a broad band of nodes in fission yeast. J Cell Biol 174: 391–402. doi:10.1083/jcb.200602032.
16. Csikász-Nagy A, Gyorffy B, Alt W, Tyson JJ, Novák B (2008) Spatial controls for growth zone formation during the fission yeast cell cycle. Yeast 25: 59–69. doi:10.1002/yea.1571.
17. Martin SG, Berthelot-Grosjean M (2009) Polar gradients of the DYRK-family kinase Pom1 couple cell length with the cell cycle. Nature 459: 852–856. doi:10.1038/nature08054.
18. Csikász-Nagy A, Kapuy O, Gyorffy B, Tyson JJ, Novák B (2007) Modeling the septation initiation network (SIN) in fission yeast cells. Curr Genet 51: 245–255. doi:10.1007/s00294-007-0123-4.
19. Pollard TD, Wu J-Q (2010) Understanding cytokinesis: lessons from fission yeast. Nat Rev Mol Cell Biol 11: 149–155. doi:10.1038/nrm2834.
20. Csikász-Nagy A, Battogtokh D, Chen KC, Novák B, Tyson JJ (2006) Analysis of a generic model of eukaryotic cell-cycle regulation. Biophys J 90: 4361–4379. doi:10.1529/biophysj.106.081240.
21. Bähler J, Pringle JR (1998) Pom1p, a fission yeast protein kinase that provides positional information for both polarized growth and cytokinesis. Genes Dev 12: 1356–1370.
22. Hachet O, Berthelot-Grosjean M, Kokkoris K, Vincenzetti V, Moosbrugger J, et al. (2011) A Phosphorylation Cycle Shapes Gradients of the DYRK Family Kinase Pom1 at the Plasma Membrane. Cell 145: 1116–1128. doi:10.1016/j.cell.2011.05.014.
23. Moseley JB, Mayeux A, Paoletti A, Nurse P (2009) A spatial gradient coordinates cell size and mitotic entry in fission yeast. Nature 459: 857–860. doi:10.1038/nature08074.
24. Krapp A, Simanis V (2008) An overview of the fission yeast septation initiation network (SIN). Biochem Soc Trans 36: 411–415. doi:10.1042/BST0360411.
25. Ray S, Kume K, Gupta S, Ge W, Balasubramanian M, et al. (2010) The mitosis-to-interphase transition is coordinated by cross talk between the SIN and MOR pathways in Schizosaccharomyces pombe. J Cell Biol 190: 793–805. doi:10.1083/jcb.201002055.
26. Gupta S, McCollum D (2011) Crosstalk between NDR kinase pathways coordinates cell cycle dependent actin rearrangements. Cell Div 6: 19. doi:10.1186/1747-1028-6-19.
27. Cornils H, Kohler RS, Hergovich A, Hemmings BA (2011) Downstream of human NDR kinases: impacting on c-myc and p21 protein stability to control cell cycle progression. Cell Cycle 10: 1897–1904.
28. Hergovich A, Cornils H, Hemmings BA (2008) Mammalian NDR protein kinases: from regulation to a role in centrosome duplication. Biochim Biophys Acta 1784: 3–15. doi:10.1016/j.bbapap.2007.07.017.
29. Jensen LJ, Jensen TS, de Lichtenberg U, Brunak S, Bork P (2006) Co-evolution of transcriptional and post-translational cell-cycle regulation. Nature 443: 594–597. doi:10.1038/nature05186.
30. Rupes I, Webb BA, Mak A, Young PG (2001) G2/M Arrest Caused by Actin Disruption Is a Manifestation of the Cell Size Checkpoint in Fission Yeast. Mol Biol Cell 12: 3892–3903.
31. Liu J, Wang H, Balasubramanian M (2000) A checkpoint that monitors cytokinesis in Schizosaccharomyces pombe. J Cell Sci 113: 1223–1230.

32. Jensen LJ, Saric J, Bork P (2006) Literature mining for the biologist: from information retrieval to biological discovery. Nat Rev Genet 7: 119–129. doi:10.1038/nrg1768.
33. Pancaldi V, Sarac OS, Rallis C, McLean JR, Prevorovsky M, et al. (2012) Predicting the Fission Yeast Protein Interaction Network. G3: Genes|Genomes|Genetics 2: 453–467. doi:10.1534/g3.111.001560.
34. Wood V (2006) Schizosaccharomyces pombe comparative genomics; from sequence to systems. In: Sunnerhagen P, Piskur J, editors. Comparative Genomics using fungi as models. Comparative Genomics using fungi as models. Springer. pp. 233–285.
35. Jensen LJ, Kuhn M, Stark M, Chaffron S, Creevey C, et al. (2009) STRING 8–a global view on proteins and their functional interactions in 630 organisms. Nucleic Acids Res 37: D412–6. doi:10.1093/nar/gkn760.
36. von Mering C, Jensen LJ, Kuhn M, Chaffron S, Doerks T, et al. (2007) STRING 7–recent developments in the integration and prediction of protein interactions. Nucleic Acids Res 35: D358–62. doi:10.1093/nar/gkl825.
37. Aslett M, Wood V (2006) Gene Ontology annotation status of the fission yeast genome: preliminary coverage approaches 100%. Yeast 23: 913–919. doi:10.1002/yea.1420.
38. Wood V, Harris MA, McDowall MD, Rutherford K, Vaughan BW, et al. (2012) PomBase: a comprehensive online resource for fission yeast. Nucleic Acids Res 40: D695–9. doi:10.1093/nar/gkr853.
39. Bitton DA, Wood V, Scutt PJ, Grallert A, Yates T, et al. (2011) Augmented annotation of the Schizosaccharomyces pombe genome reveals additional genes required for growth and viability. Genetics 187: 1207–1217. doi:10.1534/genetics.110.123497.
40. Ashburner M, Ball CA, Blake JA, Botstein D, Butler H, et al. (2000) Gene ontology: tool for the unification of biology. The Gene Ontology Consortium. Nat Genet 25: 25–29. doi:10.1038/75556.
41. Gene Ontology Consortium (2012) The Gene Ontology: enhancements for 2011. Nucleic Acids Res 40: D559–64. doi:10.1093/nar/gkr1028.
42. Vaggi F, Jordan F, Csikász-Nagy A (2011) Keystone species of the molecular network of cellular functions. In: Jordan F, Jorgensen SE, editors. Models of the Ecological Hierarchy. Elsevier Press. pp. 71–86.
43. Han J-DJ, Bertin N, Hao T, Goldberg DS, Berriz GF, et al. (2004) Evidence for dynamically organized modularity in the yeast protein-protein interaction network. Nature 430: 88–93. doi:10.1038/nature02555.
44. Batada NN, Hurst LD, Tyers M (2006) Evolutionary and physiological importance of hub proteins. PLoS Comput Biol 2: e88. doi:10.1371/journal.pcbi.0020088.
45. Yu H, Kim PM, Sprecher E, Trifonov V, Gerstein M (2007) The importance of bottlenecks in protein networks: correlation with gene essentiality and expression dynamics. PLoS Comput Biol 3: e59. doi:10.1371/journal.pcbi.0030059.
46. Batada NN, Reguly T, Breitkreutz A, Boucher L, Breitkreutz B-J, et al. (2006) Stratus not altocumulus: a new view of the yeast protein interaction network. PLoS Biol 4: e317. doi:10.1371/journal.pbio.0040317.
47. Stark C, Breitkreutz B-J, Reguly T, Boucher L, Breitkreutz A, et al. (2006) BioGRID: a general repository for interaction datasets. Nucleic Acids Res 34: D535–9. doi:10.1093/nar/gkj109.
48. Barabási A-L (2009) Scale-free networks: a decade and beyond. Science 325: 412–413. doi:10.1126/science.1173299.
49. Kim D-U, Hayles J, Kim D, Wood V, Park H-O, et al. (2010) Analysis of a genome-wide set of gene deletions in the fission yeast Schizosaccharomyces pombe. Nat Biotechnol 28: 617–623. doi:10.1038/nbt.1628.
50. Decottignies A, Sanchez-Perez I, Nurse P (2003) Schizosaccharomyces pombe essential genes: a pilot study. Genome Res 13: 399–406. doi:10.1101/gr.636103.
51. Forsburg S, Nurse P (1991) CELL CYCLE REGULATION IN CEREVISIAE AND POMBE. Ann Rev Cell Biol 7: 227–56.
52. Cross FR, Buchler NE, Skotheim JM (2011) Evolution of networks and sequences in eukaryotic cell cycle control. Phil Trans R Soc Lond B Biol Sci 366: 3532–3544. doi:10.1098/rstb.2011.0078.
53. Derényi I, Palla G, Vicsek T (2005) Clique percolation in random networks. Phys Rev Lett 94: 160202.
54. Palla G, Derényi I, Farkas I, Vicsek T (2005) Uncovering the overlapping community structure of complex networks in nature and society. Nature 435: 814–818. doi:10.1038/nature03607.
55. Morrell-Falvey JL, Ren L, Feoktistova A, Haese GD, Gould KL (2005) Cell wall remodeling at the fission yeast cell division site requires the Rho-GEF Rgf3p. J Cell Sci 118: 5563–5573. doi:10.1242/jcs.02664.
56. Tajadura V, García B, García I, García P, Sánchez Y (2004) Schizosaccharomyces pombe Rgf3p is a specific Rho1 GEF that regulates cell wall beta-glucan biosynthesis through the GTPase Rho1p. J Cell Sci 117: 6163–6174. doi:10.1242/jcs.01530.
57. Sawin KE, Snaith H a (2004) Role of microtubules and tea1p in establishment and maintenance of fission yeast cell polarity. J Cell Sci 117: 689–700. doi:10.1242/jcs.00925.
58. Niccoli T, Arellano M, Nurse P (2003) Role of Tea1p, Tea3p and Pom1p in the determination of cell ends in Schizosaccharomyces pombe. Yeast 20: 1349–1358. doi:10.1002/yea.1054.
59. Mata J, Nurse P (1997) tea1 and the microtubular cytoskeleton are important for generating global spatial order within the fission yeast cell. Cell 89: 939–949.
60. Kelly FD, Nurse P (2011) Spatial control of Cdc42 activation determines cell width in fission yeast. Mol Biol Cell 22: 3801–3811. doi:10.1091/mbc.E11-01-0057.
61. Chang F, Martin SG (2009) Shaping fission yeast with microtubules. Cold Spring Harb Perspect Biol 1: a001347. doi:10.1101/cshperspect.a001347.
62. Nurse P (2000) A long twentieth century of the cell cycle and beyond. Cell 100: 71–78.
63. Krapp A, Schmidt S, Cano E, Simanis V (2001) S. pombe cdc11p, together with sid4p, provides an anchor for septation initiation network proteins on the spindle pole body. Curr Biol 11: 1559–1568.
64. Cueille N, Salimova E, Esteban V, Blanco M, Moreno S, et al. (2001) Flp1, a fission yeast orthologue of the s. cerevisiae CDC14 gene, is not required for cyclin degradation or rum1p stabilisation at the end of mitosis. J Cell Sci 114: 2649–2664.
65. Trautmann S, Wolfe BA, Jorgensen P, Tyers M, Gould KL, et al. (2001) Fission yeast Clp1p phosphatase regulates G2/M transition and coordination of cytokinesis with cell cycle progression. Curr Biol 11: 931–940.
66. Feierbach B, Chang F (2001) Roles of the fission yeast formin for3p in cell polarity, actin cable formation and symmetric cell division. Curr Biol 11: 1656–1665.
67. Matsuzawa T, Fujita Y, Tohda H, Takegawa K (2012) Snf1-like protein kinase Ssp2 regulates glucose derepression in Schizosaccharomyces pombe. Eukaryot Cell 11: 159–167. doi:10.1128/EC.05268-11.
68. Matsusaka T, Hirata D, Yanagida M, Toda T (1995) A novel protein kinase gene ssp1+ is required for alteration of growth polarity and actin localization in fission yeast. EMBO J 14: 3325–3338.
69. Toda T, Niwa H, Nemoto T, Dhut S, Eddison M, et al. (1996) The fission yeast sts5+ gene is required for maintenance of growth polarity and functionally interacts with protein kinase C and an osmosensing MAP-kinase pathway. J Cell Sci 109 (Pt 9: 2331–2342.
70. Nakayama J-I, Xiao G, Noma K-I, Malikzay A, Bjerling P, et al. (2003) Alp13, an MRG family protein, is a component of fission yeast Clr6 histone deacetylase required for genomic integrity. EMBO J 22: 2776–2787. doi:10.1093/emboj/cdg248.
71. Wang H, Vavylonis D (2008) Model of For3p-mediated actin cable assembly in fission yeast. PLoS One 3: e4078. doi:10.1371/journal.pone.0004078.
72. Martin SG, McDonald WH, Yates JR, Chang F (2005) Tea4p links microtubule plus ends with the formin for3p in the establishment of cell polarity. Dev Cell 8: 479–491. doi:10.1016/j.devcel.2005.02.008.
73. Nakano K, Mutoh T, Arai R, Mabuchi I (2003) The small GTPase Rho4 is involved in controlling cell morphology and septation in fission yeast. Genes Cells 8: 357–370.
74. Gauthier NP, Jensen LJ, Wernersson R, Brunak S, Jensen TS (2010) Cyclebase.org: version 2.0, an updated comprehensive, multi-species repository of cell cycle experiments and derived analysis results. Nucleic Acids Res 38: D699–702.
75. Madrid M, Soto T, Khong HK, Franco A, Vicente J, et al. (2006) Stress-induced response, localization, and regulation of the Pmk1 cell integrity pathway in Schizosaccharomyces pombe. J Biol Chem 281: 2033–2043.
76. Cortés JCG, Konomi M, Martins IM, Muñoz J, Moreno MB, et al. (2007) The (1,3)beta-D-glucan synthase subunit Bgs1p is responsible for the fission yeast primary septum formation. Mol Microbiol 65: 201–217.
77. Valbuena N, Moreno S (2012) AMPK phosphorylation by Ssp1 is required for proper sexual differentiation in fission yeast. J Cell Sci 125: 2655–64.
78. Kurischko C, Kim HK, Kuravi VK, Pratzka J, Luca FC (2011) The yeast Cbk1 kinase regulates mRNA localization via the mRNA-binding protein Ssd1. J Cell Biol 192: 583–598. doi:10.1083/jcb.201011061
79. Rustici G, Mata J, Kivinen K, Lió P, Penkett CJ, et al. (2004) Periodic gene expression program of the fission yeast cell cycle. Nat Genet 36: 809–817. doi:10.1038/ng1377
80. Alberghina L, Mavelli G, Drovandi G, Palumbo P, Pessina S, et al. (2012) Cell growth and cell cycle in Saccharomyces cerevisiae: basic regulatory design and protein-protein interaction network. Biotechnol Adv 30: 52–72. doi:10.1016/j.biotechadv.2011.07.010.
81. Kovács IA, Palotai R, Szalay MS, Csermely P (2010) Community Landscapes: An Integrative Approach to Determine Overlapping Network Module Hierarchy, Identify Key Nodes and Predict Network Dynamics. PLoS ONE 5: e12528. doi:10.1371/journal.pone.0012528
82. Orr SJ, Boutz DR, Wang R, Chronis C, Lea NC, et al. (2012) Proteomic and protein interaction network analysis of human T lymphocytes during cell-cycle entry. Mol Sys Biol 8: 573. doi:10.1038/msb.2012.5
83. Fankhauser C, Reymond A, Cerutti L, Utzig S, Hofmann K, et al. (1995) The S. pombe cdc15 gene is a key element in the reorganization of F-actin at mitosis. Cell 82: 435–444.
84. Wiley DJ, Marcus S, D'urso G, Verde F (2003) Control of cell polarity in fission yeast by association of Orb6p kinase with the highly conserved protein methyltransferase Skb1p. J Biol Chem 278: 25256–25263. doi:10.1074/jbc.M209703200
85. Szappanos B, Kovács K, Szamecz B, Honti F, Costanzo M, et al. (2011) An integrated approach to characterize genetic interaction networks in yeast metabolism. Nat Genet 43: 656–662. doi:10.1038/ng.846
86. Nguyen T-P, Liu W, Jordán F (2011) Inferring pleiotropy by network analysis: linked diseases in the human PPI network. BMC Syst Biol 5: 179. doi:10.1186/1752-0509-5-179

87. Martin SG (2009) Microtubule-dependent cell morphogenesis in the fission yeast. Trends Cell Biol 19: 447–454. doi:10.1016/j.tcb.2009.06.003
88. Kurischko C, Kuravi VK, Herbert CJ, Luca FC (2011) Nucleocytoplasmic shuttling of Ssd1 defines the destiny of its bound mRNAs. Mol Microbiol 81: 831–849. doi:10.1111/j.1365-2958.2011.07731.x
89. Koyano T, Kume K, Konishi M, Toda T, Hirata D (2010) Search for kinases related to transition of growth polarity in fission yeast. Biosci Biotechnol Biochem 74: 1129–1133.
90. Tatebe H, Shimada K, Uzawa S, Morigasaki S, Shiozaki K (2005) Wsh3/Tea4 is a novel cell-end factor essential for bipolar distribution of Tea1 and protects cell polarity under environmental stress in S. pombe. Curr Biol 15: 1006–1015. doi:10.1016/j.cub.2005.04.061
91. Williams T, Brenman JE (2008) LKB1 and AMPK in cell polarity and division. Trends Cell Biol 18: 193–198. doi:10.1016/j.tcb.2008.01.008
92. Waskiewicz AJ, Cooper JA (1995) Mitogen and stress response pathways: MAP kinase cascades and phosphatase regulation in mammals and yeast. Cur Opin Cell Biol 7: 798–805. doi:10.1016/0955-0674(95)80063-8
93. Aves SJ, Durkacz BW, Carr A, Nurse P (1985) Cloning, sequencing and transcriptional control of the Schizosaccharomyces pombe cdc10 "start" gene. EMBO J 4: 457–463.
94. Agarwal S, Deane CM, Porter M a, Jones NS (2010) Revisiting date and party hubs: novel approaches to role assignment in protein interaction networks. PLoS Comput Biol 6: e1000817. doi:10.1371/journal.pcbi.1000817
95. Hakes L, Pinney JW, Robertson DL, Lovell SC (2008) Protein-protein interaction networks and biology–what's the connection? Nat Biotechnol 26: 69–72. doi:10.1038/nbt0108-69
96. Rhee SY, Wood V, Dolinski K, Draghici S (2008) Use and misuse of the gene ontology annotations. Nat Rev Genet 9: 509–515. doi:10.1038/nrg2363
97. Newman MEJ (2003) The Structure and Function of Complex Networks. SIAM Review 45: 58. doi:10.1137/S003614450342480
98. Strogatz SH (2001) Exploring complex networks. Nature 410: 268–276. doi:10.1038/35065725
99. Fortunato S (2010) Community detection in graphs. Physics Rep 486: 75–174. doi:10.1016/j.physrep.2009.11.002
100. Hagberg A, Daniel S, Swart P (2008) Exploring Network Structure, Dynamics, and Function using NetworkX. In: Varoquaux G, Vaught T, Millman J, editors. Proceedings of the 7th Python in Science conference; 19–24 August 2008; Pasadena, California, United States. SciPy 2008. pp. 11–15.
101. Bähler J, Wu JQ, Longtine MS, Shah NG, McKenzie A, et al. (1998) Heterologous modules for efficient and versatile PCR-based gene targeting in Schizosaccharomyces pombe. Yeast 14: 943–951. doi:10.1002/(SICI)1097-0061(199807)14:10<943::AID-YEA292>3.0.CO;2-Y.
102. Sato M, Dhut S, Toda T (2005) New drug-resistant cassettes for gene disruption and epitope tagging in Schizosaccharomyces pombe. Yeast 22: 583–591. doi:10.1002/yea.1233.
103. Moreno S, Klar A, Nurse P (1991) Molecular genetic analysis of fission yeast Schizosaccharomyces pombe. Methods Enzymol 194: 795–823.
104. De Chaumont F, Dallongeville S, Olivo-Marin J-C (2011) ICY: A new open-source community image processing software. IEEE International Symposium on Biomedical Imaging ISBI. IEEE. pp. 234–237. doi:10.1109/ISBI.2011.5872395
105. Yook S-H, Oltvai ZN, Barabási A-L (2004) Functional and topological characterization of protein interaction networks. Proteomics 4: 928–942. doi:10.1002/pmic.200300636
106. Joy MP, Brock A, Ingber DE, Huang S (2005) High-betweenness proteins in the yeast protein interaction network. J Biomed Biotechnol 2005: 96–103. doi:10.1155/JBB.2005.96
107. Zotenko E, Mestre J, O'Leary DP, Przytycka TM (2008) Why do hubs in the yeast protein interaction network tend to be essential: reexamining the connection between the network topology and essentiality. PLoS Comput Biol 4: e1000140. doi:10.1371/journal.pcbi.1000140
108. Gkantsidis C, Mihail M, Zegura E (2003) The Markov Chain Simulation Method for Generating Connected Power Law Random Graphs. In: Proceedings of the Fifth Workshop on Algorithm Engineering and Experiments; 11 January 2003; Baltimore, Maryland; United States. ALENEX 03. pp. 16–25.
109. Sokal RR, Rohlf FJ (1994) Biometry: The Principles and Practices of Statistics in Biological Research. W. H. Freeman.

dc_836_14

7.9 A sejtosztódás szabályzásának aszimmetriája

Bajpai A., Feoktistova A., Chen JS., McCollum D., Sato M., Carazo-Salas RE., Gould KL., **Csikász-Nagy A.** (2013) Dynamics of SIN Asymmetry Establishment. *PLOS Computational Biology* **9(7)**:e1003147 **Impakt faktor: 4.867**

OPEN ACCESS Freely available online

PLOS | COMPUTATIONAL BIOLOGY

Dynamics of SIN Asymmetry Establishment

Archana Bajpai[1], Anna Feoktistova[2], Jun-Song Chen[2], Dannel McCollum[3], Masamitsu Sato[4,5], Rafael E. Carazo-Salas[6], Kathleen L. Gould[2], Attila Csikász-Nagy[1,7,8]*

1 The Microsoft Research-University of Trento Centre for Computational Systems Biology, Piazza Manifattura 1, Rovereto, Italy, **2** Howard Hughes Medical Institute and Department of Cell and Developmental Biology, Vanderbilt University, Nashville, Tennessee, United States of America, **3** Department of Microbiology and Physiological Systems and Program in Cell Dynamics, University of Massachusetts Medical School, Worcester, Massachusetts, United States of America, **4** Department of Biophysics and Biochemistry, University of Tokyo, Tokyo, Japan, **5** Department of Life Science and Medical Bioscience, Waseda University, Tokyo, Japan, **6** The Gurdon Institute, University of Cambridge, Cambridge, United Kingdom, **7** Department of Computational Biology, Research and Innovation Center, Fondazione Edmund Mach, San Michele all'Adige, Italy, **8** Randall Division of Cell and Molecular Biophysics and Institute for Mathematical and Molecular Biomedicine, King's College London, London, United Kingdom

Abstract

Timing of cell division is coordinated by the Septation Initiation Network (SIN) in fission yeast. SIN activation is initiated at the two spindle pole bodies (SPB) of the cell in metaphase, but only one of these SPBs contains an active SIN in anaphase, while SIN is inactivated in the other by the Cdc16-Byr4 GAP complex. Most of the factors that are needed for such asymmetry establishment have been already characterized, but we lack the molecular details that drive such quick asymmetric distribution of molecules at the two SPBs. Here we investigate the problem by computational modeling and, after establishing a minimal system with two antagonists that can drive reliable asymmetry establishment, we incorporate the current knowledge on the basic SIN regulators into an extended model with molecular details of the key regulators. The model can capture several peculiar earlier experimental findings and also predicts the behavior of double and triple SIN mutants. We experimentally tested one prediction, that phosphorylation of the scaffold protein Cdc11 by a SIN kinase and the core cell cycle regulatory Cyclin dependent kinase (Cdk) can compensate for mutations in the SIN inhibitor Cdc16 with different efficiencies. One aspect of the prediction failed, highlighting a potential hole in our current knowledge. Further experimental tests revealed that SIN induced Cdc11 phosphorylation might have two separate effects. We conclude that SIN asymmetry is established by the antagonistic interactions between SIN and its inhibitor Cdc16-Byr4, partially through the regulation of Cdc11 phosphorylation states.

Citation: Bajpai A, Feoktistova A, Chen J-S, McCollum D, Sato M, et al. (2013) Dynamics of SIN Asymmetry Establishment. PLoS Comput Biol 9(7): e1003147. doi:10.1371/journal.pcbi.1003147

Editor: Christopher V. Rao, University of Illinois at Urbana-Champaign, United States of America

Received January 31, 2013; **Accepted** June 5, 2013; **Published** July 11, 2013

Funding: The authors gratefully acknowledge support from a Human Frontier Science Program (HFSP.org) Young Investigator Grant (HFSP RGY0066/2009-C; ACN, MS, RECS), an European Research Council (ERC) Starting Researcher Investigator Grant (RECS; SYSGRO). The funders had no role in study design, data collection and analysis, decision to publish, or preparation of the manuscript.

Competing Interests: The authors have declared that no competing interests exist.

* E-mail: attila.csikasz-nagy@fmach.it

Introduction

Cell division is a fundamental and conserved process in all eukaryotes. The fission yeast *Schizosaccharomyces pombe* has already proved to be a very simple yet interesting model system to study and analyze eukaryotic cell division [1–3]. The onset of cytokinesis must be tightly coupled to the completion of mitosis for proper segregation of chromosomes into two daughter cells. In fission yeast, the initiation of cell division is controlled by a conserved signaling pathway known as the Septation Initiation Network or SIN [4–9]. Regulation of the SIN happens at the spindle pole bodies (SPBs) of fission yeast cells, where the scaffold proteins Cdc11 and Sid4 localize the rest of the molecules in the network [10,11]. At the top of the pathway sits the GTPase Spg1, which controls a protein kinase pathway that triggers actomyosin ring contraction and positively regulates septum formation [12]. The Cdc16-Byr4 GAP complex negatively regulates SIN by inactivating Spg1 [13]. During interphase Cdc16-Byr4 keeps Spg1 inactive, but in metaphase the GAP complex is removed from SPBs, allowing the accumulation of the Cdc7 kinase to both SPBs [14]. As cells enter into anaphase Spg1-GTP gets hydrolyzed by the appearing Cdc16-Byr4 complex and Cdc7 disappears from the old SPB (that was existing already in the mother cell [15]). At the same time Cdc7 level rises at the new SPB with Spg1 remaining in GTP bound form and without the presence of Cdc16-Byr4 [16–18]. Such asymmetric segregation of the active SIN (Spg1-GTP and Cdc7), and its inhibitory complex (Cdc16-Byr4) is essential for proper activation and eventual inactivation of the SIN [19].

The role of this asymmetry was investigated recently and it was found that phosphorylation-dephosphorylation events on the scaffold protein Cdc11 by the downstream SIN kinase Sid2 and the SIN Inhibitory Phosphatase complex (SIP) play important roles in the establishment of SIN asymmetry between SPBs [20,21]. Still the detailed molecular mechanisms that ensure efficient and fast asymmetry establishment and turning off of SIN activity after cell division is not well understood [19]. Here we develop mathematical models of increasing complexity to understand what basic features such an asymmetry generating system might contain and what known interactions of SIN and its regulators might be important for such features.

Mathematical modeling was already successfully used to capture dynamical features of the timing of SIN activation [4] and the orthologous pathway in budding yeast was also investigated this way [22]. Future experimental and modeling work will be needed

Author Summary

Rod shaped fission yeast cells, as the name suggests, divide by medial fission. The proper timing of this cytokinesis and septation event is controlled by a signaling pathway called the Septum Initiation Network, or SIN. The SIN is activated only after chromosomes start to separate in anaphase. At this stage, the two daughter spindle pole bodies (SPBs - the yeast analog of centrosomes) have separated and are on their way to the distant tips of the cell. SIN components are localized to SPBs, but the SIN is active only at one SPB, while the Cdc16-Byr4 complex keeps the SIN inactive at the other SPB. This asymmetric activation of the SIN is important for proper cell division as perturbation of this can lead to appearance of multiple septa or total lack of septation. The molecular mechanisms that are important for asymmetry establishment are emerging, but we lack a complete picture. Here we develop computational models to capture the dynamical features of asymmetry establishment and to determine the key components and interactions that are needed for proper asymmetric SIN activation. Our predictions and their experimental tests reveal some basic features of the system and highlight missing points in our knowledge.

to merge all knowledge on the spatio-temporal regulation of the SIN into a detailed model that could capture all molecular regulatory interactions in a quantitative way. Here we make the first steps on this line by focusing on the dynamics and regulation of SIN asymmetry establishment in a qualitative fashion.

Results

A minimal model of asymmetry establishment between two SPBs

The minimal mechanism whereby asymmetry could be established between the two SPBs needs to contain some type of positive feedback loop, which involves a non-linear step [23,24]. These are the minimal requirements to reach bistability, where one SPB ends up in a steady state with active SIN, while the other settles in an inactive SIN steady state. The two SPBs communicate through releasing and anchoring molecules from the cytoplasmic pool, thus these binding-unbinding steps could be the ideal ones to be controlled by the interacting molecules. Pure autocatalytic positive feedbacks could enforce collection of most of these autocatalytic molecules at one SPB, but that would not ensure that the other molecule type ends up at the other SPB (not shown). Thus the simplest way of implementing a positive feedback loop that can bring the two molecule types to the opposite SPBs should be based on a double-negative type positive feedback loop [25]. In such a minimal model molecule X removes molecule Y from the SPBs, while molecule Y induces the unbinding of molecule X (Fig. 1A). In this way both components remove their own inhibitor and with this they positively influence their own binding to the SPB. If X has a little bias at one of the SPBs it will remove all of Y from this place and help its own recruitment to this SPB. At the same time Y can pile up at the other SPB, since its inhibitor X was moved to the other SPB. Indeed Y speeds up the removal of X from this place and by this, speeds up the establishment of asymmetry. Computational simulation of such a minimal model shows that with a little noise in the initial amounts of X and Y at SPBs or a minimal (0.1%) bias in the binding rate to the old SPB is enough to induce asymmetry from a symmetric initial condition (Fig. 1B). The molecular interactions of Fig. 1A were translated into the computational model with a non-linear enzymatic reaction step for the action of X on Y unbinding (see Materials and Methods for details). Thus a model with antagonistic interactions of two molecule types, with (in biology often observed) non-linear kinetics can serve as a minimal model of asymmetry establishment between two SPBs.

Minimal molecular network to drive asymmetry establishment

Next we investigated if we have any evidence for the existence of such an antagonistic, double-negative feedback loop among regulators of cytokinesis timing in fission yeast cells. The SIN can be considered as a linear pathway from Spg1 through Cdc7 and Sid1 activation, leading eventually to the recruitment and activation of Sid2 [6,7]. The Cdc16-Byr4 complex inhibits Spg1 and as a result Cdc7 binding to the SPB, thus it is a negative regulator of SIN. It was also shown that Byr4 can bind to an SPB only if Cdc11 is fully dephosphorylated [26] and Sid2 is responsible for part of the phosphorylation on Cdc11 [20]. Cdc11 is known to be (at least partially) dephosphorylated by the SIN Inhibitory Phosphatase Complex SIP [21], which we also consider as a regulator of the proposed minimal system. In summary Cdc16-Byr4 inhibits SIN and SIN inhibits Cdc16-Byr4 localization to SPB, giving an antagonistic double-negative feedback loop (Fig. 1C). We can update the wiring diagram of Fig. 1A with the basics of the molecular details of this antagonistic interaction by joining the SIN members in a single variable and representing the Cdc16-Byr4 complex by its limiting component Byr4. The wiring has to be further extended as SIN is not directly inhibiting Byr4, but through phosphorylating Cdc11, which form cannot support Byr4 recruitment to SPB. Thus, instead of direct activation of Byr4 removal (as it is on Fig. 1A), SIN inhibits the facilitator of Byr4 binding (Fig. 1D). This adds an extra step in the system, but does not change the signs of the interactions proposed above.

This system can be also turned into a computational model and in this case we can move the non-linearity to the Cdc11 multistep phosphorylation-dephosphorylation reactions (captured by an appropriate non-linear function [24,27,28]). Simulation of this model shows that asymmetry of SIN can be established from an initial metaphase state (high SIN, low Byr4 at both SPBs). After the transition, the active SIN is localized together with phosphorylated Cdc11 to the new SPB, while Byr4 is at the old SPB with dephosphorylated Cdc11 (Fig. 2A). Cdc11 is not moving between the two SPBs, it just changes its phosphorylation state depending on the presence of regulators at a given SPB. To reach this asymmetry all we had to assume is that Byr4 has a 0.1% higher affinity to bind to the old SPB than to the new SPB. This (or a much higher) initial bias could come from inherited phosphorylated proteins that are specifically present at the old SPB [15].

It is known that proper cytokinesis greatly depends on the total amount of SIN components and its regulators [29,30]. Overexpression of Spg1, the uppermost member of SIN leads to hyperactivation of SIN and to a multiseptated phenotype when cells periodically lay down septa without cleaving them [12]. A similar phenotype is observed when Cdc16, Byr4 or to some extent SIP function is lost [21,31,32]. On the other hand mutations in SIN components and Byr4 overexpression lead to SIN inactivation and to a multinucleate phenotype when septum formation and cell division is totally abolished [12,14,32]. We observe similar behavior in the simulations of the model if the total cellular levels of SIN and Byr4 are perturbed (Fig. 2B–E). SIN level can be changed only in a very narrow window, even very small changes lead to delays in asymmetry establishment and doubling or halving

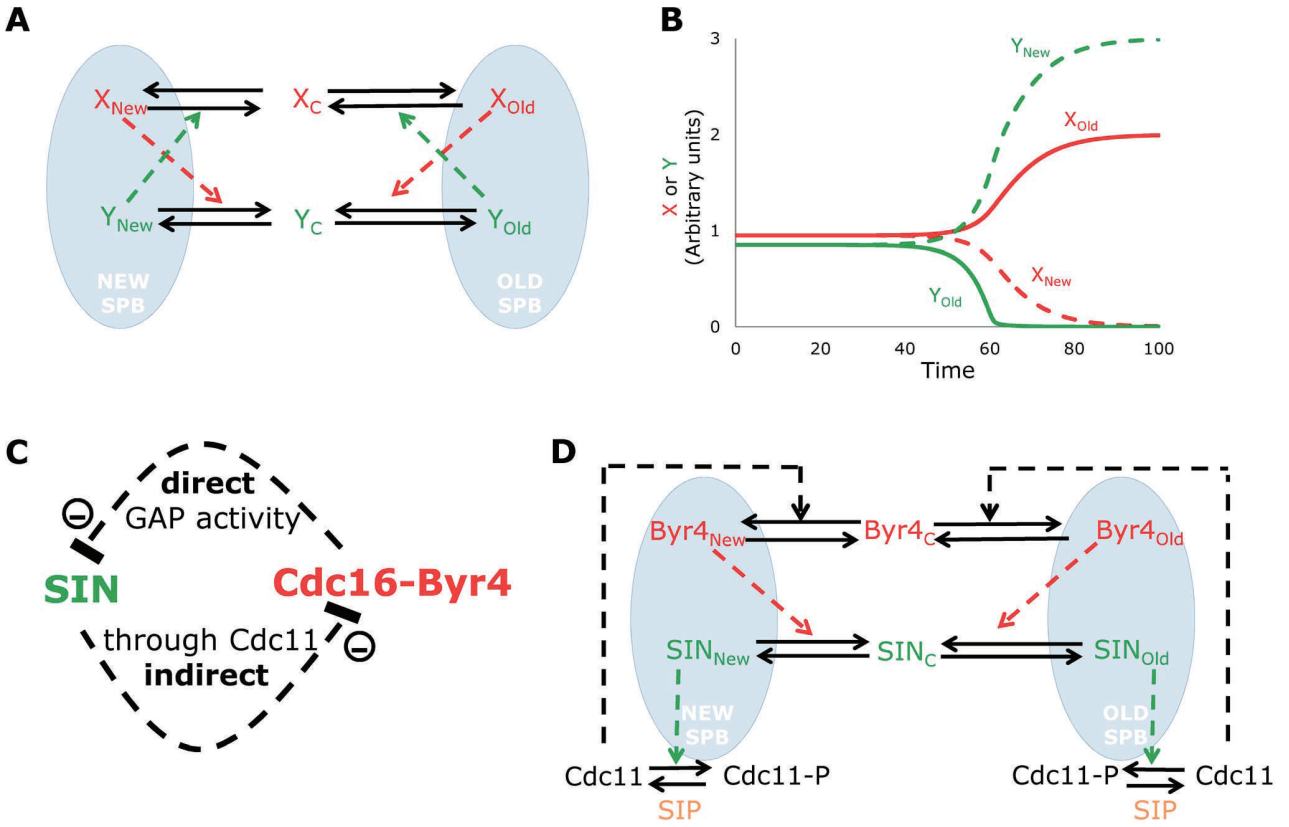

Figure 1. A minimal model for SIN asymmetry establishment. (**A**) Direct antagonistic interactions between molecule X and Y at the two SPBs. Both molecules induce the removal of the other from the SPB they are both bound. Solid lines are transitions, dashed arrows show catalytic effects. (**B**) A less than 0.1% difference in the SPB binding rates or in initial conditions (not shown) can induce quick asymmetry establishment. Solid lines for molecules at old SPB, dashed lines for molecules at new SPB, time is in arbitrary units. (**C**) The proposed antagonistic double-negative (= positive) feedback between SIN components and Cdc16-Byr4. (**D**) Merging ideas from panels A and C to create a minimal molecular model of asymmetry establishment.
doi:10.1371/journal.pcbi.1003147.g001

of the original amount already shows the experimentally observed terminal phenotypes (Fig. 2B). Byr4 cannot be increased either, small reductions do not lead to major delays in asymmetry but below a certain threshold the observed phenotype reveals (Fig. 2C). The simulated high sensitivity to Cdc11 levels (Fig. 2D) is contradicting the literature data as overexpression should not lead to a phenotype [10], while mutations in Cdc11 function should lead to multinucleate phenotype [33]. This latter problem comes from the fact that we initiate the model in late mitosis with high SIN levels, which cannot be reached in Cdc11 mutants as SIN binding to SPB requires Cdc11 function. Furthermore Cdc11 is also needed for the activity of downstream SIN components (Sid1, Sid2) [10]. A major extension of the model with the whole mitotic regulation of SIN could resolve this issue, here we keep our focus on asymmetry establishment after anaphase onset.

Overexpression of Csc1, a member of the SIP complex leads to multinucleate cells and some SIP mutant cells (*csc1Δ*) show multiple septa [21]. Although it is not clear if overexpression of one of the components of the SIP complex is enough to induce higher SIP phosphatase activity or if it has a dominant negative effect, the simulated high sensitivity to SIP levels (Fig. 2E) resembles experimental observations [21]. In summary the minimal molecular model of SIN asymmetry regulation properly simulates most experimental observations. The major failure of the model is on the high sensitivity to Cdc11 levels. The experimentally observed low sensitivity to Cdc11 overexpression [34] might be explained by a limiting effect of Sid4, which helps Cdc11 to recruit SIN members to SPB [35], but we can also investigate Cdc11 in more detail if we consider its different phosphorylation sites.

Revealing the importance of the phosphorylation states of Cdc11

Cdc11 is known to be phosphorylated on multiple sites by SIN (specifically shown for Sid2 in [20]) but Cdc11 also contains Cdk phosphorylation sites [20,35]. SIP was discovered as a SIN Inhibitory PP2A Phosphatase Complex as it can remove phosphate groups from Cdc11 [21]. PP2A complexes often counteract Cdk phosphorylations [36], so it could be that SIP is working on the Cdk phosphorylation sites of Cdc11 and either SIP or another phosphatase removes the phosphates from SIN sites. Furthermore, it was observed that removal of SIN phosphorylation sites from Cdc11 (mutating five serine to alanine) leads to advanced asymmetry establishment [20], which could not be captured by the minimal model. To overcome these issues we extended the model with Cdk phosphorylation of Cdc11 (Fig. 3A). Cdc11 can exist in at least four different forms: Cdk phosphorylated (Cdc11-CP), SIN phosphorylated (Cdc11-SP), phosphorylated by both (Cdc11-PP) and non-phosphorylated (Cdc11) and only this latest form can support Byr4 binding to SPBs. As we have

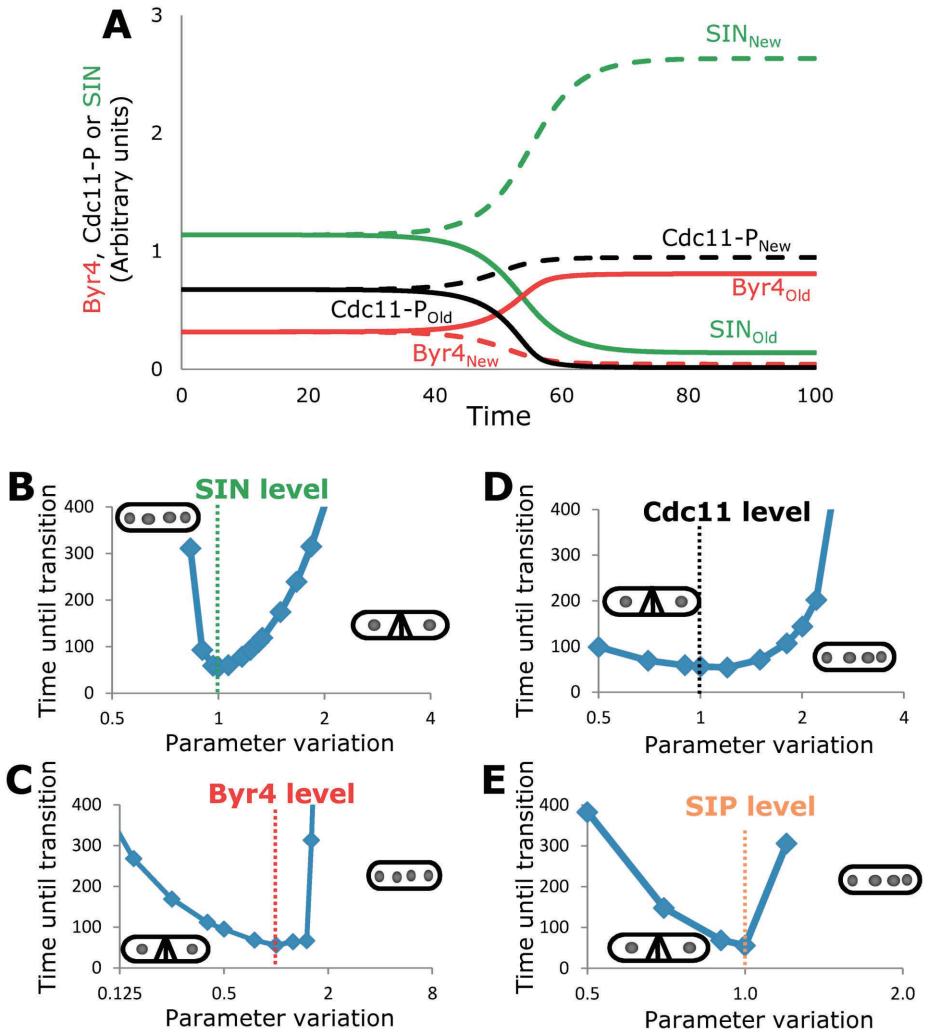

Figure 2. Behavior of the minimal molecular model of SIN asymmetry establishment. (**A**) A small bias in Byr4 binding to SPB is enough to establish asymmetry from an initial condition corresponding to metaphase-anaphase transition. Solid lines for molecules at old SPB, dashed lines for molecules at new SPB, time in arbitrary units. (**B–E**) Timing of transition (reaching the inflection point in the SIN_{New} curve) greatly depends on total level of each of the investigated proteins (plotted on a $\log_2$ scale). In each plot the basal (wild type) parameter is normalized to 1 (dashed lines) and the final phenotype of the effect of increase and decrease are noted with the multinucleate and multiseptate *S. pombe* cartoons. SIN level cannot be varied in either direction (A), Byr4 cannot be increased, while major reduction has also a deleterious effect. (B) Cdc11 and SIP can be changed also in small regimes (C,D). The observed multiseptate phenotype at reduced Cdc11 levels might come from the fact that we start simulations with an initial mitotic high SIN state, which might not be even reached in this mutant, while the multinucleate phenotype of Cdc11 overexpression contradicts literature data [10,34].
doi:10.1371/journal.pcbi.1003147.g002

no information on the target sites of SIP or other phosphatases acting on Cdc11 we investigate the effects of both dephosphorylation steps separately. We assume a hypothetical phosphatase *ppC* to remove phosphates from Cdk site, while another phosphatase *ppS* works on SIN sites (Fig. 3A). Similarly to the simple model above, SIN and Byr4 dynamics at the two SPBs follows the experimentally observed trend (Fig. 3B). The various forms of Cdc11 are converted into each other as cytokinesis proceeds, with ~75% Cdc11 becoming dephosphorylated and 25% remaining Cdk phosphorylated at the old SPB (solid black line of Fig. 3C) and most of Cdc11 at the new SPB is phosphorylated mostly by SIN (dashed green on Fig. 3C).

This model is sensitive to changes in SIN and Byr4 levels (Fig. S1A,B) as the minimal model was (Fig. 2B,C), but now the sensitivity of Cdc11 overexpression and the simulated multinucleate phenotype of the minimal model (Fig. 2D) is lost, since Cdk can phosphorylate even high levels of Cdc11 and by this inhibit Byr4 binding to the Cdc11, which is present in excess (Fig. S1C). With these we fixed the simulations of the major phenotypes. Literature data suggest that the timing of asymmetry establishment is highly sensitive to the Cdc11 phosphorylation state [20]. Fig. 4 shows how perturbations in the SIN and Cdk phosphorylation efficiencies and in the phosphatase efficiencies of ppC and ppS affect the timing of asymmetry establishment in the detailed model. Small decreases in SIN efficiency advance asymmetry, while severely reduced SIN phosphorylation on Cdc11 leads to a multinucleate phenotype. Advances were observed for the Sid2 phosphorylation site removed *cdc11-S5A* mutant [20], which is matched with an

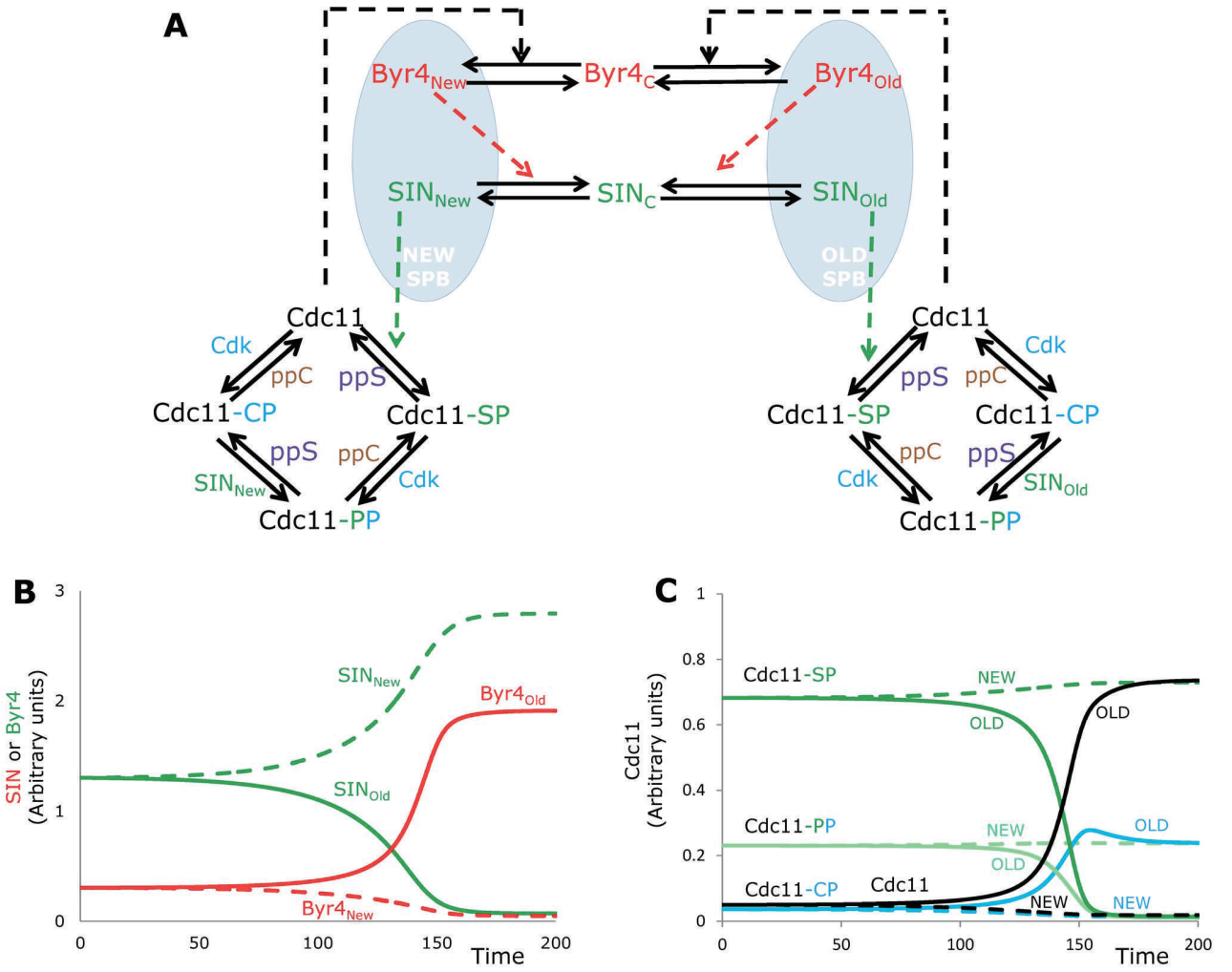

Figure 3. Model expansion on Cdc11 regulation. The minimal model was extended by multiple phosphorylation forms of Cdc11 (**A**). It can be phosphorylated by SIN (green), Cdk (light blue) and both. The Cdk sites are assumed to be dephosphorylated by the unknown phosphatase "ppC", while the SIN sites are dephosphorylated by an unknown phosphatase, "ppS". (**B**) Simulation time course of SIN and Byr4 activities at the two SPBs (solid for Old, dashed for New). (**C**) Changes in the various phosphorylated forms of Cdc11. Notations and color code on forms on panel A.
doi:10.1371/journal.pcbi.1003147.g003

approximate halving of SIN efficiency on Cdc11 (arrow on Fig. 4A). Since the phosphorylation of SIN on Cdc11 in the model captures all negative effects of SIN on Byr4 activation and the experimentally observed effect of SIN sites removal from Cdc11 can be captured by a partial reduction of this effect, suggesting that SIN has to phosphorylate other targets which are regulating Byr4 activity/localization (see details on this in the discussion). On the other hand, total reduction in Cdk phosphorylation efficiency has no effect on asymmetry timing, while an increase in the Cdk site phosphorylation, similar to high SIN efficiency led to serious delays and eventually to a multinucleate phenotype (Fig. 4A). Thus, Cdk mostly serves as an initiator of the Cdc11 phosphorylation state and it is not directly involved in asymmetry timing, but if Cdk (or SIN) phosphorylation on Cdc11 is constantly high then Byr4 cannot bind to SPBs and this leads to multinucleate phenotype.

Serious reduction in either hypothetic phosphatase activity leads to multinucleate phenotype, while milder reduction causes a delay. Interestingly increase in ppC efficiency (overexpression of the hypothetical phosphatase) does not cause any phenotype in the model, while ppS overexpression leads to multinucleate phenotype (Fig. 4B). If we assume that the overexpression of the SIP component, Csc1, induces higher SIP activity (if this is the only limiting factor in the complex) leading to the observed multinucleate phenotype [21], then the model predicts that SIP should have roles in removing phosphates catalyzed by Sid2 to Cdc11 (at least when it is overexpressed). Since other mitotic phosphatases, like the Cdc14 phosphatase, Clp1/Flp1 [37,38] or the PP2A phosphatases Par1 and Pab1 [39,40] have been associated with SIN function and recent results suggests a role for Clp1 in Cdc11 dephosphorylation [41], we cannot conclude on the exact role of SIP only by simulating single perturbations on Cdc11 phosphorylation.

Predictions and experimental tests on double and triple mutants

In our first double perturbation test we investigated the interactions between perturbations in SIN and Cdk efficiency on Cdc11 phosphorylation versus mutations in the Byr4 effector Cdc16 efficiency on SIN inactivation (Fig. 5A). Cdc16 mediates

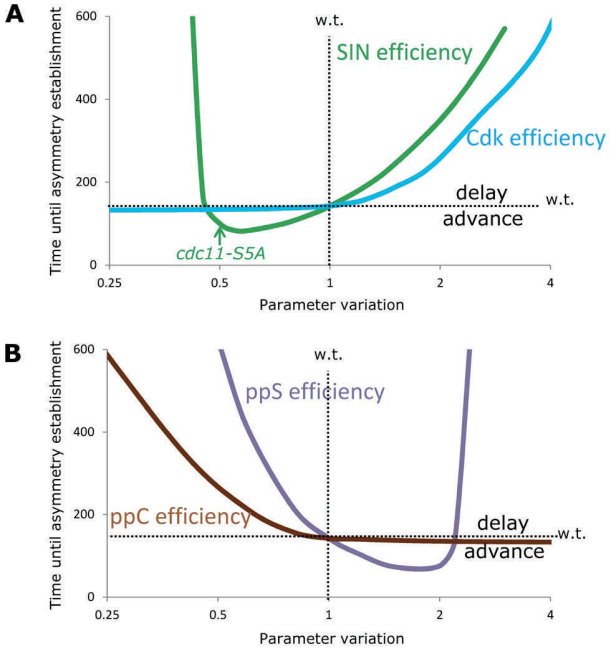

Figure 4. Sensitivity of asymmetry establishment timing on Cdc11 modification efficiencies. Efficiencies of SIN and Cdk phosphorylation (**A**) and ppC and ppS dephosphorylation (**B**) on the time it takes to reach asymmetry in SIN activity (inflection point in $Byr4_{Old}$ curve). Small decrease in SIN efficiency on Cdc11 phosphorylation advances asymmetry (this is what was observed for the *cdc11-S5A* mutant, noted with a green arrow), while major decrease in this efficiency delays the transitions and eventually leads to high Byr4 (~multinucleate) phenotype. Increase in this efficiency leads to SIN hyperactivation (~multisetpate) phenotype. Decrease in Cdk efficiency has no major effect on asymmetry, but increase in this delays the transition and can lead to SIN hyperactivation. Increase in ppC seems to have no effect on asymmetry timing, while increase in ppS can lead to Byr4 hyperactivation. All wild type parameter values are normalized to 1, thus horizontal dotted lines show the wild type timing of asymmetry establishment.
doi:10.1371/journal.pcbi.1003147.g004

the GAP-activity that induces Spg1 inactivation and it is localized by Byr4 [13], thus mutations in Cdc16 can be simulated in our model by changing the efficiency of Byr4 on SIN inactivation (k_{Soff} in Supplementary Text S1). The temperature sensitive *cdc16-116* mutant can proliferate at 25°C while at higher temperatures the activity of this mutant protein is gradually reduced and eventually the cells are unable to inactivate SIN leading to a multiseptated phenotype at 36°C [31]. Simulation of this mutant by setting Byr4 efficiency on SIN to 20% of the wild type value shows a strong delay in asymmetry establishment (Fig. 5A). The model predicts that this delay can be compensated for mildly by removal of Cdk phosphorylation sites from Cdc11 but very efficiently by the *cdc11-S5A* mutants of SIN phosphorylation on Cdc11 (Fig. 5A). To test this prediction first we used a Cdk site mutant version of Cdc11 [35] that substitutes the eight Cdk phosphorylation sites from Cdc11 [20] and tested its effects on cell viability. As reported previously [35], removal of Cdk phosphorylation sites from Cdc11 has no major effect on cell viability, matching the simulation results (Fig. 4A). The *cdc11-S8A* mutant could indeed mildly compensate for the defects of *cdc16-116* (Fig. 5B), while the SIN (Sid2) sites removed *cdc11-S5A* mutation instead of rescuing the phenotype rather exacerbated it (Fig. 5B).

It was shown that SIP phosphatase complex removes phosphate groups from Cdc11 and that mutations in SIP components give an additive effect to *cdc16* mutations [21]. To investigate the discrepancy between model and experiment further, we tested if *cdc11-S5A* and *cdc11-S8A* mutants can compensate this additive effect of SIP and *cdc16* mutations. First we simulated the *cdc16* mutation by reducing the effect of Byr4 on SIN to the half of the original value and the *csc1Δ* SIP mutation by setting both ppC and ppS to 75% of the wild type values. The simulations indeed match the additive effects of these mutations (Fig. 5C). Greater decreases lead to even greater delays in asymmetry establishment and eventually to a multiseptate phenotype (not shown). The simulations of cdc11 phosphosite mutants predict that major SIN sites removal (*cdc11-S5A*) can compensate the additive effect of SIP and Cdc16 quite well, while Cdk site removal has only minor compensatory effects (Fig. 5C). Experimental tests show that the double mutants of *cdc16-116* and *csc1Δ* is mildly compensated by Cdk phosphorylation sites removal from Cdc11, matching the prediction (Fig. 5D). At the same time the double mutant phenotype becomes more severe after Sid2 phosphorylation site removal (Fig. 5D). Phenotypic analysis of these cells show that the number of multiseptated and cut cells increased in the *cdc16-116 csc1Δ cdc11-S5A* triple mutants (Fig. 5E), suggesting that SIN might come too early and stays active longer in some of these cells.

The discrepancies between simulations and experimental results show that blocking Sid2 phosphorylation of Cdc11 has consequences other than allowing enhanced Byr4 binding to SPBs [26], furthermore, perturbation in the SIP phosphatase complex (*csc1Δ*) does not change the severe phenotype of *cdc16-116 cdc11-S5A* mutants. These, and other earlier findings [20,21,41] suggest that Sid2 phosphorylation might prime Cdc11 for dephosphorylation at other sites and Byr4 binding, making SIN an indirect activator of Byr4. Recent results suggest that such dephosphorylation events might be catalyzed by the Cdc14-like Clp1/Flp1 phosphatase, even in the absence of SIP activity [41]. Removal of both SIN and Cdk phosphorylation sites from Cdc11 (*cdc11-S13A*) does not have a major effect on cell viability, furthermore SIP activity still has an effect on the phosphorylation state of Cdc11 in *cdc11-S13A* cells [41], indicating that SIP dephosphorylates Cdc11 at sites modified by other kinases. Thus our findings, together with recent literature data, indicate that our understanding of Cdc11 regulation by phosphorylation-dephosphorylation events is incomplete.

Simulations of peculiar observations on SIN activation/inactivation dynamics

We have shown above that the model can capture the basic behavior of SIN mutants in asymmetry establishment and can accurately predict the behavior of some mutant combinations. There are a few, so far, unresolved experimental findings that ask for computational models to help understand them. Magidson et al. [42] found that if in anaphase, when SIN asymmetry is already established, the new SPB containing active SIN was ablated with a laser, then the SIN starts to get activated at the old SPB. To simulate this experiment we stopped the simulations when asymmetry was reached and uncoupled the new SPB from the rest of the cell. Fig. 6A shows that if some SIN from the ablated new SPB can fall back to the cytoplasm (or constantly produced there – not shown) then it can move to the old SPB and remove Byr4 activity there. This happens because the free cytoplasmic SIN now can start to bind to the only existing old SPB. Although this is slow at the beginning, as SIN starts to phosphorylate Cdc11, Byr4 cannot be as efficiently recruited anymore. As this positive feedback of SIN activation (through inhibiting the binding of its

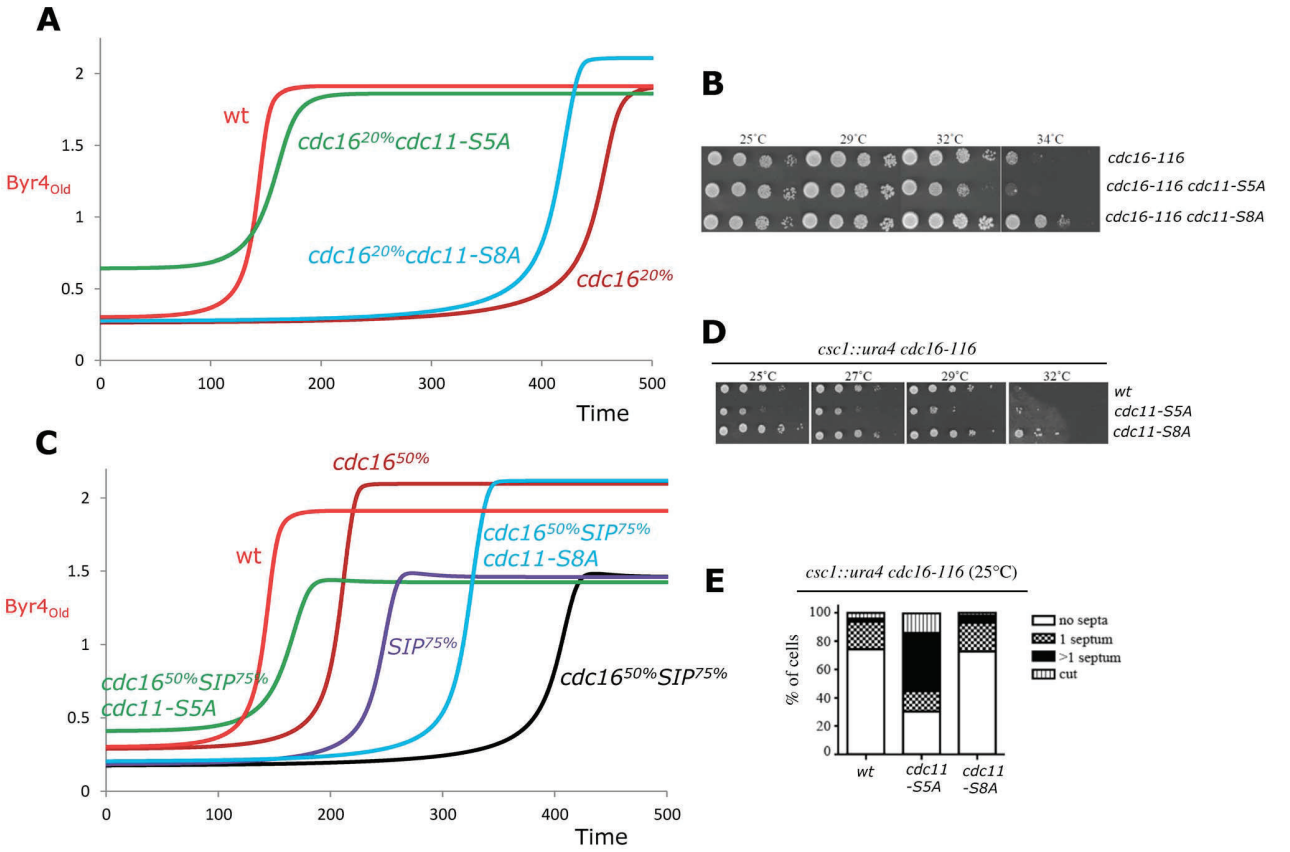

Figure 5. Predictions and experimental tests on collective effects of multiple mutations on SIN asymmetry establishment timing. (**A–C**) Simulations of interactions of *cdc16*^{ts} (**A**) and *cdc16*^{ts} *sip*$^{-}$ (**C**) mutations with mutations in *cdc11* phosphorylation sites. Reduced level of Cdc16 activity was simulated by the indicated reduction in Byr4 efficiency on SIN inactivation. Mutations in SIP was captured by 25% reduction in both *ppC* and *ppS* efficiency. As shown on Fig. 4 we assume that 50% SIN efficiency corresponds to the *cdc11-S5A* mutation. Time courses of Byr4 level changes at the old SPB are plotted as a representative proxy of SIN asymmetry establishment (other variables follow this as on Fig. 3). (**B–D**) Spot assays: The indicated cultures were serially diluted and spotted on YES agar medium, and grown at the specified temperatures. (**B**) At 32°C *cdc11-S8A* can partially compensate effects of the temperature sensitive *cdc16-116* mutation, while *cdc11-S5A* makes it even more severe. (**D**) *cdc11-S5A* decreases while *cdc11-S8A* minimally increases viability of *cdc16*^{ts} *sip*$^{-}$ mutants. (**E**) Phenotypes observed in the colonies of panel D at 25°C. n>300 cells for each strain.

doi:10.1371/journal.pcbi.1003147.g005

inhibitor) speeds up, more and more SIN gets to the only existing SPB and at the same time Byr4 is getting removed.

In another interesting experiment, by cleverly creating dikarions Garcia-Cortes and McCollum [43] investigated cells with four SPBs present at the time of mitosis. They found that when two SPBs with active SIN go to one daughter cell and two with inactive SPBs to the other, then cells separate properly and SIN gets inactivated right after division. In contrast, when both daughters inherit one active and one inactive SPB then the SIN could not turn off properly. We simulated these two scenarios by removing (separated) or maintaining (non-separated) the communication between the inactive, old SPB and the cytoplasm of the new SPB and followed the speed of SIN inactivation at the new SPB (Fig. 6B). To mimic the unknown factors that induce SIN inactivation after cell separation we started to increase the cytoplasmic Byr4 level in the cells. We followed this approach as in our small model Byr4 acts as the only inhibitor of SIN, but any other abrupt change in the SIN/Byr4 ratio as a result of cytokinesis would have a similar effect in the model. Although the exact mode of SIN inactivation after completion of cytokinesis is not clear, the simulation results show that the same inactivation strength lead to a much faster SIN inactivation when the two SPBs were separated (Fig. 6B). This happens, because in the separated case all inhibitors of SIN can start to work on the SPB with the active SIN, while in the non-separated case the newly produced inhibitors are still recruited to the already inactive SPB, thus they cannot reach the active SIN on the other SPB. A mechanical metaphor explains both situations on Fig. 6C. The antagonistic, double-negative feedback loop leads to situations when on one SPB SIN can always win against Byr4. If two or more SPBs are in the same cytoplasm then this antagonism leads to asymmetry establishment and strong maintenance of this state. These results suggest that cells are sensitive to SIN/Byr4 ratio before establishing the asymmetry, but once they established SIN asymmetry the strong antagonism can compensate small changes in the SIN/Byr4 balance. After communication between the daughter nuclei is halted by the septum, the balance is important again and the SIN-Byr4 antagonism can help the fast inactivation of SIN.

Discussion

Asymmetric activation of the SIN on one of the two SPBs is a necessary feature of proper cell division timing in fission yeast cells

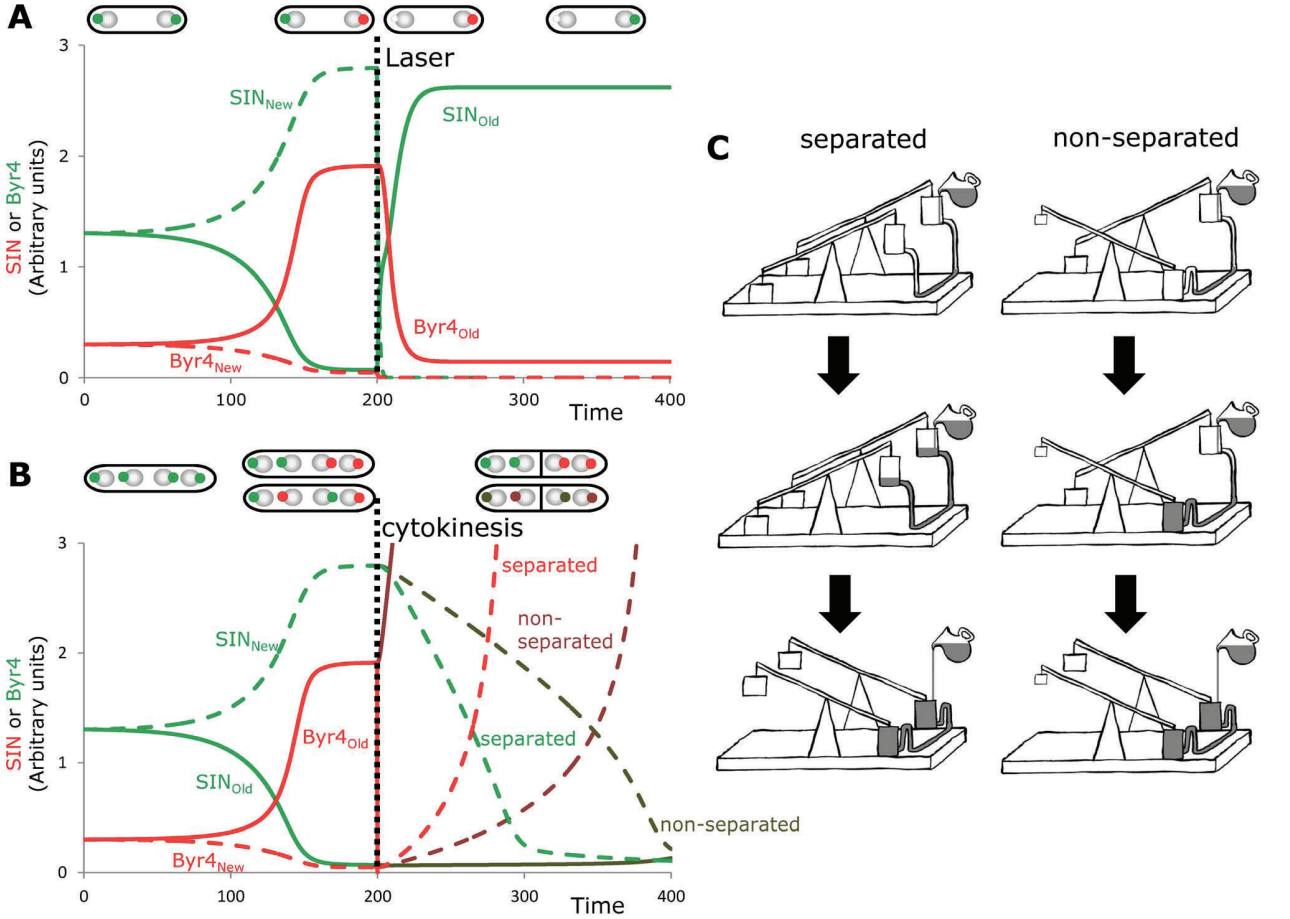

Figure 6. Simulations of the most peculiar observations in SIN asymmetry establishment. (**A**) We simulated the laser ablation of the new SPB after anaphase (top), what leads to SIN activation at the old SPB [42]. At 200 time steps (horizontal dotted line) we stopped transport towards the new SPB and let all its content diffuse into the cytoplasm. (**B**) Simulation of the termination of SIN activity. At 200 time steps we induced the production (or reduced degradation) of new Byr4 molecules (as a proxy for the unknown signal that turns off SIN). At the same time we cut the communication between the two SPBs as it happens at the end of cytokinesis ("separated", lighter color curves) or let the two SPBs communicate through the cytoplasm as it happens in some dikarions [43] (Non-separated, darker color lines and dots on top panel). If the cells are separated the newly formed Byr4 goes to the only existing new SPB, while if the cells did not separate it will be constantly recruited to the old SPB, thus SIN at the new SPB will turn off much later. (**C**) Seesaw metaphors of the two cases of panel B (seesaws are common examples of antagonistic interactions with two opposing steady states). The right arm of the seesaws represent SIN activity at the two SPBs, and they are connected to each other (water can flow between them in the metaphor - molecules can diffuse between SPBs in cells). The situation where the active and inactive SPBs are separated is captured on the left, where both SPBs are active, water is poured in (signals induce SIN inactivation) they both can turn together. On the right (non-separated active and inactive SPB) one SPB has high SIN, the other has low SIN. When water is poured in, first it flows to the lower (already inactive SIN) bucket and the upper seesaw will turn only if the lower bucket and the pipe are full.
doi:10.1371/journal.pcbi.1003147.g006

[18,19]. Similar asymmetry is established between the SPBs of the budding yeast *Saccharomyces cerevisiae* [44,45]. In the case of such asymmetrically dividing organisms, the asymmetry establishment is better characterized [46] and mathematical modeling has already facilitated discoveries of the detailed mechanism [22]. Here we establish a minimal model to understand the major driving forces of symmetry breaking in SIN activity at the two SPBs in fission yeast. This minimal model is based on the antagonistic interaction of two molecules that are inhibiting each other's localization to the SPB (Fig. 1A). This system resembles the basic models of Notch-Delta antagonism that is used to model lateral inhibition [47]. Indeed the underlying dynamics in both cases leads to a pitchfork bifurcation ([23] and Fig. S2). The model behaves as an efficient switch [48], which brings one molecule type to one SPB and its antagonist to the other, with some remaining in the cytoplasm. In the case of SIN asymmetry establishment the clear candidates for such antagonistic interactions are the members of the SIN and its inhibitory complex Byr4-Cdc16. Byr4-Cdc16 inhibits SIN activity [13], while there is also some evidence that SIN indirectly inhibits Byr4 localization [20,26]. Such antagonism is a special case of a positive feedback loop, where the two components cannot coexist, either one of them is winning and inhibiting the other [25]. In the case of SIN asymmetry establishment, the two antagonists are winning at different SPBs. Indeed when the new SPB is starting to get enriched in SIN, it means SIN has to drop a bit on the other SPB, which enables Byr4 to win on the old SPB. In this way SIN activation at one SPB helps Byr4 activation on the other SPB explaining some controversial observations which suggest that SIN components and mitotic phosphatases seem to activate both SIN and Byr4 [19]. Thus any signal that leads to the induction of asymmetry establish-

ment basically activates SIN (at the new SPB) as well as Byr4 (at the old SPB). The major initiating step is the drop in Cdk activity in anaphase in parallel with spindle elongation that moves the SPBs far apart. Our simulations are initiated exactly at this step. Possible spatial extensions of the model might reveal some role for SPB positioning, although the quick turnover of active Sid2 [20] might rule out any major effect of space in SIN asymmetry establishment.

A crucial point here is that such a system with an antagonistic switch works properly only if the total amounts of the two antagonists are present in a given ratio (1 in our case, but this value is determined by the exact rate constants), any perturbation of this balance can lead to a situation where either SIN or Byr4 wins on both SPBs. Indeed fission yeast cells are very sensitive to the overexpression of either Byr4 or the SIN limiting factor Spg1, but the joint overexpression of these two can be greatly tolerated by the cells [30] suggesting that indeed their ratio is important for proper asymmetry establishment. The model suggests that once the asymmetry is established this balance is not that crucial anymore, but later the same antagonism can help the fast inactivation of SIN after septation. At this stage only the new SPB inheriting daughter has active SIN signaling, but this is turned off for an unknown signal that most probably flips the SIN/Byr4 balance.

The extended minimal model (Fig. 3A) is still a simplification of the whole system of SIN regulation as here we concentrated only on the interactions that are important for the asymmetry establishment in SIN activity (see [4] for a model on SIN activation timing). Still this simple model was able to capture qualitatively multiple experimental results on single molecule perturbations (Fig. 2B–E and Fig. S1), explain results of experiments when the number of SPBs were perturbed in the cells (Fig. 6) and predict the behavior of some double and triple mutants (Fig. 5). The prediction on the compensatory effects of Cdk sites removal from Cdc11 in a *cdc16* and *cdc16-116 csc1Δ* mutants were verified experimentally (Fig. 5A,B), the additive effects of SIP and Cdc16 mutants were also properly simulated, but the predictions on the double and triple mutants with *cdc11-S5A* failed (Fig. 5C–E). The *cdc11-S5A* mutation amplified the phenotype of *cdc16* and *cdc16-116 csc1Δ* mutants instead of compensating them. This does not mean that the model is totally wrong; it rather means that there is a hole in our knowledge about the backup mechanisms that regulate SIN activity when some of the major players are perturbed. Cdc11 is likely phosphorylated by other kinases (perhaps Cdc7 [26]) and proteomics screens found Clp1/Flp1 as a phosphatase acting on Cdk sites on Cdc11 [41], adding extra layers to the interaction system. Another possibility is that the Cdc11 phosphomutants may not recapitulate the result of asymmetric loss of phosphorylation in which only one SPB is affected and/or the investigated mutant combinations show a phenotype that is a result of other functions of Cdc16 [49]. Furthermore, it was earlier proposed that Clp1 might form another positive feedback loop with the SIN [19,50], which could also play a role in the robustness of SIN asymmetry establishment. The proposed core mechanism of antagonistic interactions between activators and inhibitors of SIN should hold in all cases, just the main players might change as kinases and phosphatases as well as their target molecules might be perturbed in various mutants. There could be several other layers, where SIN and Byr4 antagonistically interact, as many other SIN regulators are targets of Cdk, SIN and Polo kinase dependent phosphorylation events [19]. A related prediction of the model is that SIN components have to act on other Byr4 regulator targets than Cdc11, as we could match the SIN phosphorylation sites removed *cdc11-S5A* phenotype only with a reduced efficiency of SIN, not with the total abolishment of this effect (Fig. 4A). The simplest possible solution would be if one of the SIN components could directly phosphorylate and by this mechanism inactivate Byr4. Since Byr4 has several candidate phosphorylation sites [29,51] we cannot rule out this possibility.

The modeling results also predicted and the experiments verified that Cdk phosphorylation on Cdc11 is not a major factor in asymmetry establishment (Fig. 5A), it might rather play a role in setting up the initial state in early mitosis, when the top components of the SIN pathway are bound to both SPBs and Byr4 is removed from there. Interestingly, all of our simulation results show that in the initial mitotic state Byr4 is not totally absent from SPBs. This assumption on the initial conditions we needed to take to be able to achieve a fast asymmetry establishment. If Byr4 is completely absent from both SPBs in mitosis then it would be difficult for Byr4 to appear at one SPB in sufficient amounts (as it is sent away by active SIN) to turn on the positive feedback loop and establish asymmetry. Since Byr4 is a low abundance protein, it is hard to visualize [29], but the model suggests that even in mitosis some Byr4 might be localized at both SPBs.

It is still unknown what signal(s) turns off SIN activity in the daughter inheriting the new SPB after the completion of cytokinesis. The model of SIN and Byr4 antagonistic interactions successfully simulated the experimental results, which have shown that SIN activity can take over Byr4 at the old SPB if the new SPB was laser ablated before cell division ([42] and Fig. 6A) and it could also explain why SIN has a harder time to turn off when the two spindle pole bodies remain in the same cell after cell division ([43] and Fig. 6B). As we do not have information on the molecular details of the trigger that induces SIN inactivation in the daughter cell that inherited the SPB with active SIN, we needed to make a simple assumption that Byr4 production speeds up at this point, alternatively Byr4 degradation slows down when the daughters get separated [29]. Inactivation of SIN might happen even with a minor increase in Byr4 level, since once the old SPB is not in the same cytoplasm anymore it cannot serve as a sink for Byr4, thus Byr4 can pile up at the daughter with the active SIN and eventually turn SIN off. The prerequisite for this mechanism to work is a very fast turnover of Byr4, which has been suggested [29]. This and many other questions on the detailed regulation of SIN signaling still need to be addressed and as we have shown here, the system level view and computational modeling of the network can help our understanding and guide experimental discoveries. Here we could reach predictions on a semi-quantitative fashion (e.g.: what happens earlier/later in various mutants), measurements on molecular levels of the regulators and kinetic contacts of the reactions will enable the development of quantitative models that contain all molecular details of SIN activity regulation.

Materials and Methods

Model development

The wiring diagrams of Fig. 1A, 1D, 3A were converted into systems of ordinary differential equations (ODEs). Parameters of the models were identified by fitting their qualitative behavior to experimental observations. Molecular concentrations defined in arbitrary units. Future measurements of molecular levels could be used to convert the inferred parameter values to real biologically meaningful reaction rates. We assume fast diffusion between SPBs until cell separation cuts communication between SPBs. Parameter values, initial conditions and equations can be found in the Supplementary Text S1. Equations were numerically solved and simulated by the freely available software WINPP (http://www.math.pitt.edu/~bard/xpp/xpponw95.html).

Experimental procedures

S. pombe strains were grown in yeast extract (YE) medium. Strain construction was accomplished through standard methods. The relevant genotypes and strain numbers used in this study were *cdc16-116 cdc11-S5A-GFP::kanR* (KGY1411), *cdc16-116 cdc11-GFP::kanR* (KGY3342), *cdc16-116 cdc11-S8A-GFP::kanR* (KGY8684), *cdc16-116 cdc11-GFP::kanR csc1::ura4*$^+$ (KGY12982), *cdc16-116 cdc11-S5A-GFP::kanR csc1::ura4*$^+$ (KGY12982), and *cdc16-116 cdc11-S8A-GFP::kanR csc1::ura4*$^+$ (KGY12984).

Supporting Information

Figure S1 Dependence of timing of asymmetry establishment on total protein levels in the extended minimal model of Figure 3A. Similar figures as figure 2B–D for the more complex model. SIN dependence looks the same as in the minimal model just here the wild type behavior is not at the minimal time to reach asymmetry (**A**). Byr4 is similarly sensitive for reduction and for small increases as before (Fig. 2C), just here at higher values the time to asymmetry is advanced and eventually at a rate ~2.5 times wild type the initial early mitotic state contains higher amount of Byr4 than SIN, thus these cells might not be able to perform the earliest steps of SIN activation (**B**). Cdc11 is now insensitive for overexpression, while its removal causes again a perturbed initial mitotic state, which cannot support high SIN activity in early mitosis (**C**).
(PDF)

Figure S2 Symmetric steady state solutions for SIN levels at the two SPBs in the minimal model of SIN asymmetry establishment show that asymmetry emerges through a pitchfork bifurcation. Stable (solid lines) and unstable (dashed) steady states of SIN activity at the old or new SPB. The two solutions totally overlap as the system is fully symmetrical. The calculations were performed with $kbias = 0$ to keep the system symmetric. Steady state solutions were calculated by Oscill8 (http://sourceforge.net/projects/oscill8/).
(PDF)

Text S1 Description of parameters and variables of each model, together with equations, initial conditions and parameter values.
(PDF)

Acknowledgments

The authors are thankful to M.K. Balasubramanian and F. Vaggi for comments and C. Stocker for the drawing of Fig. 6C.

Author Contributions

Conceived and designed the experiments: KLG ACN. Performed the experiments: AF JSC. Analyzed the data: AB ACN. Contributed reagents/materials/analysis tools: DM MS RECS. Wrote the paper: AB KLG ACN. Developed the model and ran simulations: AB ACN.

References

1. Balasubramanian MK, Bi E, Glotzer M (2004) Comparative analysis of cytokinesis in budding yeast, fission yeast and animal cells. Current Biology 14: R806–R818.
2. Guertin DA, Trautmann S, McCollum D (2002) Cytokinesis in eukaryotes. Microbiology and Molecular Biology Reviews 66: 155–178.
3. Pollard TD (2010) Mechanics of cytokinesis in eukaryotes. Current Opinion in Cell Biology 22: 50–56.
4. Csikasz-Nagy A, Kapuy O, Gyorffy B, Tyson JJ, Novak B (2007) Modeling the septation initiation network (SIN) in fission yeast cells. Curr Genet 51: 245–255.
5. Krapp A, Gulli MP, Simanis V (2004) SIN and the art of splitting the fission yeast cell. Current biology: CB 14: R722.
6. Krapp A, Simanis V (2008) An overview of the fission yeast septation initiation network (SIN). Biochemical Society Transactions 36: 411–415.
7. McCollum D, Gould KL (2001) Timing is everything: regulation of mitotic exit and cytokinesis by the MEN and SIN. Trends Cell Biol 11: 89.
8. Simanis V (2003) Events at the end of mitosis in the budding and fission yeasts. J Cell Sci 116: 4263–4275.
9. Wolfe BA, Gould KL (2005) Split decisions: coordinating cytokinesis in yeast. Trends Cell Biol 15: 10–18.
10. Krapp A, Schmidt S, Cano E, Simanis V (2001) S. pombe cdc11p, together with sid4p, provides an anchor for septation initiation network proteins on the spindle pole body. Current Biology 11: 1559–1568.
11. Tomlin GC, Morrell JL, Gould KL (2002) The spindle pole body protein Cdc11p links Sid4p to the fission yeast septation initiation network. Mol Biol Cell 13: 1203–1214.
12. Schmidt S, Sohrmann M, Hofmann K, Woollard A, Simanis V (1997) The Spg1p GTPase is an essential, dosage-dependent inducer of septum formation in Schizosaccharomyces pombe. Genes Dev 11: 1519–1534.
13. Furge KA, Wong K, Armstrong J, Balasubramanian M, Albright CF (1998) Byr4 and Cdc16 form a two-component GTPase-activating protein for the Spg1 GTPase that controls septation in fission yeast. Current Biology 8: 947–954.
14. Fankhauser C, Simanis V (1994) The cdc7 protein kinase is a dosage dependent regulator of septum formation in fission yeast. EMBO J 13: 3011.
15. Grallert A, Krapp A, Bagley S, Simanis V, Hagan IM (2004) Recruitment of NIMA kinase shows that maturation of the S. pombe spindle-pole body occurs over consecutive cell cycles and reveals a role for NIMA in modulating SIN activity. Genes Dev 18: 1007–1021.
16. Cerutti L, Simanis V (1999) Asymmetry of the spindle pole bodies and spg1p GAP segregation during mitosis in fission yeast. J Cell Sci 112 (Pt 14): 2313–2321.
17. Li C, Furge KA, Cheng Q, Albright CF (2000) Byr4 localizes to spindle-pole bodies in a cell cycle-regulated manner to control Cdc7 localization and septation in fission yeast. Journal of Biological Chemistry 275: 14381–14387.
18. Sohrmann M, Schmidt S, Hagan I, Simanis V (1998) Asymmetric segregation on spindle poles of the Schizosaccharomyces pombe septum-inducing protein kinase Cdc7p. Genes Dev 12: 84–94.
19. Johnson AE, McCollum D, Gould KL (2012) Polar opposites: Fine-tuning cytokinesis through SIN asymmetry. Cytoskeleton (Hoboken) 69: 686–99.
20. Feoktistova A, Morrell-Falvey J, Chen JS, Singh NS, Balasubramanian MK, et al. (2012) The fission yeast septation initiation network (SIN) kinase, Sid2, is required for SIN asymmetry and regulates the SIN scaffold, Cdc11. Mol Biol Cell 23: 1636–1645.
21. Singh NS, Shao N, McLean JR, Sevugan M, Ren L, et al. (2011) SIN-inhibitory phosphatase complex promotes Cdc11p dephosphorylation and propagates SIN asymmetry in fission yeast. Curr Biol 21: 1968–1978.
22. Caydasi AK, Lohel M, Grunert G, Dittrich P, Pereira G, et al. (2012) A dynamical model of the spindle position checkpoint. Mol Syst Biol 8: 582.
23. Ferrell JE, Jr. (2012) Bistability, bifurcations, and Waddington's epigenetic landscape. Curr Biol 22: R458–466.
24. Novak B, Tyson JJ (2008) Design principles of biochemical oscillators. Nat Rev Mol Cell Biol 9: 981–91.
25. Ferrell JE, Jr. (2002) Self-perpetuating states in signal transduction: positive feedback, double-negative feedback and bistability. Curr Opin Cell Biol 14: 140–148.
26. Krapp A, Cano E, Simanis V (2003) Mitotic hyperphosphorylation of the fission yeast SIN scaffold protein cdc11p is regulated by the protein kinase cdc7p. Curr Biol 13: 168–172.
27. Goldbeter A, Koshland DE (1981) An amplified sensitivity arising from covalent modification in biological systems. Proceedings of the National Academy of Sciences 78: 6840.
28. Domingo-Sananes MR, Novak B (2010) Different effects of redundant feedback loops on a bistable switch. Chaos 20: 045120.
29. Krapp A, Collin P, Cano del Rosario E, Simanis V (2008) Homoeostasis between the GTPase Spg1p and its GAP in the regulation of cytokinesis in S. pombe. J Cell Sci 121: 601–608.
30. Moriya H, Chino A, Kapuy O, Csikasz-Nagy A, Novak B (2011) Overexpression limits of fission yeast cell-cycle regulators in vivo and in silico. Mol Syst Biol 7: 556.
31. Minet M, Nurse P, Thuriaux P, Mitchison JM (1979) Uncontrolled septation in a cell division cycle mutant of the fission yeast Schizosaccharomyces pombe. J Bacteriol 137: 440–446.
32. Song K, Mach KE, Chen CY, Reynolds T, Albright CF (1996) A novel suppressor of ras1 in fission yeast, byr4, is a dosage-dependent inhibitor of cytokinesis. J Cell Biol 133: 1307–1319.
33. Nurse P, Thuriaux P, Nasmyth K (1976) Genetic control of the cell division cycle in the fission yeast Schizosaccharomyces pombe. Molecular and General Genetics MGG 146: 167–178.
34. Krapp A, Cano E, Simanis V (2004) Analysis of the S. pombe signalling scaffold protein Cdc11p reveals an essential role for the N-terminal domain in SIN signalling. FEBS Lett 565: 176–180.
35. Morrell JL, Tomlin GC, Rajagopalan S, Venkatram S, Feoktistova AS, et al. (2004) Sid4p-Cdc11p assembles the septation initiation network and its regulators at the S. pombe SPB. Curr Biol 14: 579–584.

36. Queralt E, Uhlmann F (2008) Cdk-counteracting phosphatases unlock mitotic exit. Current Opinion in Cell Biology 20: 661–668.
37. Cueille N, Salimova E, Esteban V, Blanco M, Moreno S, et al. (2001) Flp1, a fission yeast orthologue of the S. cerevisiae CDC14 gene, is not required for cyclin degradation or rum1p stabilisation at the end of mitosis. Journal of cell science 114: 2649.
38. Trautmann S, Wolfe BA, Jorgensen P, Tyers M, Gould KL, et al. (2001) Fission yeast Clp1p phosphatase regulates G2/M transition and coordination of cytokinesis with cell cycle progression. Current Biology 11: 931–940.
39. Jiang W, Hallberg RL (2001) Correct regulation of the septation initiation network in Schizosaccharomyces pombe requires the activities of par1 and par2. Genetics 158: 1413–1429.
40. Lahoz A, Alcaide-Gavilán M, Daga RR, Jimenez J (2010) Antagonistic roles of PP2A-Pab1 and Etd1 in the control of cytokinesis in fission yeast. Genetics 186: 1261–1270.
41. Chen J-S, Broadus MR, McLean JR, Feoktistova A, Ren L, et al. (2013) Comprehensive proteomics analysis reveals new substrates and regulators of the fission yeast Clp1/Cdc14 phosphatase. Molecular & Cellular Proteomics 12: 1074–86.
42. Magidson V, Chang F, Khodjakov A (2006) Regulation of cytokinesis by spindle-pole bodies. Nat Cell Biol 8: 891–893.
43. Garcia-Cortes JC, McCollum D (2009) Proper timing of cytokinesis is regulated by Schizosaccharomyces pombe Etd1. J Cell Biol 186: 739–753.
44. Barral Y, Liakopoulos D (2009) Role of Spindle Asymmetry in Cellular Dynamics. Int Rev Cell Mol Biol 278: 149–213
45. Pereira G, Tanaka TU, Nasmyth K, Schiebel E (2001) Modes of spindle pole body inheritance and segregation of the Bfa1p-Bub2p checkpoint protein complex. EMBO J 20: 6359–6370.
46. Monje-Casas F, Amon A (2009) Cell Polarity Determinants Establish Asymmetry in MEN Signaling. Dev Cell 16: 132–145.
47. Collier JR, Monk NAM, Maini PK, Lewis JH (1996) Pattern formation by lateral inhibition with feedback: a mathematical model of delta-notch intercellular signalling. Journal of Theoretical Biology 183: 429–446.
48. Cardelli L, Csikasz-Nagy A (2012) The cell cycle switch computes approximate majority. Sci Rep 2: 656.
49. Fankhauser C, Marks J, Reymond A, Simanis V (1993) The S. pombe cdc16 gene is required both for maintenance of p34cdc2 kinase activity and regulation of septum formation: a link between mitosis and cytokinesis? EMBO J 12: 2697.
50. Chen CT, Feoktistova A, Chen JS, Shim YS, Clifford DM, et al. (2008) The SIN Kinase Sid2 Regulates Cytoplasmic Retention of the *S. pombe* Cdc14-like Phosphatase Clp1. Current Biology 18: 1594–1599.
51. Johnson AE, Gould KL (2011) Dma1 ubiquitinates the SIN scaffold, Sid4, to impede the mitotic localization of Plo1 kinase. EMBO J 30: 341–354.

dc_836_14

7.10 A *Neurospora crassa* mitózisok napi ritmusos szinkronizációja

Hong CI., Zámborszky J., Baek M., Labiscsak L., Ju K., Lee H., Larrondo LF., Goity A., Chong HS., Belden WJ., **Csikász-Nagy A.** (2014) Circadian Rhythms Synchronize Mitosis in *Neurospora crassa*. *Proc Natl Acad Sci USA* **111(4):**1397-402

Impakt faktor: 9.737

Circadian rhythms synchronize mitosis in *Neurospora crassa*

Christian I. Hong[a,1], Judit Zámborszky[a], Mokryun Baek[a], Laszlo Labiscsak[a], Kyungsu Ju[a], Hyeyeong Lee[a], Luis F. Larrondo[b], Alejandra Goity[b], Hin Siong Chong[c], William J. Belden[c], and Attila Csikász-Nagy[d,e]

[a]Department of Molecular and Cellular Physiology, University of Cincinnati, Cincinnati, OH 45267; [b]Departamento de Genética Molecular y Microbiología, Facultad de Ciencias Biológicas, Pontificia Universidad Católica de Chile, Casilla 114-D, Santiago, Chile; [c]Department of Biochemistry and Microbiology, Rutgers, The State University of New Jersey, New Brunswick, NJ 08901; [d]Randall Division of Cell and Molecular Biophysics and Institute for Mathematical and Molecular Biomedicine, King's College London, London SE1 UL, United Kingdom; and [e]Department of Computational Biology, Research and Innovation Centre, Fondazione Edmund Mach, 38010 San Michele all'Adige, Italy

Edited* by Jay C. Dunlap, Geisel School of Medicine at Dartmouth, Hanover, NH, and approved December 11, 2013 (received for review October 15, 2013)

The cell cycle and the circadian clock communicate with each other, resulting in circadian-gated cell division cycles. Alterations in this network may lead to diseases such as cancer. Therefore, it is critical to identify molecular components that connect these two oscillators. However, molecular mechanisms between the clock and the cell cycle remain largely unknown. A model filamentous fungus, *Neurospora crassa*, is a multinucleate system used to elucidate molecular mechanisms of circadian rhythms, but not used to investigate the molecular coupling between these two oscillators. In this report, we show that a conserved coupling between the circadian clock and the cell cycle exists via serine/threonine protein kinase-29 (STK-29), the Neurospora homolog of mammalian WEE1 kinase. Based on this finding, we established a mathematical model that predicts circadian oscillations of cell cycle components and circadian clock-dependent synchronized nuclear divisions. We experimentally demonstrate that G1 and G2 cyclins, CLN-1 and CLB-1, respectively, oscillate in a circadian manner with bioluminescence reporters. The oscillations of *clb-1* and *stk-29* gene expression are abolished in a circadian arrhythmic *frq*^{ko} mutant. Additionally, we show the light-induced phase shifts of a core circadian component, *frq*, as well as the gene expression of the cell cycle components *clb-1* and *stk-29*, which may alter the timing of divisions. We then used a histone hH1-GFP reporter to observe nuclear divisions over time, and show that a large number of nuclear divisions occur in the evening. Our findings demonstrate the circadian clock-dependent molecular dynamics of cell cycle components that result in synchronized nuclear divisions in Neurospora.

Molecular mechanisms of circadian rhythms provide temporal information to other cellular processes, such as metabolism, to optimize their outcomes (1–3). For instance, circadian oscillations of rate-limiting genes in glucose metabolism suggest time-of-day specific regulatory mechanisms that maintain glucose homeostasis in mammals (3). Circadian clock-gated cell division cycles have been observed in various organisms, including mammals, indicating that cell divisions preferentially occur at specific times of the day (4–7). In the mouse liver, expression of the cell cycle kinase-encoding gene, *wee1*, is directly activated by a heterodimeric circadian transcription factor, CLOCK-BMAL1, providing a molecular link between the cell cycle and circadian rhythms (5). This suggests that circadian clock-regulated WEE1 promotes periodic inhibition of mitotic cycles between G2 and M phase by phosphorylating and inactivating the mitotic cyclin-dependent kinase (CDK) (8). On the other hand, circadian-independent cell divisions have been reported in rat-1 fibroblasts despite the fact that these cells maintain robust circadian rhythms (9). These data suggest that not all cells with circadian rhythms may display circadian-gated cell division cycles.

The multinucleate fungus *Neurospora crassa* has played a pivotal role in elucidating the molecular mechanism of circadian rhythms (10, 11). Briefly, circadian rhythms in *N. crassa* are regulated by positive and negative elements that create a time-delayed negative feedback loop (12). A heterodimeric transcription factor, White Collar Complex (WCC, which consists of WC-1 and WC-2), activates transcription of the *frequency* (*frq*) gene. Its product, FRQ protein, interacts with an RNA helicase, FRH (13), and inactivates the WCC by indirectly phosphorylating and removing WCC from the nucleus (14–16). FRQ is phosphorylated progressively over time, which makes it more susceptible to ubiquitination and degradation triggered by its conformational changes (17–19). The degradation of FRQ results in a new cycle of transcriptional activations by the WCC.

Previous studies in Neurospora showed asynchronous mitotic divisions, with no report of circadian-gated division cycles, despite the presence of robust circadian rhythms (20–22). On the other hand, although synchronous nuclear divisions are observed in other fungi, such as *Aspergillus nidulans*, it is unknown whether circadian rhythms play a role in the synchrony of their divisions (23). Recent use of GFP labeling has facilitated detailed observations of mitosis in germinating conidia, supporting models for asynchronous mitotic nuclear divisions (21, 24). These experiments, however, did not take into account the potential influence of circadian rhythms in mitotic division cycles. In Neurospora, robust circadian oscillations are observed in constant darkness (DD) or under entrainment regimens (e.g., light–dark cycles), but not in constant light (LL) conditions. There are no reports of experiments that address functional roles of circadian rhythms in mitotic divisions in the syncytium system.

Significance

Circadian rhythms provide temporal information to other cellular processes, such as metabolism. We investigate the coupling between the cell cycle and the circadian clock using mathematical modeling and experimentally validate model-driven predictions with a model filamentous fungus, *Neurospora crassa*. We demonstrate a conserved coupling mechanism between the cell cycle and the circadian clock in Neurospora as in mammals, which results in circadian clock-gated mitotic cycles. Furthermore, we observe circadian clock-dependent phase shifts of G1 and G2 cyclins, which may alter the timing of divisions. Our work has large implications for the general understanding of the connection between the cell cycle and the circadian clock.

Author contributions: C.I.H. and A.C.-N. designed research; J.Z., M.B., L.L., K.J., H.L., L.F.L., A.G., H.S.C., and W.J.B. performed research; J.Z. performed mathematical modeling; C.I.H., J.Z., and A.C.-N. analyzed data; and C.I.H., J.Z., L.F.L., W.J.B., and A.C.-N. wrote the paper.

The authors declare no conflict of interest.

*This Direct Submission article had a prearranged editor.

Freely available online through the PNAS open access option.

[1]To whom correspondence should be addressed. E-mail: christian.hong@uc.edu.

This article contains supporting information online at www.pnas.org/lookup/suppl/doi:10.1073/pnas.1319399111/-/DCSupplemental.

The cell cycle regulation of Neurospora has yet to be investigated thoroughly because of some technical limitations, such as adequate methods to synchronize, image, and measure doubling times of nuclear divisions in growing mycelia. We explored the Neurospora genome (25) to find the homologs of key cell cycle regulators and found that Neurospora has a low number of predicted cyclins and CDKs. Neurospora has a single *Cdk1* homolog (*cdc-2*, NCU09778), one G1 cyclin that resembles the sequence of the G1/S regulating budding yeast *Clns* (*cln-1*, NCU02114), and two B-type cyclins (*clb-1*, NCU02758, and *clb-3*, NCU01242) (26). There also exists a homolog of the CDK1 inhibitor WEE1 kinase (*stk-29*, NCU04326), which is regulated in a circadian manner in the mouse liver (5). Interactions between the above homologous proteins in budding and fission yeast have been well characterized, and their conservation among eukaryotes (27, 28) suggests they may be wired in a similar fashion in *N. crassa*.

Here, we investigate the molecular connection between the cell cycle and the circadian clock and functional consequences of this coupling in *N. crassa*. First, we show that there is a conserved connection between the cell cycle and the circadian clock in Neurospora as in mammals via STK-29, which is the Neurospora homolog of WEE1. Based on this finding and on the hypothesis of conserved cell cycle regulatory interactions, we use mathematical modeling to investigate molecular profiles of both cell cycle and circadian clock components. Our computational simulations predict circadian oscillations of cell cycle components, such as CLN-1 and CLB-1. We experimentally validate this prediction with luciferase bioluminescence reporters to track both cell cycle and circadian clock components in real time in vivo. Moreover, we demonstrate circadian clock-induced phase shifts of cell cycle components, which may alter the timing of divisions. The circadian oscillations of key cell cycle components suggest circadian clock-gated synchronized nuclear divisions. By observing nuclear morphology over time at 25 °C in DD, we indicate that most divisions occur in the evening. We propose that there is a significant coupling between the cell cycle and the circadian clock, which might result in immediate changes in the dynamics of cell cycle regulation upon alterations in circadian rhythms.

Results

There Is a Conserved Coupling Between the Cell Cycle and the Circadian Clock in *N. crassa* as in *Mus musculus*. A heterodimeric circadian transcription factor, WCC, recognizes light-responsive elements (LREs) to activate target genes (13, 29, 30). We found four putative LREs (GAGATCC, CCGATCC, CCGATCG, and TCGATCT) within 1.75 kb of the *stk-29* gene 5′ upstream region (Fig. 1*A*). To test WCC-dependent activation of *stk-29*, we performed a light induction experiment. WC-1 is also a photoreceptor that undergoes a light induction response, which is described by a sharp increase in its expression followed by a decrease to its basal level of expression when Neurospora is transferred from dark to light conditions (Fig. 1*B*). Light-induced WC-1 activates many downstream target genes by recognizing LREs (31). We observe light response from *stk-29* mRNA in the wild type, which is abolished in the *wc-1*^{ko} (Fig. 1 *C* and *D*). In contrast, we do not observe a light response of *cln-1* mRNA in wild-type strains (Fig. 1*E*). The WC-1–dependent light response of *stk-29* indicates that *stk-29* is activated by WCC and that it is a potential target for circadian regulation. To verify direct binding of WCC to the promoter of *stk-29*, we performed a WC-2 ChIP experiment and show that the WC-2 binds to the region close to LRE1 (Fig. 1*F*). Based on the finding that *stk-29* is activated by WCC, we tested a mathematical model of the Neurospora circadian clock and cell cycle as a coupled oscillator and explored coupled dynamics (Figs. S1–S4 and Tables S1–S5).

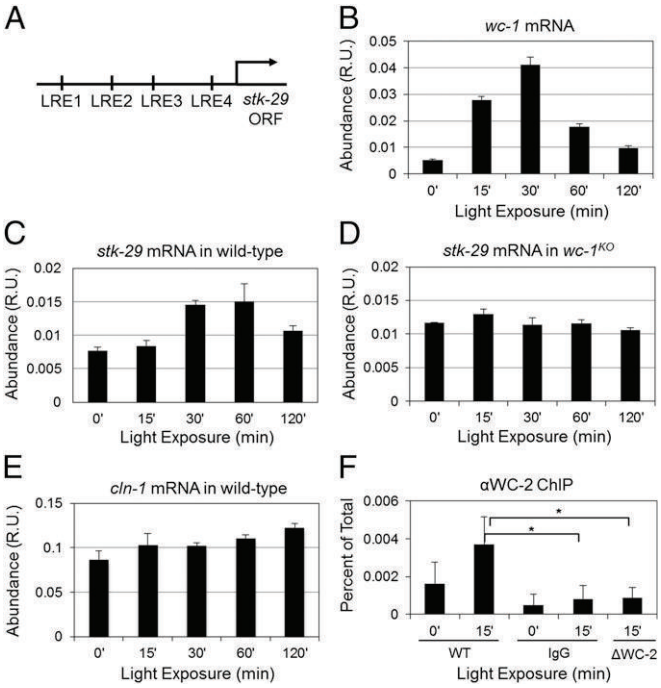

Fig. 1. *stk-29* mRNA shows WC-1–dependent light response, and WC-2 directly binds to the *stk-29* promoter. (*A*) There are four LREs within 1.75 kb of the *stk-29* gene 5′ upstream region. The first LRE, GAGATCC, is located ∼1.75 kb upstream (LRE1); the second LRE, CCGATCC, is located ∼1.2 kb upstream (LRE2); the third LRE, CCGATCG, is located ∼0.8 kb upstream (LRE3); and the fourth LRE, TCGATCT, is located ∼0.25 kb upstream (LRE4) of the *stk-29* gene. (*B*) *wc-1* mRNA undergoes light response when Neurospora is moved from dark to light conditions. (*C* and *D*) *stk-29* mRNA shows light response in the wild type (*C*), which is abolished in *wc-1*^{ko} (*D*). (*E*) *cln-1* mRNA does not show light response in the wild type. The above data are relative units (R.U.) normalized with *actin* mRNA. The average ± SD is shown. The above data are representative of two or more independent experiments. (*F*) WC-2 directly binds to the promoter of *stk-29*. ChIP assay was performed on a wild-type strain (FGSC2489), with samples grown in the dark (0′) or in response to a 15-min light pulse (15′) using a polyclonal antibody that recognizes WC-2 protein and oligos specific for a region of the *stk-29* promoter. A nonspecific IgG and a strain lacking the *wc-2* gene (*Δwc-2*) were used as controls. The results are an average of five experiments, and the error bars represent the SDs. The asterisks indicate a *P* value <0.001.

***cln-1* and *clb-1* Gene Expression and Protein Abundance Show Circadian Clock-Dependent Oscillations.** Our mathematical model predicts circadian oscillations of cell cycle components such as CLN-1 and CLB-1 proteins if intermediate to strong coupling exists between the circadian clock and the cell cycle (Figs. S1–S4). To validate circadian-dependent oscillations of cell cycle factors, we constructed bioluminescence reporters to track in vivo gene expression of *cln-1* (NCU02114), *clb-1* (NCU02758), *stk-29* (NCU04326), and *cdc-2* (NCU09778) in real time. Bioluminescence reporters were constructed by fusing the fully codon-optimized luciferase from firefly with a promoter of interest (32). Our data indicate that expression of *cln-1*, *clb-1*, and *stk-29* from populations of Neurospora nuclei show circadian oscillations (Fig. 2*A*). We also observe circadian oscillations of *cln-1* and *clb-1* mRNA expressions (Fig. S5). Expression of *cdc-2*, however, does not follow circadian regulation (Fig. 2*A*). This is in accord with the cell cycle model that we adapted (33), which assumes constitutive expression of *cdc-2*. We then constructed translational bioluminescence reporters of CLN-1^{luc}, CLB-1^{luc}, and CDC-2^{luc} by fusing luciferase to genes of interest as previously described for FRQ^{luc} (34), and followed protein abundances of CLN-1, CLB-1, and CDC-2. The abundance of both CLN-1 and CLB-1

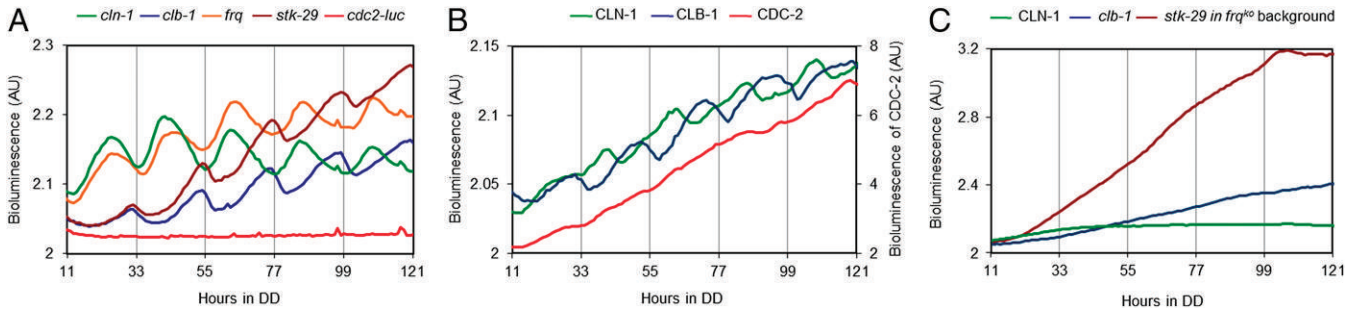

Fig. 2. *cln-1*, *clb-1*, and *stk-29* demonstrate circadian oscillations. (*A*) *cln-1*, *clb-1*, *stk-29*, and *cdc-2* promoters are fused to the codon-optimized firefly luciferase (32) for real-time analyses of their gene expressions in vivo. A strain carrying *frq-luciferase* reporter, an established core circadian component, is used as a positive control. (*B*) *cln-1*, *clb-1*, and *cdc-2* genes are fused with the codon-optimized firefly luciferase for real-time observation of CLN-1, CLB-1, and CDC-2 protein abundances. (*C*) A strain housing *clb-1–luciferase* or *stk-29–luciferase* reporter is crossed with frq^{ko} mutant resulting in *clb-1–luciferase* and *stk-29–luciferase* reporters in frq^{ko} background that show loss of circadian oscillations of *clb-1* and *stk-29* gene expression. Similarly, the CLN-1^{luc} translational reporter is crossed with frq^{ko} mutant, resulting in a CLN-1^{luc} reporter strain in frq^{ko} background, which shows an arrhythmic phenotype. The above data are representative of three or more independent experiments. Arbitrary units (AU) are shown.

shows circadian oscillations with phase information similar to that of their gene expression profiles (Fig. 2*B*). The observed phase relationship between CLN-1 and CLB-1 is expected based on their cell cycle functions in G1 and G2/M phases, respectively. In contrast, the abundance of CDC-2 increases continuously over time, corresponding to the growth in mass of Neurospora, and does not exhibit circadian oscillations (Fig. 2*B*). The data suggest that CDC-2 is stable with a constant rate of expression, consistent with findings in budding yeast (35). Importantly, circadian oscillations of CLN-1 protein and *clb-1* and *stk-29* gene expression are lost in the frq^{ko} strain, an arrhythmic mutant in which the circadian clock is nonfunctional (Fig. 2*C*). This indicates that the synchronized oscillations of cell cycle elements are under the influence of circadian rhythms.

Based on the above data, we hypothesized that the expression of cell cycle genes such as *clb-1* might be altered in a circadian manner. We performed light-pulse experiments to phase-shift circadian rhythms and investigated the circadian-dependent phase shifts of cell cycle components. We tracked bioluminescence of *frq*, *clb-1*, and *stk-29* gene expression after a 90-min light pulse at specific time points in DD. We observed ~3–5-h phase advances and delays in the expression of *frq*, *clb-1*, and *stk-29* when light pulses were given at DD32 [circadian time 23 (CT23)] and DD48 (CT16), respectively (Fig. 3). This demonstrates that the phases of *clb-1* and *stk-29* gene expression are influenced by phase

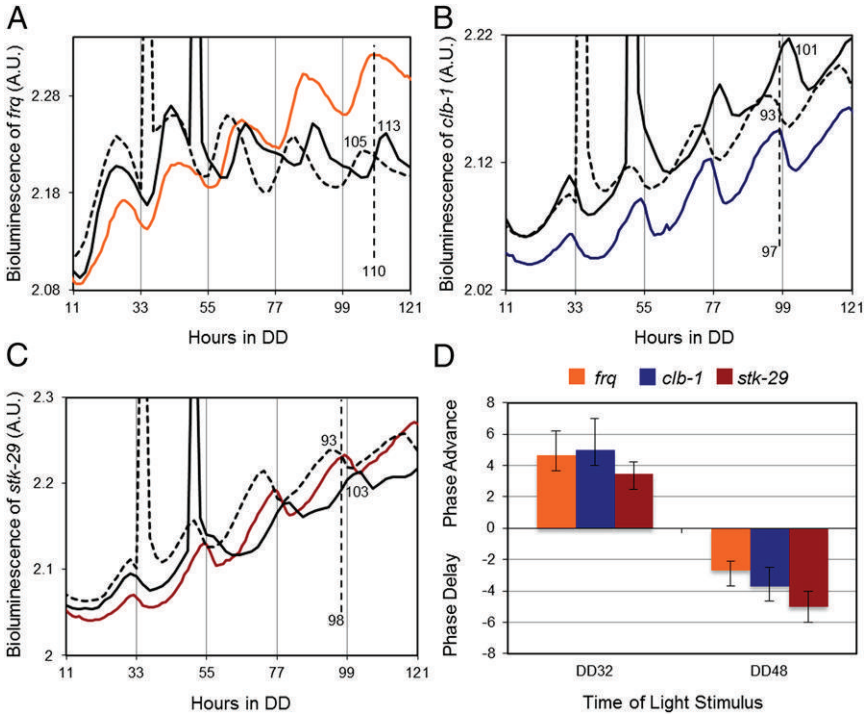

Fig. 3. *clb-1* and *stk-29* gene expressions indicate circadian clock-dependent phase shifts. (*A–C*) A 90-min light pulse is given at either DD32 (dashed black) or DD48 (solid black), and the phases of peak expressions of *frq*, *clb-1*, and *stk-29* genes are compared with unperturbed data (*frq*, orange; *clb-1*, blue; *stk-29*, maroon) at the fourth peak of unperturbed data (dashed straight line). Corresponding peaks are labeled in each figure. The data shown represent three independent experiments. (*D*) A 90-min light stimulus at DD32 and DD48 creates ~3–5-h phase advances and delays, respectively. The data are from three independent experiments (Fig. S6), and the average ± SD is shown. Arbitrary units (AU) are shown.

changes of the circadian clock that are similar in degree and direction, which may alter the timing of nuclear divisions in *N. crassa*.

Circadian Clock-Dependent Synchronized Nuclear Divisions Occur in the Middle of the Night. The lack of circadian oscillations of *clb-1* gene expression in frq^{ko} does not necessarily indicate altered mitosis (Fig. 2*C*). Rather, it suggests asynchronous mitotic divisions uncoupled from circadian rhythms. To verify this, we investigated circadian clock-dependent synchronized nuclear divisions. In Neurospora, nuclei are visualized readily by using an *hH1-sgfp* strain in which histone H1 is fused to GFP (21, 24). By using this strain, the stages of the cell cycle can be visualized and categorized. We performed a time-course experiment under circadian conditions (i.e., DD at 25 °C) and classified the populations of nuclei into two categories: interphase and mitotic phase (Fig. 4*A*). At CT4, or during the subjective day, most nuclei are in interphase, as shown by round nuclear morphology (Fig. 4*B*). In contrast, many nuclei undergo mitosis at around CT17, which corresponds to late subjective evening (Fig. 4*C*). Although there is variability in mitotic stage, around 60% of nuclei are actively dividing in the evening (Fig. 4*D*). These data clearly demonstrate circadian oscillations in Neurospora mitotic divisions. The synchronized nuclear divisions are not observed in the frq^{ko} strain (Fig. 4*E*), which indicates that circadian rhythms are necessary for this daily synchronization of cell cycles. These observations are in accord with the arrhythmic *clb-1* and *stk-29* gene expression in frq^{ko} (Fig. 2*C*). We also used an established mitosis marker, phospho-histone H3 (pH3) antibody, as an independent measurement of mitosis (36, 37). We observed more pH3-positive nuclei at DD25 (CT15) than at DD35 (CT2) (Fig. S7 *A* and *B*).

The above experiments are performed by harvesting Neurospora from liquid culture media in DD and counting the number of nuclei present in fixed cells. It is important to note that we observe similar results via live cell imaging from Neurospora grown in defined solid agar media, in which we observe a second cycle of increased and decreased mitosis at DD47 and DD57, respectively (Fig. S8 and Movies S1–S4).

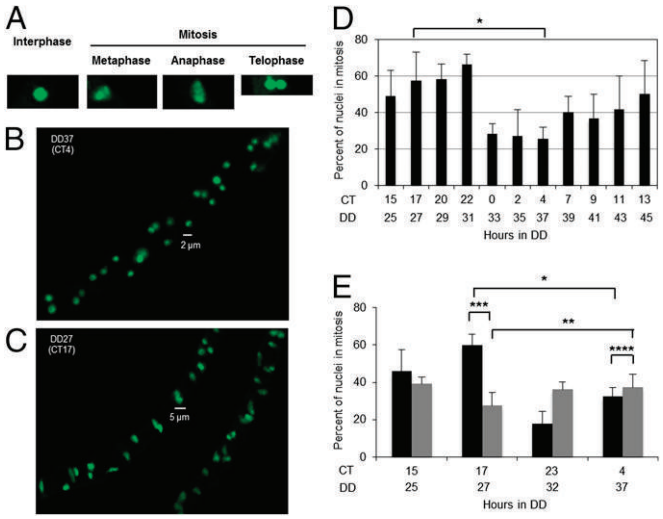

Fig. 4. Circadian clock-gated synchronized nuclear divisions are observed in Neurospora. (*A*) Different stages of mitotic cycles can be visualized with the *hH1-sgfp* strain and categorized based on the morphology of nuclei. (*B* and *C*) Microscopy data showing strands of hyphae at two different time points: CT4 and CT17. CT denotes circadian time in a free-running period in DD, in which subjective day begins at CT0 and subjective night begins at CT12. (*D*) Percentages of nuclei in mitosis are calculated as a time course with 2-h resolution. The average ± SD is shown. DD27 is statistically different from DD37 (**P* = 0.021). The values are obtained from a time-course experiment with four to six samples from each time point. (*E*) Percentages of nuclei in mitosis are calculated and compared between the wild type (black) and frq^{ko} (gray) at four different time points (CT15, CT17, CT23, and CT4). The average ± SEM is shown. The data are from three or more independent experiments. Two-way ANOVA indicates there is a significant difference between DD27 and DD37 in the wild type (**P* = 0.012) but not in the frq^{ko} strain (***P* = 0.33). There is a significant difference between the wild type and the frq^{ko} at DD27 (****P* = 0.005) but not at DD37 (*****P* = 0.609). Similar data are shown from live cell imaging (Fig. S8 and Movies S1–S4).

Discussion

In silico, we investigated various scenarios of coupled dynamics between the circadian clock and the cell cycle, which demonstrated circadian oscillations of cell cycle components if significant coupling exists between the two oscillators (Figs. S2–S4). We have demonstrated experimentally that elements of the cell cycle (e.g., *cln-1* and *clb-1*) undergo circadian oscillations, which manifest a circadian clock-dependent synchronized mitotic division in Neurospora. We also show that both *clb-1* and *stk-29* gene expression undergo light-dependent phase shifts in a length and direction similar to those of *frq* gene expression. This suggests circadian clock-dependent phase shifts of cell cycle components, which might be used to alter the timing of mitotic divisions.

The fundamental molecular regulatory architecture of circadian rhythms that highlight the time-delayed negative feedback mechanism is conserved from *N. crassa* to *M. musculus* (38). Coupling between circadian rhythms and the DNA damage response pathway is also conserved between Neurospora and mammals. Checkpoint kinase 2 (CHK2) is activated upon DNA damage and phosphorylates one of the core clock components (i.e., PER1 in mammals and FRQ in Neurospora), resulting in a subsequent degradation of PER1 or FRQ that leads to predominantly phase advances in circadian rhythms (39–43). We demonstrate that WC-2 binds to the promoter of *stk-29* (NCU04326) and that *stk-29* undergoes WC-1–dependent light-response and circadian oscillations, which shows conserved coupling between the cell cycle and circadian rhythms. The binding of WC-2 to the *stk-29* promoter was not reported in the recent WC-2 ChIP-sequencing data (44). This is probably a result of the low expression of *stk-29* and the less dramatic light response of *stk-29* compared with other targets. Further investigations are needed to understand the detailed dynamics of these connections as well as other possible coupling factors. We have shown circadian oscillations in a few cell cycle regulators. However, it is unclear whether these cycling components are genuine coupling components or mere reflections of the circadian-gated cell cycle determined by the currently known coupling factor STK-29. Recently, microarray data have suggested that several genes in cell cycle control show oscillatory behavior in Neurospora (45). Identification of other factors that couple the cell cycle and circadian rhythms will elucidate distinct points of interactions in which the circadian clock influences the cell cycle.

Identified conserved coupling components (i.e., CHK2 and WEE1) among the circadian clock, DNA damage response, and cell cycle mechanisms pose Neurospora as an ideal model organism to investigate the fundamental wiring of this network. However, one of the main disadvantages of Neurospora is that it is technically difficult to assess the doubling time of mitotic cycles in Neurospora mycelium grown on solid agar media. Previous measurements in liquid culture media showed a range in doubling time from 72 to 239 min, depending on growth conditions from young germinating conidia (46), which is in good agreement with our measurements in noncircadian conditions (e.g., LL) (Fig. S9). However, the doubling time in mature mycelium in circadian conditions (i.e., DD) might be different because of the presence of the circadian clock. Therefore, measuring the doubling time of nuclear divisions in DD for an extended period will be critical for future experiments. Real-time fluorescence and bioluminescence reporters, in addition to the use of

microfluidic devices for single-nucleus imaging, may facilitate measurement of doubling times for Neurospora growing in both liquid culture and solid agar media.

In this report, we demonstrate that many nuclear divisions occur during a specific window of circadian time. However, our experimental data also show that synchronized divisions are spread out over 6 h, with less frequent nuclear divisions also occurring at other times of the day (Fig. 4*D*). This does not imply that a single nucleus spends 6 h in the mitotic state; rather, our data suggest an increase in mitosis as a population within that 6-h window. It is also possible to hypothesize that a weak coupling might exist that enables the circadian clock to modulate the total abundance of CLB-1, which might allow more divisions during the evening in a threshold-dependent manner while keeping the cell cycle time short (Figs. S2*B* and S3*B*). Another hypothesis that might result in the observed phenotype is context-dependent (e.g., aging, nutrient conditions) weak to strong coupling. Our modeling work and other mathematical models predict quasi-periodic multimodal doubling times depending on the strength of the coupling and the frequency of the two oscillators (8, 47). In our future work, we plan to assess the strength of the coupling and the doubling time by using both computational simulations and experiments observing both cell cycle and circadian components with bioluminescence assays. Our discovery of circadian clock-dependent synchronized mitotic cycles in Neurospora will serve as a stepping-stone for further investigations to uncover conserved principles of coupled mechanisms between the cell cycle and circadian rhythms.

Materials and Methods

Strains. Strains used for the experiments are a clock wild-type *ras-1^{bd}*;a (328-4) and three arrhythmic mutants from the laboratories of Drs. J. Dunlap and J. Loros (Dartmouth Medical School, Hanover, NH) [*ras-1^{bd}*; *frq^{ko}*;a (358-6), *ras-1^{bd};wc-1^{ko}* (S38), and *ras-1^{bd};wc-2^{ko}* (*Δwc-2*)]. Wild-type strain FGSC#2489 (Mat A) was used for the ChIP experiment. Strain *hH1-sgfp* (FGSC#9518) was obtained from the Fungal Genetics Stock Center (FGSC, University of Missouri–Kansas City) (48). *cln-1-luc*, *clb-1-luc*, and *cdc-2-luc* strains were made by integrating these reporter constructs into the *csr-1* locus as previously described (49). CLN-1^{luc}, CLB-1^{luc}, and CDC-2^{luc} translational fusion strains were made by knock-in strategies as previously described (50). The strain *clb-1-luc;frq^{ko}* is a progeny from a cross between *clb-1-luc;ras-1^{bd};A* and 358–6 (*ras-1^{bd}*; *frq^{ko}*; a). The strain *stk-29-luc;frq^{ko}* is a progeny from a cross between *stk-29-luc;ras-1^{bd};A* and 358–6 (*ras-1^{bd}*; *frq^{ko}*;a). The strain CLN-1^{luc}; *frq^{ko}* is a progeny from a cross between CLN-1^{luc}*;ras-1^{bd};A* and 358–6 (*ras-1^{bd}*; *frq^{ko}*;a). The strain *hH1-sgfp;frq^{ko}* is a cross-progeny between *hH1-sgfp* (FGSC#9518) and 358–6 (*ras-1^{bd}*; *frq^{ko}*;a).

Quantitative RT-PCR. Neurospora was grown in liquid culture media containing Vogel's medium (pH 5.8) with 2% (wt/vol) glucose, 0.5% arginine, and 50 ng/mL biotin, and harvested as previously described (31). Total RNA was isolated using Tri Reagent (Molecular Research Center, Inc.), and quantitative RT-PCR (qRT-PCR) was performed as previously described (31). The *actin* mRNA is used to normalize real-time qRT-PCR data.

ChIP. ChIP was performed in a manner similar to methods previously described, with slight modifications (51, 52). One hundred-milliliter cultures of Neurospora mycelia were cross-linked with 1% formaldehyde for 15 min and then quenched with 0.1 M glycine for an additional 15 min. The Neurospora was harvested by filtration and ground with a mortar and pestle, and the tissue was added to 10 mL FA lysis buffer (0.05 M Hepes, pH 7.4/0.15 M NaCl/0.001 M EDTA/1% Triton TX-100/0.1% SDS) containing protease inhibitors (0.002 mg/mL leupeptin, 0.002 mg/mL pepstatin A, 0.001 M PMSF). To improve cell disruptions, the tissue was subjected to a single sonication at 50% power and the cellular debris was removed by centrifugation at 2500 × *g* for 10 min. A chromatin-enriched fraction then was obtained by a high-speed spin at 60,000 × *g* for 30 min. The pellet was suspended in the lysis buffer plus protease inhibitors and sonicated to an average size of 500 bp. Equal amounts of sheared chromatin were incubated with WC-2 antibody (53) plus protein A Dynabeads overnight at 4 °C with constant mixing. The beads were washed with the lysis buffer and eluted two times with 50 mL 0.1 M sodium bicarbonate and 1.0% SDS. The cross-links were reversed by incubating for 4 h at 65 °C in the presence of 0.1 M NaCl. The DNA was recovered by treatment with proteinase K for 1 h followed by a phenol/chloroform extraction, then suspended in 10 mM Tris, pH 7.5/1.0 mM EDTA. Two milliliters of the purified DNA was used in a quantitative PCR with primers specific to the *stk-29* promoter.

Bioluminescence Assay. In all experiments, Neurospora was grown at 25 °C in constant white fluorescent light (LL) overnight before being transferred into constant darkness (DD) for time-course experiments. For bioluminescence assays, we used standard race tubes containing Vogel's medium (pH 5.8) with 0.1% glucose, 0.17% arginine, 50 ng/mL biotin, 1.5% (wt/vol) agar, and 12.5 μM luciferin (Fig. 2). In vivo luciferase activity was collected for 10 min every hour with a PIXIS CCD camera from Princeton Instruments controlled by WinView/32 software from Roper Scientific. A 90-min pulse of white fluorescent light (80 μmol photons·m^{-2}·s^{-1}) was given at indicated time points for phase-shift experiments, and in vivo luciferase activity was collected for 10 min every 2 h.

Microscopy. For microscopy experiments, Neurospora conidia suspensions were grown in 500-mL baffled flasks in liquid culture media containing Vogel's medium (pH 5.8) with 2% (wt/vol) glucose, 0.5% arginine, and 50 ng/mL biotin. Neurospora was grown at 25 °C in constant white fluorescent light (LL) overnight before being transferred into constant dark (DD) for time-course experiments. Samples were grown on a shaker at 125 rpm. Random samples of mycelia were collected and fixed in 2% (wt/vol) paraformaldehyde/PBS at indicated time points and observed under a confocal fluorescence microscope (Zeiss LSM710). Two to three slides were prepared from each time point, and four to six images of mycelia were captured from each slide. Nuclei from each image were analyzed to calculate the average number of nuclei undergoing mitosis.

ACKNOWLEDGMENTS. We thank P. Stambrook, M. Montrose, N. Horsemen, K. Lee, and C. H. Chen for discussions. We thank S. Yoo, S. Moon, D. Ruter, and S. Kim for technical assistance. We thank C. Closson at the Live Microscopy Core for his help with confocal microscopy, and the Fungal Genetics Stock Center for providing the *hH1-sgfp* strain (FGSC#9518) (48). We are pleased to acknowledge use of materials generated by Grant P01 GM0668087, "Functional Analysis of a Model Filamentous Fungus" (54). C.I.H. was supported by Department of Interior Grant D12AP00005 and startup funds from the Department of Molecular and Cellular Physiology, University of Cincinnati. L.F.L. was supported by Fondo Nacional de Desarrollo Cientifico y Tecnologico 1090513. W.J.B. is supported by National Institutes of Health Grant R01 GM101378 and is a member of the National Institute on Environmental Health Sciences Center for Environmental Exposure and Disease (P30 ES005022).

1. Fu L, Pelicano H, Liu J, Huang P, Lee C (2002) The circadian gene Period2 plays an important role in tumor suppression and DNA damage response in vivo. *Cell* 111(1):41–50.
2. Green CB, Takahashi JS, Bass J (2008) The meter of metabolism. *Cell* 134(5):728–742.
3. Panda S, et al. (2002) Coordinated transcription of key pathways in the mouse by the circadian clock. *Cell* 109(3):307–320.
4. Edmunds LN, Jr., Funch RR (1969) Circadian rhythm of cell division in Euglena: Effects of random illumination regimen. *Science* 165(3892):500–503.
5. Matsuo T, et al. (2003) Control mechanism of the circadian clock for timing of cell division in vivo. *Science* 302(5643):255–259.
6. Sweeney BM, Hastings JW (1958) Rhythmic cell division in populations of Gonyaulax polyedra. *J Eukaryot Microbiol* 5:217–224.
7. Yang Q, Pando BF, Dong G, Golden SS, van Oudenaarden A (2010) Circadian gating of the cell cycle revealed in single cyanobacterial cells. *Science* 327(5972):1522–1526.
8. Zámborszky J, Hong CI, Csikász Nagy A (2007) Computational analysis of mammalian cell division gated by a circadian clock: Quantized cell cycles and cell size control. *J Biol Rhythms* 22(6):542–553.
9. Yeom M, Pendergast JS, Ohmiya Y, Yamazaki S (2010) Circadian-independent cell mitosis in immortalized fibroblasts. *Proc Natl Acad Sci USA* 107(21):9665–9670.
10. Dunlap JC, et al. (2007) A circadian clock in Neurospora: How genes and proteins cooperate to produce a sustained, entrainable, and compensated biological oscillator with a period of about a day. *Cold Spring Harb Symp Quant Biol* 72:57–68.
11. Liu Y, Bell-Pedersen D (2006) Circadian rhythms in Neurospora crassa and other filamentous fungi. *Eukaryot Cell* 5(8):1184–1193.
12. Aronson BD, Johnson KA, Loros JJ, Dunlap JC (1994) Negative feedback defining a circadian clock: Autoregulation of the clock gene frequency. *Science* 263(5153):1578–1584.
13. Cheng P, He Q, He Q, Wang L, Liu Y (2005) Regulation of the Neurospora circadian clock by an RNA helicase. *Genes Dev* 19(2):234–241.
14. Cha J, Chang SS, Huang G, Cheng P, Liu Y (2008) Control of WHITE COLLAR localization by phosphorylation is a critical step in the circadian negative feedback process. *EMBO J* 27(24):3246–3255.

15. Hong CI, Ruoff P, Loros JJ, Dunlap JC (2008) Closing the circadian negative feedback loop: FRQ-dependent clearance of WC-1 from the nucleus. *Genes Dev* 22(22): 3196–3204.
16. Schafmeier T, et al. (2008) Circadian activity and abundance rhythms of the Neurospora clock transcription factor WCC associated with rapid nucleo-cytoplasmic shuttling. *Genes Dev* 22(24):3397–3402.
17. Baker CL, Kettenbach AN, Loros JJ, Gerber SA, Dunlap JC (2009) Quantitative proteomics reveals a dynamic interactome and phase-specific phosphorylation in the Neurospora circadian clock. *Mol Cell* 34(3):354–363.
18. Querfurth C, et al. (2011) Circadian conformational change of the Neurospora clock protein FREQUENCY triggered by clustered hyperphosphorylation of a basic domain. *Mol Cell* 43(5):713–722.
19. Tang CT, et al. (2009) Setting the pace of the Neurospora circadian clock by multiple independent FRQ phosphorylation events. *Proc Natl Acad Sci USA* 106(26): 10722–10727.
20. Gladfelter AS (2006) Nuclear anarchy: Asynchronous mitosis in multinucleated fungal hyphae. *Curr Opin Microbiol* 9(6):547–552.
21. Roca MG, Kuo HC, Lichius A, Freitag M, Read ND (2010) Nuclear dynamics, mitosis, and the cytoskeleton during the early stages of colony initiation in Neurospora crassa. *Eukaryot Cell* 9(8):1171–1183.
22. Serna L, Stadler D (1978) Nuclear division cycle in germinating conidia of Neurospora crassa. *J Bacteriol* 136(1):341–351.
23. Rosenberger RF, Kessel M (1967) Synchrony of nuclear replication in individual hyphae of Aspergillus nidulans. *J Bacteriol* 94(5):1464–1469.
24. Freitag M, Hickey PC, Raju NB, Selker EU, Read ND (2004) GFP as a tool to analyze the organization, dynamics and function of nuclei and microtubules in Neurospora crassa. *Fungal Genet Biol* 41(10):897–910.
25. Galagan JE, et al. (2003) The genome sequence of the filamentous fungus Neurospora crassa. *Nature* 422(6934):859–868.
26. Borkovich KA, et al. (2004) Lessons from the genome sequence of Neurospora crassa: Tracing the path from genomic blueprint to multicellular organism. *Microbiol Mol Biol Rev* 68(1):1–108.
27. Nurse P (1990) Universal control mechanism regulating onset of M-phase. *Nature* 344(6266):503–508.
28. Csikász-Nagy A, Battogtokh D, Chen KC, Novák B, Tyson JJ (2006) Analysis of a generic model of eukaryotic cell-cycle regulation. *Biophys J* 90(12):4361–4379.
29. Froehlich AC, Liu Y, Loros JJ, Dunlap JC (2002) White Collar-1, a circadian blue light photoreceptor, binding to the frequency promoter. *Science* 297(5582):815–819.
30. He Q, et al. (2002) White collar-1, a DNA binding transcription factor and a light sensor. *Science* 297(5582):840–843.
31. Chen CH, Ringelberg CS, Gross RH, Dunlap JC, Loros JJ (2009) Genome-wide analysis of light-inducible responses reveals hierarchical light signalling in Neurospora. *EMBO J* 28(8):1029–1042.
32. Gooch VD, et al. (2008) Fully codon-optimized luciferase uncovers novel temperature characteristics of the Neurospora clock. *Eukaryot Cell* 7(1):28–37.
33. Tyson JJ, Novak B (2001) Regulation of the eukaryotic cell cycle: Molecular antagonism, hysteresis, and irreversible transitions. *J Theor Biol* 210(2):249–263.
34. Larrondo LF, Loros JJ, Dunlap JC (2012) High-resolution spatiotemporal analysis of gene expression in real time: In vivo analysis of circadian rhythms in Neurospora crassa using a FREQUENCY-luciferase translational reporter. *Fungal Genet Biol* 49(9): 681–683.
35. Spellman PT, et al. (1998) Comprehensive identification of cell cycle-regulated genes of the yeast Saccharomyces cerevisiae by microarray hybridization. *Mol Biol Cell* 9(12): 3273–3297.
36. Hendzel MJ, et al. (1997) Mitosis-specific phosphorylation of histone H3 initiates primarily within pericentromeric heterochromatin during G2 and spreads in an ordered fashion coincident with mitotic chromosome condensation. *Chromosoma* 106(6):348–360.
37. Plikus MV, et al. (2013) Local circadian clock gates cell cycle progression of transient amplifying cells during regenerative hair cycling. *Proc Natl Acad Sci USA* 110(23): E2106–E2115.
38. Dunlap JC (1999) Molecular bases for circadian clocks. *Cell* 96(2):271–290.
39. Gamsby JJ, Loros JJ, Dunlap JC (2009) A phylogenetically conserved DNA damage response resets the circadian clock. *J Biol Rhythms* 24(3):193–202.
40. Gery S, et al. (2006) The circadian gene per1 plays an important role in cell growth and DNA damage control in human cancer cells. *Mol Cell* 22(3):375–382.
41. Hong CI, Zámborszky J, Csikász-Nagy A (2009) Minimum criteria for DNA damage-induced phase advances in circadian rhythms. *PLOS Comput Biol* 5(5):e1000384.
42. Oklejewicz M, et al. (2008) Phase resetting of the mammalian circadian clock by DNA damage. *Curr Biol* 18(4):286–291.
43. Pregueiro AM, Liu Q, Baker CL, Dunlap JC, Loros JJ (2006) The Neurospora checkpoint kinase 2: A regulatory link between the circadian and cell cycles. *Science* 313(5787): 644–649.
44. Smith KM, et al. (2010) Transcription factors in light and circadian clock signaling networks revealed by genomewide mapping of direct targets for neurospora white collar complex. *Eukaryot Cell* 9(10):1549–1556.
45. Dong W, et al. (2008) Systems biology of the clock in Neurospora crassa. *PLoS One* 3(8):e3105.
46. Martegani E, Levi M, Trezzi F, Alberghina L (1980) Nuclear division cycle in Neurospora crassa hyphae under different growth conditions. *J Bacteriol* 142(1):268–275.
47. Gérard C, Goldbeter A (2012) Entrainment of the mammalian cell cycle by the circadian clock: Modeling two coupled cellular rhythms. *PLOS Comput Biol* 8(5):e1002516.
48. McCluskey K, Wiest A, Plamann M (2010) The Fungal Genetics Stock Center: A repository for 50 years of fungal genetics research. *J Biosci* 35(1):119–126.
49. Chen CH, DeMay BS, Gladfelter AS, Dunlap JC, Loros JJ (2010) Physical interaction between VIVID and white collar complex regulates photoadaptation in Neurospora. *Proc Natl Acad Sci USA* 107(38):16715–16720.
50. Larrondo LF, Colot HV, Baker CL, Loros JJ, Dunlap JC (2009) Fungal functional genomics: Tunable knockout-knock-in expression and tagging strategies. *Eukaryot Cell* 8(5):800–804.
51. Belden WJ, Lewis ZA, Selker EU, Loros JJ, Dunlap JC (2011) CHD1 remodels chromatin and influences transient DNA methylation at the clock gene frequency. *PLoS Genet* 7(7):e1002166.
52. Belden WJ, Loros JJ, Dunlap JC (2007) Execution of the circadian negative feedback loop in Neurospora requires the ATP-dependent chromatin-remodeling enzyme CLOCKSWITCH. *Mol Cell* 25(4):587–600.
53. Denault DL, Loros JJ, Dunlap JC (2001) WC-2 mediates WC-1-FRQ interaction within the PAS protein-linked circadian feedback loop of Neurospora. *EMBO J* 20(1-2): 109–117.
54. Colot HV, et al. (2006) A high-throughput gene knockout procedure for Neurospora reveals functions for multiple transcription factors. *Proc Natl Acad Sci USA* 103(27): 10352–10357.